THE ASTROPHYSICAL JOURNAL SUPPLEMENT SERIES, 90:317–432, 1994 January

A HIGH-RESOLUTION SPECTRAL ATLAS OF CARBON STARS

CECILIA BARNBAUM
Department of Astronomy, University of California, Berkeley, CA 94720
Received 1993 April 12; accepted 1993 July 8

ABSTRACT

We present a spectral atlas of six bright carbon stars (U Hya, TX Psc, RZ Peg, V Oph, Y CVn, and UV Cam) observed with the Hamilton Echelle Spectrograph at coudé using the 3 m telescope at Lick Observatory. These data are of high resolution (0.13 Å at 6100 Å) and high signal-to-noise. The spectral range spans from 5080 to 7850 Å; however, there are gaps due to the unmatched size of the echelle format and the CCD. We have observed a total of 87 carbon stars in the solar neighborhood over the period from 1988 May through 1991 September, with two or more observations for 67 stars of the sample. The reduced spectra (40 orders per observation for a total of nearly 9200 individual spectra) will be available to the scientific community via the Astrophysics Data System (ADS). The current study has produced the most detailed multi-epoch observations to date of a large number of carbon stars.

Presented here, along with spectra of the six sample stars, are separate template plots to be used as a tool for the ADS on-line database. These templates are of atomic features, as well as ^{12}CN and $^{12}C_2$ transitions taken from the tables of Davis & Phillips (1963) and Phillips & Davis (1968), respectively. We have calculated band head positions for the isotopic species $^{13}C^{14}N$, $^{12}C^{13}C$, and $^{13}C^{13}C$, whose transitions contribute significantly to the spectra of carbon stars with enhanced ^{13}C abundance, known as *J*-type carbon stars.

Subject headings: atlases — stars: AGB and post-AGB — stars: carbon

1. INTRODUCTION

Asymptotic giant branch (AGB) stars are important for a number of reasons. They determine, in large part, the elemental composition of the interstellar medium, directing the next generation of star formation. Their dusty circumstellar envelopes are chemical laboratories in which compounds form that will seed the interstellar medium with siliceous and carbonaceous grains, chains, and perhaps even Buckminsterfullerenes. AGB stars are enormously bright (e.g., from 6×10^3 to several $\times 10^4$ $L_\odot$; Claussen et al. 1987; Kastner et al. 1993) and, therefore, they are resolvable at large distances in the Milky Way and even in some nearby galaxies. Carbon stars, the subject of this atlas, make up a subgroup of stars on the AGB which have an inverted carbon-to-oxygen ratio (C/O > 1). Since carbon stars are approximately one bolometric magnitude brighter than oxygen-rich AGB stars of the same mass (Iben & Truran 1978), they have been used to probe the kinematics and dynamics of the Galaxy (Dean 1976; Tyson & Rich 1991) and of external systems (e.g., Reid & Mould 1990). Carbon stars have also played a role in attempts to answer questions of cosmological significance. Radial velocity measurements of bright carbon stars in dwarf halo galaxies of the Milky Way have provided observational evidence for a large amount of dark matter in these systems (Seitzer & Frogel 1985; Aaronson 1983; Aaronson & Olszewski 1987; Mateo et al. 1991), although these results have been disputed (Jura 1986; Godwin & Lynden-Bell 1987; Barnbaum 1992a).

Carbon stars have peculiar atmospheric and circumstellar chemical abundances due to the dredge-up of freshly processed material from their interior (Iben & Renzini 1983; Boothroyd & Sackman 1988). A spectrum of a carbon star's atmosphere is a window into the stellar interior which normally is locked away from view. The presence or absence of certain elements, such as those produced by the *s*-process, offers insight into evolutionary status and interior structure. Optical spectra can also reveal clues to the dynamics and physical processes in the tenuous stellar atmosphere; the velocities of atomic transitions at different energies show a changing velocity structure with phase, as well as shocks, in these pulsating giants (e.g., see Barnbaum 1992b; Barnbaum & Morris 1993).

In the early days of optical spectroscopy, seminal studies were made measuring radial velocities of carbon stars using low-resolution spectra (20 Å mm^{-1} in the visual and near-infrared) taken on photographic plates (Sanford 1935, 1944, 1950; Merrill 1940; Joy 1954; Fujita 1952). These spectra initiated us into the peculiarities of these cool, swollen stars, such as strong Balmer emission and heavy molecular line blanketing in the blue spectral region. Atomic absorption lines are largely overwhelmed by molecular transitions, making line identification and velocity measurements difficult and unreliable with low or even moderate dispersion. Adding to these difficulties, photographic plates are more sensitive in the blue wavelength region where carbon stars are faint, and they are significantly less sensitive in the red region where carbon stars are brightest and most easily observed. Thus, observing a large number of carbon stars with high resolution was impractical until the advent of the red-sensitive CCD.

After Sanford and Merrill's work, optical spectroscopy of carbon stars reached higher dispersion (8 to 10 Å mm^{-1}) and extended into the near infrared; Utsumi (1963) and Utsumi (1967) obtained broad wavelength coverage of two carbon stars (Y CVn and U Cyg, respectively), and Fujita & Yamashita (1960) observed V Aql. These data and microphotometer tracings have approximately half the dispersion presented here, and do not have high signal-to-noise ratios,

although a dispersion similar to our present data was obtained by Fujita & Yamashita (1963) on Y CVn. None of these studies, however, presents either the multi-epoch observations needed to ascertain changes in velocity and profile structure of individual atomic and molecular lines or observations of a large number of carbon stars.

Starting in 1988 and ending in 1991, we observed 87 carbon stars of the solar neighborhood, 67 with two or more observations, using the Hamilton Echelle Spectrograph and TI 800 × 800 CCD with the 3 m telescope at Lick Observatory. These data are high resolution (0.13 Å at 6100 Å), high signal-to-noise (typically from 150 to 600 at 6100 Å and from 250 to 800 at 7100 Å), and span from 5080 to 7850 Å. The reduced spectra (40 orders per observation for a total of nearly 9200 individual spectra) will be available to the scientific community via the Astrophysics Data System (ADS). The current study has produced the most detailed multi-epoch observations to date of a large number of carbon stars. In this paper, we present a spectral atlas of six of the stars in the sample of 87 (U Hya, TX Psc, RZ Peg, V Oph, Y CVn, and UV Cam). Separate template-plots of molecular and atomic lines for each order are included, to be used as a tool for this atlas and the ADS on-line database: the ^{12}CN and $^{12}C_2$ transitions are taken from the tables of Davis & Phillips (1963) and Phillips & Davis (1968), respectively.

Model atmospheres of AGB stars have been difficult to develop, due to the complicated conditions in a cool, tenuous atmosphere (e.g., non-LTE effects and nonlinear opacities). However, sophisticated models of carbon star atmospheres have recently been developed (Johnson & Luttermoser 1992). The spectra in this study will allow theorists a detailed comparison of their models with high signal-to-noise spectra for many types of carbon stars over many photometric phases.

All carbon stars observed in this program whose spectra will be available with ADS are listed in Table 1, with spectral type, variability type, period, and epoch where available. In the last column are comments indicating interesting aspects of the observations, such as Hα, Mg I, and K I emission, and, for two stars, Hα absorption. Table 2 lists the dates of the observations for each star. In § 3 we describe the molecular and atomic features which characterize the optical spectra of carbon stars, presenting typical examples of variable features in Figures 1–4. The figures of the spectral atlas (Figs. 5–44) are described in § 4, and the template plots of atomic and molecular features are found in Figures 45–52 and Figures 53–65, respectively.

2. OBSERVATIONS

The program stars were selected from a flux-limited sample of Galactic carbon stars detected by the Two Micron Sky Survey (Neugebauer & Leighton 1969) and compiled by Claussen et al. (1987). For the most part, we chose stars brighter than magnitude 6.5 in the *I* band (9000 Å), observing 84 of the 215 stars listed by Claussen et al., with three additional carbon stars, EU And, DY Per, and V778 Cyg.

Optical spectra were obtained between 1988 May and 1991 September with the 120 inch (3 m) Shane Telescope at Lick Observatory. The Hamilton Echelle spectrograph at coudé produces high-resolution spectra (0.13 Å at 6100 Å) with a linear reciprocal dispersion ranging from 2.8 Å mm^{-1} in the blue to 4.3 Å mm^{-1} in the red (see Vogt 1987 for a description of the spectrograph). Note that the broad wavelength range, from 5080 to 7850 Å, has gaps due to the unmatched size of the echelle format and the CCD (see Table 3 for exact wavelength coverage). The detector, a TI 800 × 800 CCD, measures only 12 mm and must be moved over the larger echelle format to the desired wavelength region, covering ~3,000 Å at any one setting. The choice of wavelength region was based on the nature of carbon stars as well as on the properties of the echelle grating. The effective temperature, $T_{\rm eff}$, of carbon stars on the AGB is generally between ~2000 and 3600 K (Mendoza & Johnson 1965; Lambert et al. 1986). Carbon stars are very bright in the red and faint in the blue, and their meager blue light is greatly attenuated by line blanketing. In addition, the Hamilton Echelle grating, as well as the CCD detector, have their highest efficiency in the red region. Achieving adequate signal-to-noise in the blue would greatly over-saturate the red region. Therefore, the wavelength coverage was chosen to reach as far as possible into the blue with adequate signal-to-noise without necessitating multiple exposures to preserve the red region. The setup results in 40 spectral orders per observation.

Stellar spectra were taken with a 2″.5 decker and 640 μ slit, projecting 1″.2 on the sky. Focusing typically produced a FWHM of 2.3 to 2.5 pixels. A Thorium-Argon lamp was used for wavelength calibration, bracketing stellar exposures. We find the spectrograph to be stable, with a drift of 0.7 km s^{-1} (0.3 pixels) over 8 hours. The raw data were reduced with the IRAF software package. Specifics of echelle spectra reduction are given by Goodrich & Veilleux (1988). The bias was subtracted from each image. A quartz lamp was used for flat fielding with a 4″ (arcsecond) decker, which adequately covers each order of the stellar spectra, observed through a 2″.5 decker. The alternative method discussed in Vogt (1987) uses a deckerless quartz exposure for the flat-fielding, and then a 2″.5 decker quartz image is extracted as spectra and later used to divide into stellar spectra to remove the fringing resulting from the open decker flat. We experimented with both methods and found the 4″ decker flat to be adequate. Extraction of the orders was carried out using an exposure of a smooth continuum standard as a template (a rapidly rotating A or B star). The Hamilton Echelle spectrograph was designed for minimal order separation, and therefore accurate sky subtraction is not attempted (see Vogt 1987). Inter-order scattered light was found to be fairly consistent at ~12%, and is subtracted from each order. Table 3 lists the beginning and ending wavelength, number of angstroms covered, dispersion, and resolution for each of the 40 orders for a typical reduction. The exact number of angstroms plotted in each figure presented in this paper, as well as the figure number for a given order, appear in the last two columns of Table 3.

3. SPECTRAL CHARACTERISTICS OF CARBON STARS

The optical spectral region of carbon stars is characterized by very closely spaced molecular absorption lines, namely, those of CN and C_2. The continuum is obscured throughout the optical region, and atomic absorption lines are overwhelmed by the molecular transitions. Since the wings of even the strongest atomic lines are not visible and the level of the

TABLE 1

PROPERTIES OF CARBON STARS OBSERVED IN THIS STUDY

STAR	SPECTRAL TYPE[a]		VARIABILITY	APPARENT MAGNITUDE RANGE		PERIOD[b] (day)	EPOCH (JD +2,400,000)	COMMENTS
				Maximum	Minimum			
AQ And	N	C5,4	SR	9.9	11.8	346	29970	
EU And	R	C4,4J	SR	12.9	14.1p	...	...	Silicate-rich CSE;H_2O maser[c]
SU And	Nb	C6,4	Lc	8.0	8.5v	...	...	
VX And	N7	C4,5J	SRa	7.8	9.3v	...	...	
V Aql	N6	C6,4	SRb	6.6	8.4v	353	...	
V374 Aql	Ne	C7,3e	SRa	8.8	11.7v	456.5	38314	Hα emission
AU Aur	N0e	C6,3e	M	13.0	15.8p	400	29057	Hα emission
AZ Aur	N0e	C7,1e	M	10.5	17.7b	415.9	42866	Hα and Mg I emission
EL Aur	N3	C5,4	Lb	11.5	12.3p	...	...	
FU Aur	N0	C7,2	Lb	11.0	12.2b	...	...	
S Aur	N3	C4,4	SR	8.2	13.3v	590.1	42000	Hα emission
TX Aur	N3	C5,4	Lb	8.5	9.2v	...	...	
UU Aur	N3	C5,3	SRb	7.8	10.0b	234	...	
UV Aur	Ne	C6,2epJ	M	7.4	10.6v	394.4	41062	Hα and Mg I emission
S Cam	R8e	C7,3e	SRa	7.7	11.6v	327.3	43360	Hα and Mg I emission
ST Cam	N5	C5,4	SRb	9.2	12.0p	300	...	
U Cam	N5	C3,9e	SRb	11.0	12.8p	...	43060	
UV Cam	R8	C5,3J	SRb	7.5	8.1v	294	...	Hα absorption
T Cnc	N6R6	C3,8	SRb	7.6	10.5v	482	...	
X Cnc	N3	C5,4	SRb	5.6	7.5v	195	43631	
W CMa	N	C6,3	Lb	6.4	7.9v	...	...	
Y CVn	N3	C5,4J	SRb	7.4	10.0p	157	...	
R CMi	CSep	C7,1eJ	M	7.2	11.6v	337.8	41323	Hα emission
HO Cas	R	C4,3	Lb	13.4	14.0p	...	...	
HV Cas	Ne	C4,3e	M	12.9	17.2p	527	38120	Hα emission
W Cas	...	C7,1e	M	7.8	12.5v	405.6	44209	Hα and Mg I emission
X Cas	N1e	C5,4e	M	9.5	13.2v	422.8	43922	Hα emission
S Cep	N8e	C7,4e	M	7.4	12.9v	487.0	47213[b]	Hα emission
V CrB	N2e	C6,2e	M	6.9	12.6v	358.0	47342[b]	Hα and Mg I emission
RS Cyg	N0ep	C8,2e	SRa	6.5	9.5v	417.4	47270[b]	Hα emission
TT Cyg	N3e	C5,4e	SRb	10.2	11.9b	118	...	
U Cyg	Nep	C7,2e	M	5.9	12.1v	462.4	47326[b]	Hα and Mg I emission
V Cyg	Nep	C5,3e	M	7.7	13.9v	421.4	47382[b]	Hα emission
V778 Cyg	N	C4,5J	Lb	11.6	13.5p	...	...	Silicate-rich CSE;H_2O & OH maser[c]
WX Cyg	N3e	C8,2eJ	M	8.8	13.2v	410.5	47407[b]	Hα emission; ↑ Li
RY Dra	N4p	C4,5J	SRb	6.0	8.0v	172.5	...[b]	
T Dra	N0e	C6,2e	M	7.2	13.5v	421.2	47337[b]	Hα and Mg I emission
UX Dra	N0	C7,3	SRa	5.9	7.1v	168	...	
R For	Ne	C4,3e	M	7.5	13.0v	388.7	41974	Hα emission; P-Cyg K I
BM Gem	N	C5,4J	SRb	11.5	12.1p	286	...	Silicate-rich CSE[c]
TU Gem	N3	C6,4	SRb	9.4	12.5p	230	...	
VX Gem	Nep	C7,2e	M	10.8	15.1p	379.4	41280	Hα emission
ZZ Gem	Ne	C5,3e	M	12.4	16.0p	317	33999	Hα and Mg I emission
CZ Hya	Ne	Ce	M	9.7	15.5p	442	27546	Hα and Mg I emission
RY Hya	N	C6,4e	SRb	12.2	15p	529	...	Hα emission
U Hya	N2	C6,5	SRb	7.0	9.2v	450	47210[b]	
V Hya	N6e	C6,3e	M/SRa	10.9	16.0v	529.2	46900[b]	Hα emission
Y Hya	N3p	C5,4	SRb	8.3	12.0p	302.8	...	
R Lep	N6e	C7,6e	M	5.5	11.7v	427.1	42506	Hα and Mg I emission
HK Lyr	N4	C6,4	Lb	7.8	9.6v	...	...	
T Lyr	R6	C6,5J	Lb	7.8	9.6v	...	...	
U Lyr	N0e	C4,5e	M	8.3	13.5v	455.6	47088[b]	Hα emission
CL Mon	N6e	C6,3e	M	11.0	17.5p	497.2	37440	Hα emission; P-Cyg K I
CZ Mon	N5	C4,5	Lb	12.5	14.5p	...	...	
DF Mon	N	C4,4	Lb	12.5	14.8b	...	...	
GY Mon	N3R8	C6,3	Lb	9.4	11.6p	...	...	
TW Oph	N	C5,5	SRb	11.6	13.8p	185	...	
TY Oph	N	C5,5	Lb	12.7	15.1p	...	...	
V Oph	N3e	C5,2e	M	7.3	11.6v	298	47180[b]	Hα and Mg I emission
BL Ori	N	C6,3	Lb	7.9	9.7p	...	...	
GK Ori	N	C4,4	SR	9.5	11v	236	26002	
RT Ori	N	C6,4	SRb	9.7	11.8p	321	...	
W Ori	N5	C5,4	SRb	8.2	12.4p	212	...	
RZ Peg	CSe	C9,1e	M	7.6	13.6v	439.4	47413[b]	Hα and Mg I emission
AC Per	N3	C6,3	Lb	11.8	12.4p		...	

TABLE 1—*Continued*

Star	Spectral Type[a]		Variability	Apparent Magnitude Range		Period[b] (day)	Epoch (JD +2,400,000)	Comments
				Maximum	Minimum			
DY Per	R8	C4,5	SRb	10.6	13.2	900	...	
SY Per	N3e	C6,4	SRa	8.7	13.0v	474	37635	Hα emission
TX Psc	N0	C7,2	Lb	4.8	5.2v	...	...	
Z Psc	N0	C7,2	SRb	8.8	10.1p	144	...	
AC Pup	N	C5,4	Lb	8.9	10.1v	...	...	
SS Sgr	N/R3	C3,4	SRb	10.9	11.3p	...	...	
SZ Sgr	N	C7,3	SRb	11.1	11.9b	73	...	
V781 Sgr	N0	C	Lb	12.5	14.0p	...	...	
V2548 Sgr	N3	...	SRa	14.5	16.4p	159	23950	
SU Sco	N0	C5,5	SR	11.7	13.2p	414	...	Hα emission
V901 Sco	Ne	Ce	SR	13.6	15.8p	...	...	Hα emission
R Scl	Np	C6,5e	SRb	9.1	12.9p	370	...	
S Sct	N3	C6,4	SRb	9.6	10.9b	148	...	
FO Ser	R6	C4,5J	Lb	8.4	8.7v	...	...	Hα absorption
FX Ser	...	C	Lb	14.1	15.7v	...	...	Hα emission
TT Tau	N3	C4,2	SRb	10.2	12.2p	166.5	...	
TU Tau	N3	C5,4	SRb	5.9	9.2v	190	...	
Y Tau	N2e	C6,5e	SRb	6.5	9.2v	241.5	...	
TMSS−30293	...	...	...	...	...	...	...	
VY UMa	N0	C6,3	Lb	5.9	7.0v	...	...	
RU Vir	R3ep	C8,1e	M	9.0	14.2v	436.2	47322[b]	Hα and Mg I emission
SS Vir	Ne	C6,3e	M/SRa	6.0	9.6v	354.7	47177[b]	Hα emission

[a] Spectral and variability types and magnitudes are from Kholopov 1985. The J-type classification of EU And and FO Ser is based on the optical spectra obtained in this study. Note that the magnitudes are indicated as either v (visual), b (blue), or p (photographic). These designations refer to both the maximum and minimum magnitudes.

[b] Period and epoch provided by AAVSO (Mattei 1990). All others are from Kholopov 1985.

[c] See discovery papers: Little-Marenin 1986; Willems & De Jong 1986; for review, see Barnbaum et al. 1991.

TABLE 2

SUMMARY OF DATES OF ALL OBSERVATIONS

Star	1988 May	1988 Dec	1989 May	1989 Jul	1989 Dec	1990 Mar	1990 Jun	1990 Sep	1990 Oct	1990 Nov	1990 Dec	1991 Sep
AQ And					✓			✓				
EU And				✓	✓			✓	✓	✓		
SU And					✓							
VX And					✓			✓				
V Aql	✓						✓					
V374 Aql			✓					✓				
AU Aur									✓			
AZ Aur					✓				✓			
EL Aur											✓	
FU Aur											✓	
S Aur					✓				✓	✓		
TX Aur					✓						✓	
UU Aur					✓						✓	
UV Aur					✓				✓			
S Cam					✓						✓	
ST Cam					✓			✓				
U Cam					✓							
UV Cam					✓			✓	✓		✓	
T Cnc					✓	✓						
X Cnc					✓	✓				✓		
W CMa					✓	✓						
Y CVn	✓		✓			✓	✓				✓	
R CMi					✓	✓			✓	✓		
HO Cas								✓				
HV Cas					✓							
W Cas					✓					✓		
X Cas					✓			✓	✓			
S Cep				✓			✓	✓				
V CrB	✓		✓	✓		✓	✓					
RS Cyg			✓					✓				

TABLE 2—*Continued*

Star	1988 May	1988 Dec	1989 May	1989 Jul	1989 Dec	1990 Mar	1990 Jun	1990 Sep	1990 Oct	1990 Nov	1990 Dec	1991 Sep
TT Cyg			✓					✓				
U Cyg				✓				✓				
V Cyg				✓				✓				
V778 Cyg				✓			✓	✓				
RY Dra	✓		✓			✓	✓					
T Dra	✓		✓				✓	✓				
WX Cyg				✓								
UX Dra	✓											
R For								✓				✓
BM Gem					✓	✓			✓	✓	✓	
TU Gem					✓							
VX Gem						✓						
ZZ Gem					✓				✓			
CZ Hya	✓		✓		✓	✓				✓	✓	
RY Hya						✓			✓			
U Hya	✓	✓	✓✓		✓	✓	✓			✓	✓	
V Hya	✓	✓	✓		✓	✓	✓			✓	✓	
Y Hya					✓	✓						
R Lep					✓				✓			
HK Lyr			✓	✓								
T Lyr							✓					
U Lyr			✓				✓	✓				
CL Mon						✓			✓✓	✓✓	✓	
CZ Mon											✓	
DF Mon											✓	
GY Mon					✓	✓			✓	✓		
TW Oph	✓		✓				✓					
TY Oph				✓								
V Oph			✓	✓			✓					
BL Ori					✓					✓		
GK Ori					✓							
RT Ori					✓						✓	
W Ori					✓					✓		
RZ Peg				✓	✓				✓			
AC Per								✓				
DY Per								✓				
SY Per					✓			✓		✓		
TX Psc				✓	✓✓			✓✓	✓✓	✓✓	✓	✓
Z Psc					✓			✓	✓			
AC Pup					✓	✓						
SS Sgr			✓				✓					
SZ Sgr	✓						✓					
V781 Sgr			✓				✓					
V2548 Sgr	✓											
SU Sco			✓	✓			✓	✓				
V901 Sco			✓				✓					
R Scl					✓							
S Sct	✓						✓					
FO Ser				✓			✓	✓				
FX Ser								✓				
TT Tau					✓			✓		✓		
TU Tau										✓	✓	
Y Tau					✓				✓	✓		
TMSS-30293			✓				✓					
VY UMa	✓					✓						
RU Vir	✓		✓		✓	✓					✓	
SS Vir	✓					✓	✓				✓	

TABLE 3

TYPICAL SPECTRUM PARAMETERS[a]

ORDER NUMBER	λ_{begin} (Å)	λ_{end} (Å)	TOTAL RANGE (Å)	$\Delta\lambda$ PER PIXEL (Å)	DISPERSION (Å mm^{-1})	RESOLUTION[b] (Å)	THE FIGURES: Total λ in Plot[c] (Å)	THE FIGURES: Figure Number
112	5084.089	5117.969	33.880	0.0426	2.84	0.11	34.0	5
111	5129.885	5164.069	34.184	0.0429	2.86	0.11	34.4	6
110	5176.513	4211.008	34.495	0.0433	2.89	0.11	34.7	7
109	5223.997	5258.808	34.811	0.0437	2.92	0.11	35.0	8
108	5272.360	5307.493	35.133	0.0441	2.94	0.11	35.3	9
107	5321.627	5357.089	35.462	0.0446	2.97	0.11	35.7	10
106	5371.824	5407.620	35.796	0.0450	3.00	0.11	36.0	11
105	5422.977	5459.113	36.136	0.0454	3.03	0.11	36.4	12
104	5475.113	5511.596	36.483	0.0458	3.06	0.12	36.6	13
103	5528.262	5565.099	36.837	0.0463	3.09	0.12	37.1	14
102	5582.453	5619.651	37.198	0.0467	3.12	0.12	37.4	15
101	5637.717	5675.283	37.566	0.0472	3.15	0.12	37.7	16
100	5694.086	5732.027	37.941	0.0477	3.18	0.12	38.1	17
99	5751.594	5789.918	38.324	0.0482	3.21	0.12	38.5	18
98	5810.276	5848.991	38.715	0.0486	3.24	0.12	38.4	19
97	5870.167	5909.281	39.114	0.0492	3.28	0.12	39.3	20
96	5931.307	5970.827	39.520	0.0497	3.31	0.12	39.7	21
95	5993.733	6033.669	39.936	0.0502	3.35	0.13	40.2	22
94	6057.488	6097.849	40.361	0.0507	3.38	0.13	40.5	23
93	6122.614	6163.409	40.795	0.0513	3.42	0.13	41.0	24
92	6189.156	6230.393	41.237	0.0518	3.45	0.13	41.4	25
91	6257.160	6298.850	41.690	0.0524	3.49	0.13	41.9	26
90	6326.675	6368.828	42.153	0.0530	3.53	0.13	42.3	27
89	6397.752	6440.378	42.626	0.0536	3.57	0.13	42.8	28
88	6470.445	6513.555	43.110	0.0542	3.61	0.14	43.3	29
87	6544.809	6588.414	43.605	0.0548	3.65	0.14	43.8	30
86	6620.902	6665.014	44.112	0.0554	3.69	0.14	44.4	31
85	6698.786	6743.417	44.631	0.0561	3.74	0.14	44.8	32
84	6778.524	6823.686	45.162	0.0568	3.78	0.14	45.1	33
83	6860.184	6905.889	45.705	0.0574	3.83	0.14	45.9	34
82	6943.835	6990.097	46.262	0.0581	3.88	0.15	46.1	35
81	7029.552	7076.385	46.833	0.0589	3.92	0.15	47.0	36
80	7117.411	7164.829	47.418	0.0596	3.97	0.15	47.6	37
79	7207.495	7255.513	48.018	0.0604	4.02	0.15	47.6	38
78	7299.889	7348.522	48.633	0.0611	4.07	0.15	48.7	39
77	7394.682	7443.946	49.264	0.0619	4.13	0.16	49.2	40
76	7491.970	7541.882	49.912	0.0627	4.18	0.16	50.0	41
75	7591.853	7642.429	50.576	0.0636	4.24	0.16	50.5	42
74	7694.435	7745.695	51.260	0.0644	4.29	0.16	51.4	43
73	7799.827	7851.789	51.962	0.0653	4.35	0.16	52.1	44

[a] Total number of points in each spectrum is 796. These particular values are those of U Hya 1989/12/10, and the values listed are those before heliocentric correction.

[b] Resolution is based on FWHM = 2.5 pixels, each pixel measuring 15 μm.

[c] Each figure is exactly the same physical length in the x-axis. The total number of angstroms plotted in each figure is indicated here.

continuum is unknown, direct measurements of equivalent width are not possible without performing spectral synthesis using model atmospheres and all the assumptions entailed. In this paper we have identified a number of atomic features, as well as CN and C_2 absorption lines. We have calculated band head positions for the isotopic species $^{13}C^{14}N$, $^{12}C^{13}C$, and $^{13}C^{13}C$, which also affect optical spectra, particularly the spectra of stars with greatly enhanced ^{13}C abundance, known as J-type carbon stars ($^{12}C/^{13}C \sim 3$ for J-types vs. $^{12}C/^{13}C \sim 50$ for other carbon stars; Lambert et al. 1986). This section describes the general characteristics of carbon star spectra resulting from the complex combination of molecular and atomic absorption features in their cool atmospheres.

3.1. *Molecular Lines*

3.1.1. $^{12}C^{14}N$ *and* $^{12}C_2$

The spectral region from ~5600 to 7850 Å is dominated by the vibration-rotation transitions of CN, specifically, by the Red System, $A^2\Pi$–$X^2\Sigma$. The Swan bands of C_2, $A^3\Pi_g$–$X^3\Pi_u$, dominate the blue region and extend into the red region, up to near 6600 Å, overlapping with those of CN. The CN and C_2 transitions connect the ground state to the first electronic excited state, with orbital angular momentum change from the ground state $\Delta\Lambda = -1$ for CN and $\Delta\Lambda = 0$ for C_2. These states are split into vibrational terms whose energy intervals are closely spaced, and the vibrational terms are split by the even

more closely spaced rotational transitions. It is the combination of electronic, vibrational, and rotational transitions that produces the complex bands characteristic of these spectra. The direction in which a molecular band degrades, to the blue or red, depends on whether the internuclear distance increases or decreases, respectively, as the result of the vibration-rotation change from the upper to lower state. CN branches of the Red System degrade to the red, and the band heads are significantly more diffuse than the sharp, well-separated band heads of C_2 (Swan bands), which degrade toward the blue. The rotational transitions are the P, Q, and R branches which represent a change in the rotational quantum number K of -1, 0, and $+1$, respectively, and each with spin splitting, producing eight branches of P, Q, and R for CN and six branches of P and R for C_2. These branches overlap both within a given vibrational transition and among the many vibrational transitions for each molecular species, creating a jumble of absorption features in carbon star spectra which are very difficult to sort out. To complicate matters further, an isotope of carbon, ^{13}C, forms molecules whose absorption lines mingle with those of ^{12}CN and $^{12}C_2$.

With the tables of Davis & Phillips (1963) and Phillips & Davis (1968), we have identified a number of CN and C_2 transitions over the region of interest through pattern recognition, although these identifications are a small fraction of the total number of absorption dips in the spectrum. Isotopic species are likely contributors to the optical spectra of carbon stars, and therefore, we have calculated the positions of isotopic band heads within our spectral window.

3.1.2. *Isotopes* $^{13}C^{14}N$, $^{12}C^{13}C$, *and* $^{13}C^{13}C$

Isotopic species of CN and C_2 have been known for some time to occur in the spectra of carbon stars (e.g., Sanford 1950). These molecules are especially evident in carbon stars with greatly enhanced ^{13}C, the J-type carbon stars. The increased strength of the ^{13}C isotopic species in J-type stars causes their spectra to have a clearly different appearance from those of carbon stars with normal ^{13}C abundance. The effect of a heavier isotope on the band structure of a diatomic molecule both shifts the band origin and contracts the entire vibration-rotation band, with respect to the lighter molecule. For example, for a given vibration transition, the rotational branches of ^{13}CN are more contracted about the band origin than those of ^{12}CN (Herzberg 1950), and additionally, the band origin itself is shifted redward. The superposition of isotopic shifts with the normal line positions might be the cause of the smeared appearance of many regions of the spectra of J-type carbon stars (e.g., see the figures of Y CVn in this atlas).

No detailed atlas, such as those of Davis & Phillips (1963) and Phillips & Davis (1968), exists for the isotopic species of CN and C_2; therefore, we have calculated the location of a number of isotopic band heads. The position of an absorption line is the sum of its electronic, vibrational and rotational terms. Since the isotopic shift of the electronic term is negligible (Herzberg 1950), the adjustment comes from the vibrational and rotational terms, where each is a function of the reduced mass, $\mu = (m_1 m_2)/(m_1 + m_2)$, where m_1 and m_2 are the masses of the atoms of the diatomic molecule. The equation for the band head, in wavenumbers (cm^{-1}), is

$$\nu_{bh} = \nu_0 - \frac{(B_{\nu'} + B_{\nu''})^2}{4(B_{\nu'} - B_{\nu''})} .$$

The B_ν's are the rotational constants,

$$B_\nu = \rho^2 B_e - \rho^3 \alpha_e (\nu + \tfrac{1}{2}) ,$$

where $\rho^2 = \mu/\mu_i$ is the ratio of the reduced masses (the subscript i indicating the reduced mass of the isotopic molecule), and B_e and α_e are constants and functions of the moment of inertia of the molecule. The symbols ν' and ν'' refer to upper and lower vibration states, respectively. The band origin, ν_0, is equal to the electronic term, ν_e, and the vibrational term:

$$\nu_0 = \nu_e + [\rho \omega_e'(\nu' + \tfrac{1}{2}) - \rho^2 \omega_e' \chi_e'(\nu' + \tfrac{1}{2})^2] - [\rho \omega_e''(\nu'' + \tfrac{1}{2}) - \rho^2 \omega_e'' \chi_e''(\nu'' + \tfrac{1}{2})^2] .$$

For our calculations, the constants, ν_e, α_e, ω_e, and $\omega_e \chi_e$ were taken from Phillips & Davis (1968) and Davis & Phillips (1963), for C_2 and CN, respectively. The R_2 bandheads for CN are found by calculating the transition of the R_2 branch for various rotational quantum numbers, J, as given in Herzberg (1950), and then finding the minimum wavelength, the vertex of the parabolic branch.

As a check on our calculations, we compared our results for ^{12}CN with the laboratory data of Davis and Phillips, shown in Table 4. The first column lists the vibrational transitions for the bandheads occurring in the spectral region of this atlas. The mean difference between observed and calculated wavelengths of ^{12}CN band heads is 0.15 Å. The results for ^{13}CN are in the last column, and are calculated for all vibrational transitions from 5080 to 7850 Å. The band heads which fall off order, yet whose individual lines away from the band head might affect our spectra, are so indicated.

Calculating band head locations for C_2 is nontrivial. Phillips and Davis describe the difficulties due to perturbations. We were unable to use their experimental values of ν_0 for specific upper and lower vibration states, since ν_0 is a function of ρ, which is not equal to unity for isotopic species. However, we were able to use their experimental values for ω_e and $\omega_e \chi_e$ to calculate the B_ν's. The difference between our calculated band heads for $^{12}C^{12}C$ and those presented in the tables of Phillips and Davis are substantially larger than for ^{12}CN. The differences were smallest for the lower vibrational transitions, and we present the results for $^{12}C^{12}C$ in Table 5, as well as the calculations for the same vibrational transitions for the isotopic species, $^{12}C^{13}C$ and $^{13}C^{13}C$. These band head locations give a general idea of the spectral regions likely to be affected by an increase in ^{13}C abundance.

3.2. *Atomic Lines*

3.2.1. *General Characteristics of Atomic Lines*

Atomic absorption lines in the optical spectra of carbon stars are so severely blended by molecular features that in almost all cases only their line cores are present. The strongest lines, Na

TABLE 4

R_2 BAND HEADS OF $^{12}C^{14}N$ AND $^{13}C^{14}N$ FOR THE RED SYSTEM $A^2\Sigma$–$X^2\Pi$

		$^{12}C^{14}N$			$^{13}C^{14}N$
v'	v''	Davis & Phillips Measured	R_2 Band Head Calculated	O–C	R_2 Band Head Calculated
10,	3	5043.46	5043.35[a]	0.11	5093.81
6,	0	5129.62	5129.45[a]	0.17	5183.76
7,	1	5239.26	5239.25	0.01	5292.46
8,	2	5354.09	5353.70	0.39	5406.02
9,	3	5473.28	5473.11[a]	0.17	5524.22[a]
5,	0	5606.93	5606.88[a]	0.05	5661.67
10,	4	5597.90	5597.79	0.11	5647.55
15,	8	5659.70	5659.42	0.28	5702.31
11,	5	5728.15	5728.13	0.02	5776.34
6,	1	5729.92	5729.85	−0.07	5783.51
7,	2	5858.17	5858.16[a]	−0.01	5910.53
12,	6	5864.42	5864.49	−0.07	5910.97
8,	3	5992.62	5992.16[a]	0.46	6043.08[a]
9,	4	6132.40	6132.24	0.16	6181.52[a]
4,	0	6192.09	6192.15	−0.06	6246.25[a]
10,	5	6278.82	6278.82	0.00	6326.25[a]
5,	1	6332.18	6332.14	0.04	6384.80[a]
11,	6	6432.20	6432.36	−0.16	6477.71
12,	7	6593.00	6593.37[a]	−0.37	6636.37
7,	3	6631.29	6631.30	−0.01	6680.52[a]
8,	4	6791.88	6791.37	0.51	6838.54[a]
3,	0	6925.82	6926.12[a]	−0.30	6977.39
9,	5	6959.20	6959.11	0.09	7003.97[a]
4,	1	7088.69	7088.76[a]	−0.07	7138.12
5,	2	7259.01	7258.95[a]	0.06	7306.16
6,	3	7437.32	7437.22	0.10	7482.03[a]
7,	4	7624.08	7624.16	−0.08	7666.27[a]
8,	5	7820.91	7820.43	0.48	7859.51[a]

[a] The location of the band head is outside the spectral ranges of Figs. 5–44, but lines belonging to this vibrational transition might affect the observed spectra.

D (λ5895.93 and λ5889.96), K I (λ7698.96), Mg Ib (λ5183.61), and Li I (λ6707.84), are clearly present in all stars. Even for these strong lines, the wings are completely obscured, with the exception of Na D in a few stars where the absorption is so deep and broad that the effect of these two lines is seen over the full 40 Å spectral order. However, even in the case of Na D only a suggestion of profile wings is evident, and these wings are severely mottled by the overlapping and closely spaced molecular absorption lines. Figure 1 shows an example of the broad Na D lines in UV Aur before minimum light (ϕ = 0.26) and the narrower Na D lines at maximum light (ϕ = 0.03). Broadening and narrowing of Na D was described as early as 1920 by Shane, who noticed this phenomenon in a number of carbon stars, and was also noted by Sanford (1950) in the spectrum of U Cyg; temperature variations are likely to contribute to the effect (Alksne & Ikaunieks 1981). However, the extreme change in the Na D lines with phase does not occur in all Miras of our sample of carbon stars.

The spectra of carbon stars show other interesting changes with phase. In addition to the broadening and narrowing of Na D, emission lines brighten and fade. For a given observation, atomic line velocities differ from each other, and the magnitude of these differences changes with phase. The differences among atomic line velocities are smallest at minimum light and are largest at photometric maximum. Miras have larger velocity variations and differences among atomic line velocities than do SR or Lb variables. Additionally, their cross-correlated optical velocities[1] are consistently redshifted with respect to center-of-mass velocity, as measured by circumstellar CO (J = 1–0), whereas the optical velocities of SR and Lb variables vary equally to the red and blue of the center-of-mass motion (Barnbaum 1992a). Figure 2 shows the measured velocities of Li, K, and Mg absorption lines as well as the cross-correlated optical velocities and circumstellar CO (J = 1–0) for a typical Mira, SR, and Lb star. The velocities are plotted versus phase for the SR and Mira variables (U Hya and CZ Hya); the Lb variable (TX Psc) has no regular period and so the velocities are plotted versus Julian Day. The velocity variations of atomic lines with phase and the dispersion among them for a given observation have been described in Barnbaum (1992b); although opacity changes and differential atmospheric bulk motion throughout a pulsation are likely to play a role (Hinkle 1978), the phenomenon is not well understood.

[1] These velocities were measured by cross-correlating the entire spectrum, over 25–30 orders, with a template. See legend of Fig. 2.

TABLE 5

BAND HEADS OF $^{12}C^{12}C$, $^{12}C^{13}C$, AND $^{13}C^{13}C$ FOR THE SWAN SYSTEM $A^3\Pi_g$–$X^3\Pi_u$

		$^{12}C^{12}C$			$^{12}C^{13}C$	$^{13}C^{13}C$
v'	v''	Phillips & Davis Measured	Band Head Calculated	O–C	Band Head Calculated	Band Head Calculated
1,	1	5129.36[a]	5128.56	0.80	5129.4[a]	5130.2[a]
0,	0	5165.24[a]	5165.11	0.13	5165.2[a]	5165.4[a]
2,	3	5540.70	5537.65	3.05	5530.3	5522.8[a]
1,	2	5585.49	5584.56	0.93	5576.2[a]	5567.6[a]
0,	1	5635.50[a]	5635.29	0.21	5625.6[a]	5615.8
1,	3	6122.15[a]	6121.04	1.11	6100.1[a]	6078.8
0,	2	6191.27	6190.96	0.31	6167.9[a]	6144.4

[a] The location of the band head is outside the spectral ranges of Figs. 5–44, but lines belonging to this vibrational transition might affect the observed spectra.

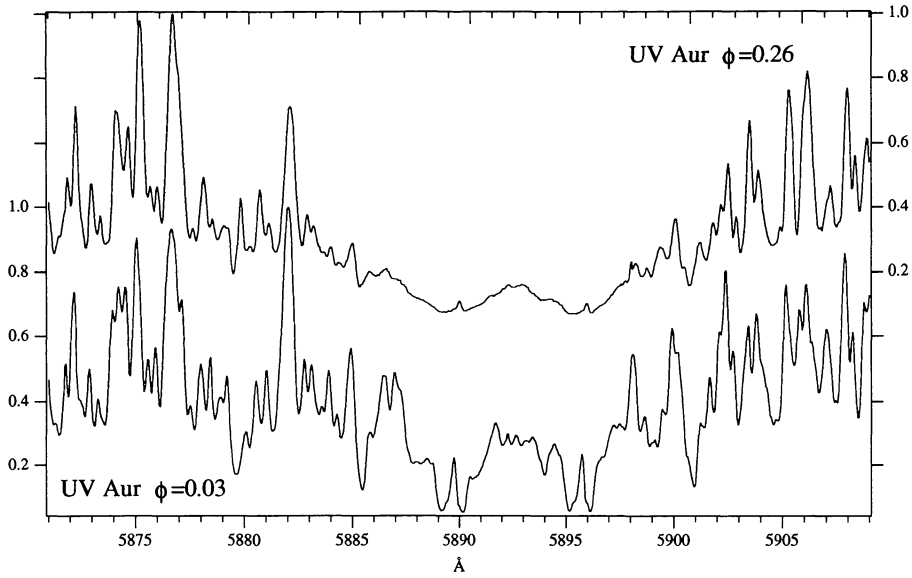

FIG. 1.—Spectral region of Na D in UV Aur over two epochs. Each spectrum is normalized to its maximum point, with the scale for $\phi = 0.03$ on the left and for $\phi = 0.26$ on the right.

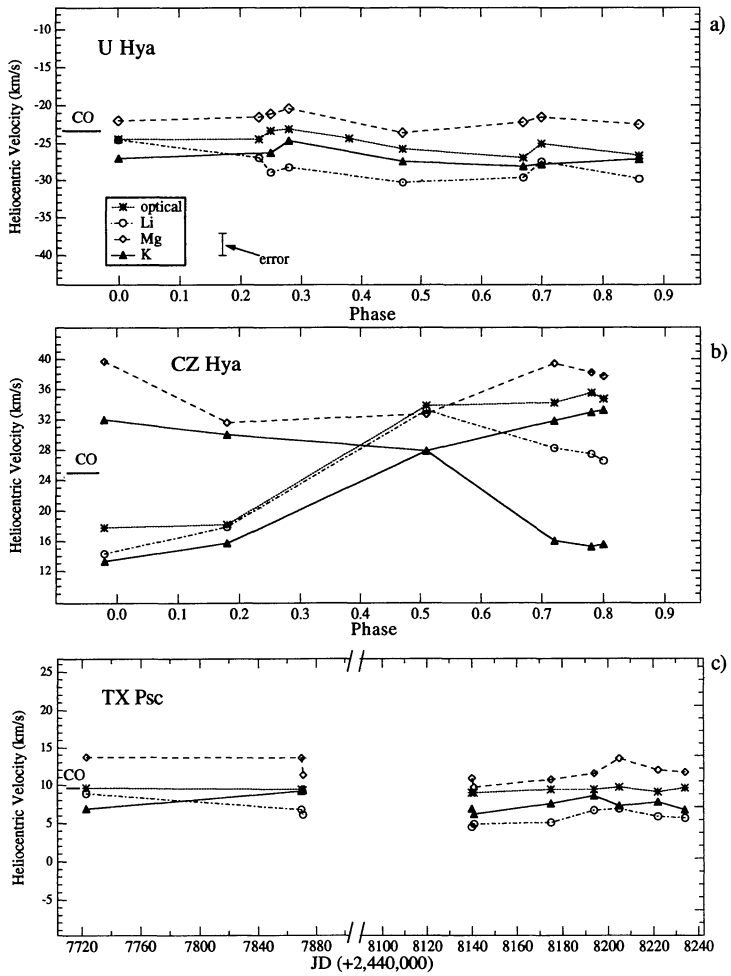

FIG. 2.—Heliocentric velocities as a function of phase. The legend and the error bars for the line velocities (± 1.5 km s^{-1}) are indicated in panel (*a*). Cross-correlated (labeled "optical") velocities were obtained by cross-correlating spectra with a template over 25 to 30 spectral orders, and represent a statistical average of the molecular and atomic line shifts, taken together (see Barnbaum 1992b for discussion). (*a, b*) Velocities are plotted as a function of phase for SR variable U Hya and Mira CZ Hya. The observations have been folded and plotted by phase, not chronology. (*c*) Velocities for Lb variable TX Psc are plotted chronologically, according to Julian Day, since Lb variables do not have regular periods. Note that the velocity scale is the same for all three plots. The *heliocentric* circumstellar emission line velocity of CO ($J = 1$–0) is indicated on the left-hand side of each plot, being −23.3, +25, and +11.2 km s^{-1} for U Hya, CZ Hya, and TX Psc, respectively (taken from Olofsson et al. 1990; Olofsson et al. 1993; Olofsson et al. 1987).

Emission lines, such as Hα, Mg I, and K I, arise with changes in phase. Hα emission is present in 34 stars of our sample of 87 and is noted in Table 1. Its presence is ascribed to shocks propagating through the pulsating atmospheres of AGB stars (Hill & Willson 1979; Willson & Hill 1979). In the absence of shocks, Hα is not expected to be in absorption since in atmospheres of $T_{\rm eff} \sim 3000$ K, the $n = 2$ level is not greatly populated. However, two stars of this sample, UV Cam and FO Ser, show Hα in absorption (see UV Cam in Fig. 30*b* below). It is interesting to note that both of these stars have enhanced ^{13}C (J-types) and are classified as late R spectral type. The variation of the cross-correlated velocities of both stars is only 3 km s^{-1} (the error of each measurement is ±1.5 km s^{-1}), and is not likely due to a companion (Barnbaum 1992b).

Hα absorption has been reported in a number of carbon-rich stars in the Galactic bulge, although these stars are thought to be too faint to be on the AGB (Tyson & Rich 1991). A possible mechanism to populate the $n = 2$ level would be the presence of a chromosphere. Eaton et al. (1985) successfully observed with *IUE* a number of R carbon stars, including UV Cam, and attributed the Mg II emission and ultraviolet flux to chromospheres. However, these chromospheres appear weaker than those of other late-type giants (such as K and M giants). Of the eight R carbon stars in our sample, only two have Hα absorption. Johnson et al. (1986) and Johnson & Luttermoser (1987) found evidence for chromospheres in a few N carbon stars (presumably cooler than the R stars). Four of these stars, BL Ori, U Hya, UU Aur, and TX Psc, are contained in our sample, and none shows Hα in absorption or emission. The cause of the Hα absorption lines in UV Cam and FO Ser remains uncertain, although a chromospheric origin is possible.

Mg I (5183.61 Å) presents an inverse P-Cygni profile in 13 of the 34 Hα emission stars in the sample and appears to be well correlated with the strength of Hα. Two of the 34 emission line stars show K I (7698.96 Å) as a P-Cygni profile (R For and CL Mon); neither of these has any observable Mg I emission. In R For, K I and Hα emission do not appear to reach maximum strength at the same time, but only two observations are not enough to be certain. The Mg I and K I profiles are displayed in Figure 3, along with concurrent Hα emission profiles over two phases, for V CrB and R For.

Finally, the spectra of some Miras show a doubling of various molecular and atomic absorption features. Notably, K I is doubled in many stars of the sample near maximum light, and a few show significant broadening of the K I line near minimum light (e.g., RZ Peg). The velocity variation of K I is significant. As shown in this atlas, the position of K I frequently differs from the velocities of other atomic and molecular lines. When K I is doubled, the velocity of the red absorption component is often closer to the center-of-mass velocity (as is the case for RZ Peg and V Oph shown in this atlas), but sometimes it is the blue component. A discussion of the structure and possible origin of this line appears in Barnbaum (1992b). There is also a suggestion of splitting of Na D lines and/or emission, but Na D emission from San Jose, near Lick Observatory, makes even a qualitative analysis of the profile unreliable. In a few Miras, not only does the K I line double, but many features of the spectral region, particularly redward of 6000 Å, appear to double as well. In these cases, the cross-correlation function (from cross-correlating spectra with a template) is doubled-peaked, or strongly asymmetric. Figure 4 shows an example of this spectral doubling in AZ Aur. Phillips & Freedman (1969) noticed a possible doubling of absorption lines near 6200 Å in R Lep. Our two observations of R Lep are, unfortunately, both near minimum light when splitting would not be expected.

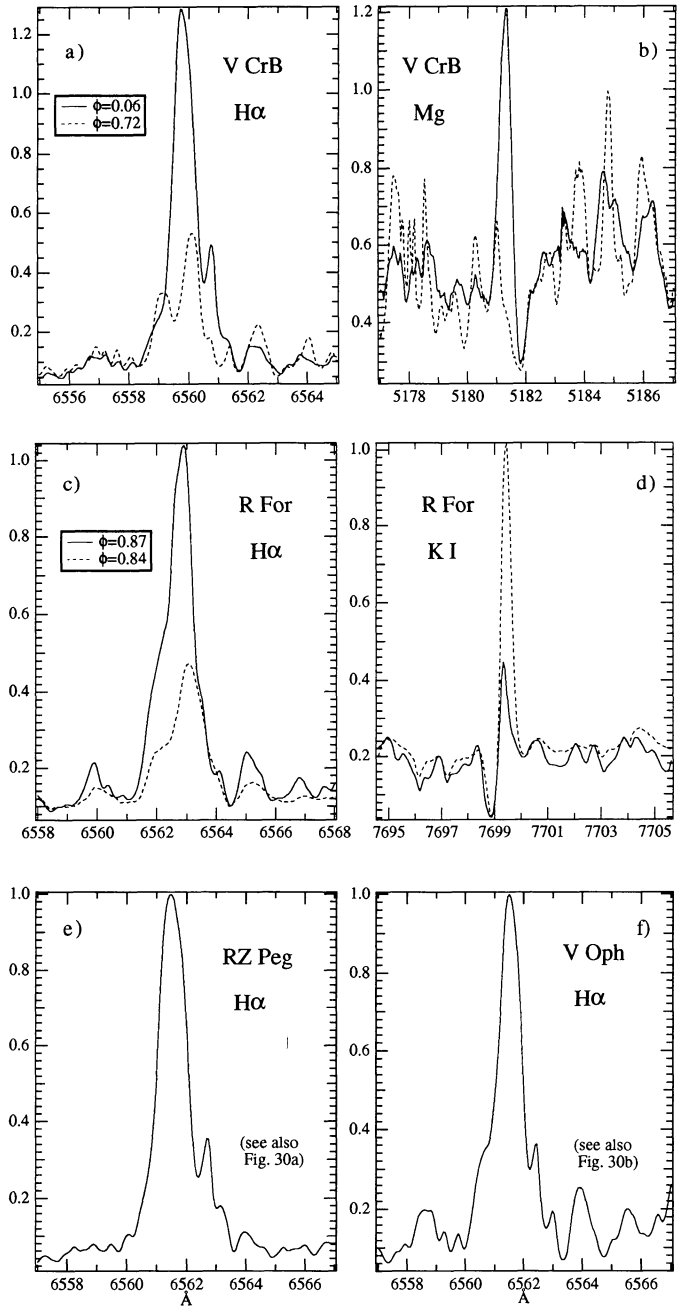

FIG. 3.—Samples of variations in emission line spectra. The spectra were each normalized to the strength of a nearby absorption feature. (*a, b*) Hα emission and Mg I inverse P-Cygni profile of V CrB at $\phi = 0.06$ and $\phi = 0.72$. (*c, d*) Hα emission and K I P-Cygni profile of R For at $\phi = 0.87$ and $\phi = 0.84$. While the phase and period for V CrB are from the AAVSO, that of R For is from Kholopov (1985) and might not be accurate. (*e, f*) These spectra of RZ Peg and V Oph show the Hα emission profiles that are truncated in Figs. 30*a* and 30*b*.

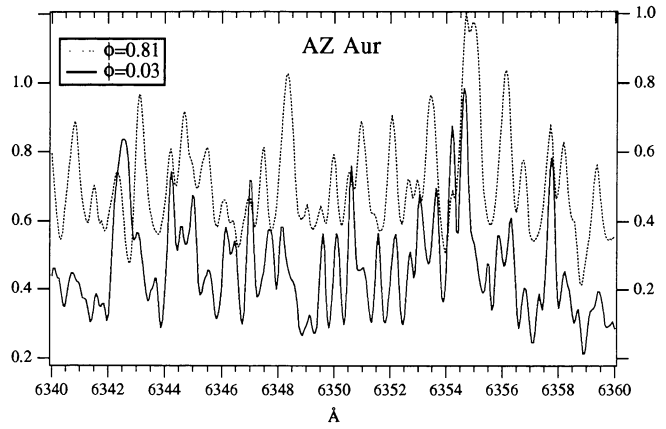

FIG. 4.—Example of molecular line doubling in AZ Aur. At phase ϕ = 0.81 the absorption lines are single, and the cross-correlation function (not shown), resulting from cross-correlation with a template, is single peaked. At ϕ = 0.03, many features appear to double, and the cross-correlation function (not shown) is double peaked. Each spectrum was normalized to the same feature. The relative intensity for ϕ = 0.03 is indicated on the left and for ϕ = 0.81 on the right.

3.2.3. *Identifications of Atomic Lines*

Fujita (1952) and Fujita & Yamashita (1963) listed atomic features identified in U Cyg (at 20 Å mm^{-1}) and Y CVn (at 4 to 8 Å mm^{-1}), respectively, and Wallerstein (1989) identified a number of lines in the spectrum of RZ Peg (at 7 Å mm^{-1}). We started with these identifications, looking for atomic features corresponding to the rest wavelengths of U Hya. Some features are weak in U Hya but appear stronger in the other stars; these have been included in the list of identifications. All elements identified and the number of transitions for each appear in Table 6, and Table 7 lists each transition and wavelength separately. Note that Table 7 should be considered a list of possible lines, not all firm identifications, since interference by molecular features make the presence of only the strongest atomic lines irrefutable. Of the 1056 atomic lines found by Fujita and Yamashita within the wavelength region of the present study, only 320 of these matched features in the spectrum of U Hya or in other stars in this atlas. Given that the dispersion in the spectra of Fujita and Yamashita is a factor of 2 lower than ours, it is reasonable to suspect that many of their identifications are severely blended with molecular lines and are not reliable.

4. THE ATLAS FIGURES

4.1. *The Stellar Spectra*

The purpose of this atlas is to present a tool for comparing and identifying atomic and CN features in the optical spectra of carbon stars, as well as to advertise the carbon star ADS database. With this in mind, we have prepared stellar spectra, as well as atomic and molecular line templates with precisely the same scale, for easy use.

The six stars presented here were chosen both as a representative sample and as a demonstration of pecularities. Although complicated in appearance optical spectra of carbon stars are very similar. Line ratios sometimes vary significantly from star to star, but nearly every absorption dip in the high signal-to-noise spectra is reproduced in the spectrum of every star. This property is clearly demonstrated in the spectra of the six carbon stars chosen for this atlas. SR, M, and Lb variables are represented here, as well as J-types and one CS star. These stars span a range of temperature and carbon abundance. Spectral classification of the six stars, period, phase (where available), date of each observation, and heliocentric velocities are listed in Table 8. The velocities are the result of cross-correlation of 25 to 30 orders with a template; the procedure is described in Barnbaum (1992b) where velocities for this entire sample of carbon stars are listed.

All stellar spectra in this atlas as well as in the ADS database are corrected to heliocentric motion. Figures 5–44 display the spectra, one order per figure, with U Hya, TX Psc, and RZ Peg in part (*a*), and V Oph, Y CVn, and UV Cam in part (*b*) of each figure. The *y*-axis units are data numbers (*DN*) where one *DN* represents 2.5 electrons. Since the readout noise is small (~7 electrons), the signal-to-noise goes as 2.5 × $\sqrt{DN}$. The *x*-axis is in angstroms, and the number of angstroms per spectrum is exactly the same for each plot of a given order, and is given in the eighth column of Table 3. This will allow perfect alignment for overlaying spectra of interest with any of the six stars.

On the left-hand side of each spectrum is a solid, half-height, vertical line which represents the zero-velocity shift of the spectrum (referred to as the "zero-velocity axis"), with respect to the wavelength range chosen for the atomic and CN plots (see below). The zero-velocity axis serves as a fiducial for all the plots in the atlas. That is, if spectra of the same order are aligned so that their zero-velocity axes coincide, their absorption features will align. When the vertical line seems absent, it is because the zero-velocity axis coincides with the *y*-axis of that spectrum (especially for the spectra of UV Cam), except in Figures 34 and 42 where no zero-velocity axis is indicated, since the domination of telluric features makes velocity difficult, if not impossible, to determine. Note that the placement of this zero-velocity axis varies from star to star due to differ-

TABLE 6

ELEMENTS IDENTIFIED

Element	Number of Lines	Element	Number of Lines
Ba	5	Na	4
Ba II	2	Nb	3
Ca	13	Nd	2
Ce	2	Nd II	13
Ce II	1	Ni	6
Co	23	Pr II	7
Cr	41	Rb	1
Fe	105	Sc	23
Gd	10	Sc II	9
Gd II	10	Sm	1
K	1	Sr	4
La	3	Ti	75
La II	13	V	36
Li	1	V II	6
Mg	1	Y	12
Mn	8	Y II	4
Mo	2	Zr	30

TABLE 7

LIST OF ATOMIC LINES IDENTIFIED IN U HYDRAE

Element	λ_0	Multiplet	Element	λ_0	Multiplet	Element	λ_0	Multiplet
Fe	5110.41	1	Fe	5324.18	553	Co	5558.83	166
Ti[a]	5147.48	4	V II	5325.71	54	V	5561.66	77
Ti[a]	5152.20	4	Fe	5328.05	15	Fe	5586.76	686
Gd II	5178.84	147	Fe	5328.53	37	Ca	5588.75	21
Mg	5183.62	2	Cr	5329.12	94	V	5592.42	37
Ca	5188.85	45	Co[a]	5331.47	39	Ca[a]	5594.45	21
Nd II[a]	5191.45	24	Fe	5332.90	36	Ca	5598.49	21
Fe	5191.47	383	Sc II	5334.23	30	Nd II	5603.65	45
Fe	5192.36	383	Mn	5334.80	36	V	5604.95	37
Nd II	5192.62	75	Ti	5338.33	35	Y II	5610.36	19
Ti	5192.98	4	Fe	5339.94	553	Nd II	5614.30	87
Fe	5194.95	36	Sc	5342.05	30	Gd II	5616.20	61
Cr	5200.19	201	Sc	5342.96	4	Fe	5617.22	626
Y II	5200.41	20	Gd	5343.02	7	Gd	5617.91	3
Fe	5202.34	66	Cr	5345.81	18	Nd	5639.54	...
Y II	5205.72	20	Cr	5348.32	18	Fe	5649.66	838
Cr[a]	5206.04	7	Ca	5349.47	33	Co	5651.73	56
Cr	5207.04	...	V II	5350.38	54	V	5656.90	127
Cr	5208.44	7	Gd	5350.41	7	Fe	5658.67	1087
Ti	5210.39	4	Ti	5351.08	300	Ti	5662.91	269
Fe	5225.53	1	Sc	5355.75	19	Zr	5664.51	47
Fe	5226.88	383	Sc	5356.10	17	V	5668.36	37
Cr	5226.89	37	Ti	5376.59	3	Nd II	5668.87	84
Fe	5227.19	114	Fe	5379.58	928	V	5670.85	36
Cr	5227.75	58	Ti	5384.63	35	Sc	5671.81	12
Fe	5228.41	1091	Zr	5385.14	26	Ti	5675.44	249
Nd II	5228.43	46	Ti	5389.18	35	Gd	5696.22	3
Fe	5229.87	553	Sc	5392.08	19	Sm II	5696.24	...
Co	5230.22	39	Mn	5394.67	1	V	5698.52	35
Cr	5230.23	58	Ti	5396.60	3	Sc	5700.14	12
Fe	5232.94	383	Fe	5404.15	1165	Fe	5701.56	209
Ti	5233.82	37	Fe	5405.78	15	La II	5703.33	48
Fe	5238.25	962	Ni	5424.65	70	V	5703.56	35
Ti	5238.58	...	Ti	5426.26	3	Nd II	5706.21	86
Cr	5238.97	59	Fe	5429.70	15	V	5706.98	35
Sc II	5239.82	26	Nd II	5431.53	80	Cr	5712.78	119
Cr	5243.40	201	Mn	5432.55	1	Ti[a]	5715.13	228
Fe	5247.06	1	Fe	5434.53	15	Ti	5716.48	249
Cr	5247.56	18	Ti	5438.32	108	Sc	5717.25	12
Co	5247.93	39	Fe	5441.32	1144	Fe	5717.84	1107
Nd II	5249.59	75	Ti	5446.64	...	Nd II	5718.12	86
Fe	5250.21	1	Fe	5446.92	15	Ti	5720.48	249
Fe	5250.65	66	La II	5447.59	112	Sc	5724.07	12
Ti	5250.95	37	Ti	5448.90	259	V	5727.03	35
Ti	5251.49	37	Ti	5449.16	107	V	5727.66	35
Ti	5252.11	4	Sr	5450.84	9	V	5731.25	36
Gd II	5252.16	99	Fe	5452.12	870	Fe	5753.14	1107
Fe	5253.48	553	Sc	5455.21	...	Ti	5762.27	309
Fe[a]	5254.96	1	Fe	5455.61	15	Y	5765.64	...
Nd II	5255.51	43	Ti	5477.71	265	Nd	5767.33	...
Zr	5277.41	27	Fe	5478.47	1062	La II	5769.07	70
Fe	5280.36	880	Sr	5480.84	9	Ce	5773.59	...
Co[a]	5280.65	172	Mn[a]	5481.40	4,31	Ti	5774.05	309
Ti	5282.39	74	La II	5486.84	68	Fe	5775.09	1087
Gd	5283.09	6	Ti	5490.85	3	Ba	5777.67	9
Ti	5283.45	156	Fe	5491.84	1031	Fe	5778.47	209
Cr[a]	5285.63	192	Fe	5493.33	873	Mo + Mn	5780.11	...
Sc	5285.75	23	Fe	5497.52	15	Cr	5781.20	119,188
Co	5287.57	175	Fe	5501.47	15	V	5782.61	35,127
Fe	5288.38	406	Ti	5503.90	287	V	5783.50	141
Fe	5288.53	929	Fe	5506.78	15	Ti	5812.84	309
Nd II	5293.17	75	Co	5530.77	38	Fe	5814.80	1086
Sc II[a]	5295.30	22	Ce	5535.23	...	Gd II	5815.85	112
Cr	5296.69	18	Nd II	5535.27	...	Sm[a]	5816.34	...
Cr	5297.36	94	Fe	5536.59	345	V	5817.06	92
Cr	5300.75	18	Fe	5543.18	926	Ti	5823.71	239
Co	5301.06	39	V[a]	5545.93	38	Co	5826.30	169
Sc	5301.94	4	Y II	5546.01	27	V	5830.72	142
La II	5301.98	36	Ce	5556.25	...	Ti	5832.47	309
Pr II	5322.78	35	Mo	5556.28		Fe	5833.93	209
Ti	5323.96	36	V	5558.75	77	Nb	5838.15	...

TABLE 7—*Continued*

Element	λ_0	Multiplet	Element	λ_0	Multiplet	Element	λ_0	Multiplet
Nb[a]	5838.64	...	V	6093.89	...	Zr	6407.00	2
Ti	5839.78	105	Fe	6094.34	...	Fe	6411.66	816
Gd II	5840.47	112	V	6097.42	33	Sc	6413.35	1
Nd	5842.39	86	Ti	6098.57	304	Ti	6419.10	196
Cr	5844.61	119	Zr	6124.84	24	Fe	6419.98	1258
Fe	5848.09	552	Ti	6126.22	69	Fe	6421.36	111
Gd II	5871.81	79	Zr	6127.44	2	Fe	6428.80	1138
Ti	5877.73	...	Fe	6127.92	1017	Co	6429.91	81
Zr	5879.80	4	V	6128.34	33	Fe	6430.85	62
Ti	5880.31	71	Ni	6128.99	42	Y	6435.00	2
La II	5880.63	35	La II	6129.55	47	V	6438.08	...
Fe	5881.76	63	Zr	6134.55	2	Ca	6439.07	18
Zr	5885.62	2	V	6135.38	34	Ca	6471.66	18
Na D	5889.95	1	Fe	6136.62	169	Mn	6491.71	39
Na D	5895.92	1	Fe	6137.00	62	Ba II	6496.90	2
Ti	5899.32	72	Fe	6137.70	207	Ti	6497.69	102
Fe	5909.99	552	Y	6138.41	3	Fe	6498.95	13
Fe	5934.66	982	Zr	6140.46	24	Ca	6499.65	18
Zr	5935.20	2	Ba II[a]	6141.72	2	Ni	6502.21	...
La II	5936.22	19	Fe	6141.76	816	V	6504.17	48
Ti	5937.82	72	Zr	6143.20	2	Zr	6506.36	...
Ti	5940.68	2	V	6150.15	20	Ti	6508.14	102
Ti	5941.76	72	Fe	6151.63	62	Ca	6508.74	18
Fe	5943.58	63	Na	6154.23	5	Fe	6546.25	268
Fe	5949.36	14	Ca	6156.29	20	Ti	6546.28	102
Pr II	5951.27	...	Fe	6157.73	1015	Fe	6547.58	13
Gd II	5951.58	95	Na	6160.75	5	Sr	6550.26	12
Ti	5953.17	154	Ca	6162.17	3	Fe	6551.68	13
Zr	5955.35	3	Zr	6192.96	24	Ti	6554.23	102
Gd II	5956.46	59	Sc	6193.67	3	Ti	6556.07	102
Fe	5956.71	14	Sc	6210.68	2	Y	6557.39	1
Fe	5958.34	63	Zr	6213.05	24	V[a]	6558.02	59
Ce II	5959.69	...	Fe	6213.44	62	Co	6563.42	80
Ti	5965.84	154	V	6216.37	19	Cr	6564.14	...
Sc	5969.19	...	Fe	6219.28	62	V	6565.88	48
Fe	5969.55	1086	Fe	6221.36	...	Pr II	6566.77	...
Zr	5995.37	...	Fe	6221.66	13	Zr	6569.43	...
Cr	5996.64	...	Y	6222.60	2	La II	6571.96	...
Ba	5997.09	7	V	6224.26	20	Ca	6572.78	1
Fe	5997.78	1175	Ti	6258.10	104	Fe	6574.24	13
Ti	5999.66	227	Ti	6258.71	104	Zr	6576.56	...
Sc II	6001.53	20	Ti	6261.10	104	La	6578.51	1
Y	6009.19	...	La II	6262.30	33	V	6578.96	32
Ti	6011.59	...	Fe	6265.14	62	Nd II	6580.94	...
Fe	6012.21	64	V	6266.32	20	Y	6584.84	1
Mn	6013.50	27	Ti	6268.53	103	Ni[a]	6586.33	64
Mn[a]	6016.64	27	V	6268.82	20	Co	6623.76	...
Ba	6017.47	...	Fe	6270.22	342	V	6624.85	48
Ti	6018.42	198	Ni	6271.77	...	Cr	6629.06	...
Fe	6019.36	780	Ti	6273.39	1	Cr	6630.02	16
Ba	6019.47	7	V	6274.65	19	V	6632.04	...
Mn[a]	6021.80	27	Sc	6276.31	2	Co	6632.45	111
Y	6023.41	3	V	6285.17	19	V	6642.73	...
Zr	6025.36	...	Fe	6291.88	...	Ni	6643.64	43
Mo	6030.66	5	V	6292.86	19	Fe	6648.08	13
Ti	6031.68	2	Ti	6295.25	1, 144	Ti	6650.36	...
Zr	6032.61	...	Ti	6295.95	144	V	6653.43	...
Sc II	6059.25	20	Ti	6296.65	1	Pr II	6656.83	...
Zr	6062.85	3	Ti	6298.08	144	Cr	6657.54	282
Fe	6062.89	63	Cr	6330.10	6	V	6659.88	...
Ti	6064.63	69	Fe	6335.34	62	Fe	6663.45	111
Fe	6065.49	207	Ti	6336.10	103	Zr[a]	6702.12	...
V	6077.40	...	Sc	6344.83	1	Fe	6703.58	268
V	6081.44	34	Sr	6347.75	...	Fe	6705.12	1197
Fe	6082.71	64	Cr	6348.36	...	Ti	6706.29	...
Ti	6085.23	69	Zr	6357.10	2	Li	6707.74	1
Tc?	6085.22	...	Fe	6358.69	13	Li	6707.89	1
V	6087.49	33	Cr	6362.87	6	Zr	6709.61	...
V	6089.47	33	La II	6399.05	104	Fe	6710.31	34
V	6090.21	34	Fe	6400.26	13	Ca	6717.69	32
Ti	6091.18	238	Y	6401.01	...	Nb	6723.62	...
Ti	6092.50	...	Y	6402.01	2	Fe	6733.17	1195

TABLE 7—*Continued*

Element	λ_0	Multiplet	Element	λ_0	Multiplet	Element	λ_0	Multiplet
Fe	6737.96	...	La II	6952.49	18	Zr	7335.97	23
Fe	6739.54	34	La II	6954.50	1	Zr	7399.30	...
Nd II	6740.11	...	Co	7052.89	54	Y II[a]	7406.21	25
Ti	6743.12	48	Ba	7059.96	5	Ti	7417.06	...
Fe	6783.71	205	Ti	7065.15	100	Co	7417.38	89
V	6785.03	...	La II	7066.21	1	Ti	7431.98	142
Sr	6791.05	3	La	7068.36	1	Zr	7439.86	23
Y	6793.70	1	Sr	7070.10	3	Nd II	7514.40	...
Y II	6795.40	26	Gd II	7135.73	...	Ce	7539.52	...
Fe	6796.13	1007	Co	7154.71	89	K	7698.96	1
Ca	6798.48	31	Ti	7160.33	98	Ni	7714.32	62
Fe	6800.87	...	Ti	7213.35	143	Y	7724.08	...
Fe	6804.00	1174	Zr	7318.08	...	Rb	7800.23	1
V	6812.37	31	Ti	7330.97	143	Sc	7821.64	...
Co	6814.94	54	Ti	7332.26	143	Gd	7846.35	...
Ti	6818.14	...	La	7334.17	...	Zr	7849.35	40

NOTE.—The multiplet numbers are taken from Moore 1972.

[a] Indicates that there is a possible blend, listed here:

Pr II	5147.48	...	V II	5280.62	55	Co	5545.94	191	Fe	6016.66	738
Fe	5151.92	16	Fe	5285.60	961	Nd II	5594.43	79	Fe	6021.82	63,1079
Co	5152.23	7	Mn II	5295.29	11	Fe	5614.29	1314	Fe	6141.73	816
Cr II	5191.46	24	Fe	5295.32	1146	Fe	5715.11	1061	Sc	6558.05	24
Ti	5206.06	276	Fe	5331.48	210	Fe	5816.36	1179	Gd	6702.12	130
Cr	5254.92	201	Ti	5481.43	265	Cr	5838.66	119	Co	7406.23	164

ences both in the instrumental set-up and in corrections for heliocentric motion of each star. In order to display the broadest wavelength coverage for each star in each order, the beginning wavelength for plots within a given order is not the same, although each spectrum of a given order is plotted with exactly the same number of angstroms, for easy comparison.

4.2. *Molecular and Atomic Line Plots*

The atomic lines identified are indicated in the spectra of U Hya. In addition, they are plotted separately in Figures 45 through 52, which can be used as templates for line identification in other spectra. Table 7 lists each of these features and the corresponding wavelengths. The CN transitions (from Davis & Phillips 1963) and the C_2 transitions (from Phillips & Davis 1968) are plotted separately on the spectra of TX Psc (Figs. 5 through 44*a*). Figures 53–60 and Figures 61–65 display the line locations of CN and C_2, respectively, as templates. All occurring transitions are shown together on the bottom of each plot, as displayed on the spectra of TX Psc, and then each separate vibrational transition is shown above, with the specific vibrational transition labeled on the left-hand side. This arrangement allows separation and identification of vibrational transitions when these templates are compared with the stellar spectra, and the specific rotational branch can be easily found in Davis & Phillips (1963) and Phillips & Davis (1968).

The zero-velocity axis is also useful when comparing spectra with the separate template plots of atomic lines or molecular transitions. Aligning the zero-velocity axis of a stellar spectrum with the *y*-axis of the corresponding atomic or molecular plot brings the stellar absorption features to rest velocity. If the wavelength tick marks of a spectrum and template are positioned to coincide, any shift in wavelength of the atomic lines to the stellar features indicates the heliocentric stellar velocity.

TABLE 8

PROPERTIES OF THE SIX CARBON STARS IN THIS ATLAS

Star	Spectral Type		Variability	Period (day)	Phase	Date of the Observation: Local	Date of the Observation: JD (+2,400,000)	Velocity[a] (km s^{-1})	$T_{\rm eff}$ (K)
U Hya	N2	C6,5	SRb	450	0.47	1989 Dec 10	47871.0	−25.7	2825[c]
TX Psc	N0	C7,2	Lb	...	...	1989 Jul 16	47724.0	9.6	3030[c]
RZ Peg	CSe[b]	C9,1e	M	439.4	0.04	1989 Dec 11	47871.6	−23.3	3100[d]
V Oph	N3e	C5,2e	M	298	0.82	1989 Jul 16	47723.7	−37.3	...
Y CVn	N3	C5,4J	SRb	157	...	1990 Dec 9	48235.0	12.0	2730[c]
UV Cam	R8	C5,3J	SRb	294	...	1990 Sep 6	48141.0	−13.6	...

[a] Heliocentric velocity from cross-correlation with a template as described in Barnbaum 1992b, ±1.5 km s^{-1}.

[b] Keenan & Boeshaar 1980 classify RZ Peg as SC 6,9e.

[c] Lambert et al. 1986.

[d] Dominy et al. 1986.

5. SUMMARY

We present high-resolution, high signal-to-noise optical spectra of six carbon stars (U Hya, TX Psc, RZ Peg, V Oph, Y CVn, and UV Cam) over 40 spectral orders. The spectra contrast Mira, SR, and Lb variables, as well as a variety of spectral types. These spectra are a sample of the 87 carbon stars we have observed from 1988 through 1991; 67 of the 87 stars have two or more observations, with a total of 228 observations in all. Approximately 9200 individual spectra will be available to the scientific community in an on-line database, archived with ADS. A number of atomic features have been identified in the spectra of U Hya, and we have plotted the Red System of CN and Swan Bands of C_2, with velocity corrections, on the spectral plots of TX Psc. Templates of atomic and molecular features are given as separate plots, to be used as a tool for identifying features in the spectra of other carbon stars.

Sincere thanks go to D. Popper for many fruitful discussions concerning the intricacies of echelle reduction. Helpful suggestions for various aspects of this atlas were made by I. Little-Marenin, H. R. Johnson, G. Wallerstein, and D. Luttermoser. Thanks are also due to J. Phillips who provided the on-line CN wavelengths. Thank you, M. Morris, J. E. Pitesky, and H. Spinrad for reading the manuscript and looking at the endless figures. I am most grateful for R. F. Wing's review and advice which improved the quality of the presentation, and for the support provided by W. J. Welch and NSF. This project was funded by AST-8714721.

This work is dedicated to the memory of Leon E. Salanave, astronomer, teacher, and friend.

REFERENCES

Aaronson, M. 1983, ApJ, 266, L11
Aaronson, M., & Olszewski, E. W. 1987, AJ, 94, 657
Alksne, Z. K., & Ikaunieks, Ya. Ya. 1981, in Carbon Stars, ed. J. H. Baumert (Tucson: Pachart Publishing House), 20
Barnbaum, C. 1992a, ApJ, 385, 694
———. 1992b, AJ, 104, 1585
Barnbaum, C., Likkel, L., Kastner, J., & Morris, M. 1991, A&A, 251, 79
Barnbaum, C., & Morris, M. 1993, in Mass Loss on the AGB and Beyond, ed. H. Schwarz (CTIO/ESO workshop), 20
Boothroyd, A. I., & Sackman, I. J. 1988, ApJ, 328, 671
Claussen, M. J., Kleinmann, S. G., Joyce, R. R., & Jura, M. 1987, ApJS, 65, 385
Davis, S. P., & Phillips, J. G. 1963, The Red System of the CN Molecule (Berkeley: Univ. California Press)
Dean, C. A. 1976, AJ, 81, 364
Dominy, J. F., Wallerstein, G., & Suntzeff, N. B. 1986, ApJ, 300, 325
Eaton, J. A., Johnson, H. R., O'Brien, G. T., & Baumert, J. H. 1985, ApJ, 290, 276
Fujita, Y. 1952, ApJ, 116, 46
Fujita, Y. & Yamashita, Y. 1960, PASJ, 12, 267
———. 1963, Publ. Dom. Astrophys. Obs. Victoria, 12, 117
Godwin, P. J., & Lynden-Bell, D. 1987, MNRAS, 229, 7P
Goodrich, R. W., & Veilleux, S. 1988, PASP, 100, 1572
Herzberg, G. 1950, Molecular Spectra and Molecular Structure Vol. I, 2d ed. (New York: Van Nostrand Co.), 193
Hill, S. J., & Willson, L. A. 1979, ApJ, 229, 1029
Hinkle, K. H. 1978, ApJ, 220, 210
Iben, I., Jr., & Renzini, A. 1983, ARA&A, 21, 271
Iben, I., Jr., & Truran, J. W. 1978, ApJ, 220, 980
Johnson, H. R., Baumert, J. H., Querci, F., & Querci, M. 1986, ApJ, 311, 960
Johnson, H. R., & Luttermoser, D. G. 1987, ApJ, 314, 329
———. 1992, ApJ, 388, 579
Joy, A. H. 1954, ApJS, 1, 39
Jura, M. 1986, AJ, 91, 539
Kastner, J. H., Forveille, T., Zuckerman, B., & Omont, A. 1993, A&A, 275, 163
Keenan, P. C., & Boeshaar, P. C. 1980, ApJS, 43, 379
Kholopov, P. N. 1985, General Catalog of Variable Stars, 4th ed. (Moscow: Nauka)
Lambert, D. L., Gustafsson, B., Eriksson, K., & Hinkle, K. H. 1986, ApJS, 62, 373
Little-Marenin, I. 1986, ApJ, 307, L15
Mateo, M., Olszewski, E., Welch, D. L., Fischer, P., & Kunkel, W. 1991, AJ, 102, 914
Mattei, J. 1990, private communication
Mendoza, V., E. E., & Johnson, H. L. 1965, ApJ, 141, 161
Merrill, P. W. 1940, Spectra of Long-Period Variable Stars, Astrophysical Monographs, ed. H. G. Gale, F. H. Seares, & O. Struve (Chicago: Univ. Chicago Press)
Moore, C. E. 1972, A Multiplet Table of Astrophysical Interest, revised ed. (Washington: NBS)
Neugebauer, G., & Leighton, R. B. 1969, Two Micron Sky Survey (NASA SP-3047)
Olofsson, H., Carlstrom, U., Eriksson, K., Gustafsson, B., & Willson, L. A. 1990, A&A, 230, L13
Olofsson, H., Eriksson, K., & Gustafsson, B. 1987, A&A, 183, L13
Oloffson, H., Eriksson, K., Gustafsson, B., & Carlstrom, U. 1993, ApJS, 87, 267
Phillips, J. G. & Davis, S. P. 1968, The Swan System of the C_2 Molecule (Berkeley: Univ. California Press)
Phillips, J. G., & Freedman, R. S. 1969, PASP, 81, 521
Reid, N., & Mould, J. 1990, ApJ, 360, 490
Sanford, R. F. 1935, ApJ, 82, 202
———. 1944, ApJ, 99, 145
———. 1950, ApJ, 111, 262
Seitzer, P., & Frogel, J. A. 1985, AJ, 90, 1796
Shane, C. D. 1920, Lick Obs. Bull., 10, 79
Tyson, N. D., & Rich, R. M. 1991, ApJ, 367, 547
Utsumi, K. 1963, PASJ, 15, 482
———. 1967, PASJ, 19, 342
Vogt, S. S. 1987, PASP, 99, 1214
Wallerstein, G. 1989, ApJS, 71, 341
Willems, F. J., & De Jong, T. 1986, ApJ, 309, L39
Willson, L. A., & Hill, S. J. 1979, ApJ, 228, 854

FIGS. 5–44.—Spectral atlas of six carbon stars, (*a*) U Hya, TX Psc, and RZ Peg, and (*b*) V Oph, Y CVn, and UV Cam. All spectra are corrected to heliocentric motion. The wavelength range displayed (i.e., total number of angstroms plotted) is the same within each order (see Table 3). Atomic absorption line velocities are plotted on the spectra of U Hya, and the CN transitions (Davis & Phillips 1963) and C_2 transitions are plotted on the spectra of TX Psc. On the left hand side of each spectrum is a solid, half-height, vertical line which represents the zero-velocity shift of the spectrum with respect to the *y*-axis of the atomic and molecular template plots (see Figs. 45–65). That is, if spectra of the same order are aligned so that their "zero-velocity axes" coincide, their absorption features will align. The zero-velocity axis serves as a fiducial for all the plots in the atlas. When the vertical line seems absent, it is because the zero-velocity axis coincides with the *y*-axis of that spectrum (especially for the spectra of UV Cam), except in Figs. 34 and 42, where the telluric features dominate. Note that where telluric features are important, spectra of a smooth continuum star (HR 2669, B9 V, $v \sin i \sim 160$ km s^{-1}) are plotted with dashed lines. In Figs. 30*a* and 30*b* the strong Hα emission lines of RZ Peg and V Oph dominate the spectra and dwarf the molecular absorption lines. Therefore, in these figures the Hα emission lines have been truncated, and the entire Hα profiles are shown, instead, in Fig. 3*e* and 3*f*.

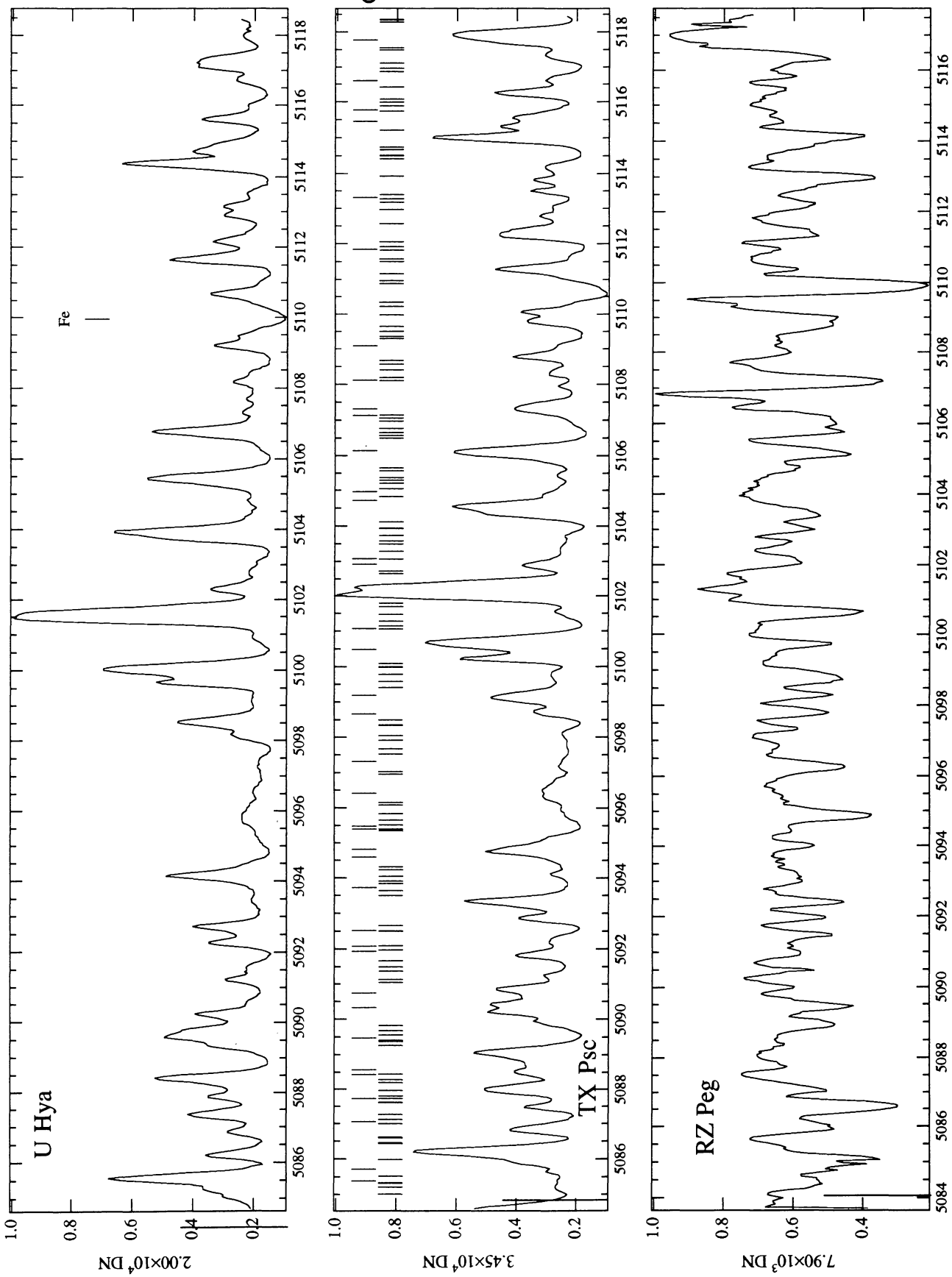

FIG. 5*a*

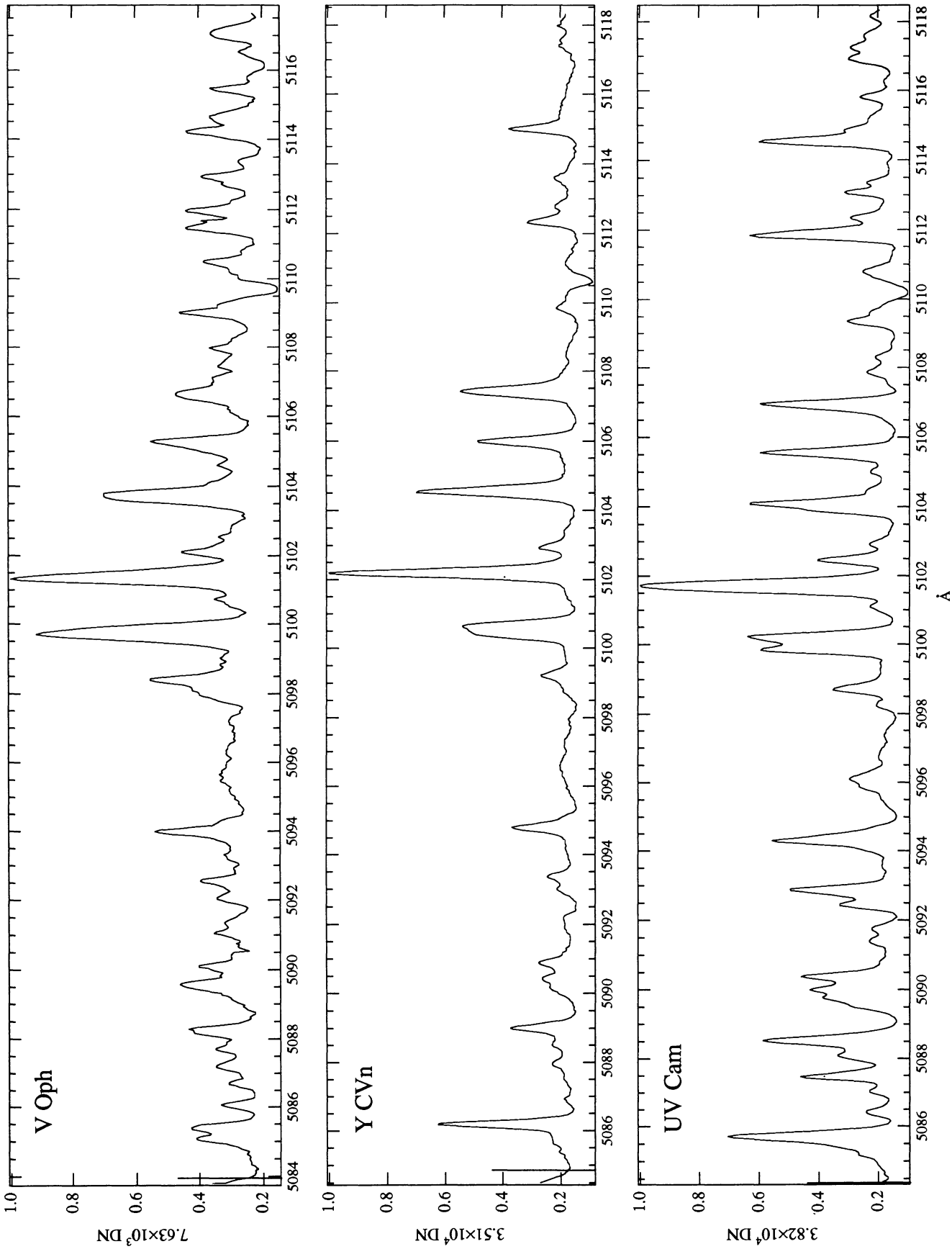

FIG. 5*b*

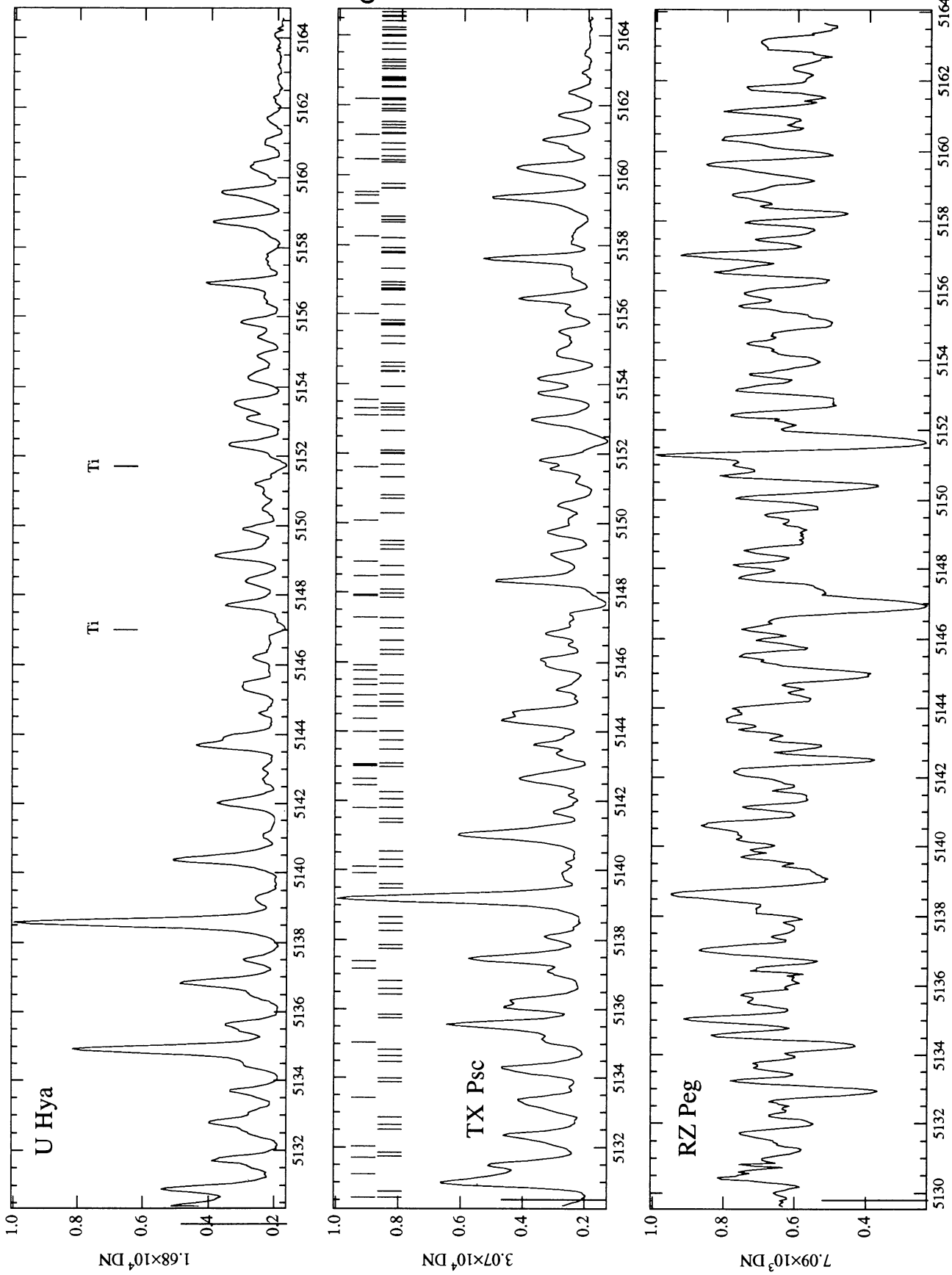

FIG. 6*a*

1994ApJS...90..317B

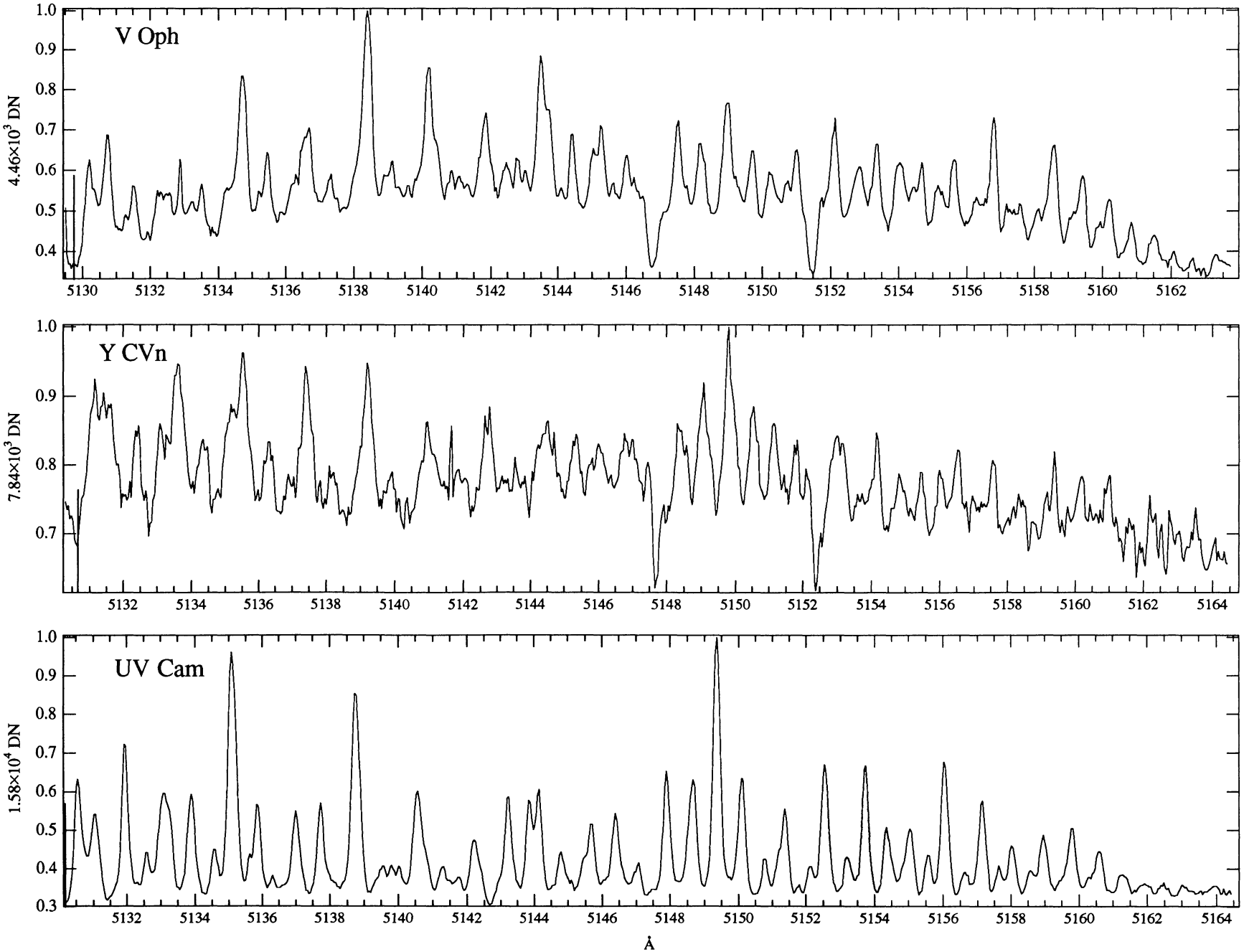

FIG. 6*b*

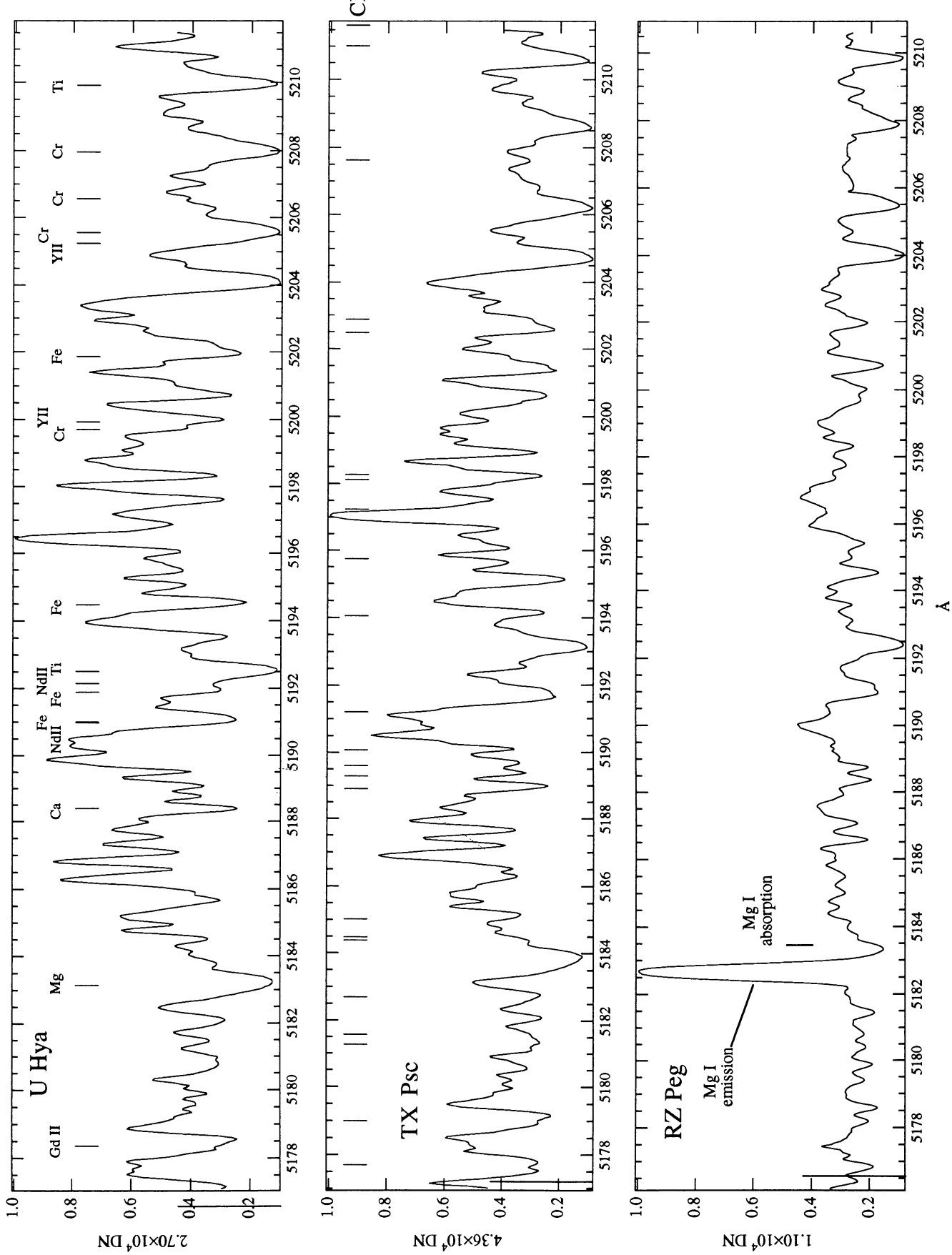

FIG. 7*a*

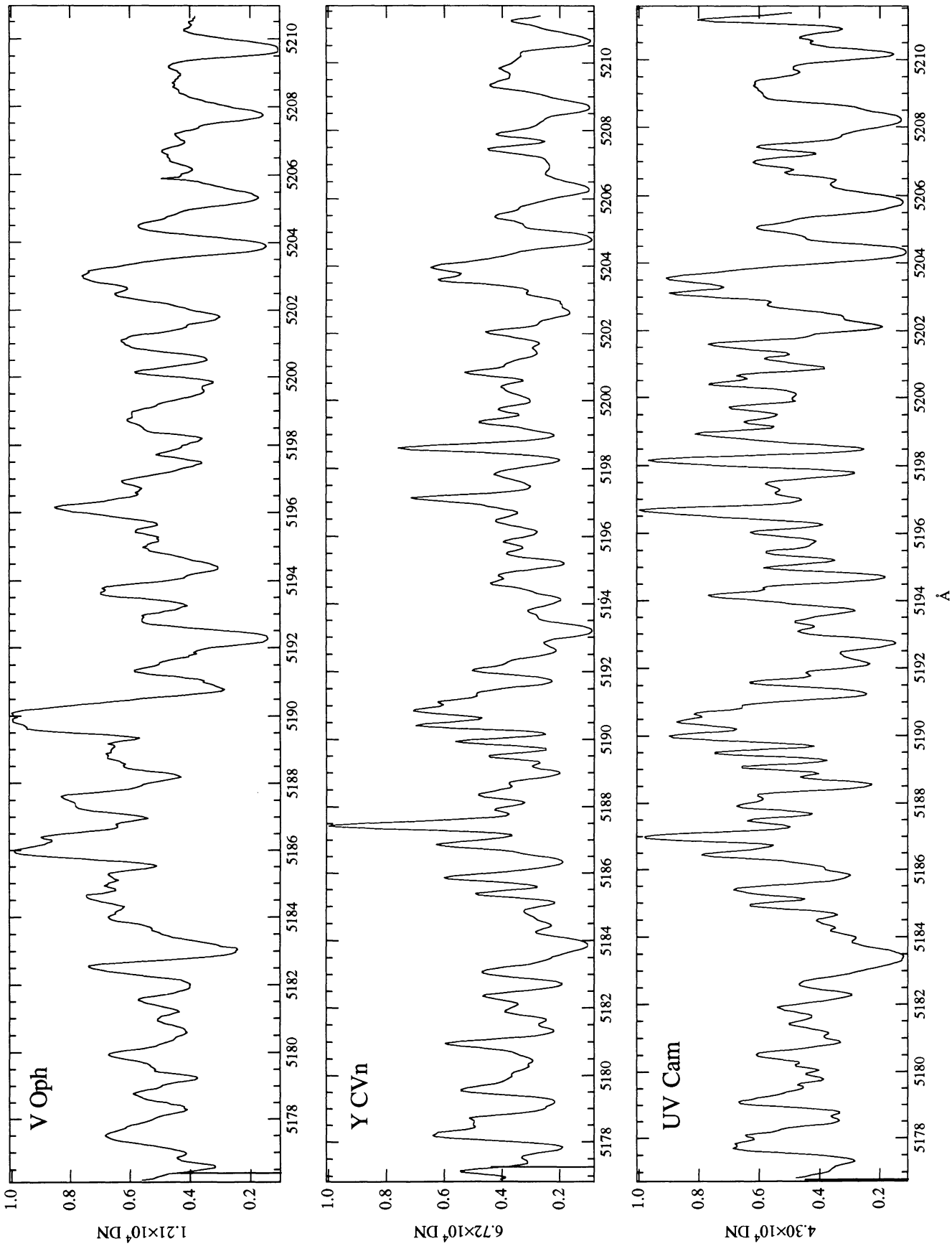

FIG. 7*b*

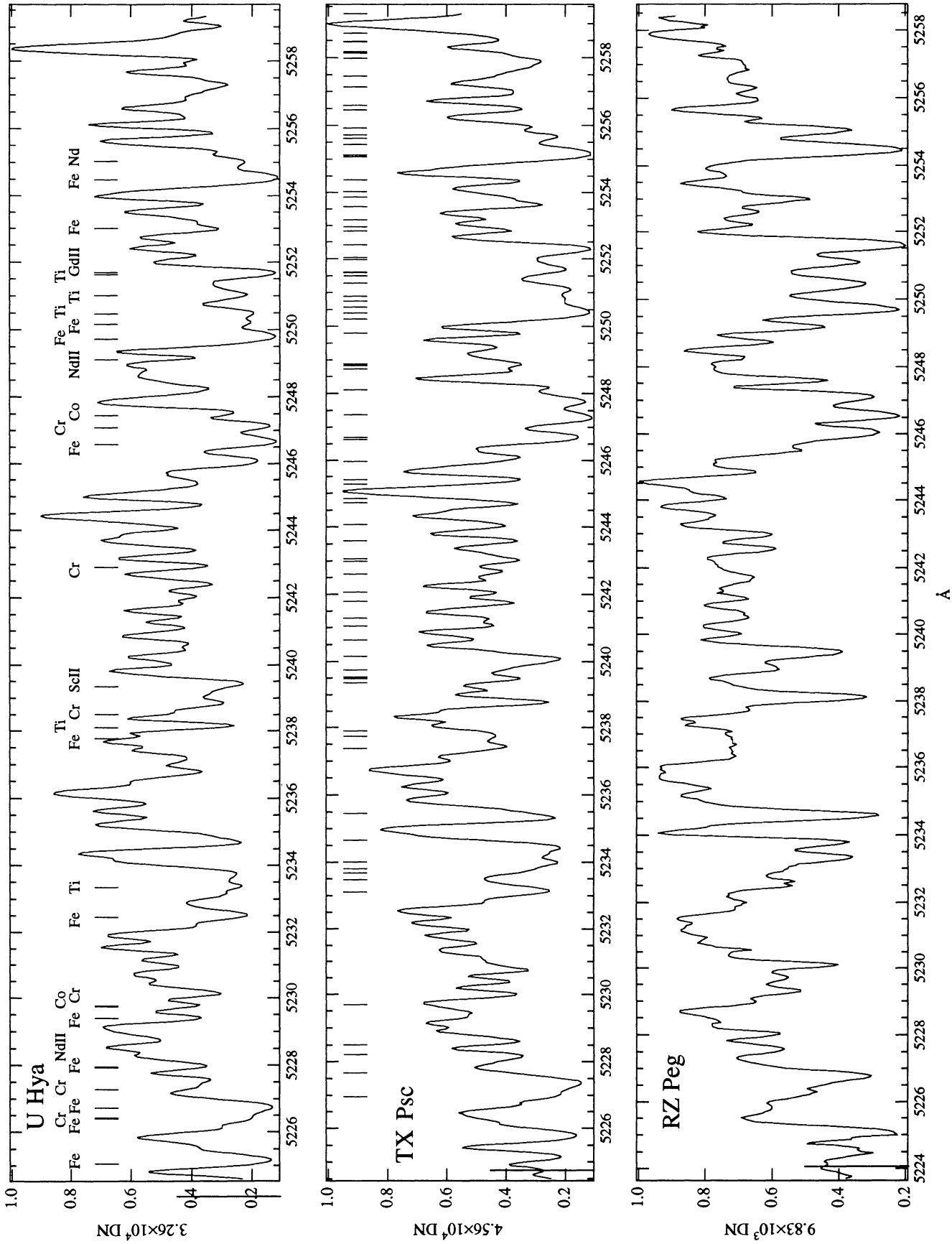

FIG. 8*a*

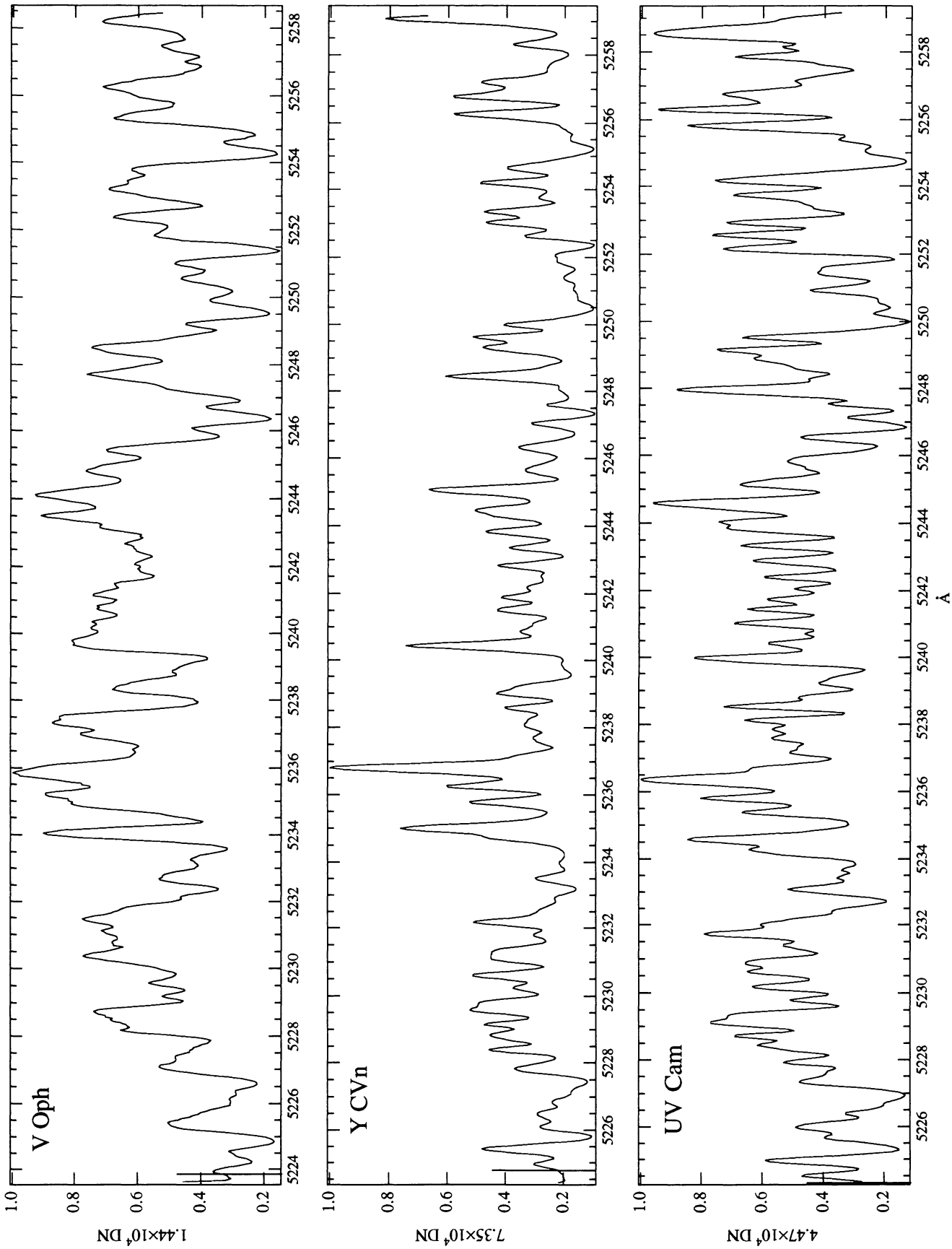

FIG. 8*b*

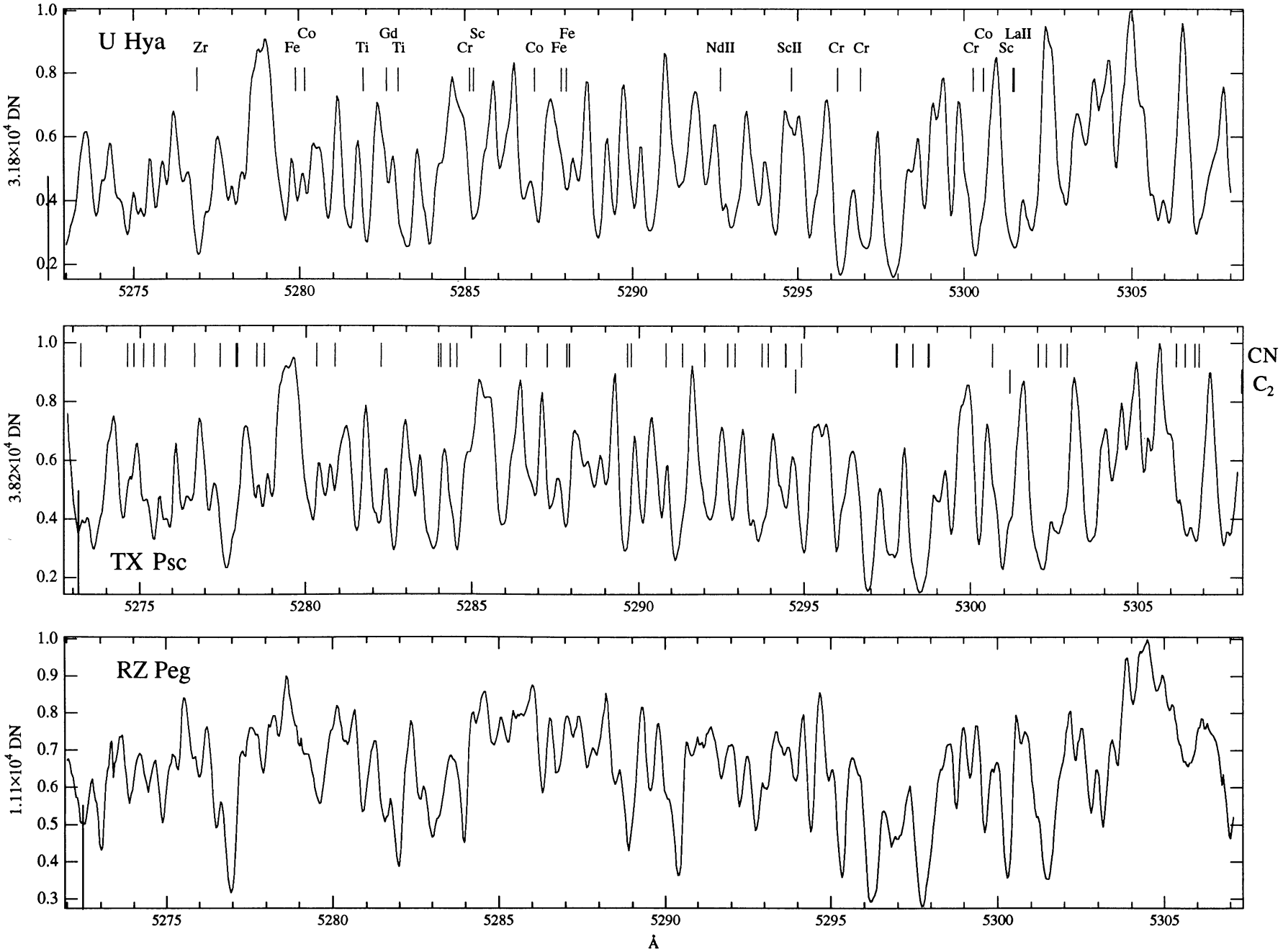

FIG. 9*a*

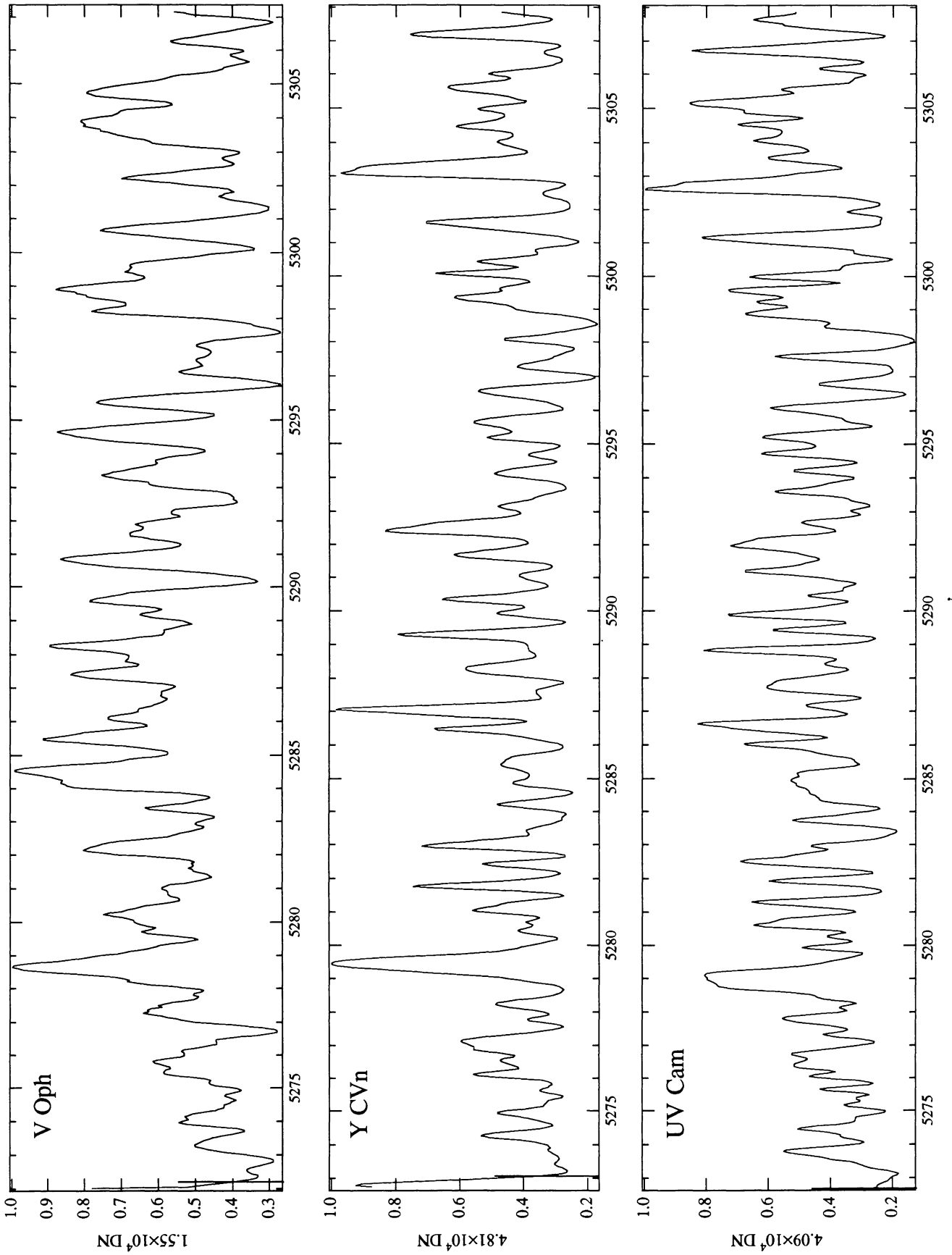

FIG. 9*b*

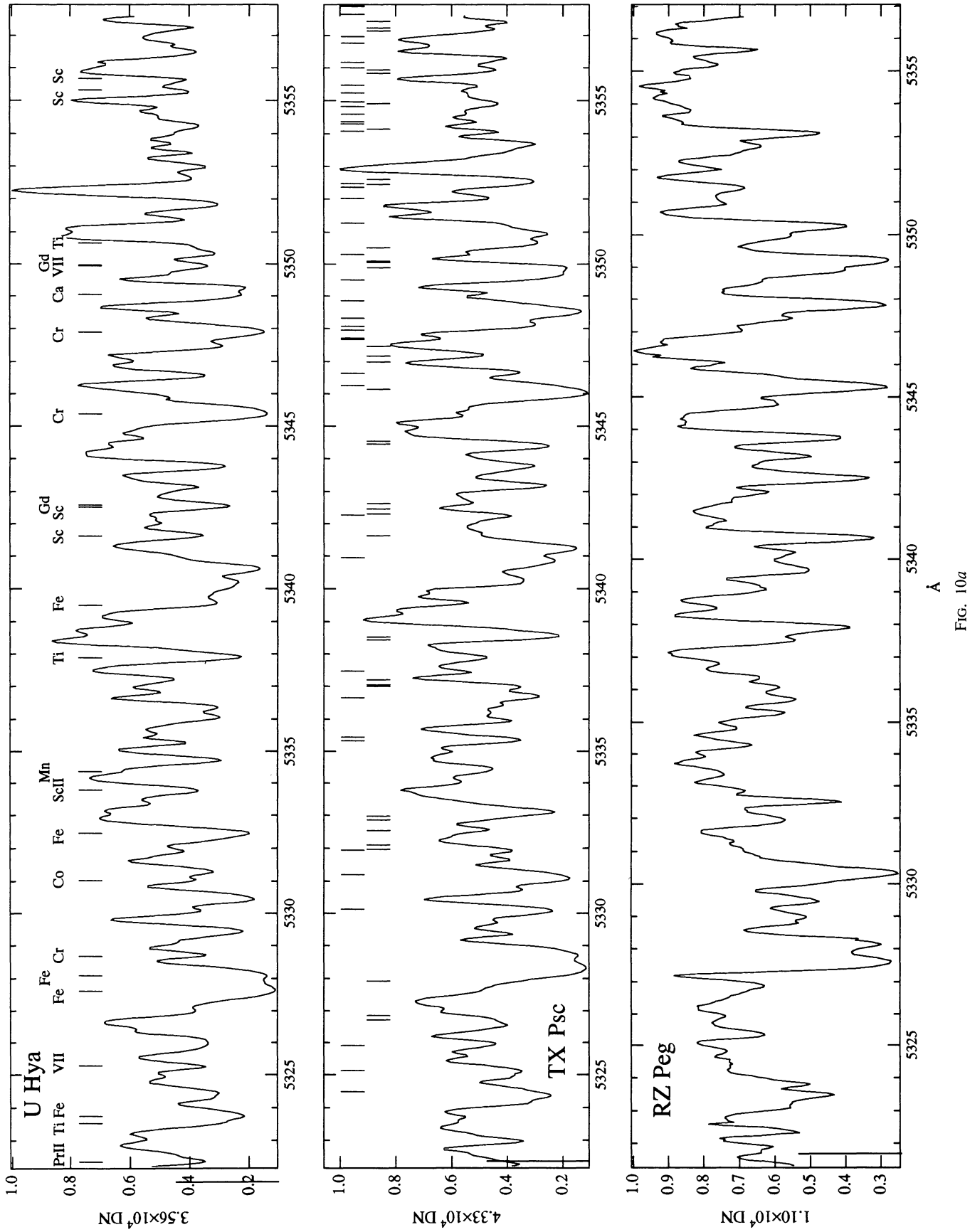

FIG. 10*a*

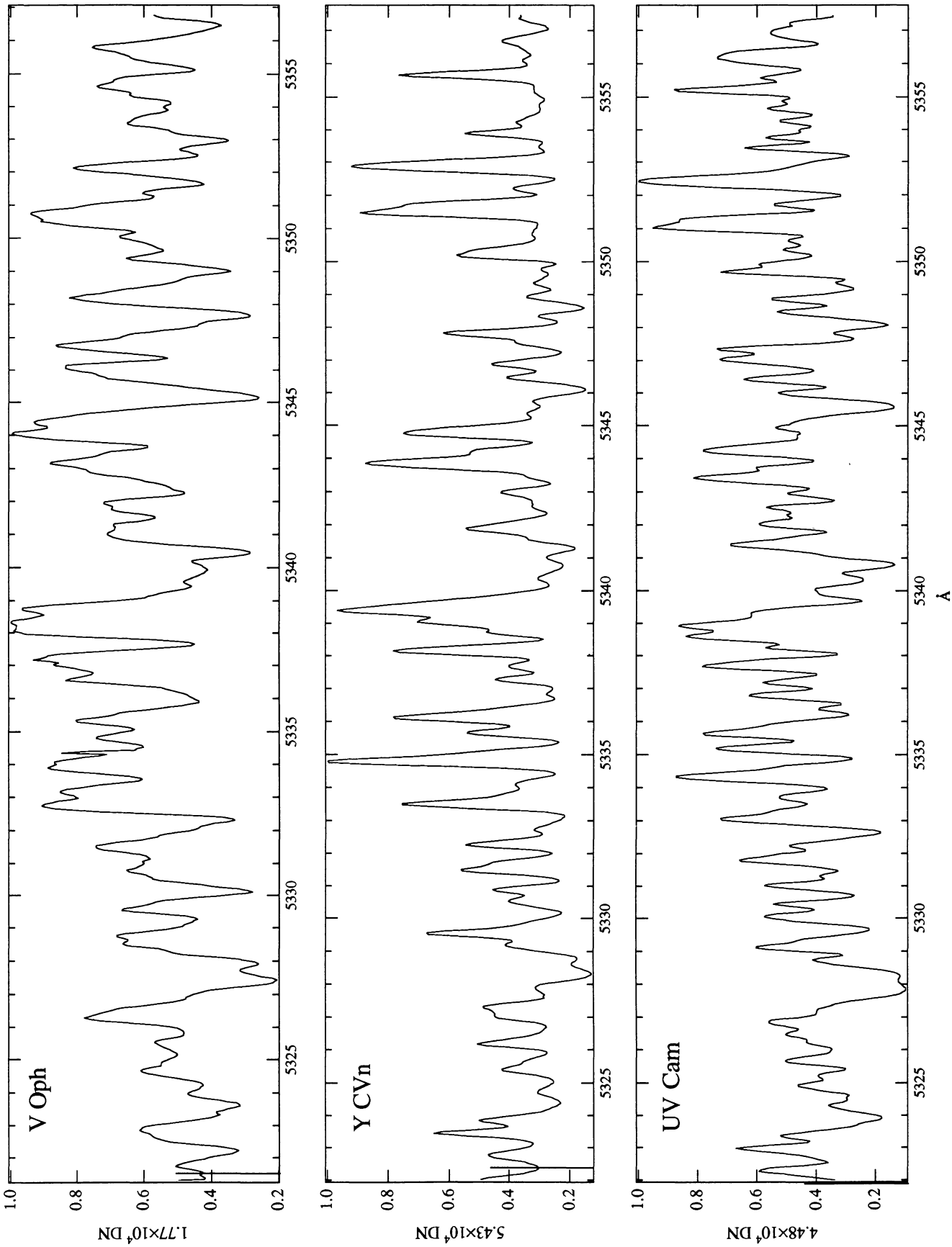

FIG. 10*b*

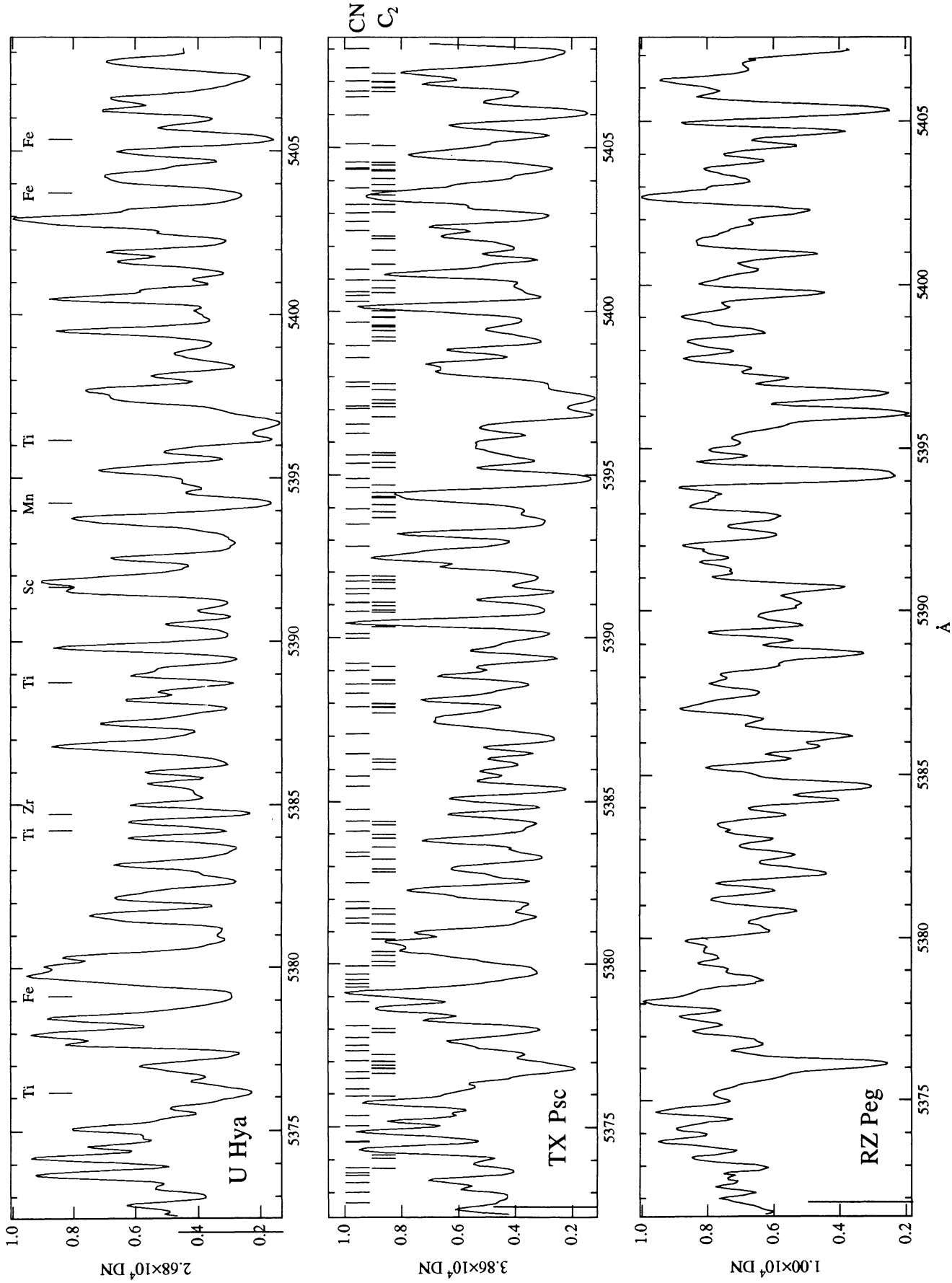

FIG. 11*a*

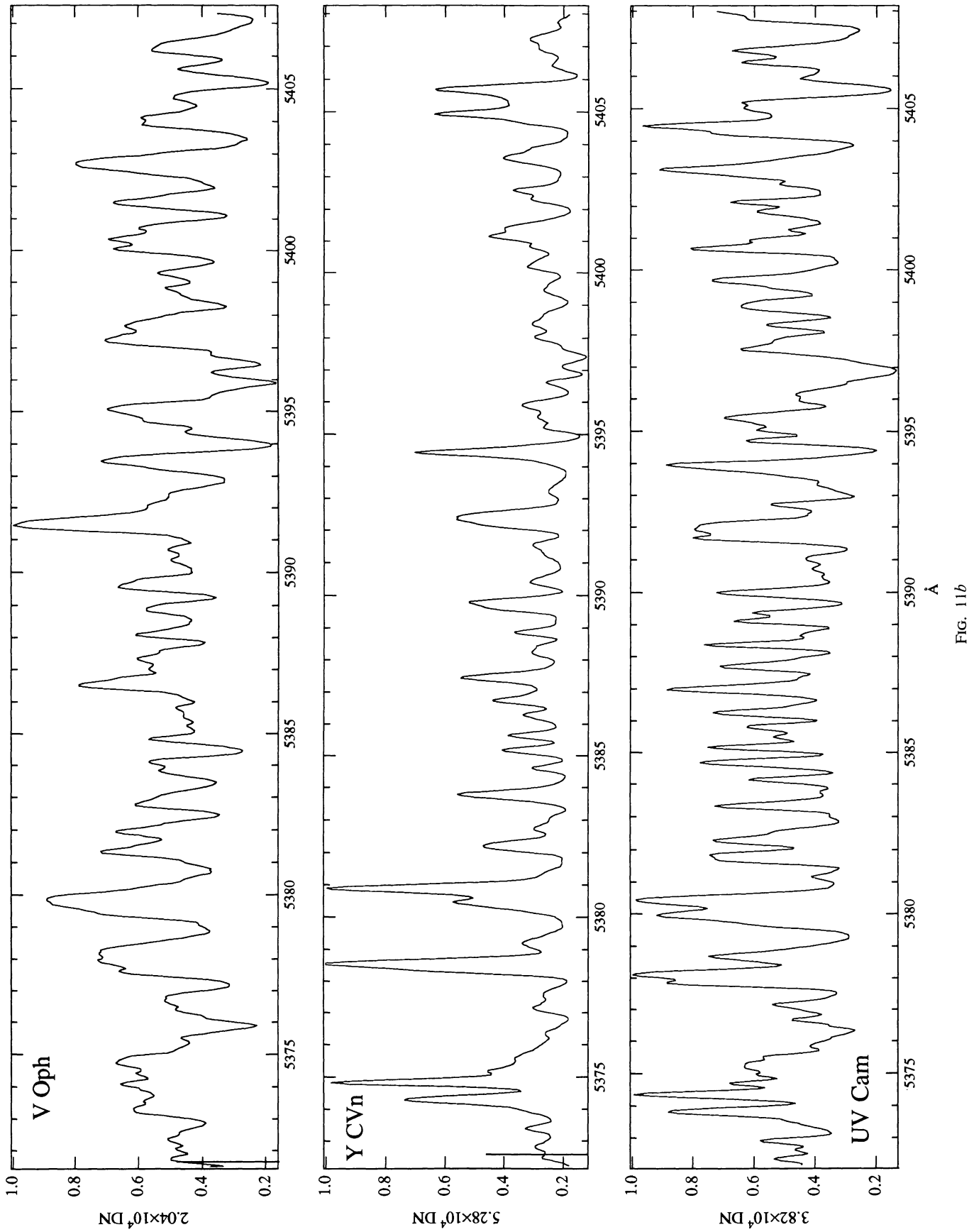

FIG. 11*b*

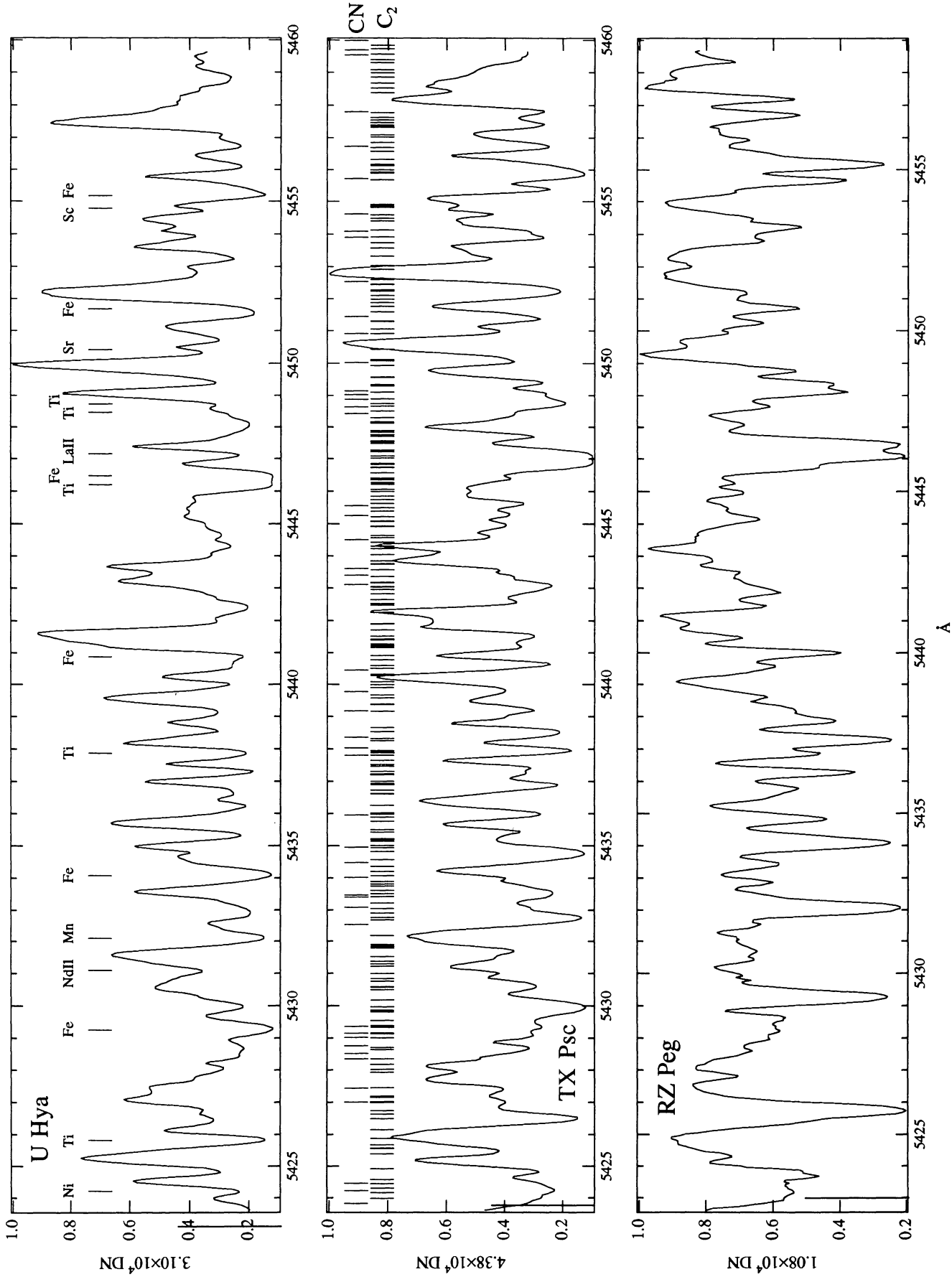

FIG. 12*a*

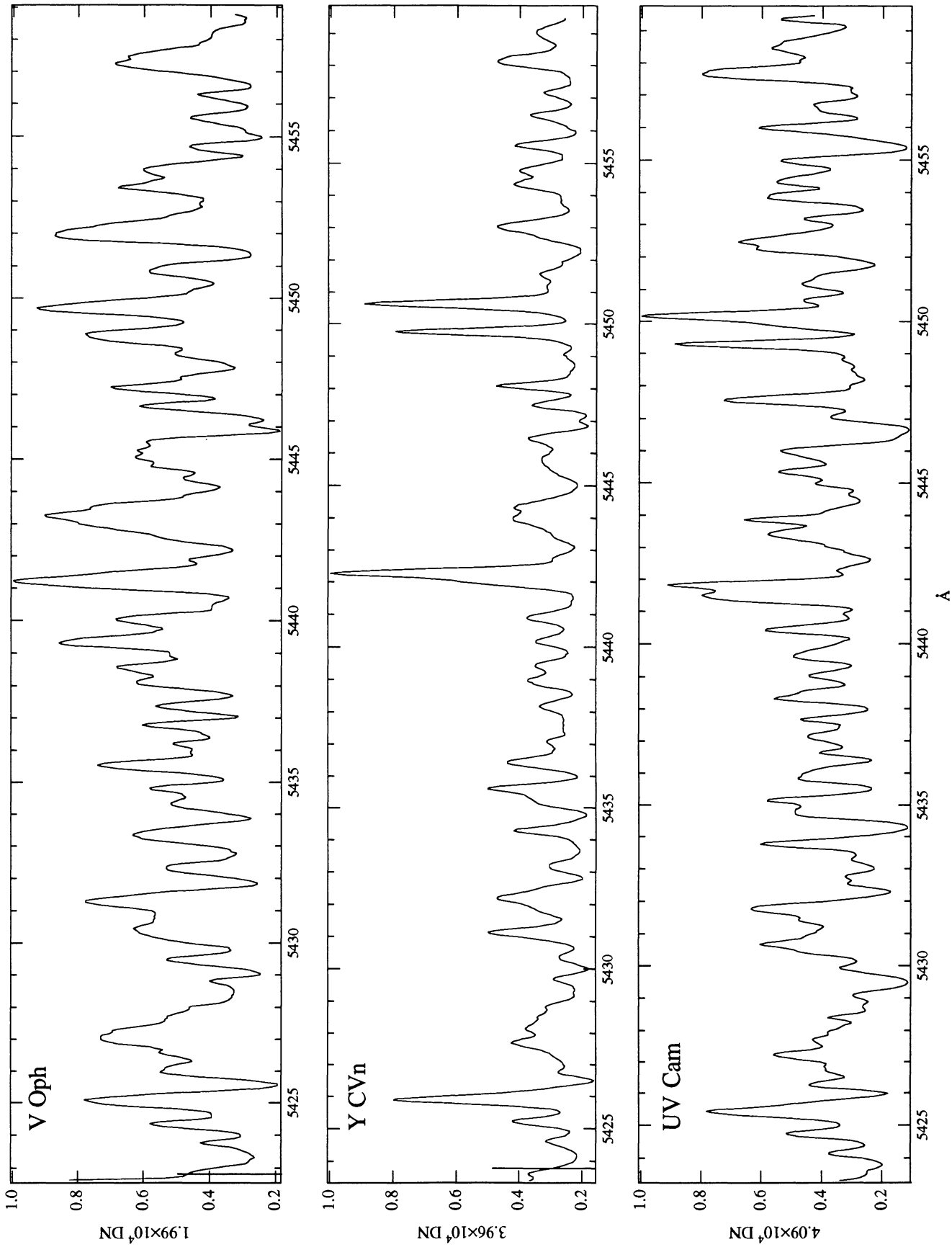

FIG. 12*b*

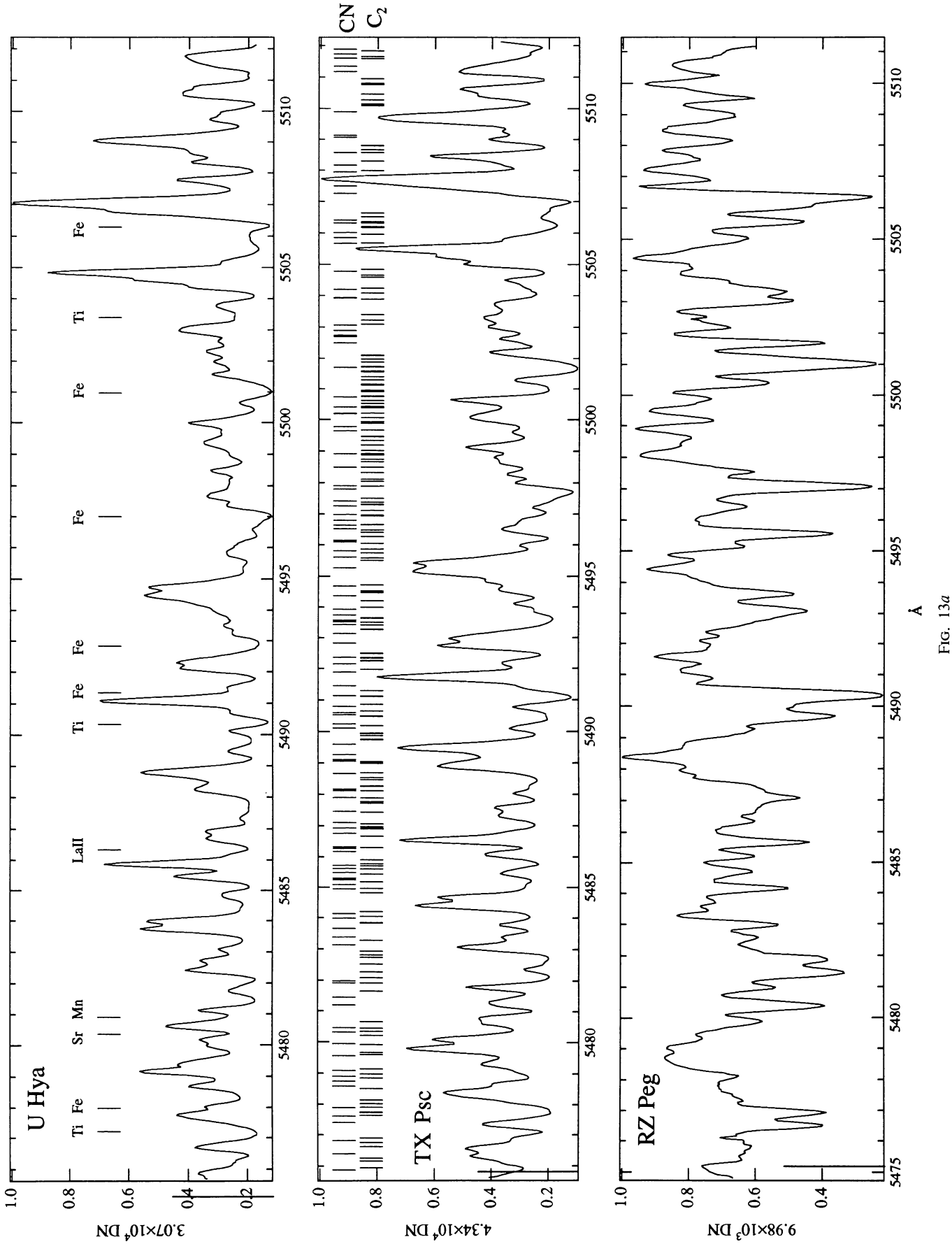

FIG. 13*a*

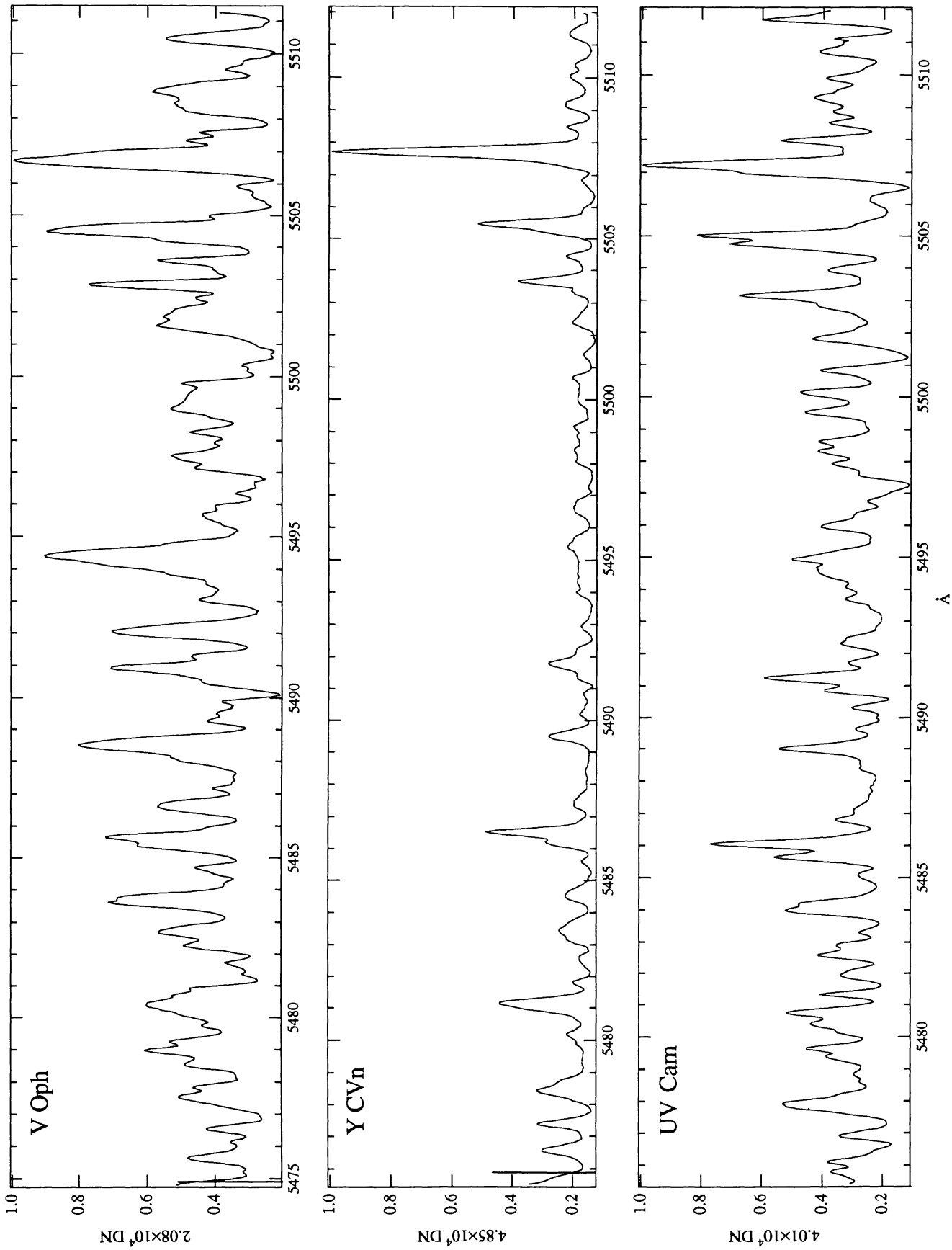

FIG. 13*b*

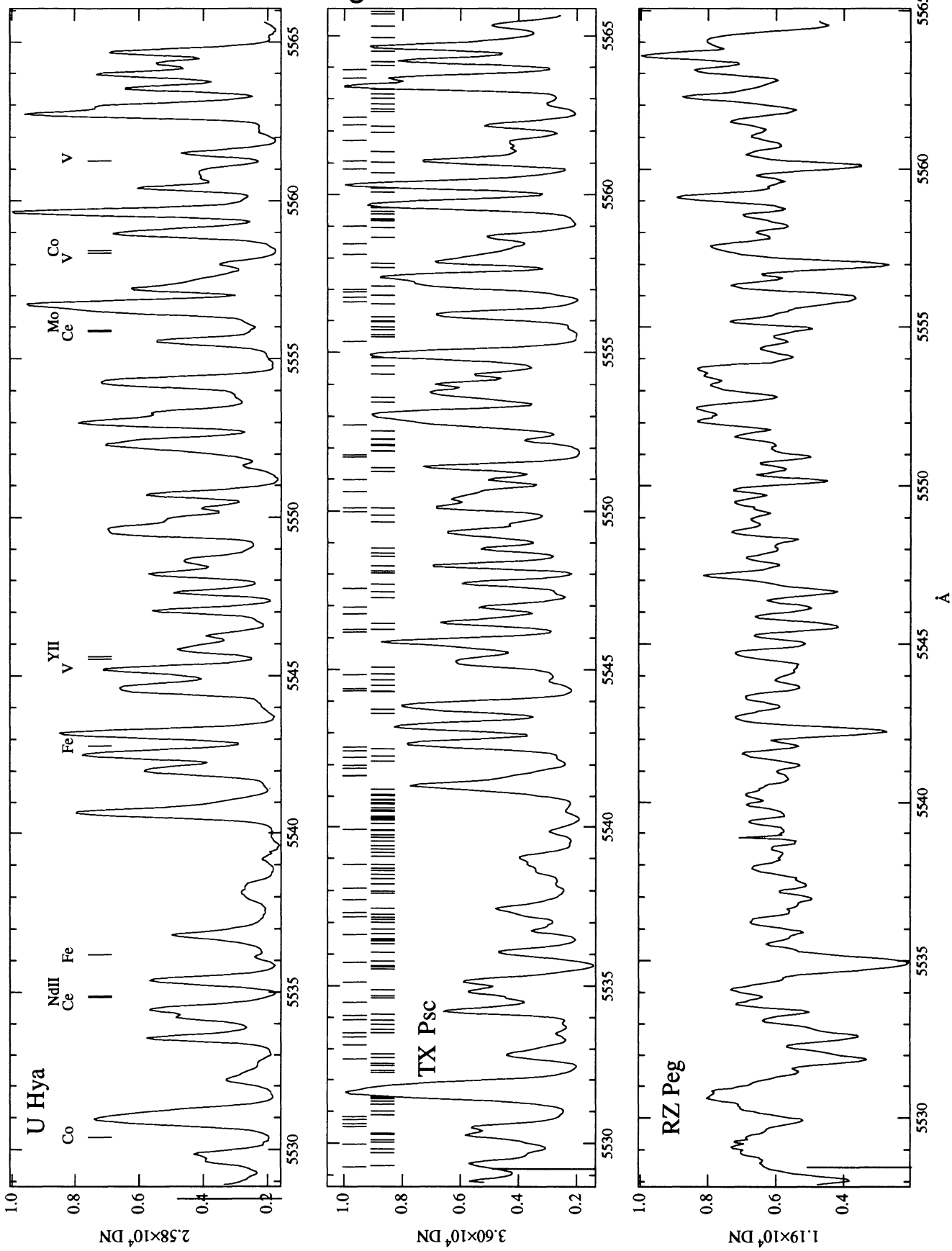

FIG. 14*a*

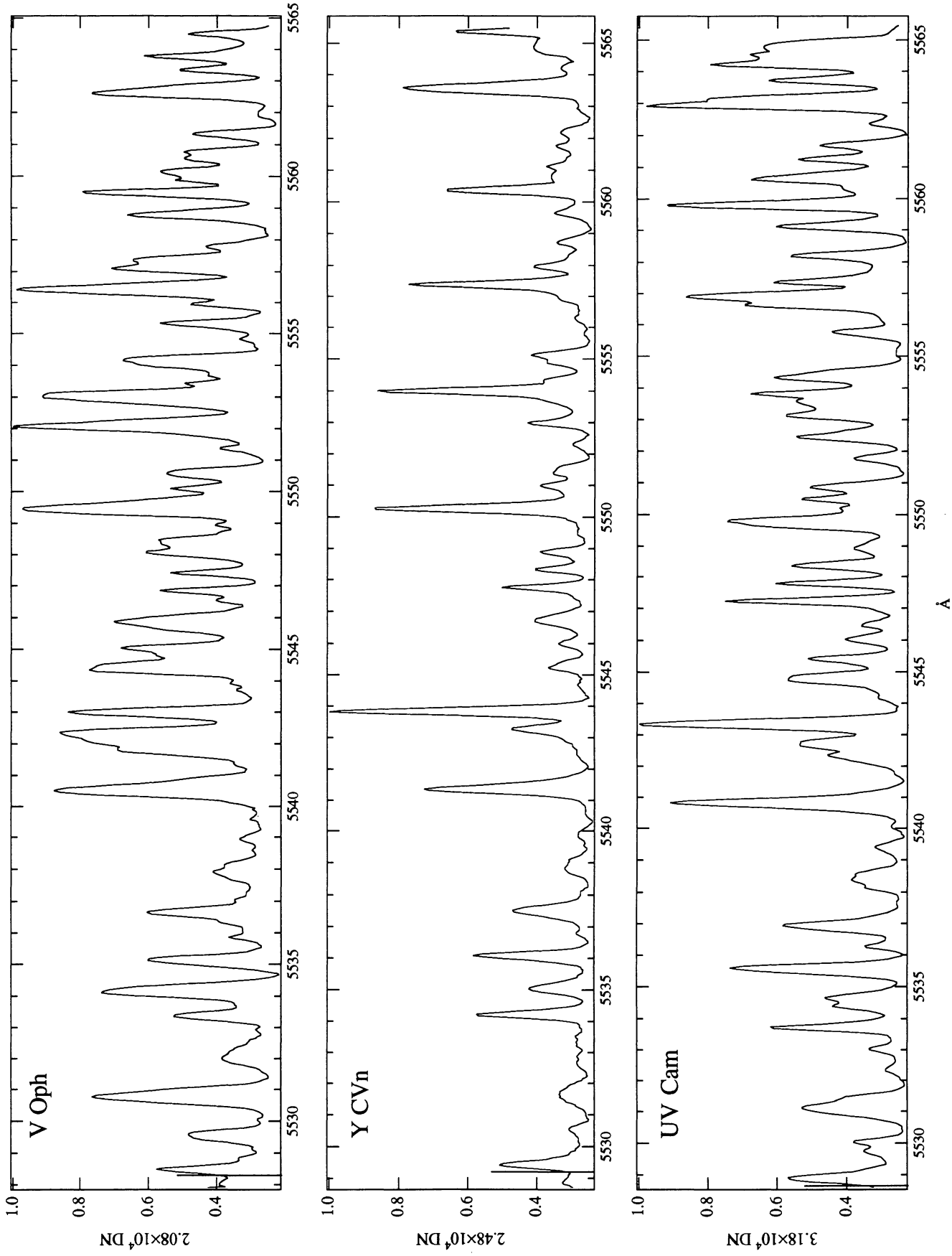

FIG. 14*b*

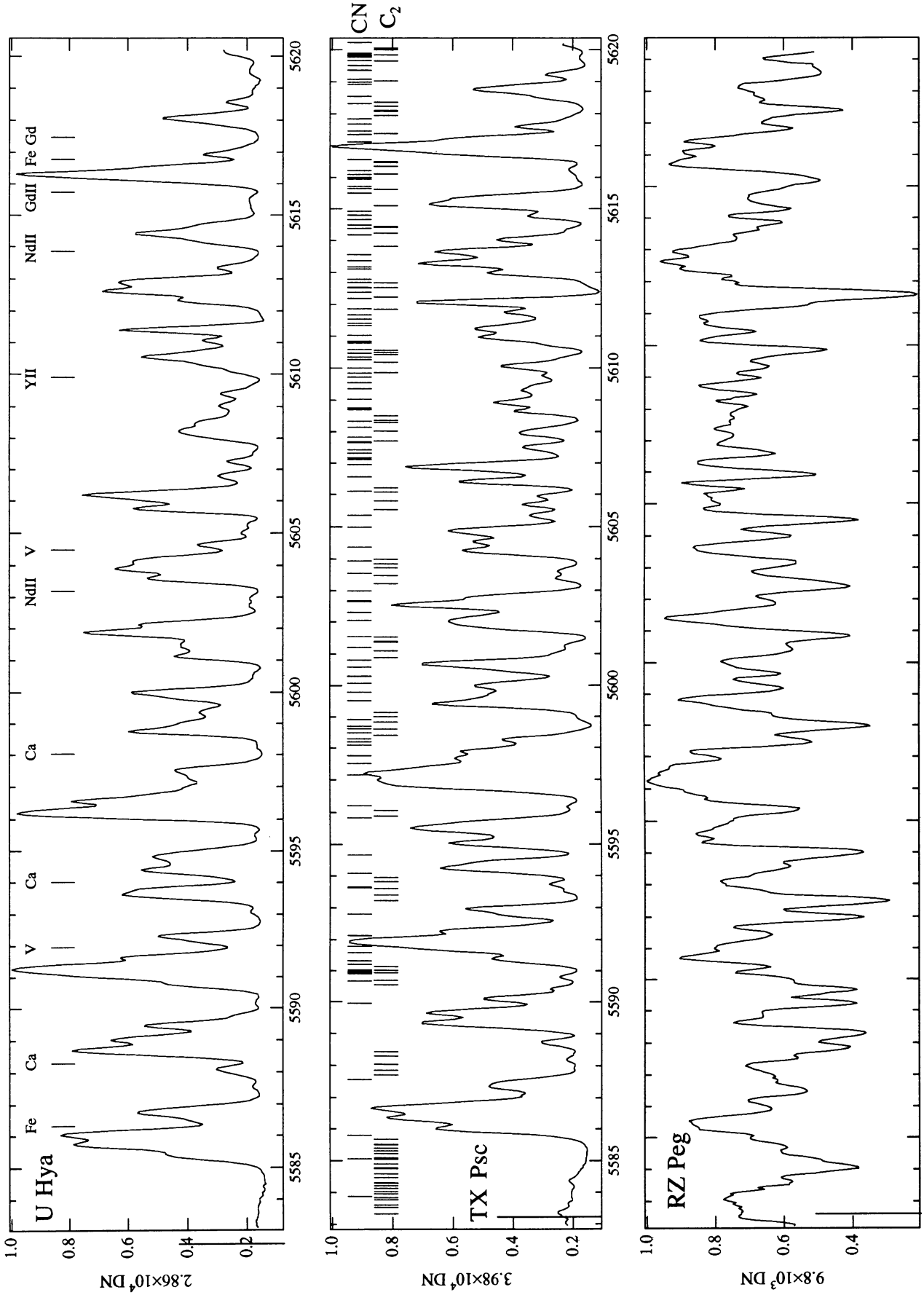

FIG. 15*a*

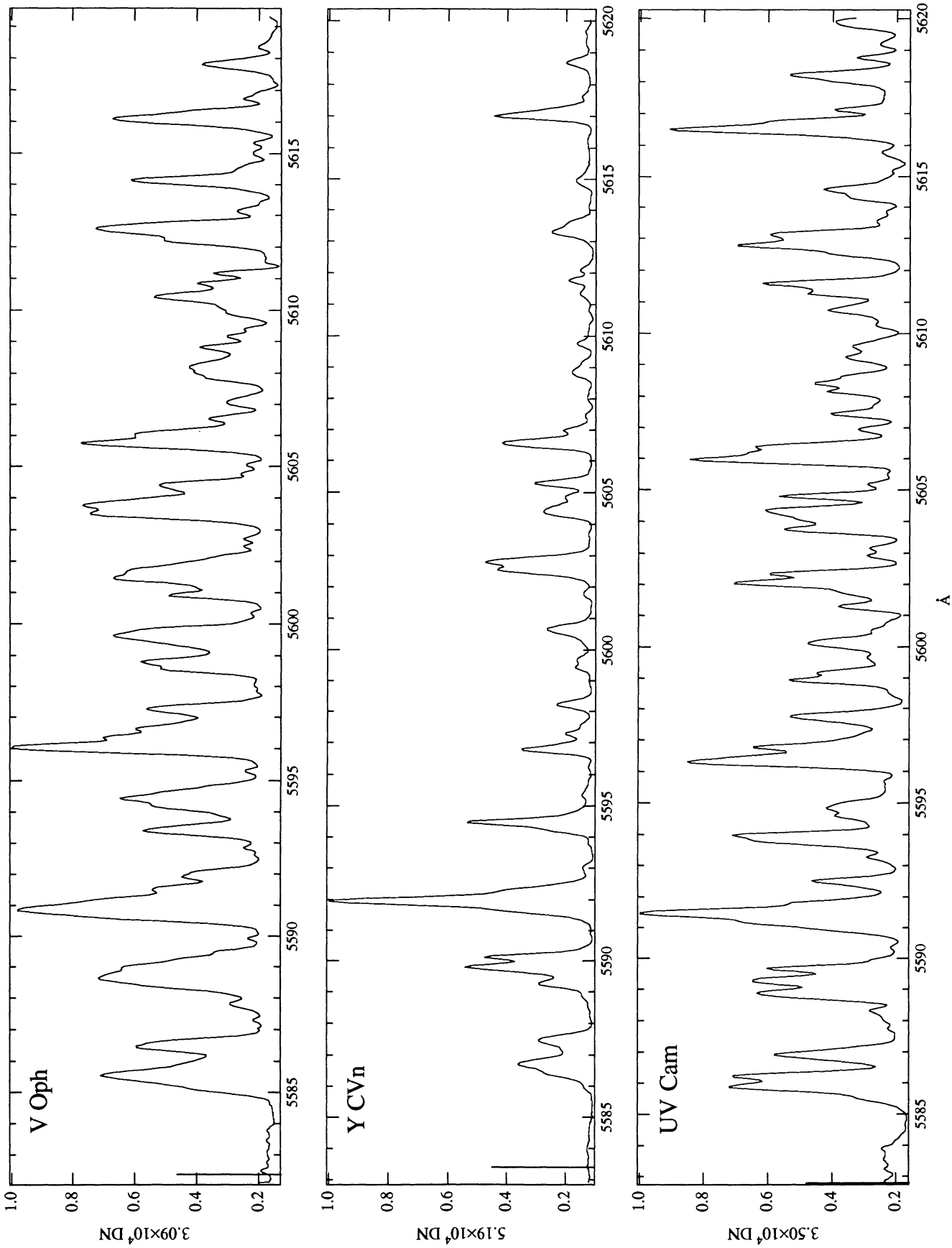

FIG. 15*b*

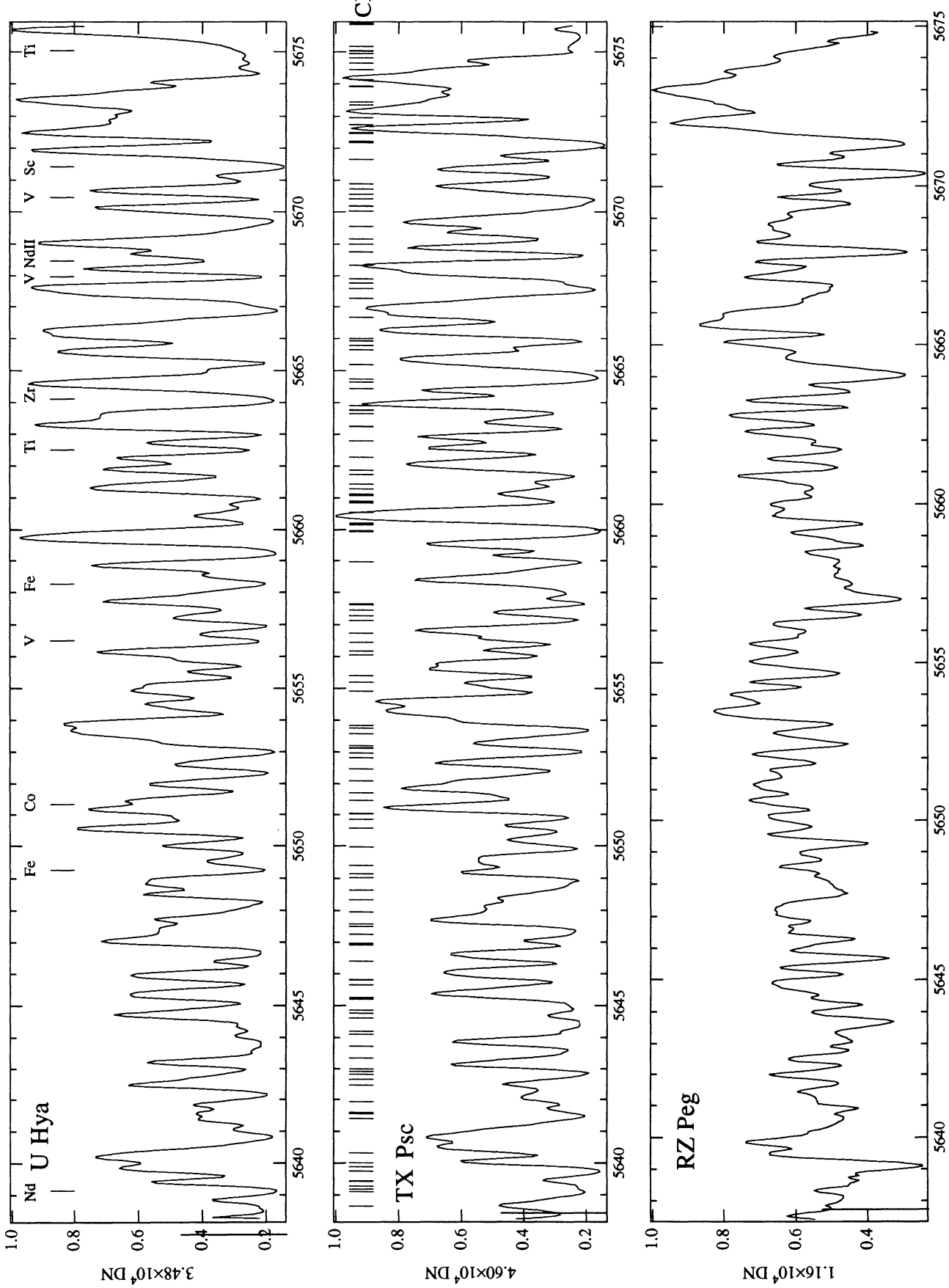

FIG. 16*a*

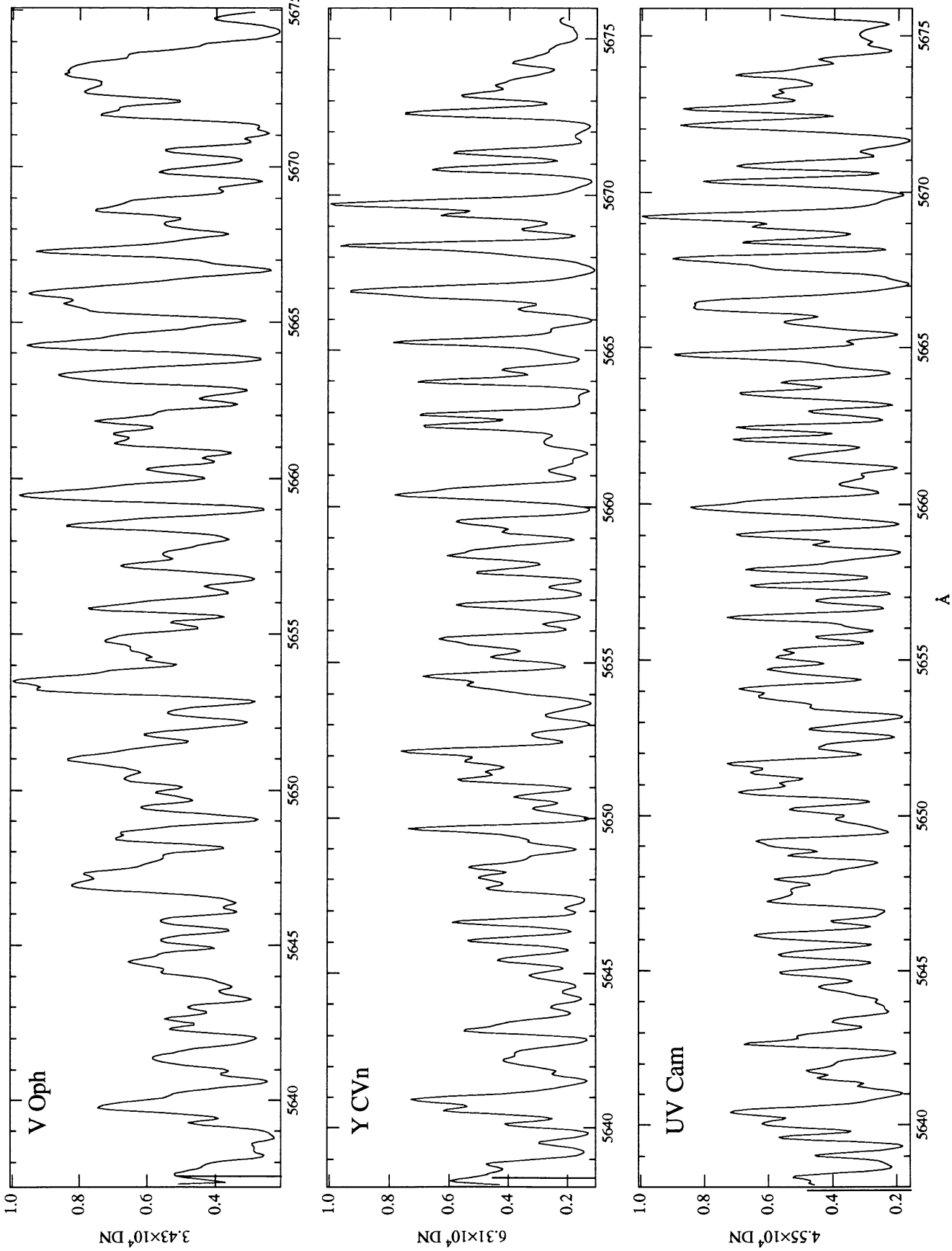

FIG. 16*b*

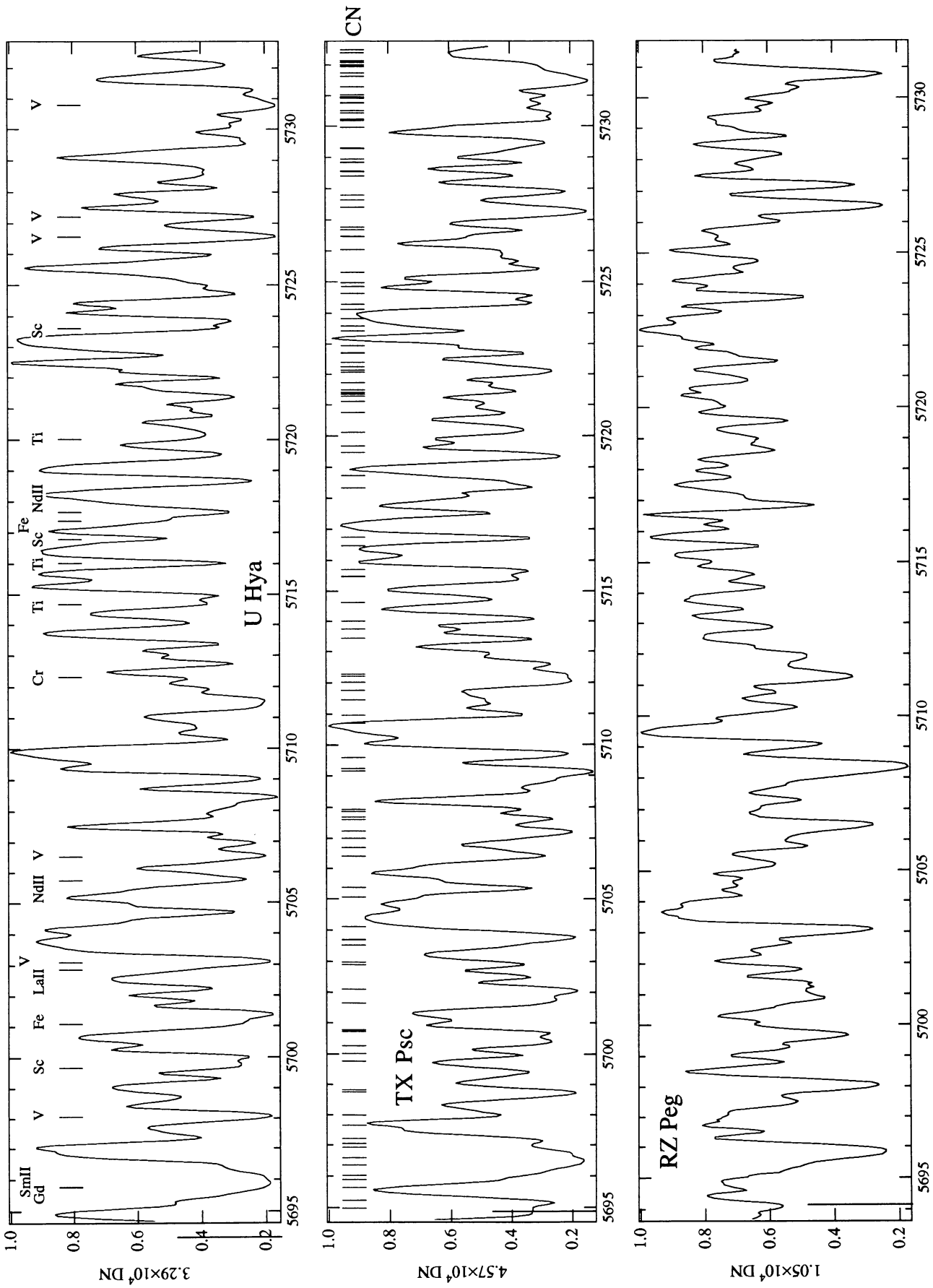

FIG. 17*a*

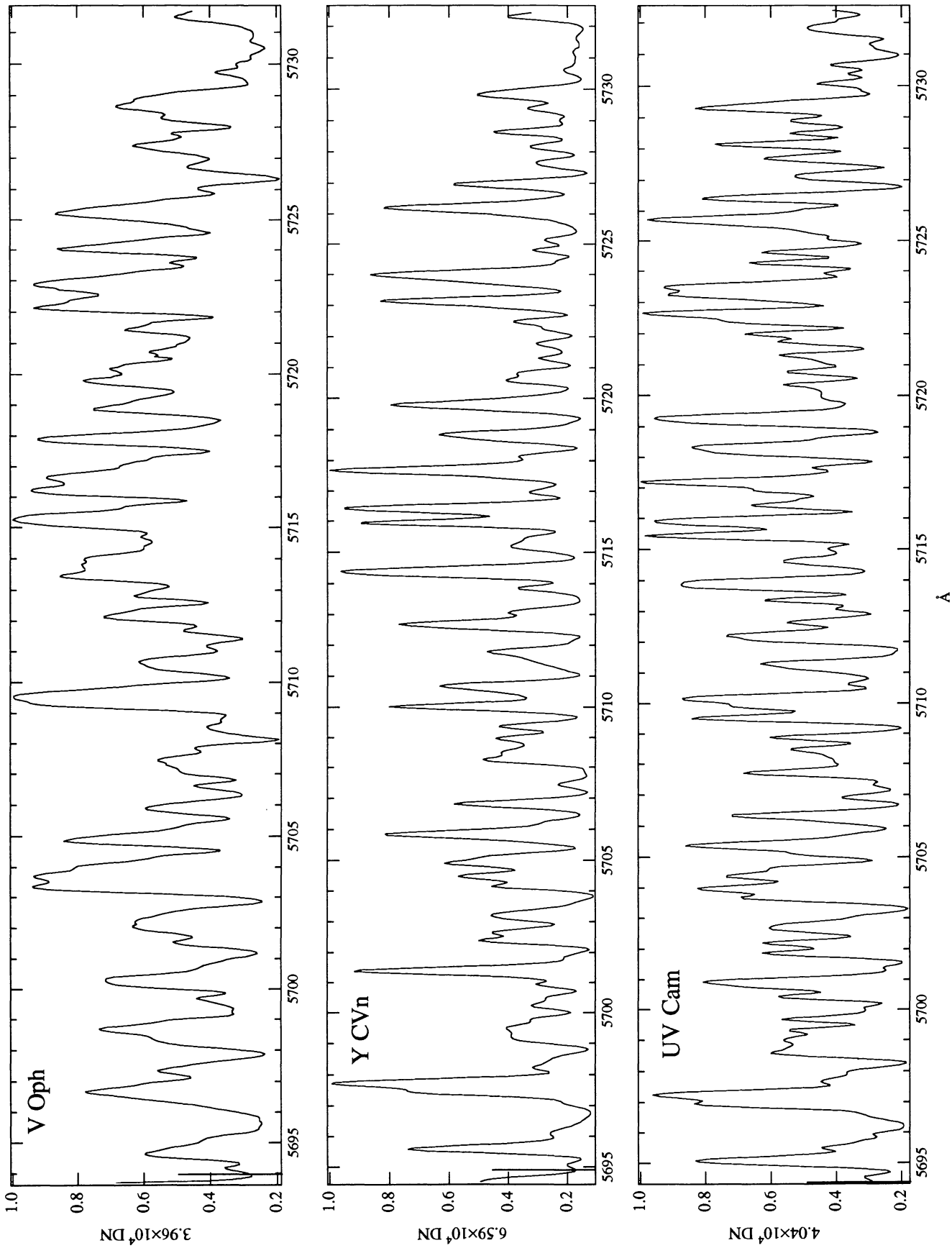

FIG. 17*b*

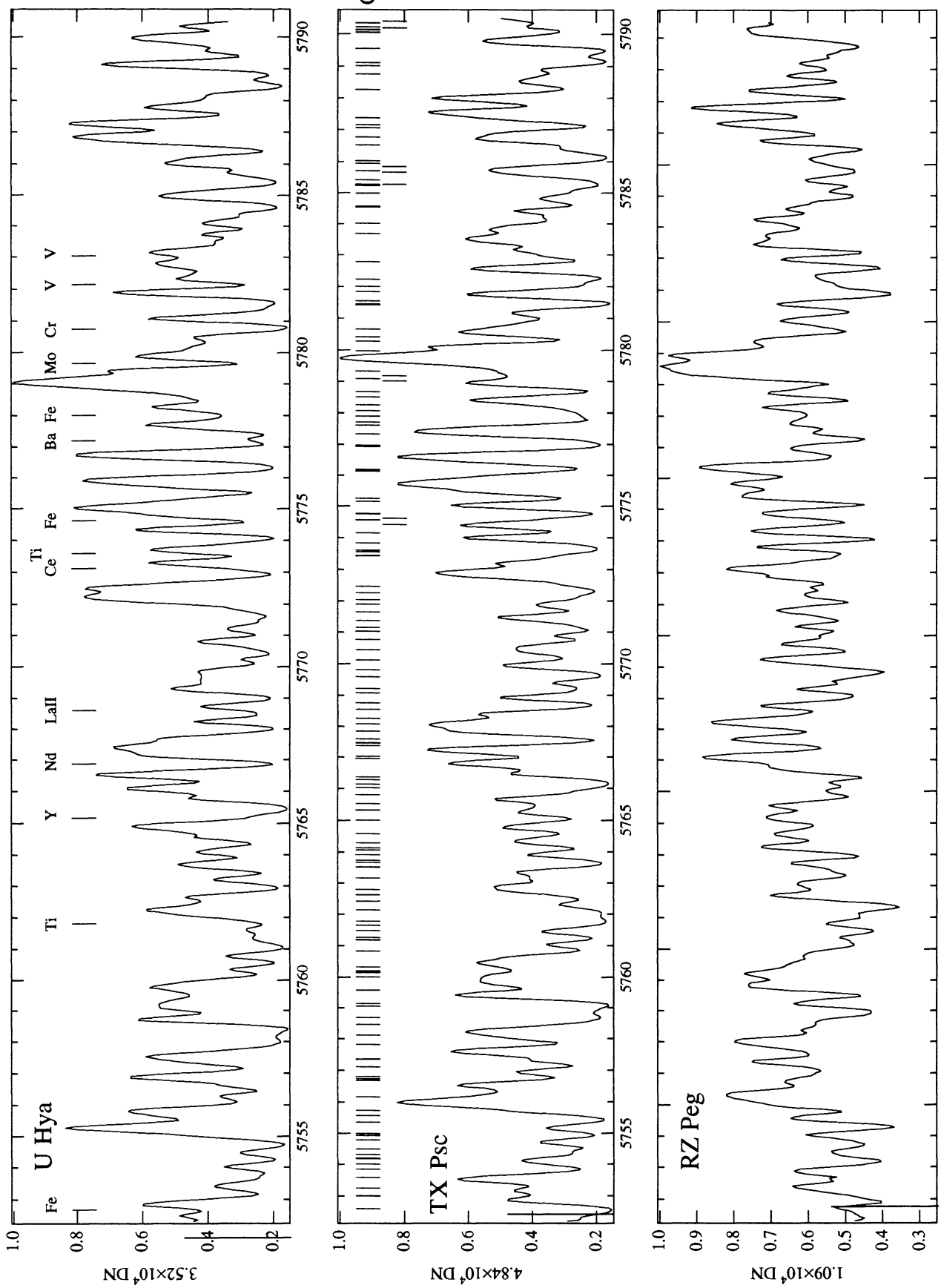

FIG. 18*a*

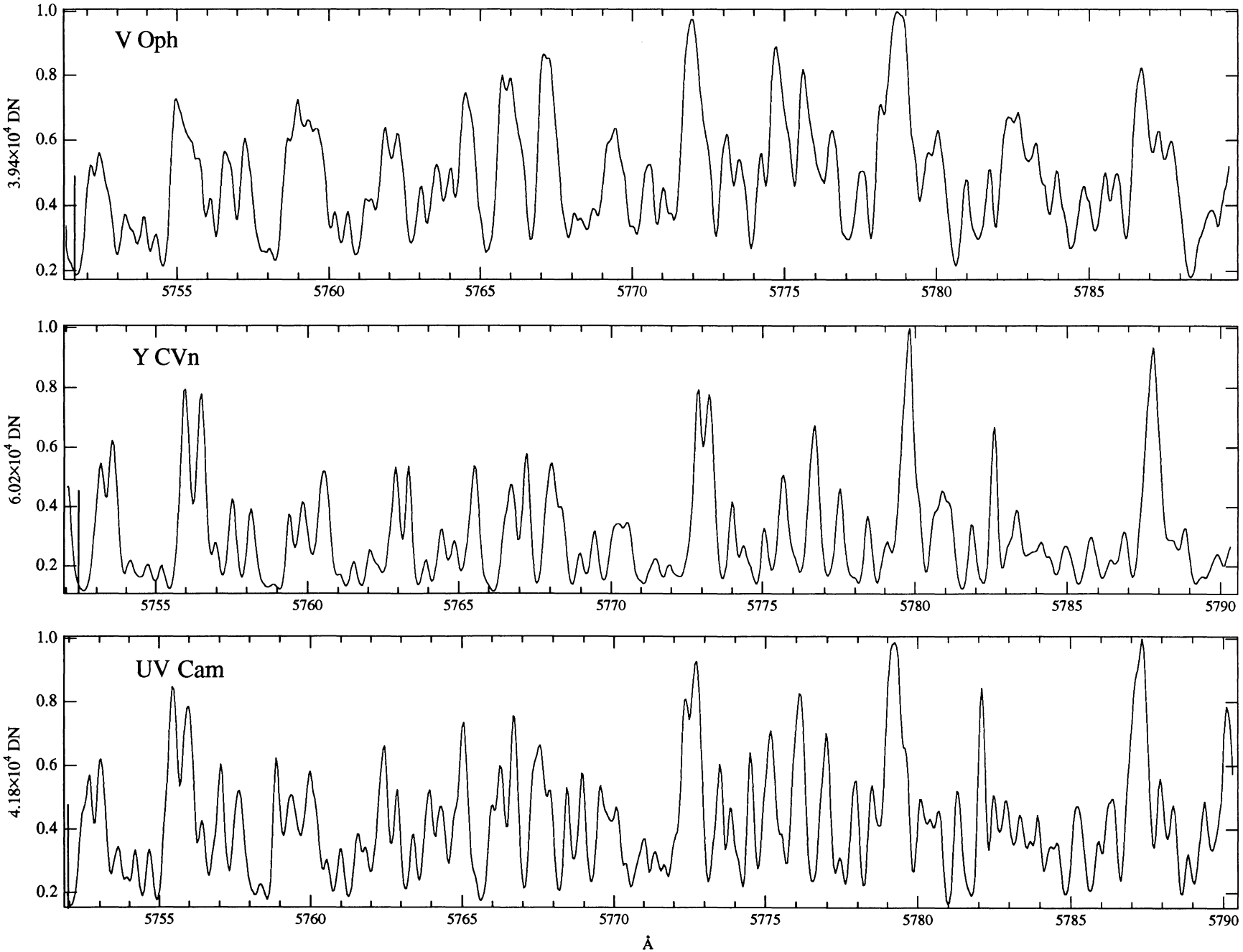

FIG. 18*b*

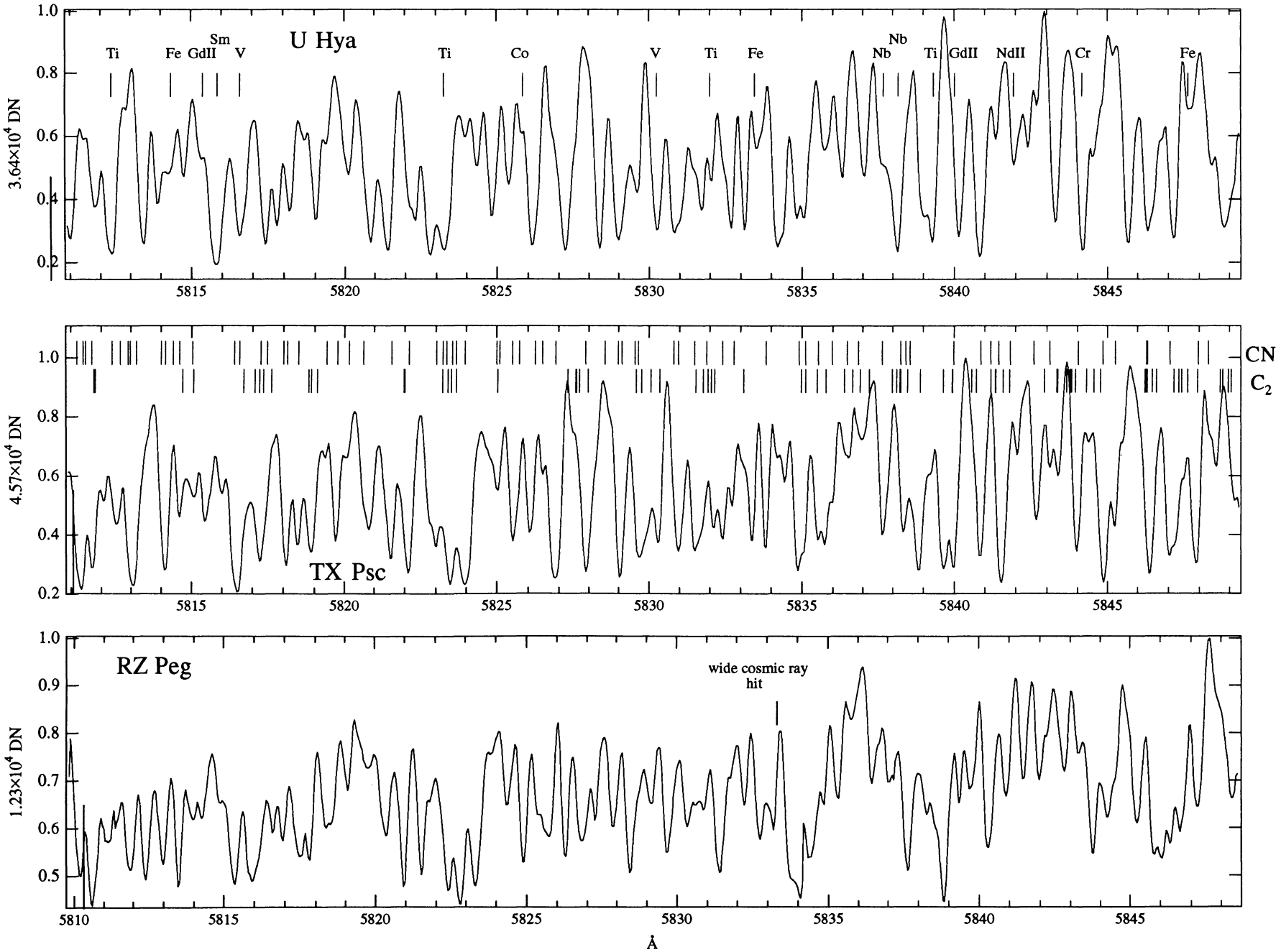

FIG. 19*a*

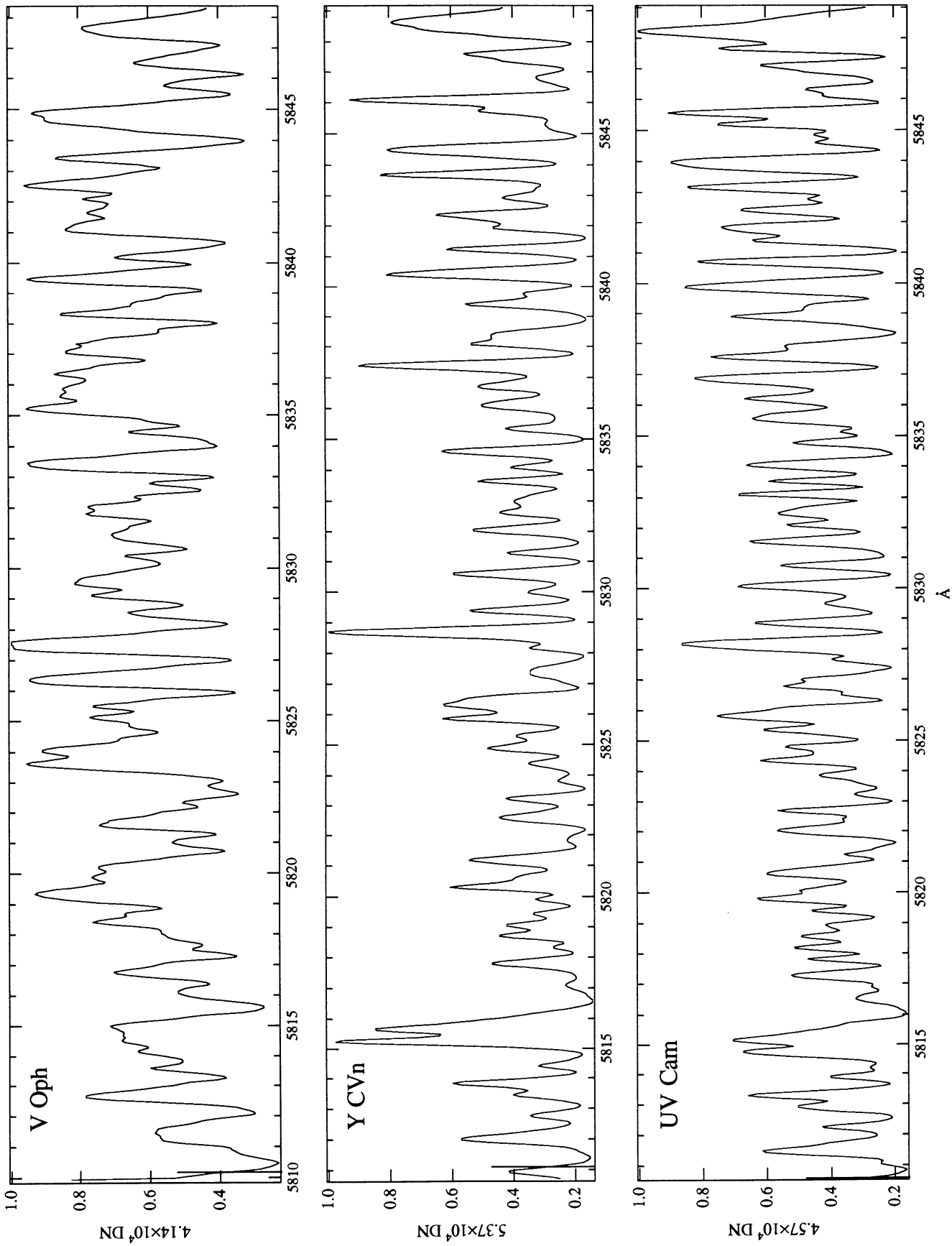

FIG. 19*b*

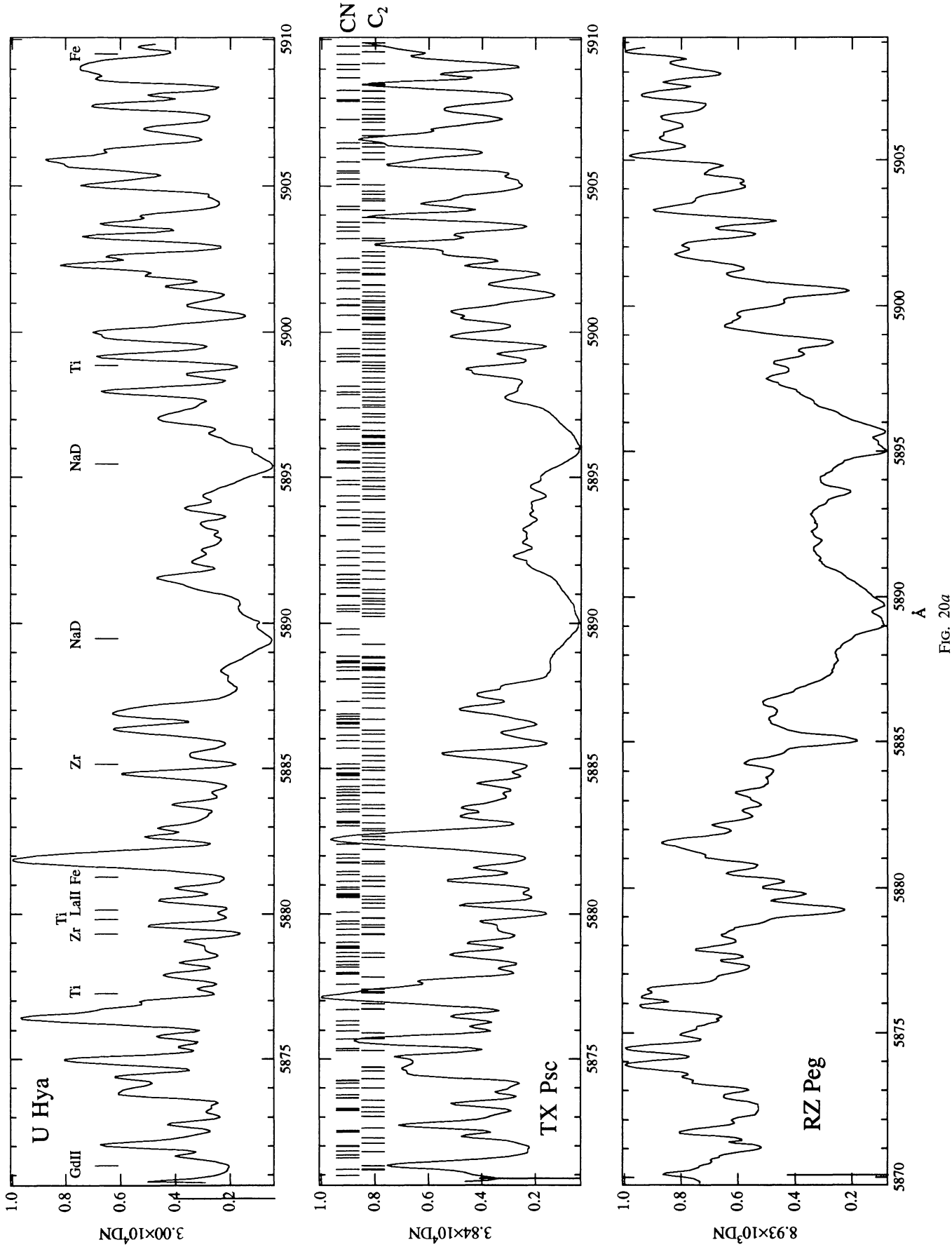

FIG. 20*a*

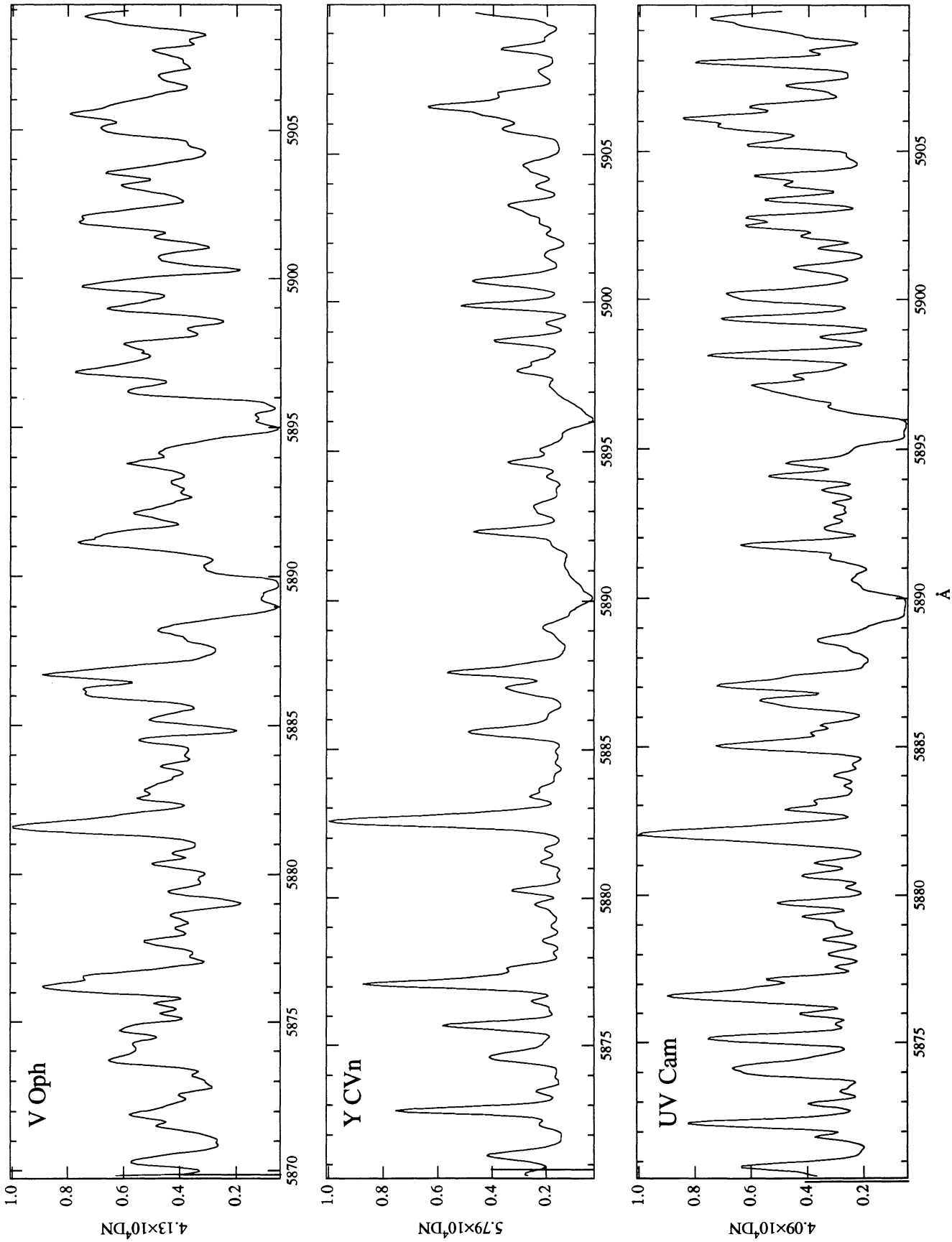

FIG. 20*b*

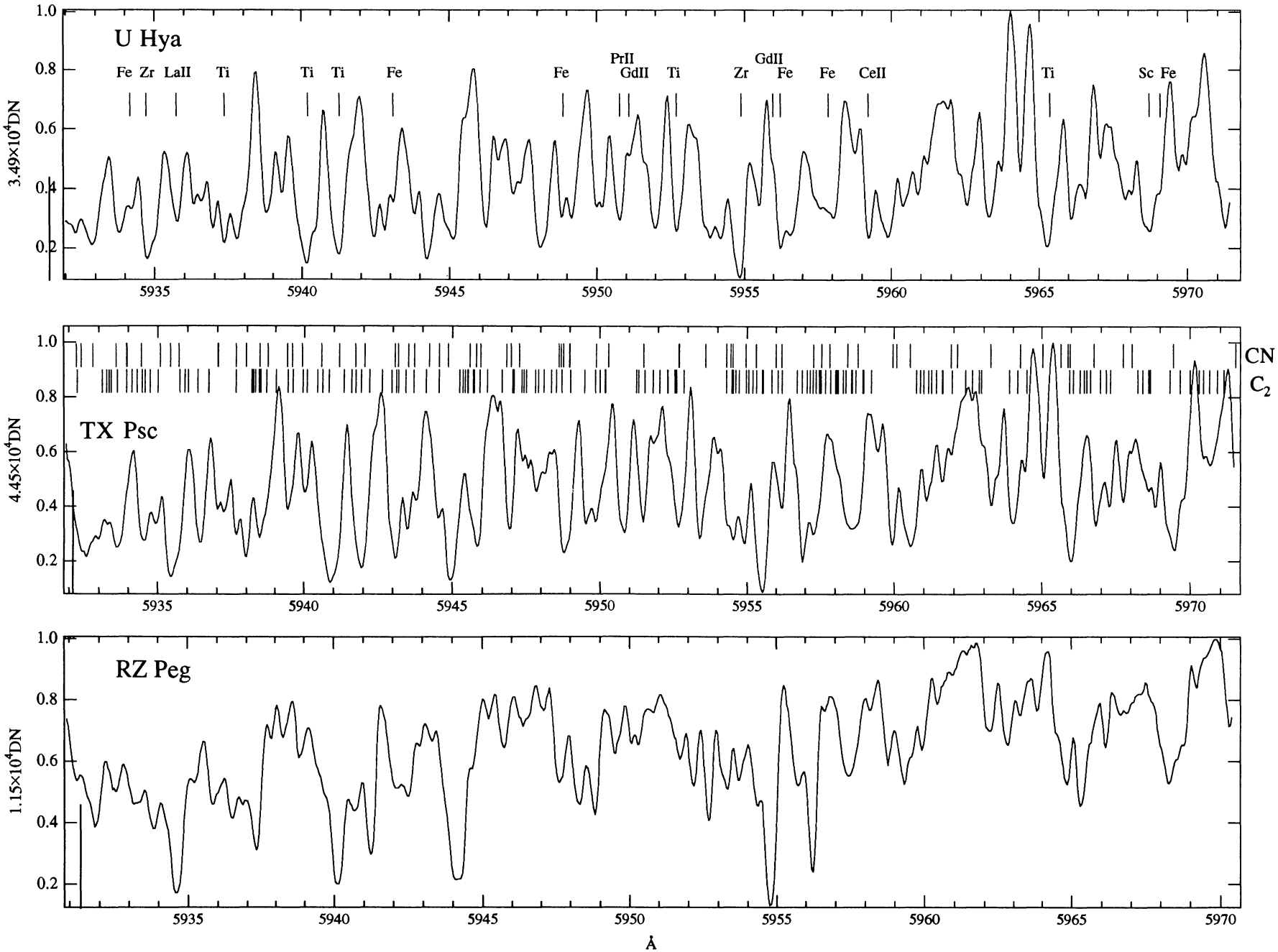

FIG. 21*a*

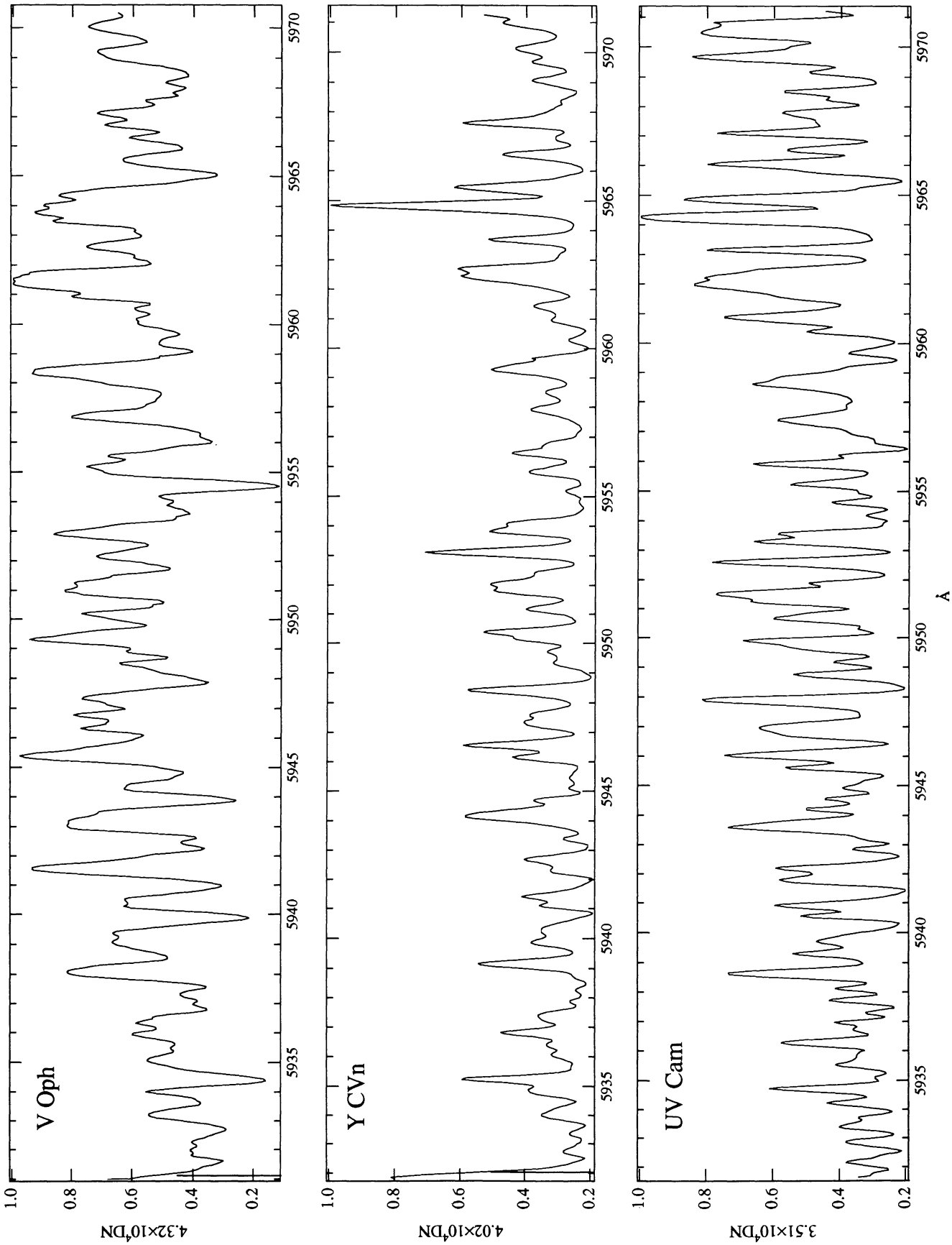

FIG. 21*b*

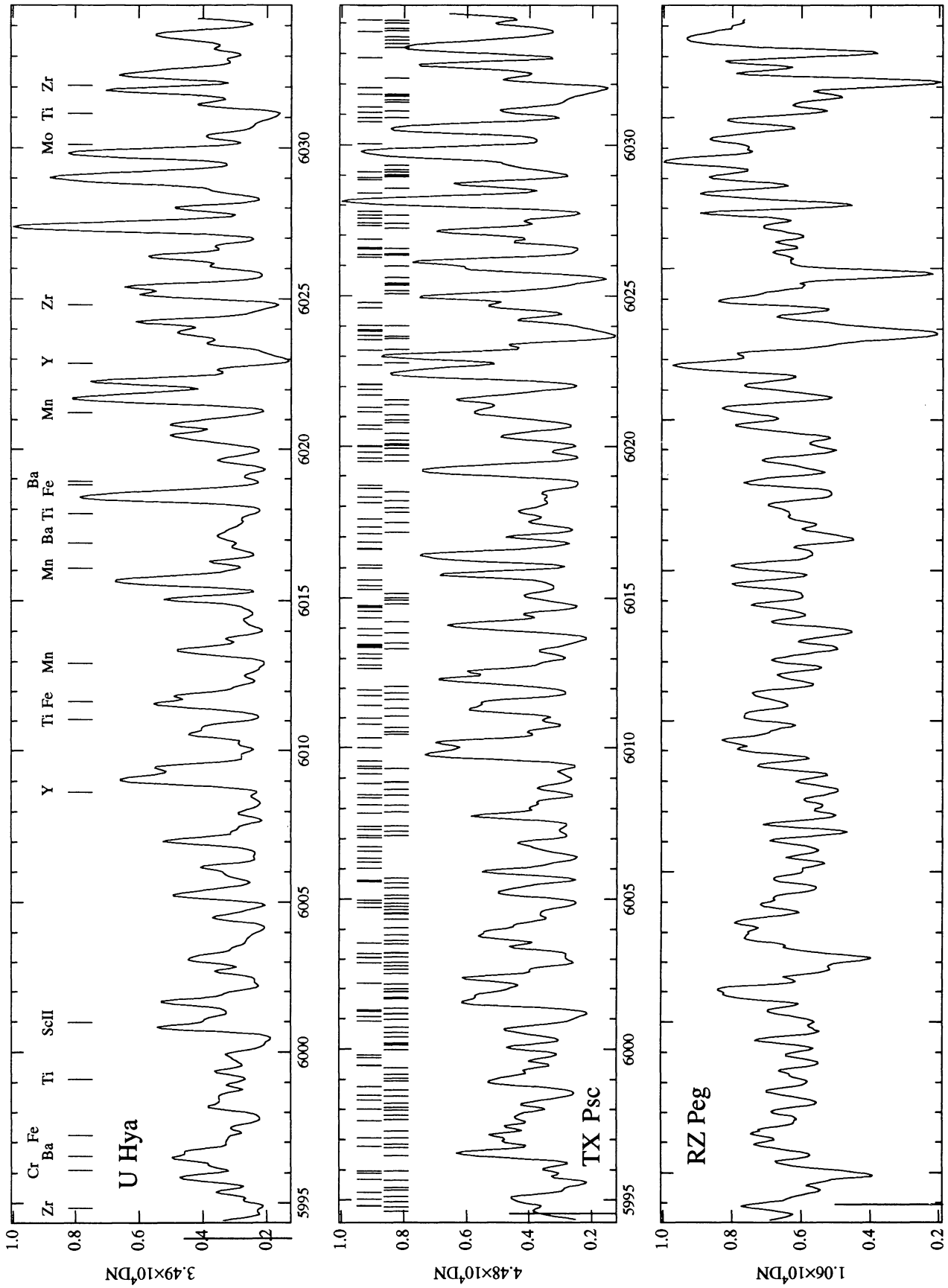

FIG. 22*a*

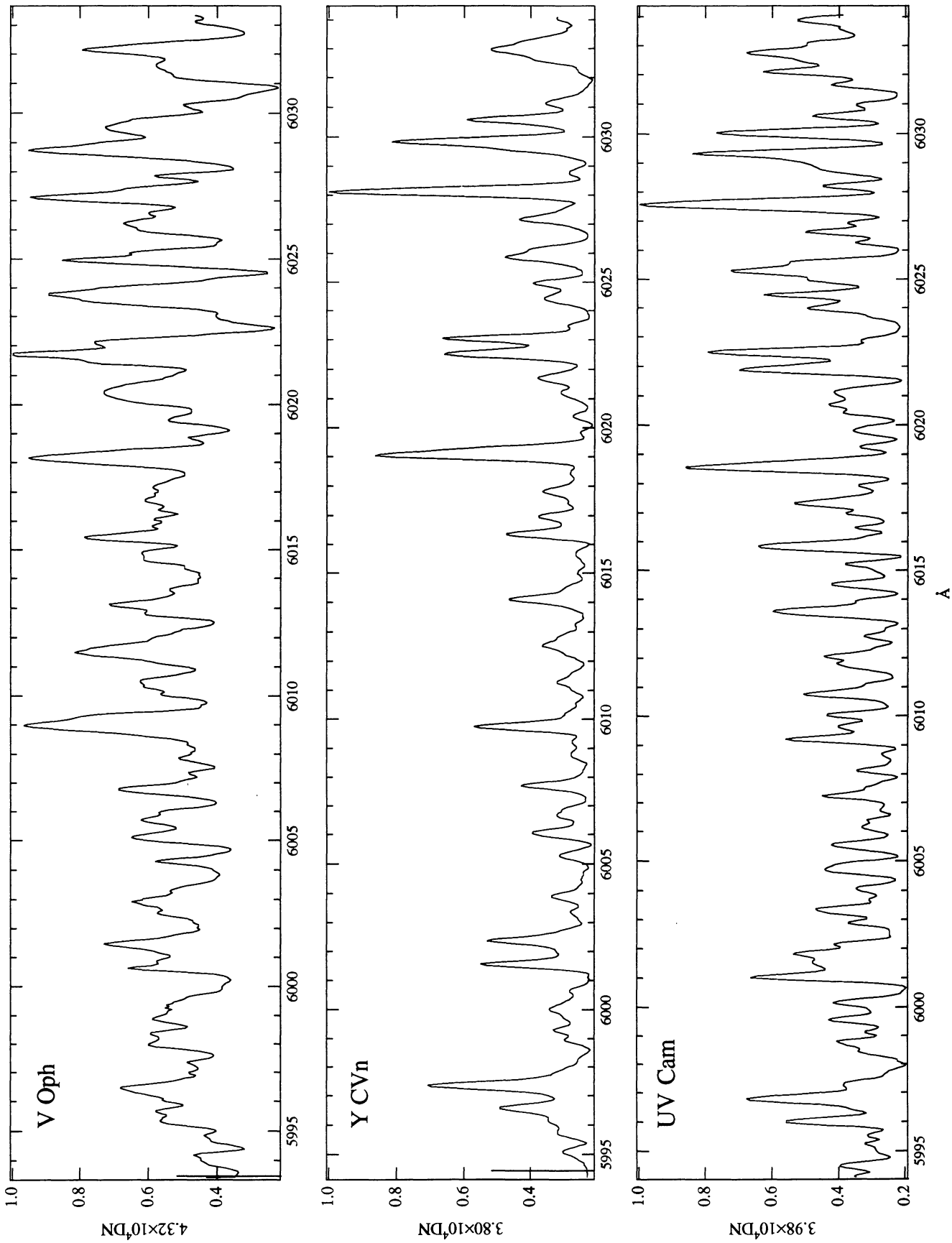

FIG. 22*b*

1994ApJS...90..317B

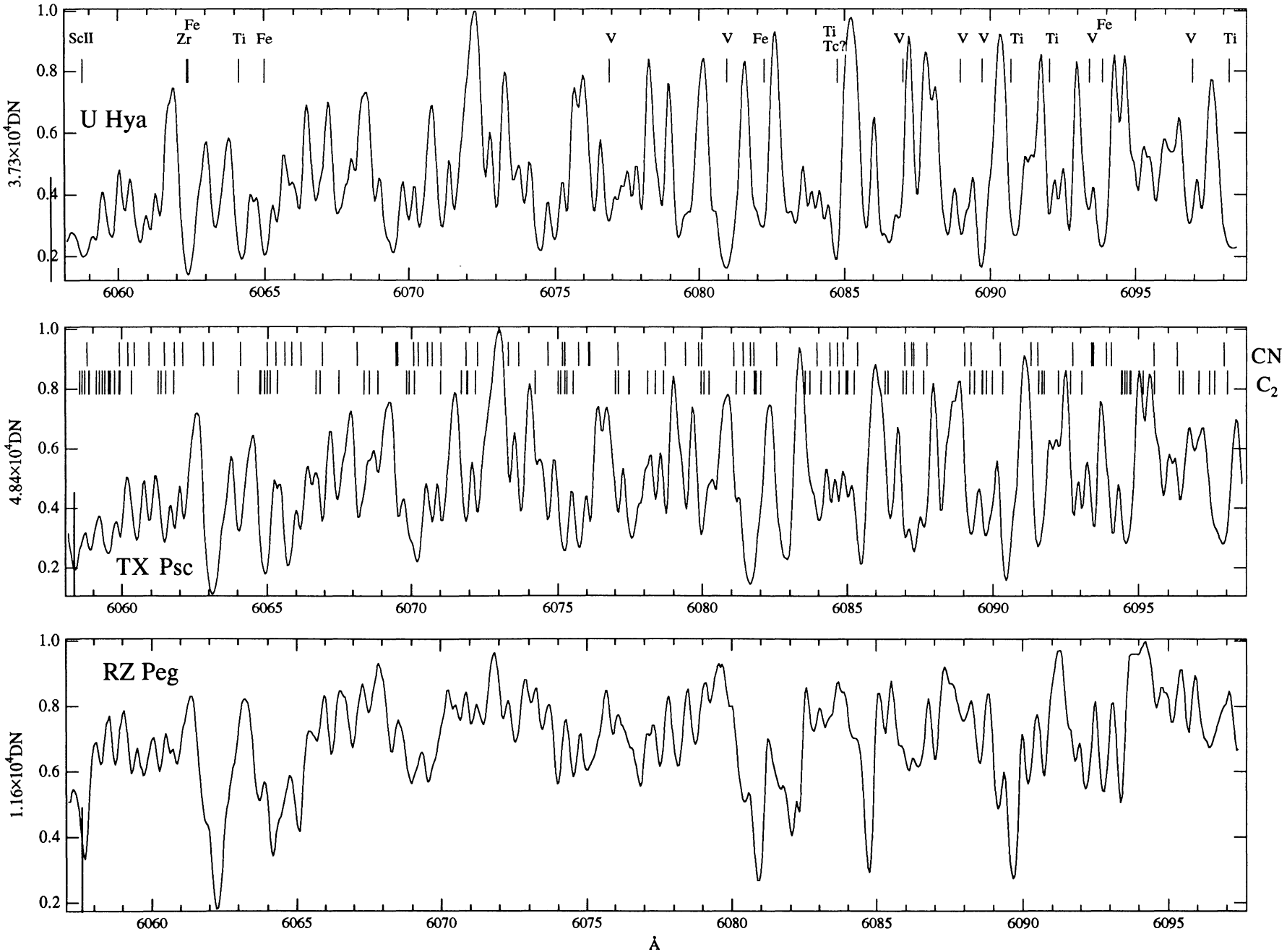

FIG. 23*a*

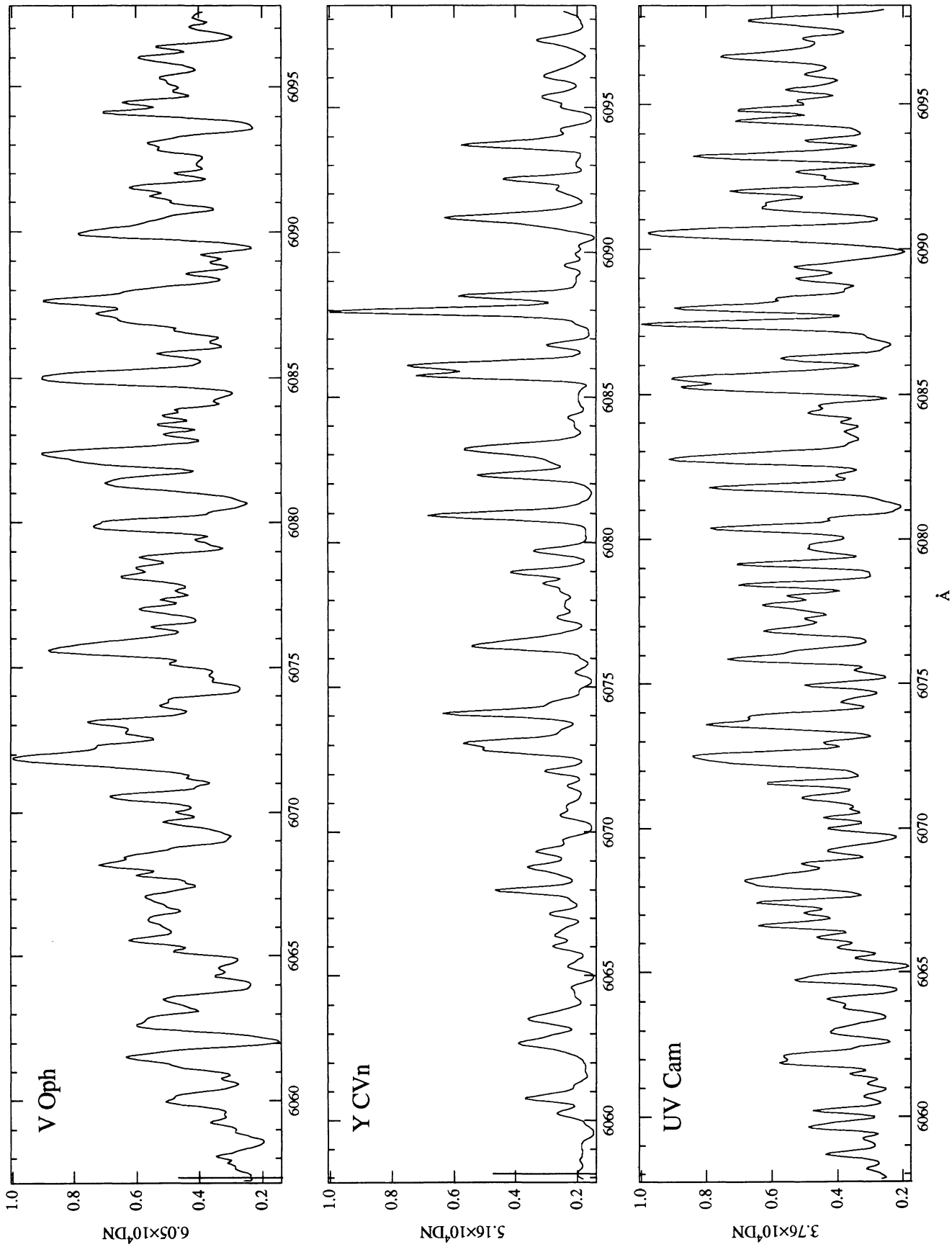

FIG. 23*b*

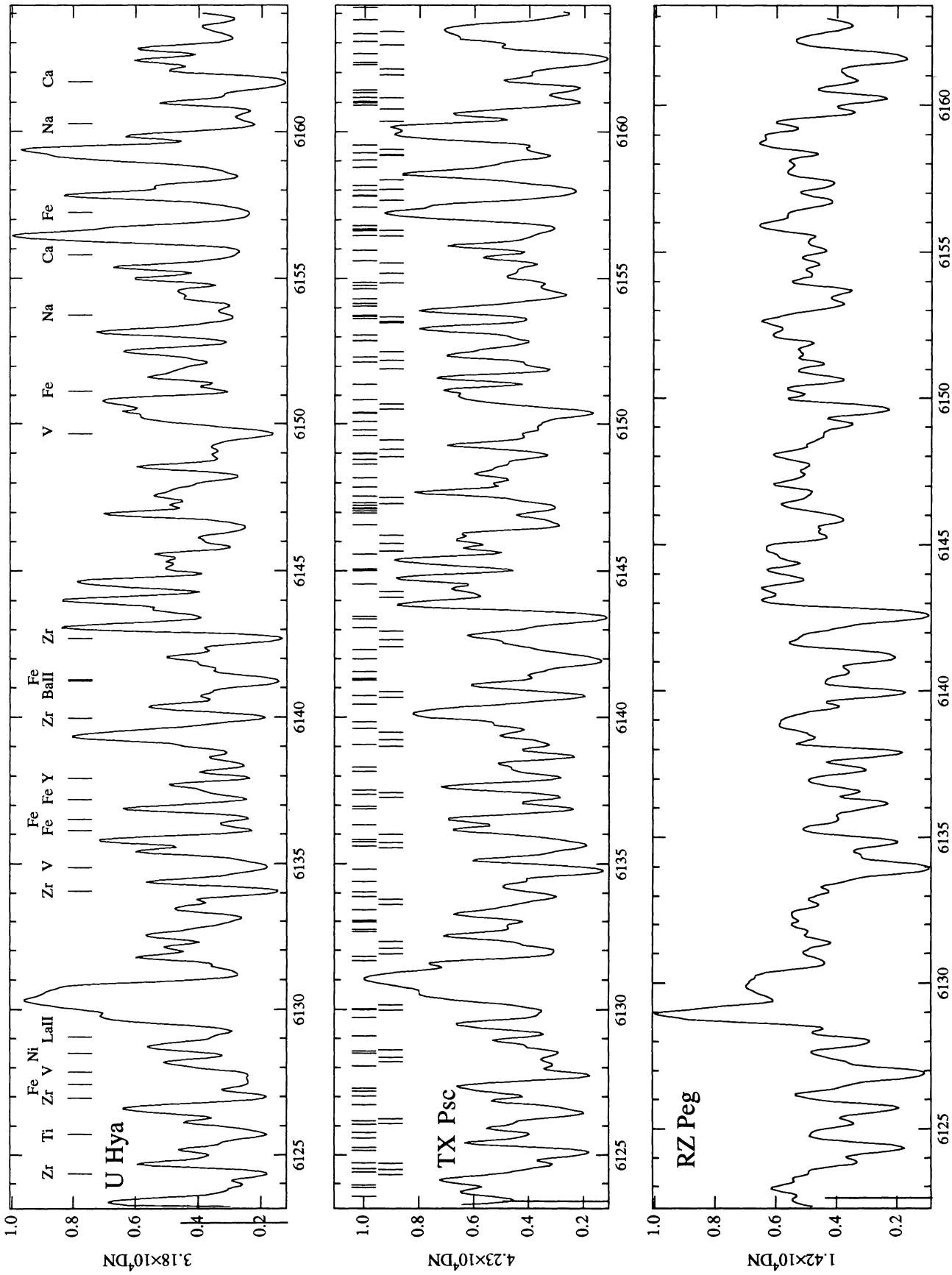

FIG. 24*a*

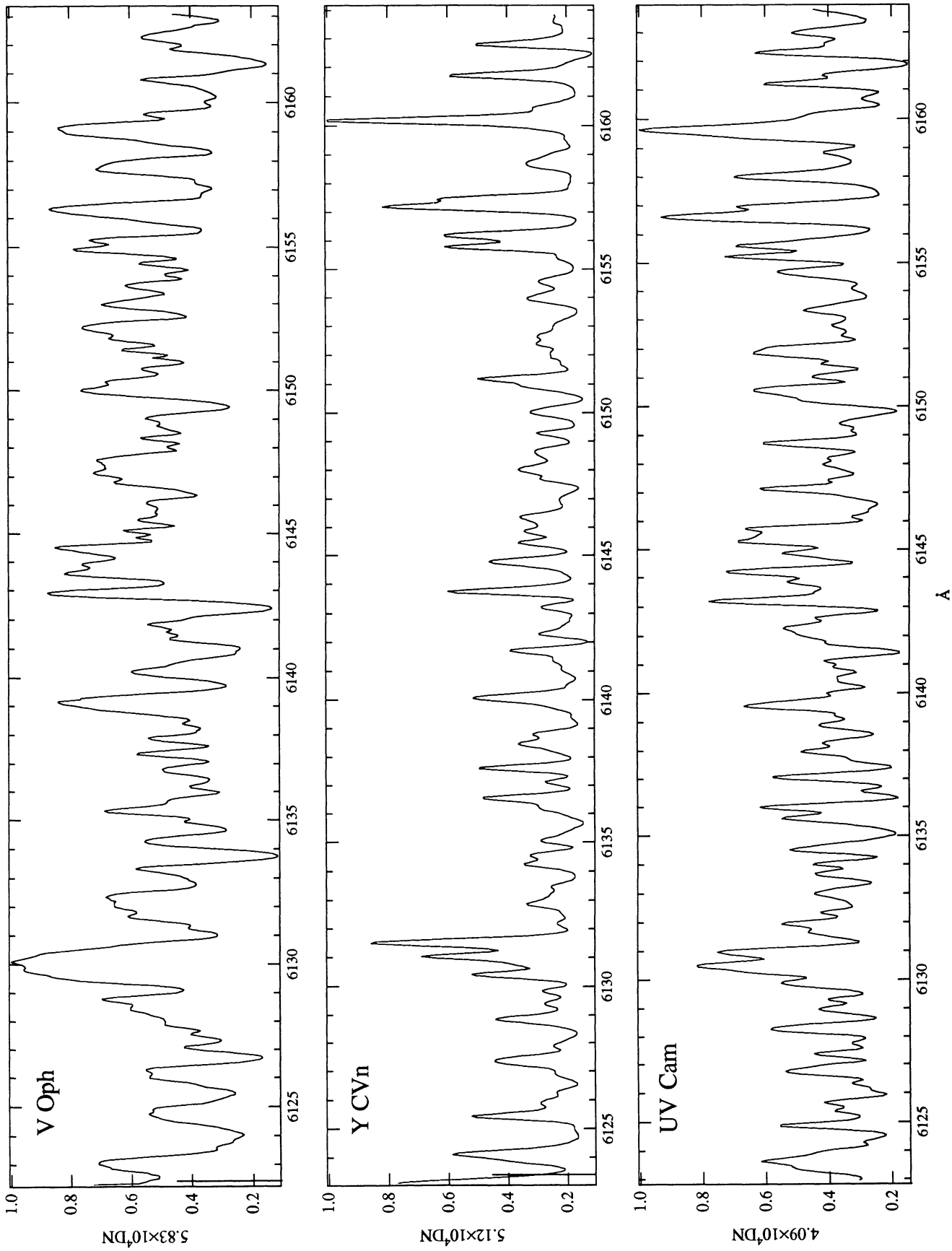

FIG. 24*b*

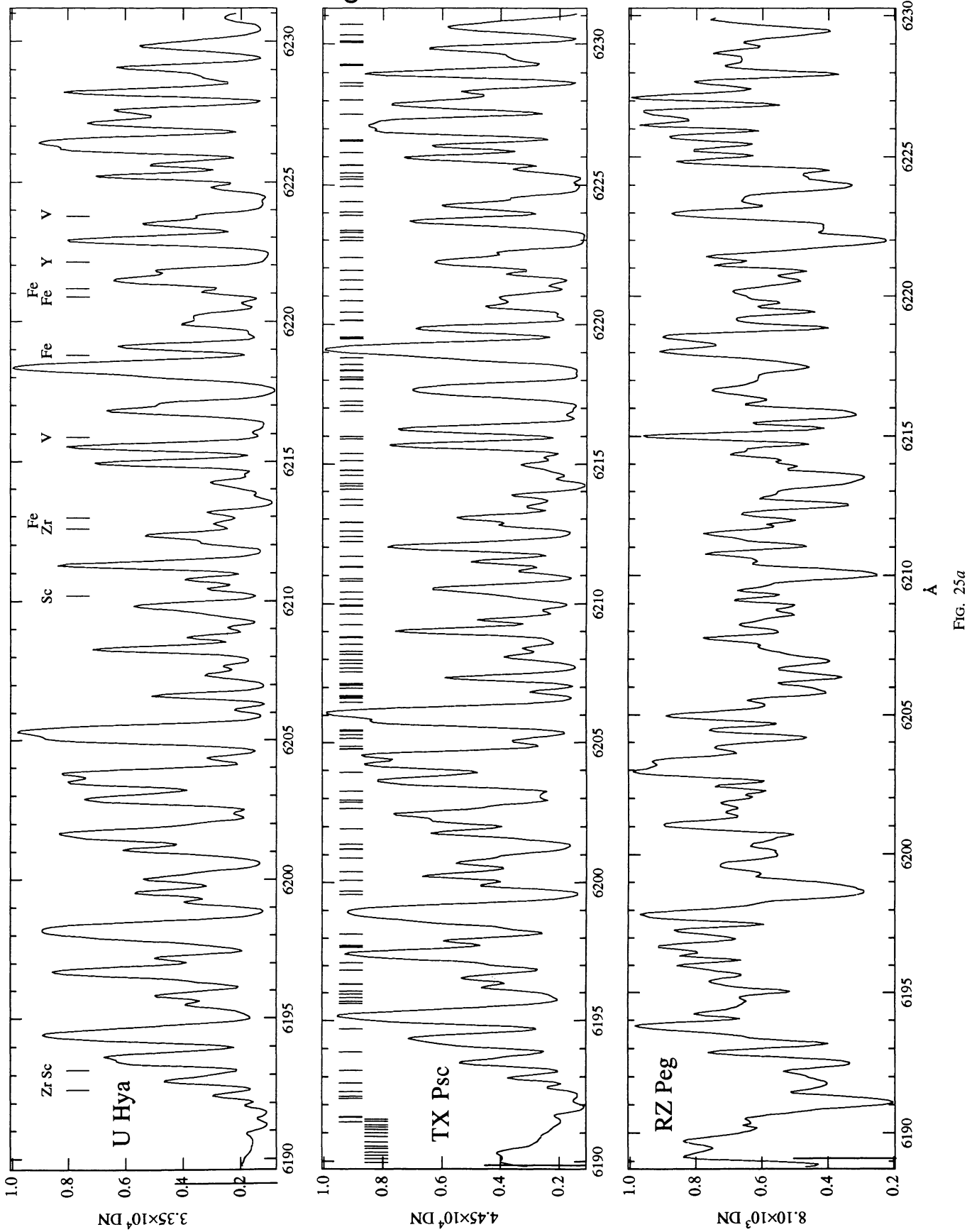

FIG. 25*a*

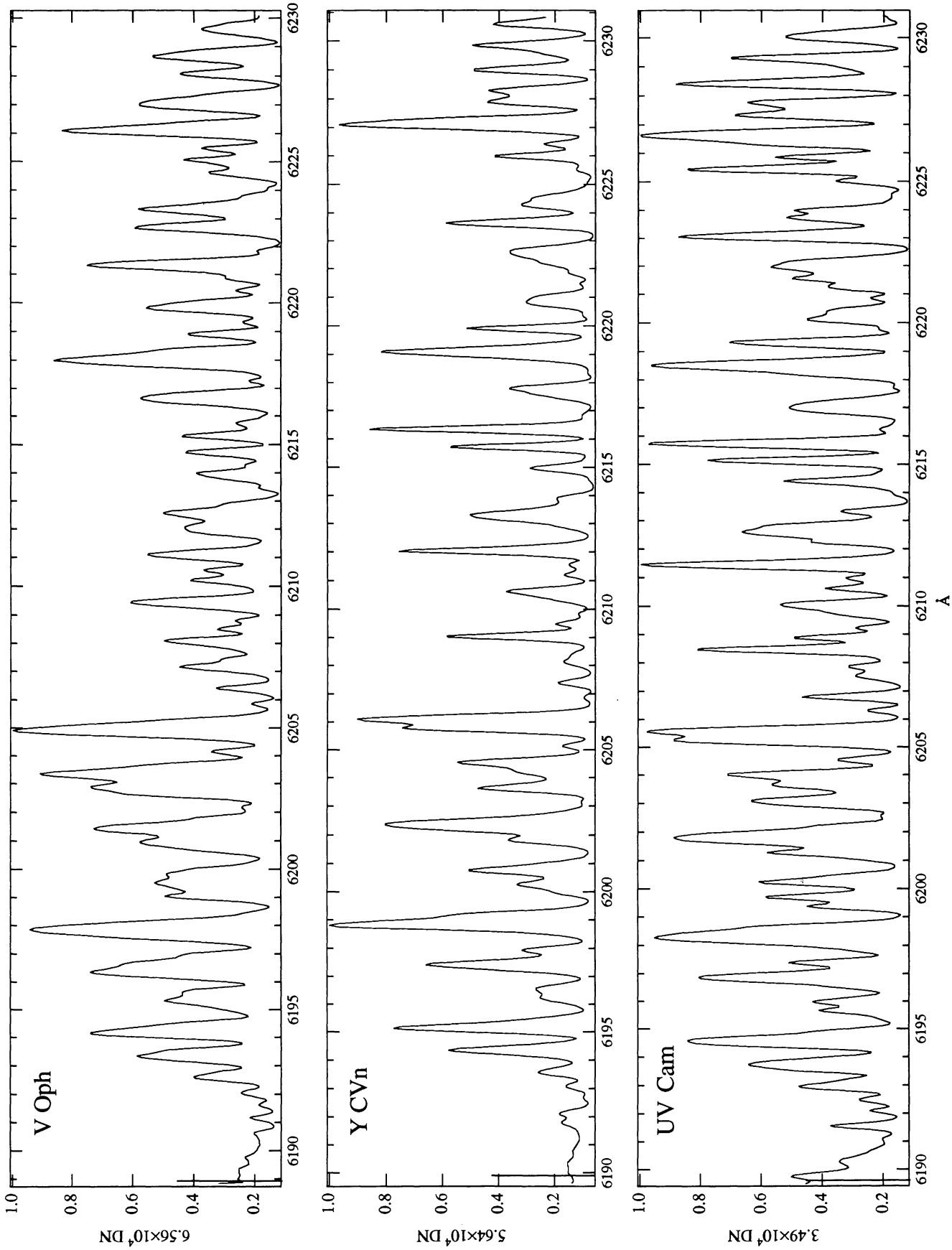

FIG. 25*b*

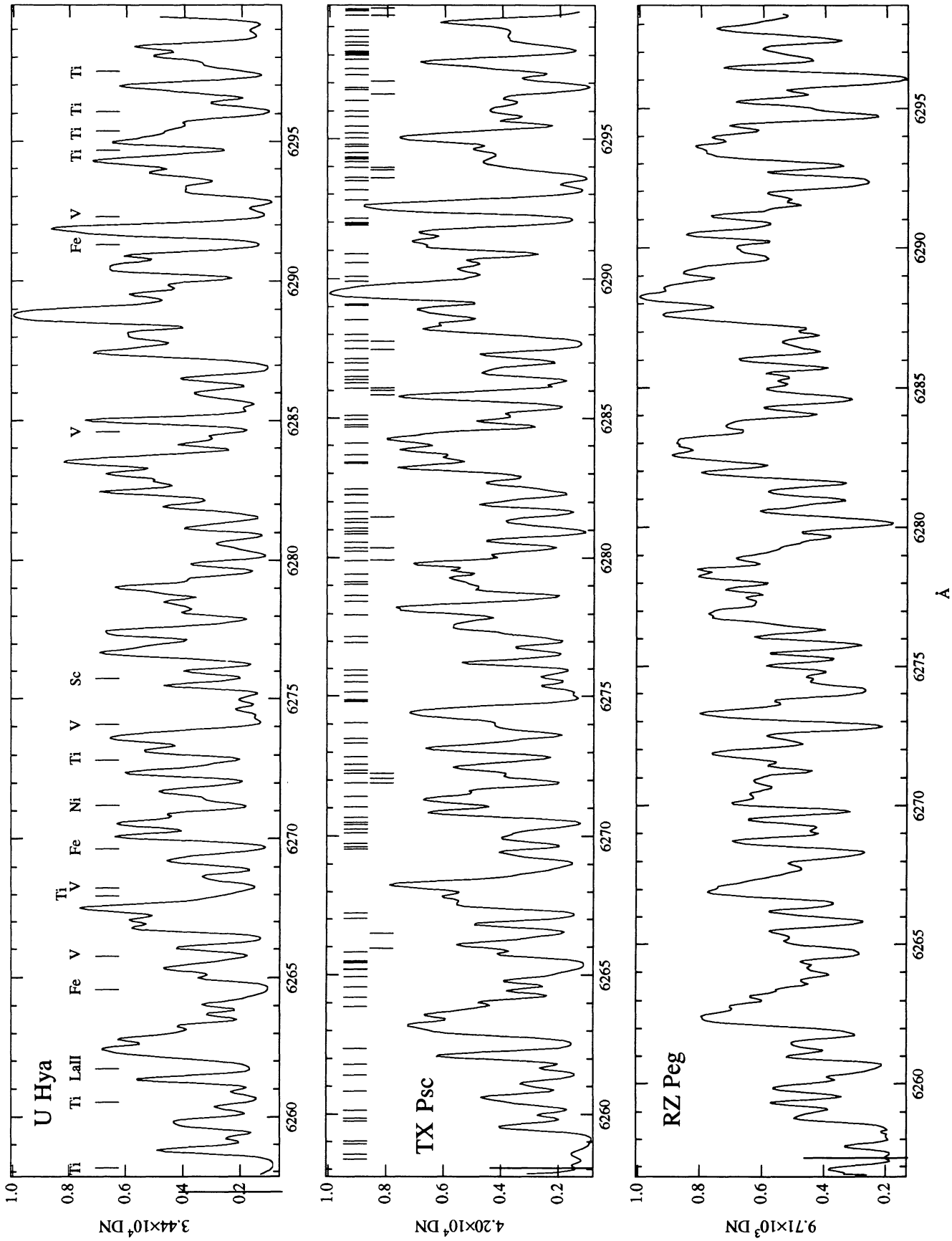

FIG. 26*a*

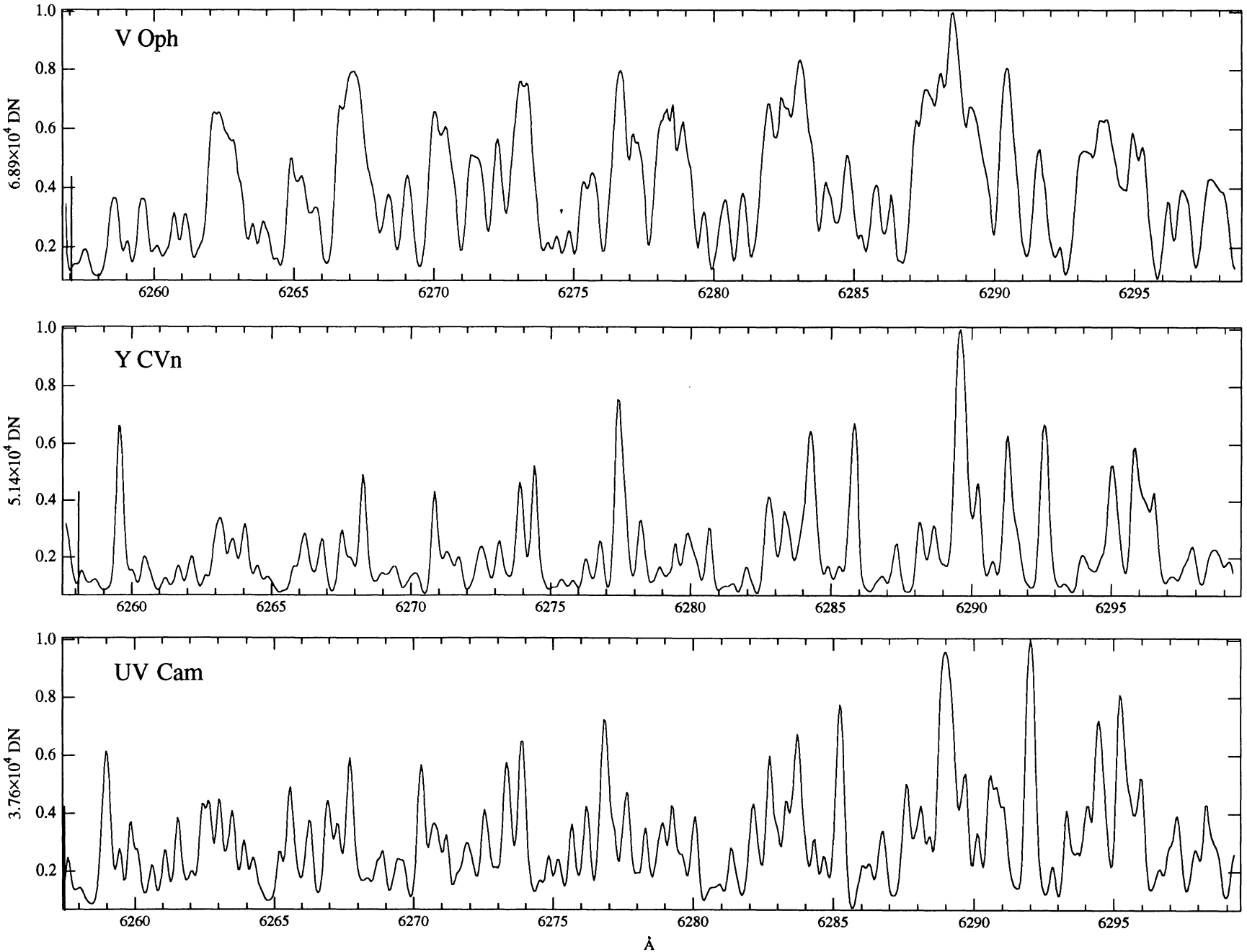

FIG. 26*b*

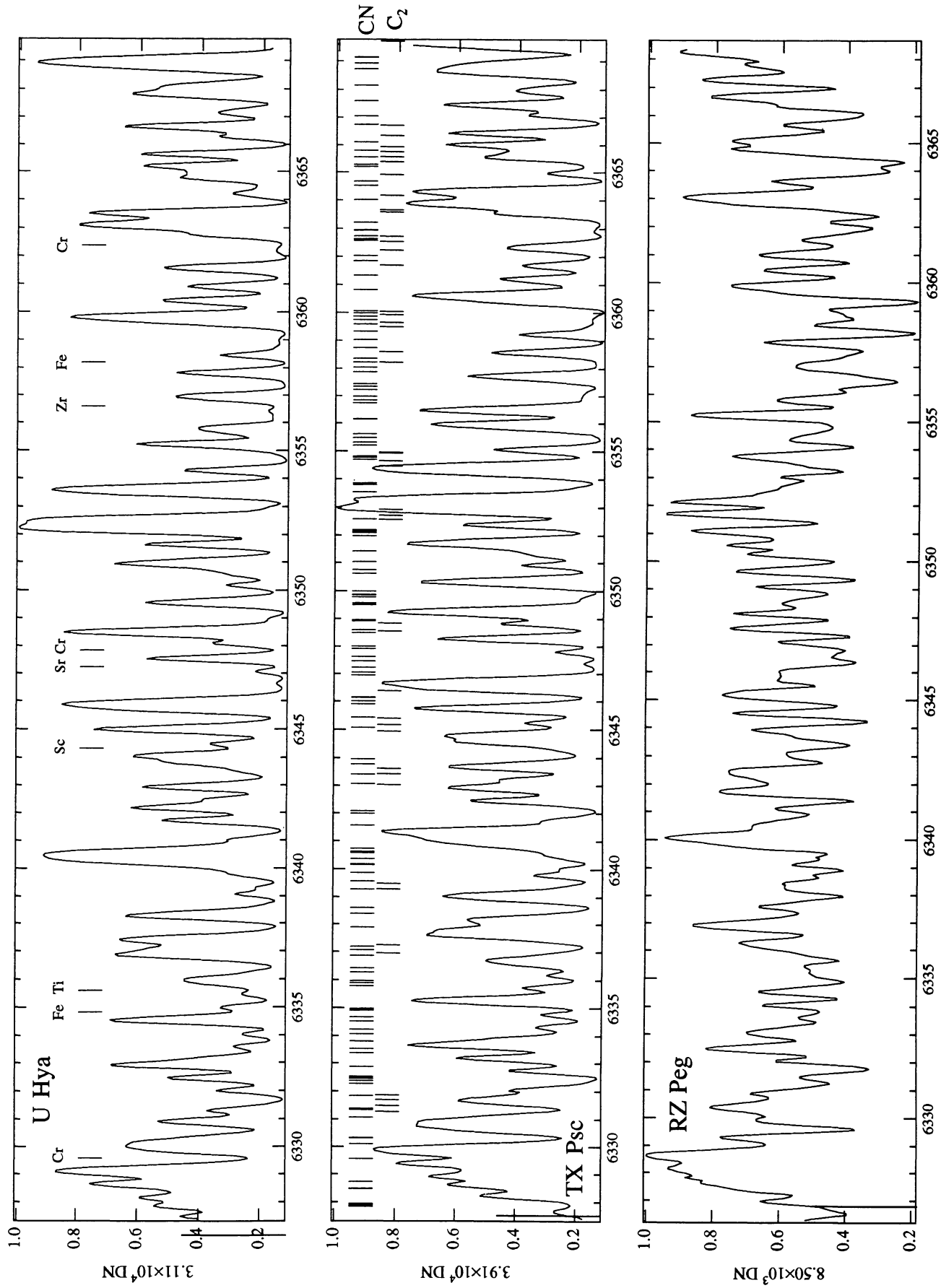

FIG. 27*a*

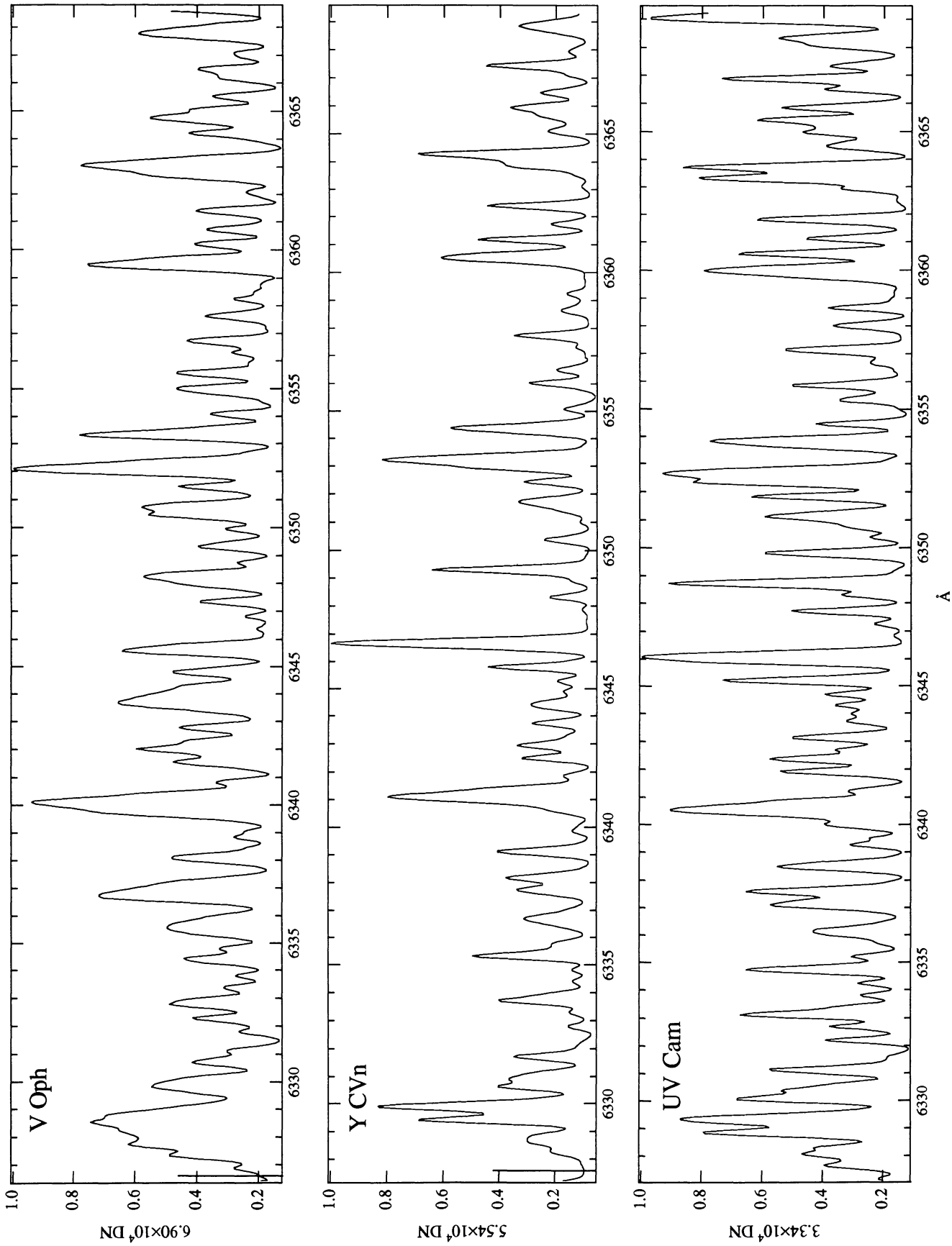

FIG. 27*b*

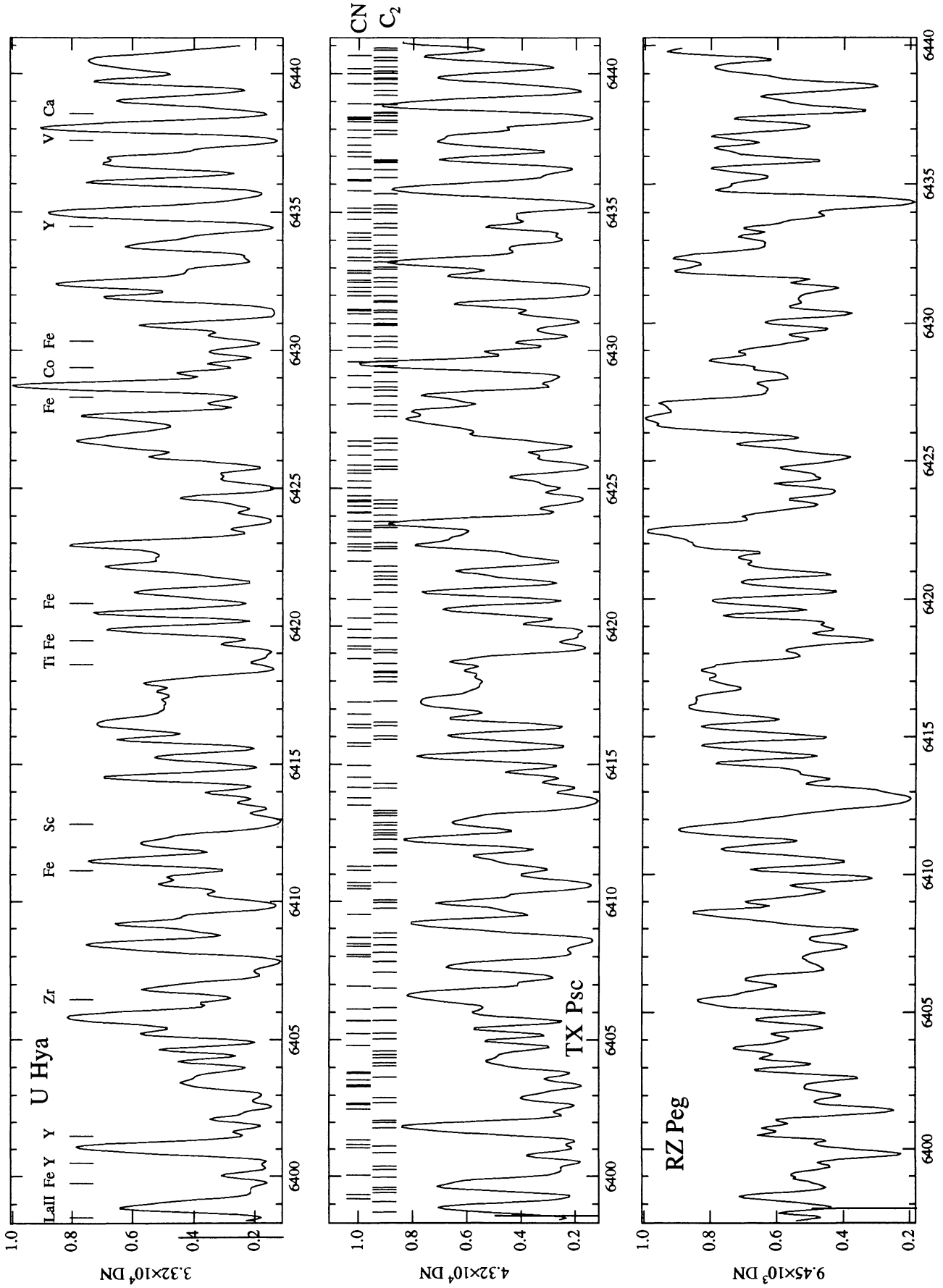

FIG. 28*a*

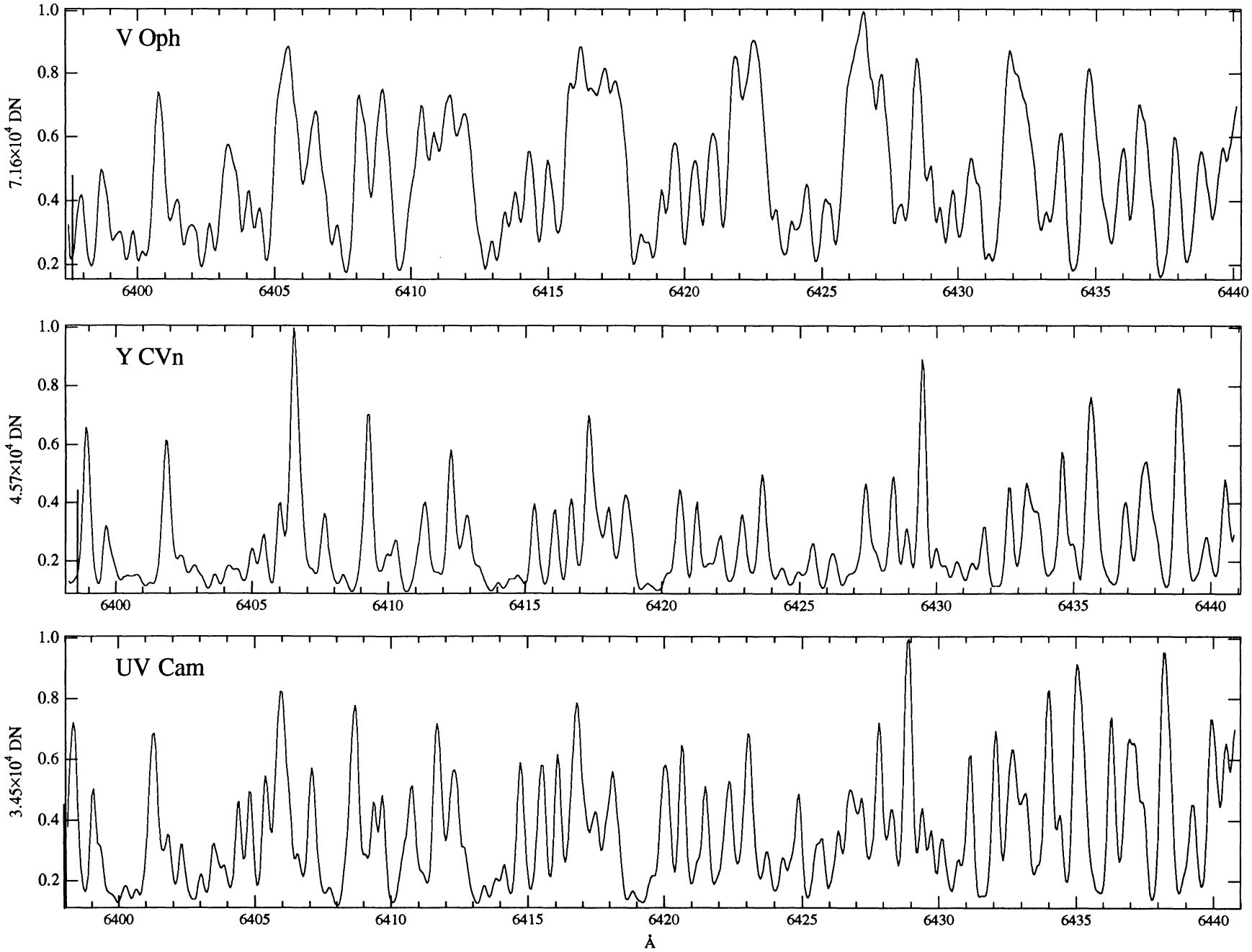

FIG. 28*b*

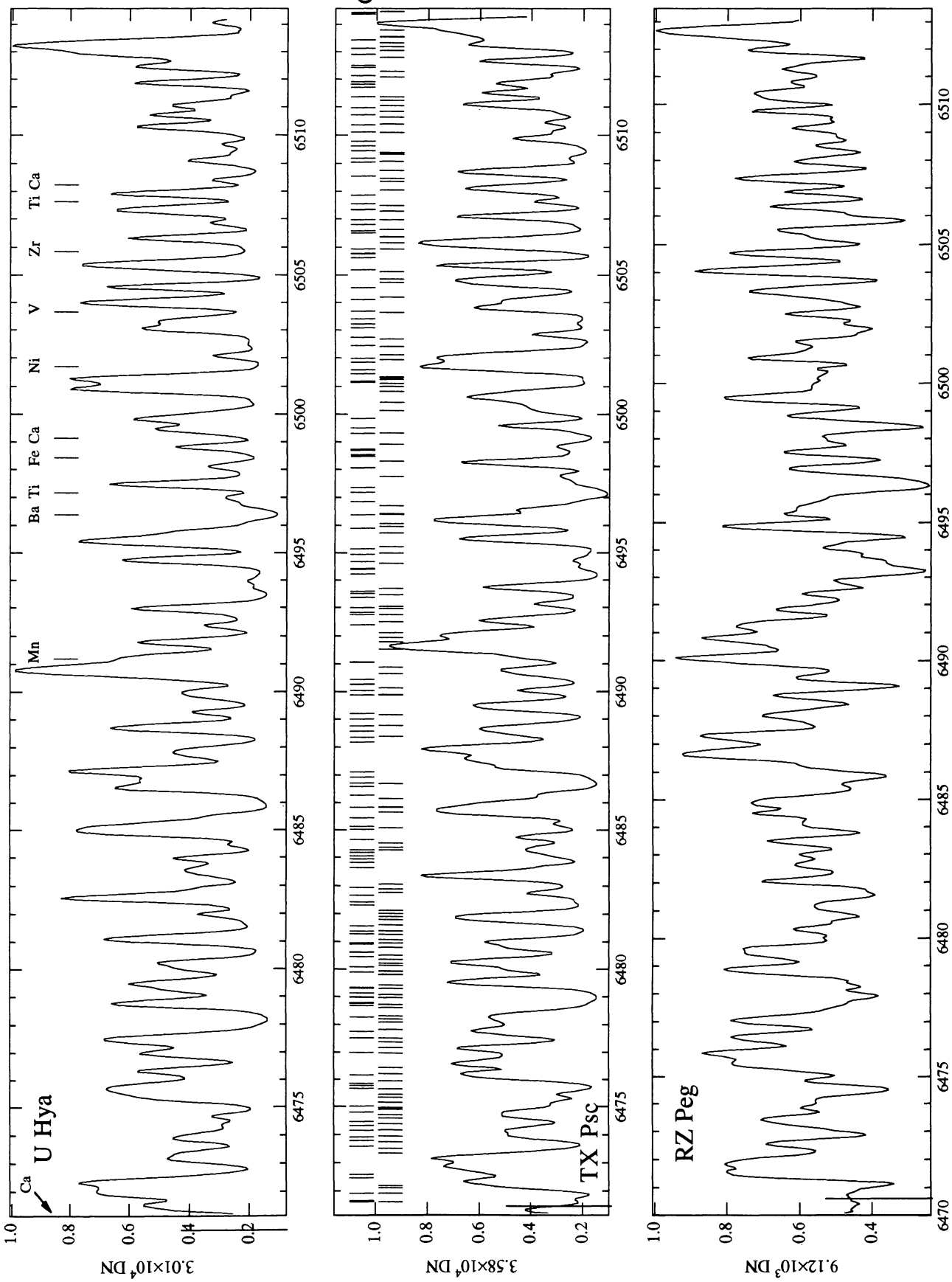

FIG. 29*a*

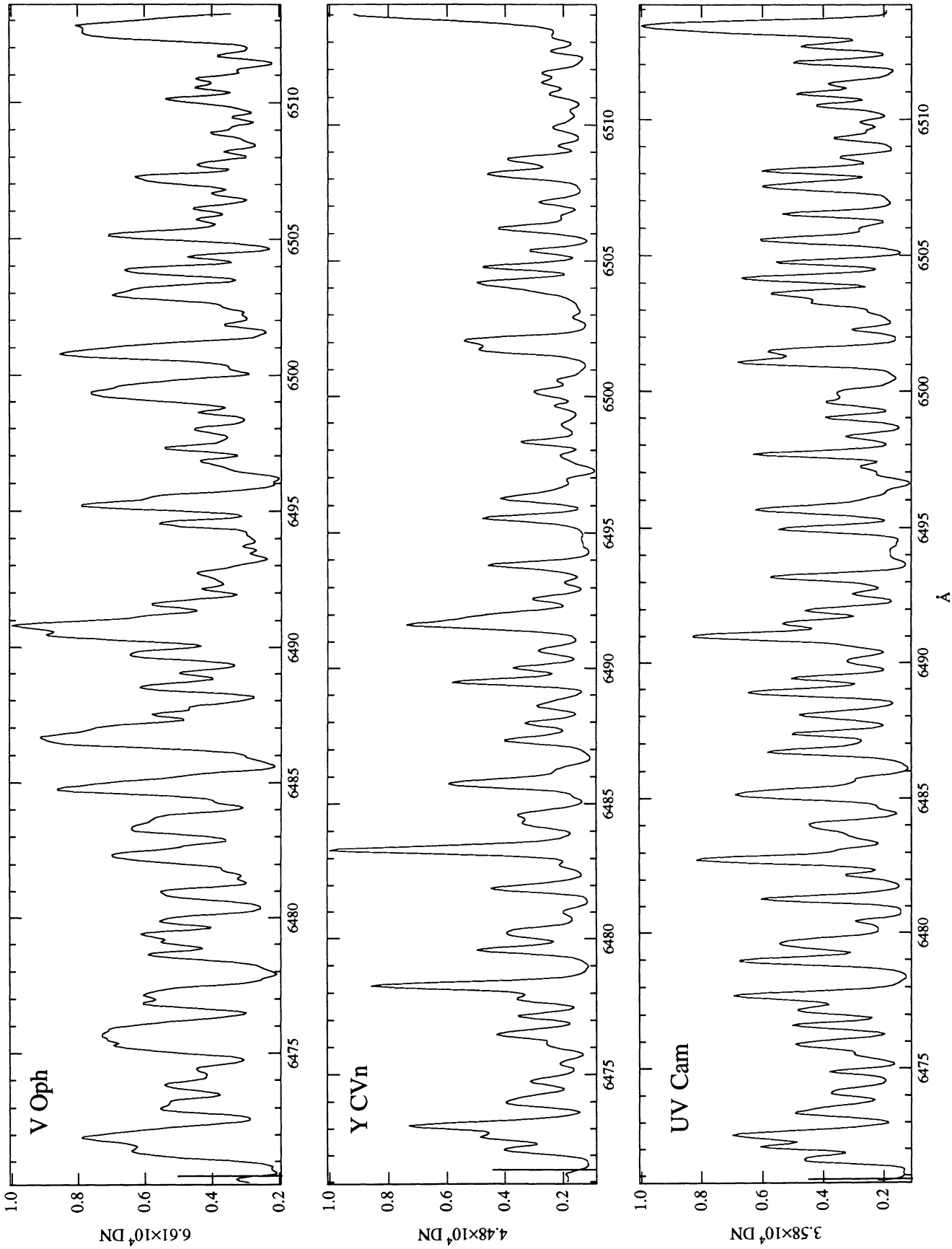

FIG. 29*b*

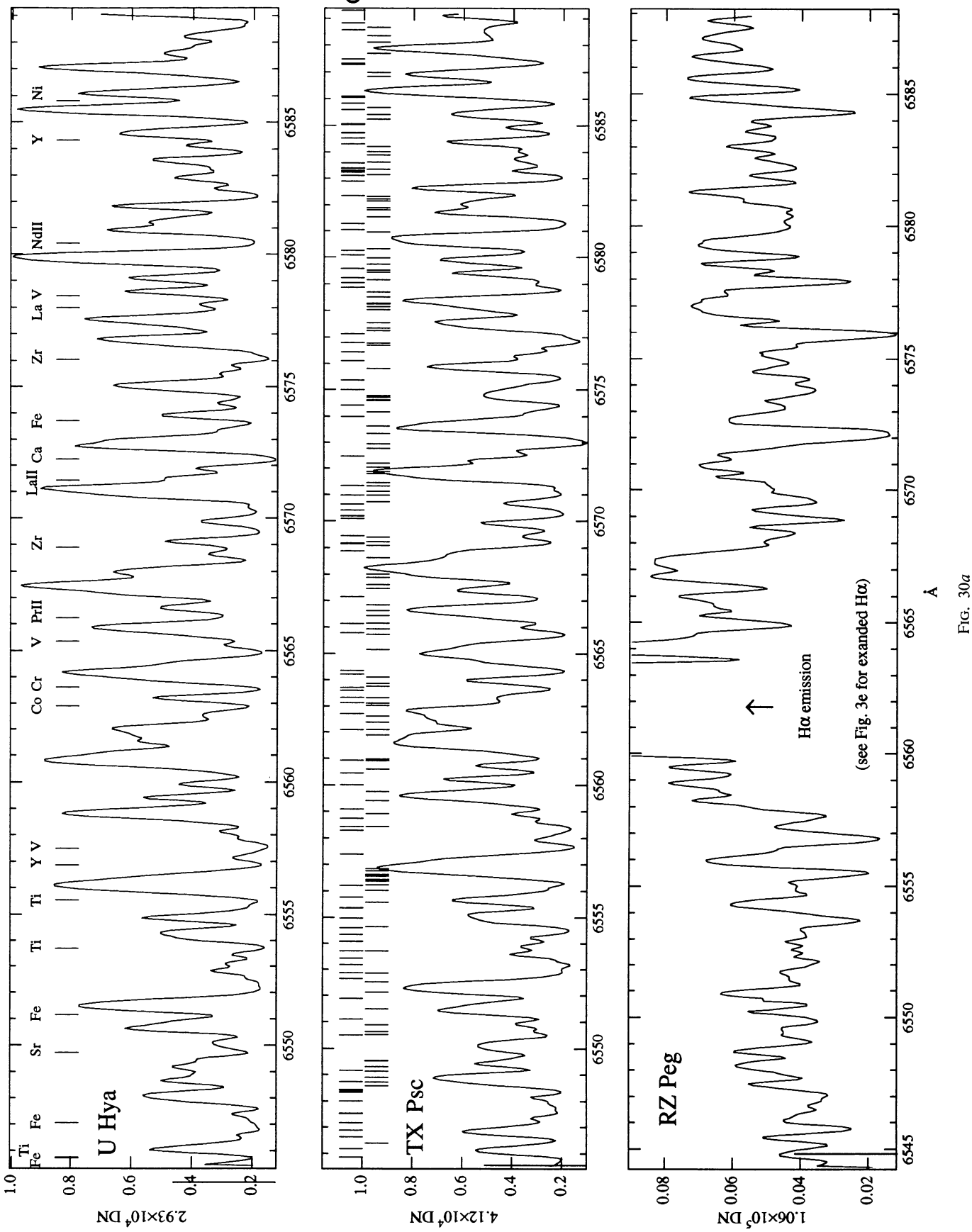

FIG. 30*a*

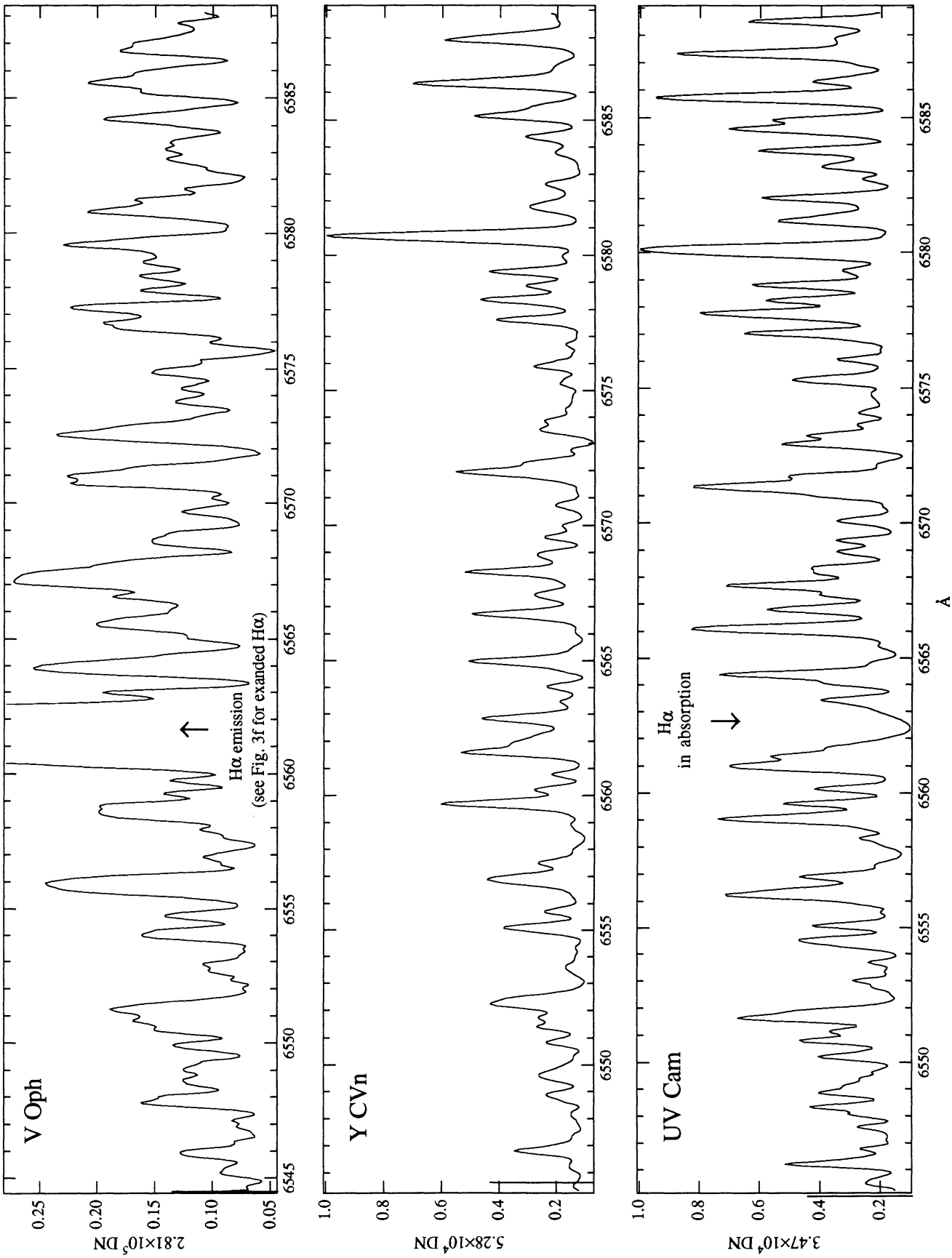

FIG. 30*b*

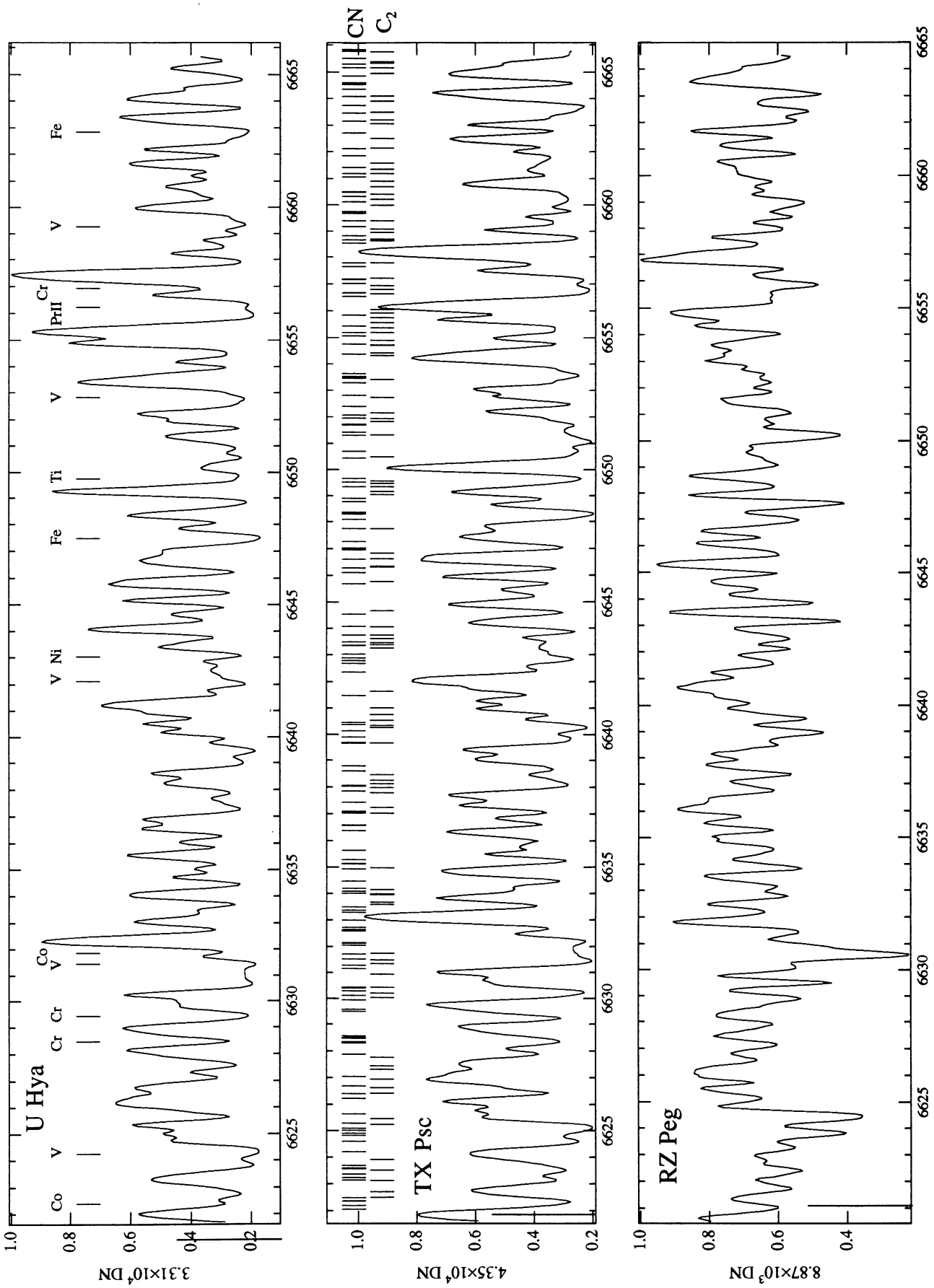

FIG. 31*a*

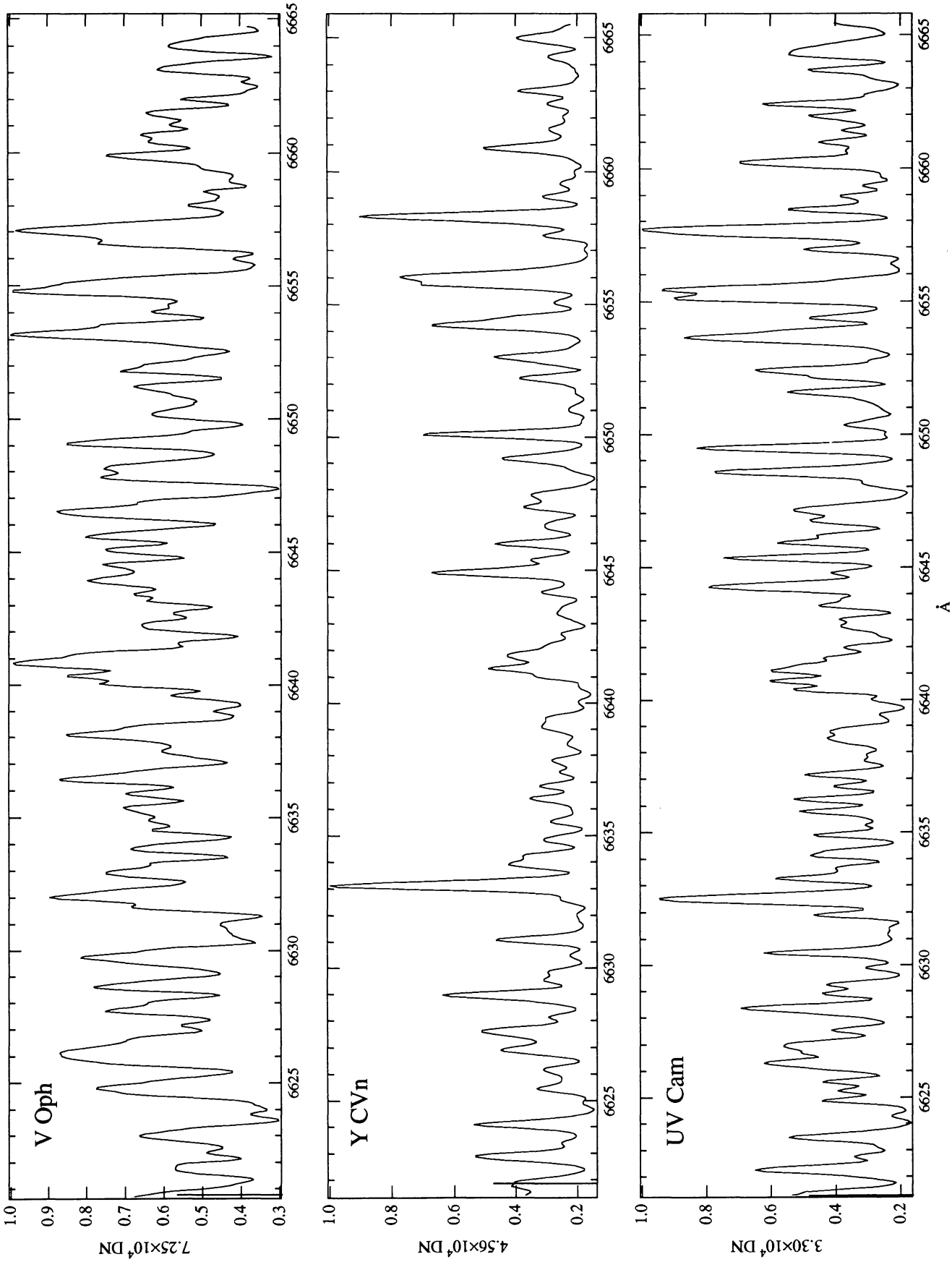

FIG. 31*b*

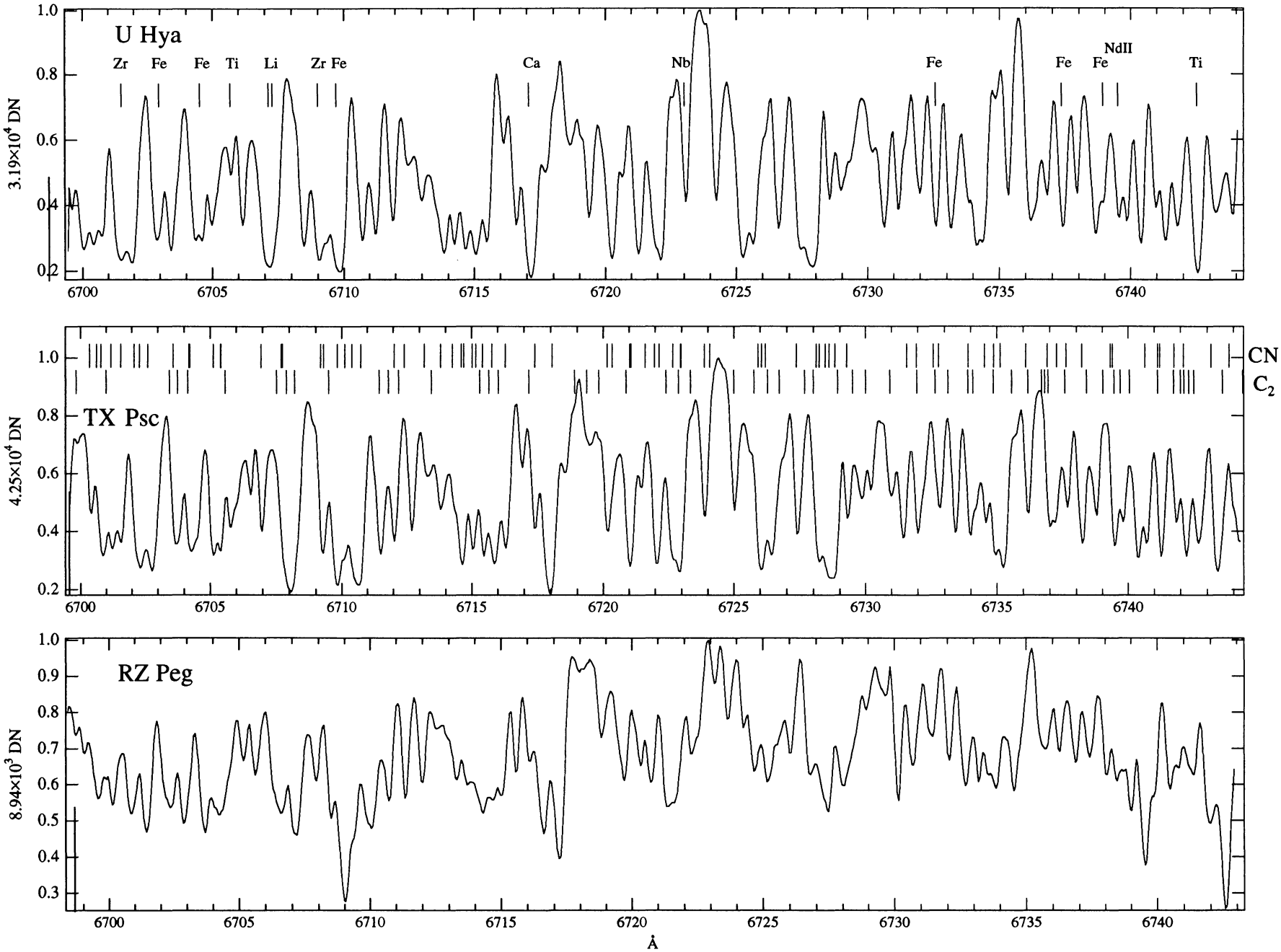

FIG. 32*a*

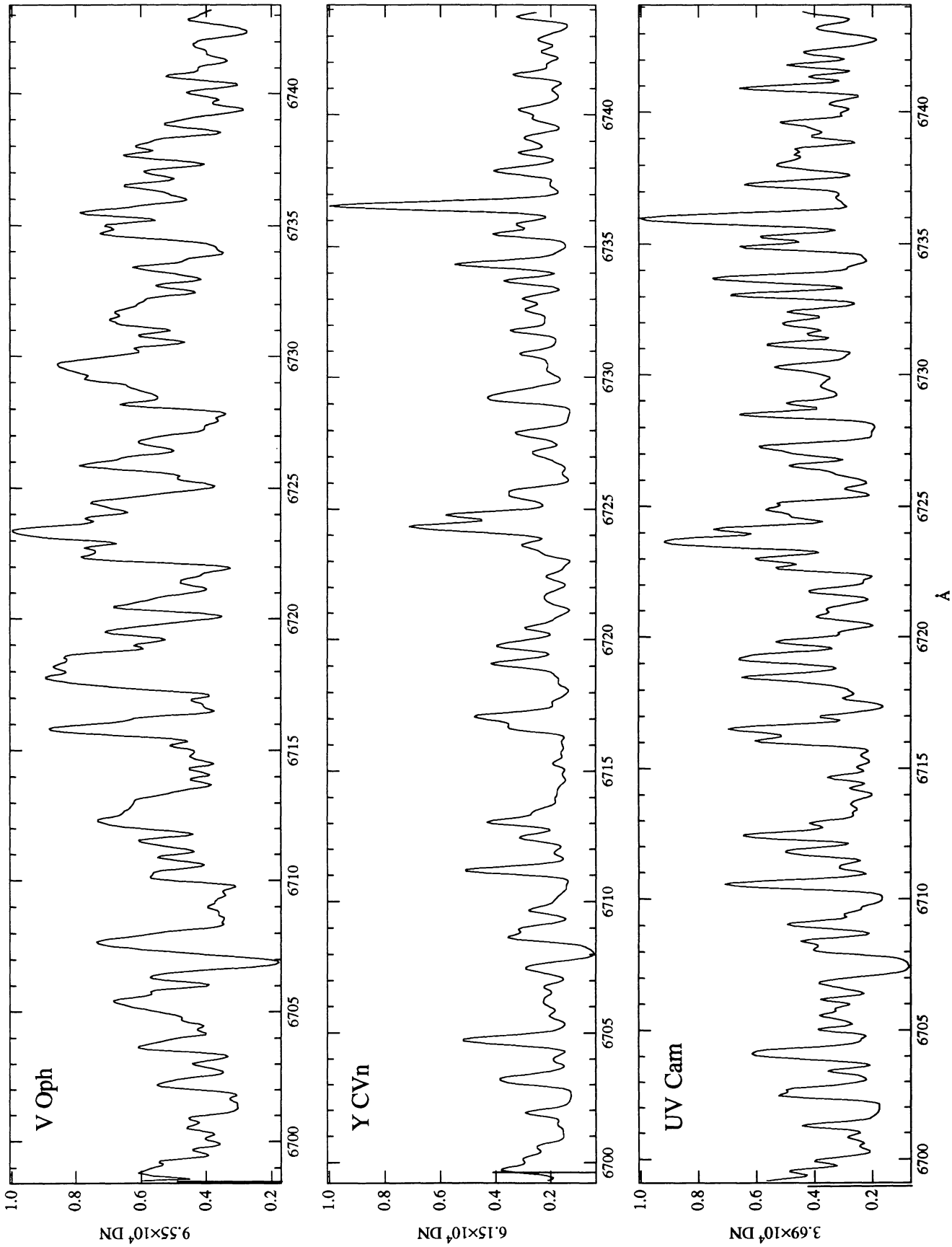

FIG. 32*b*

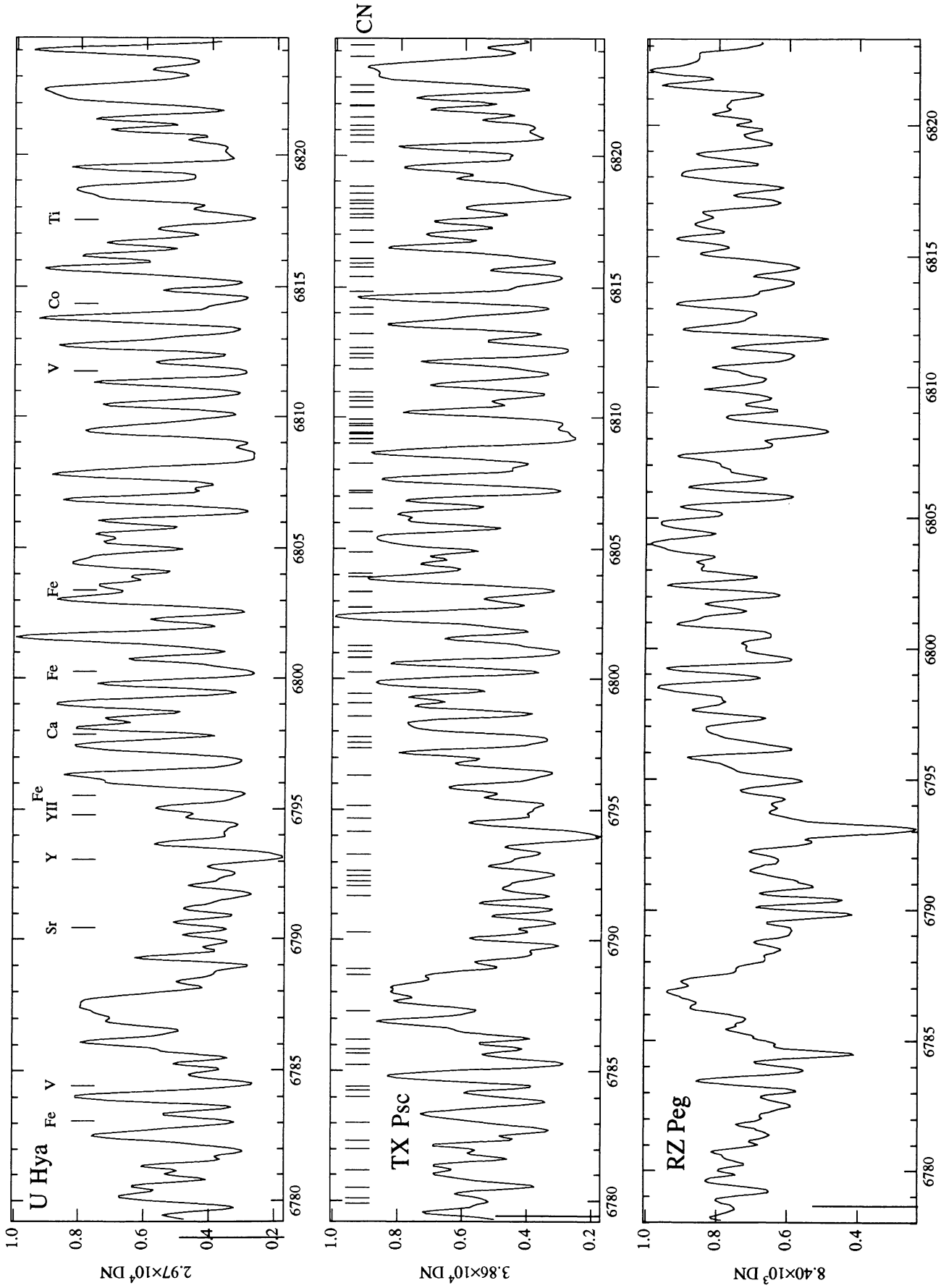

FIG. 33*a*

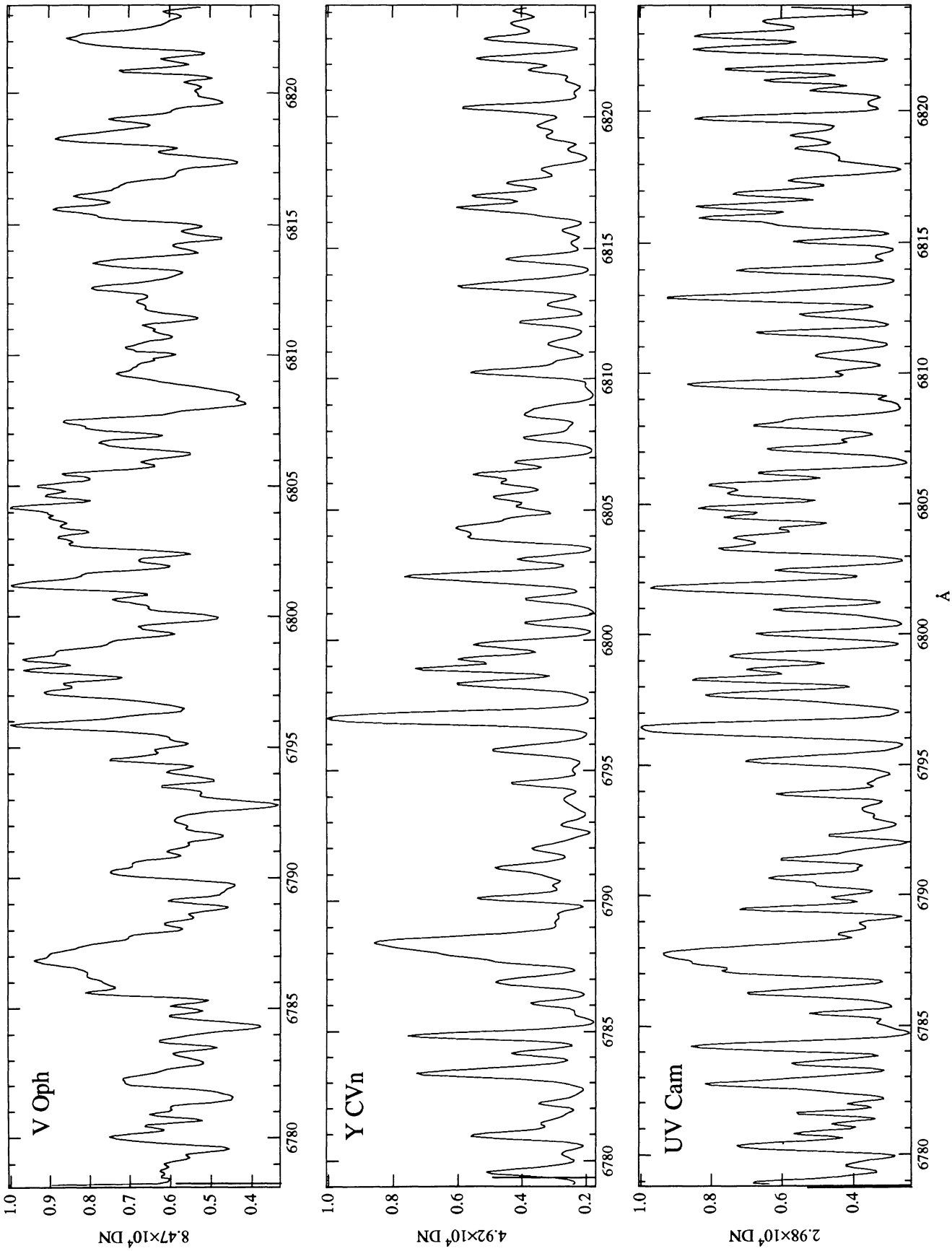

FIG. 33*b*

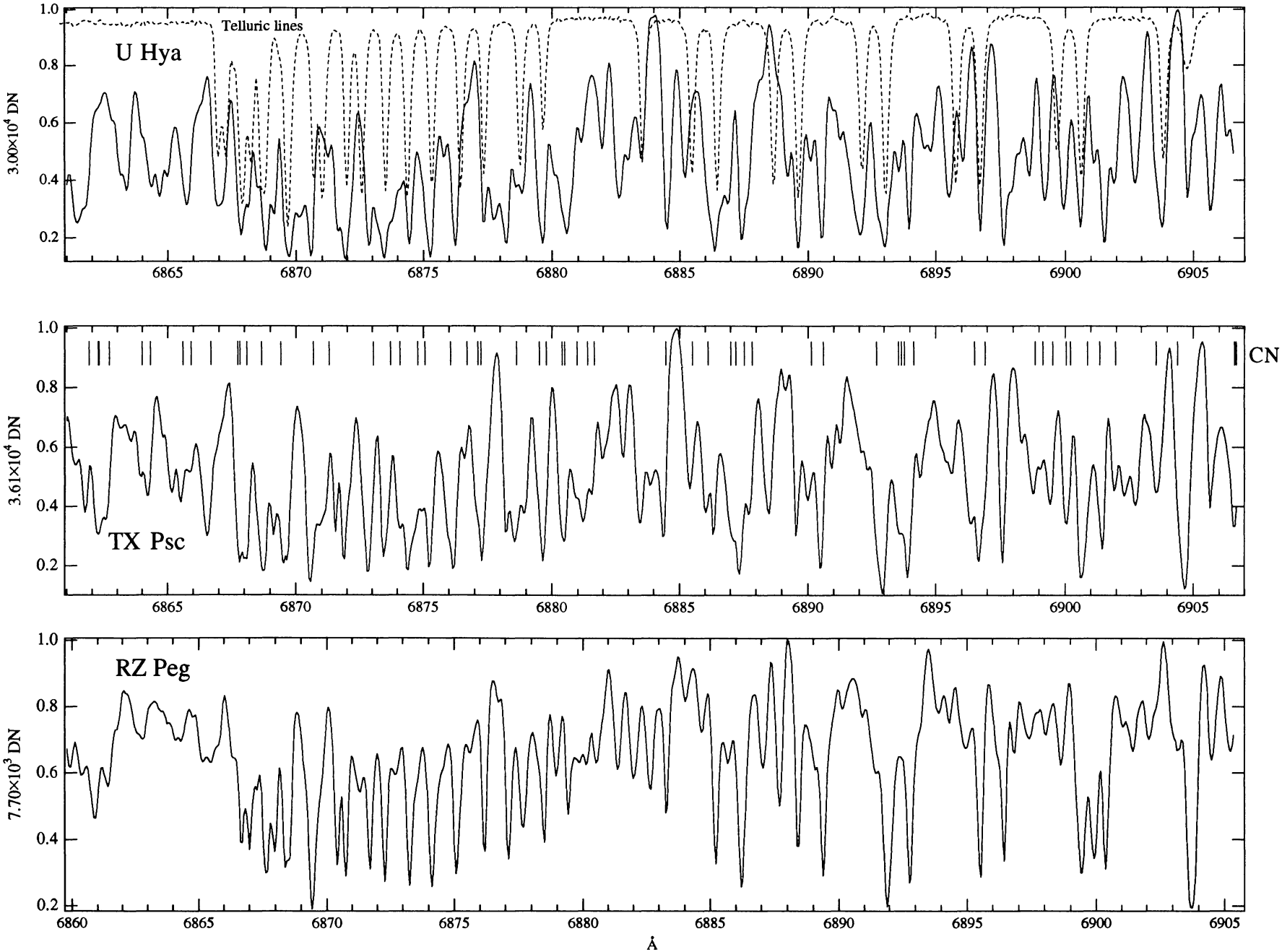

FIG. 34*a*

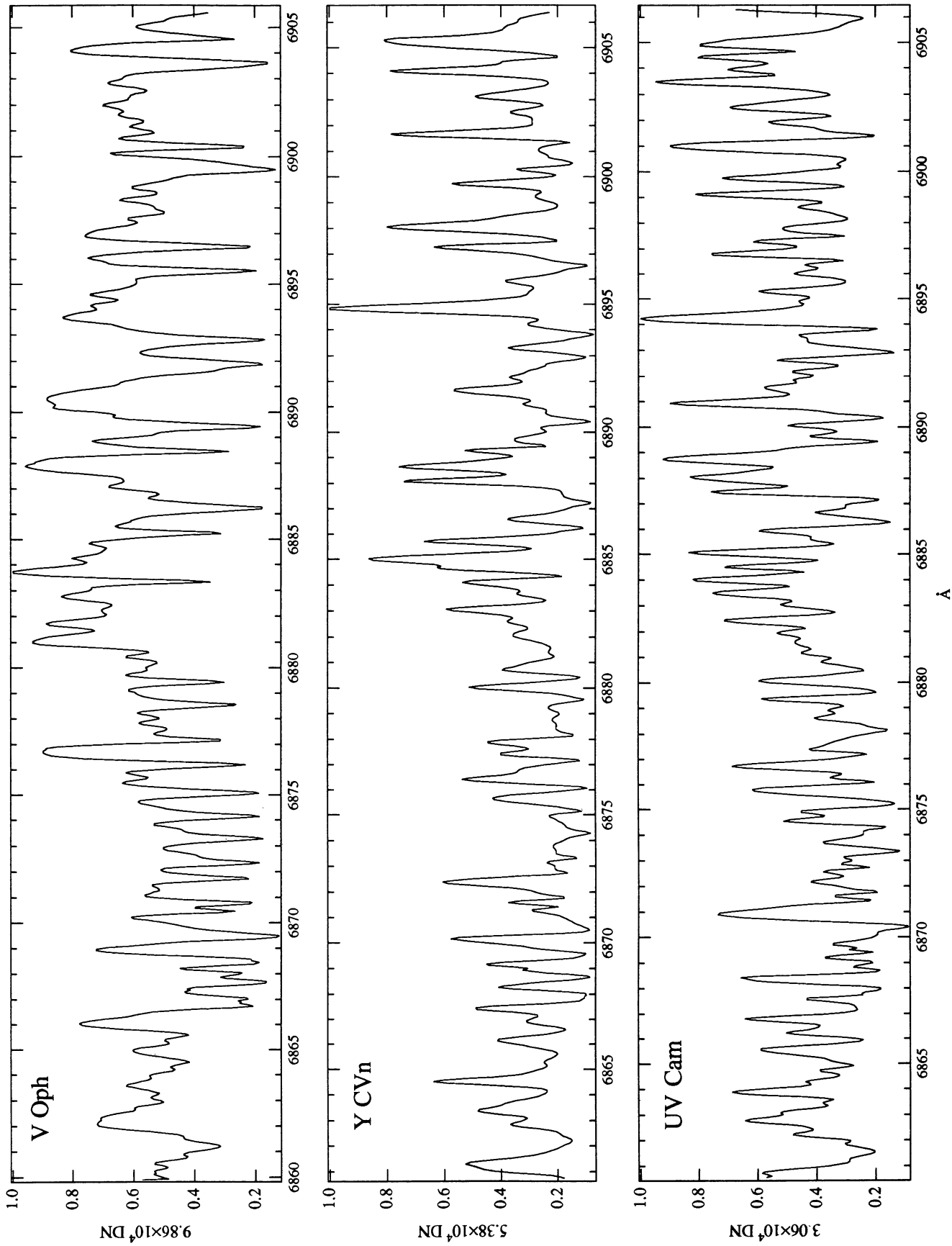

FIG. 34*b*

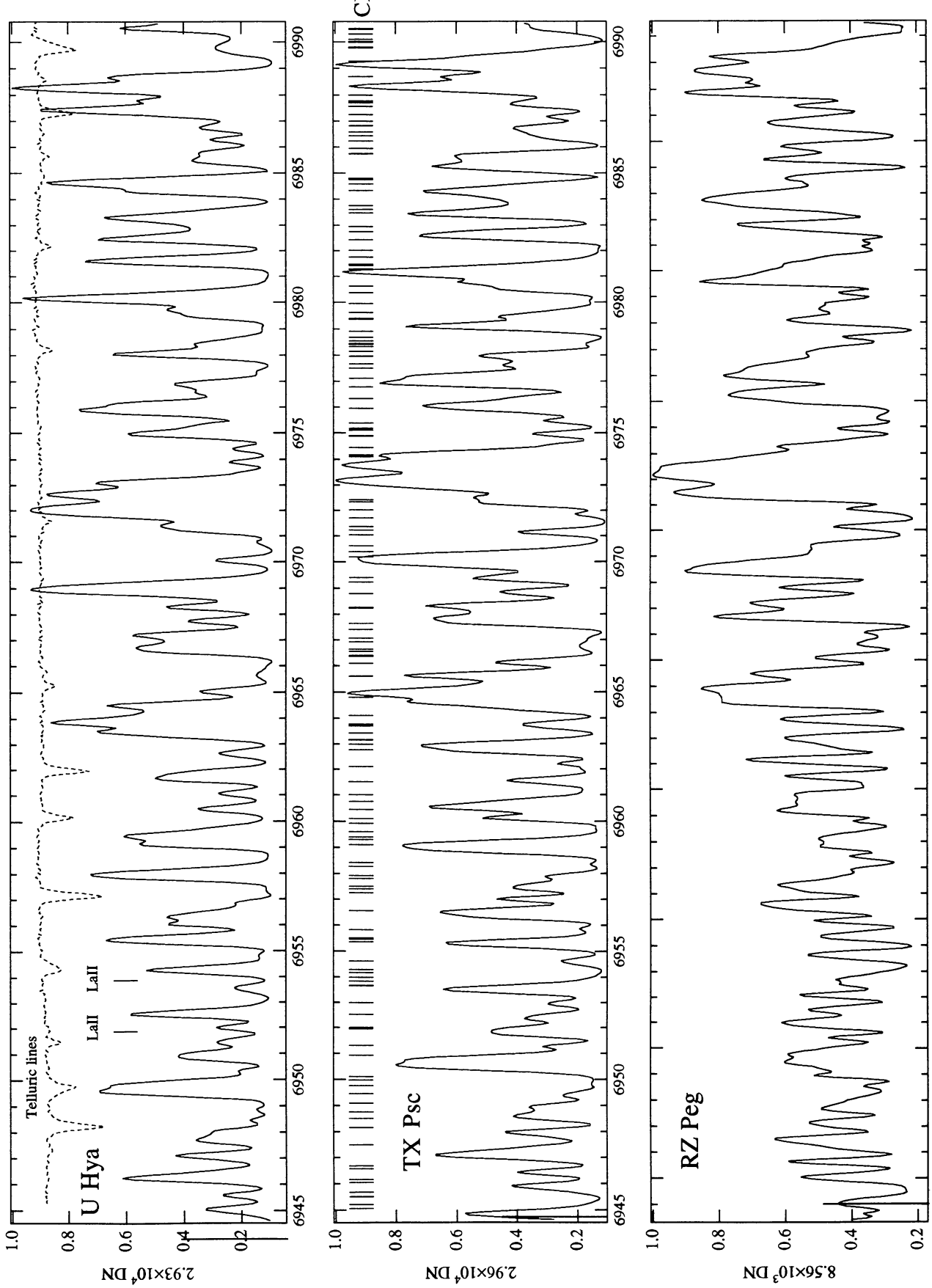

FIG. 35*a*

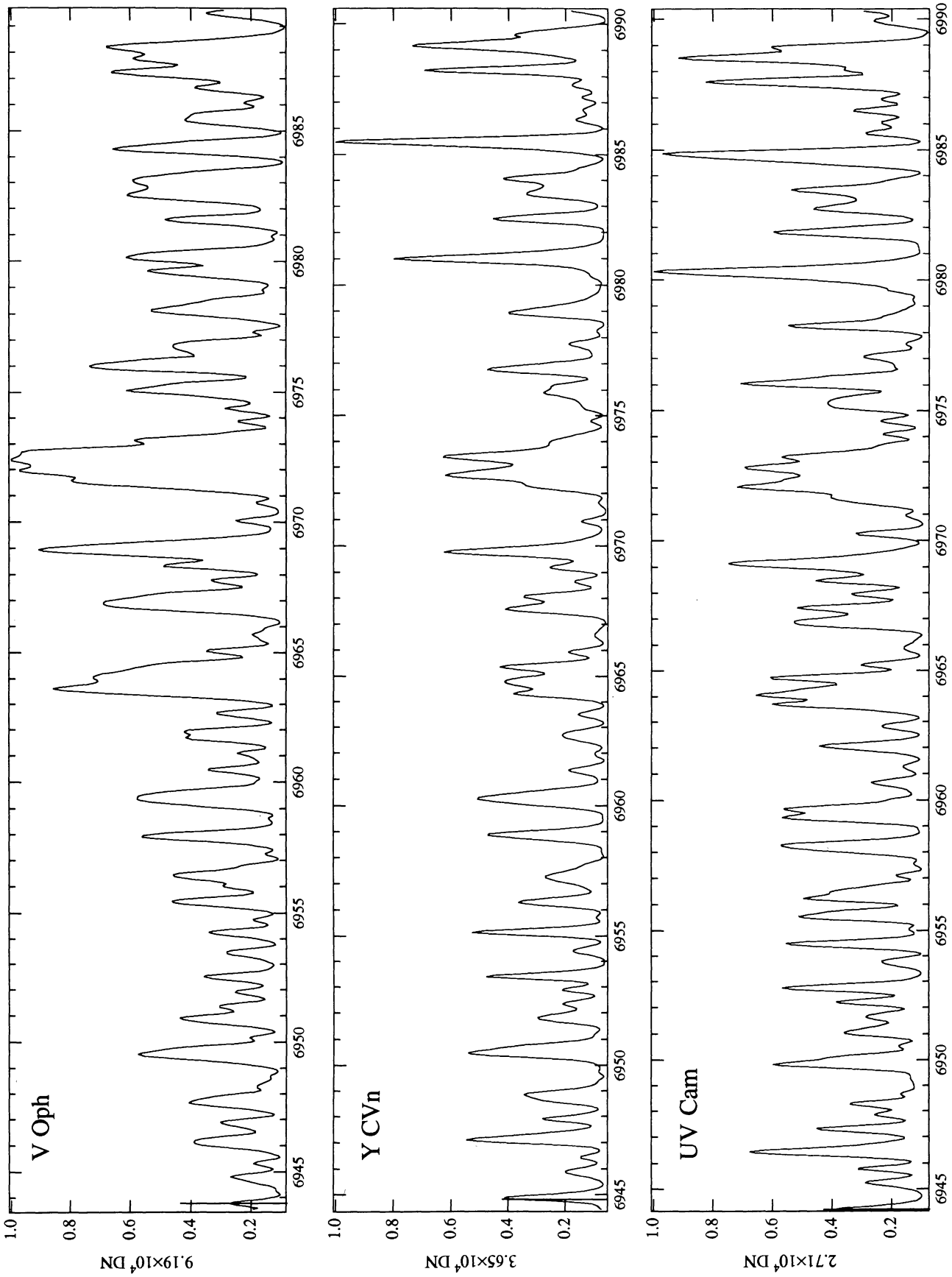

FIG. 35*b*

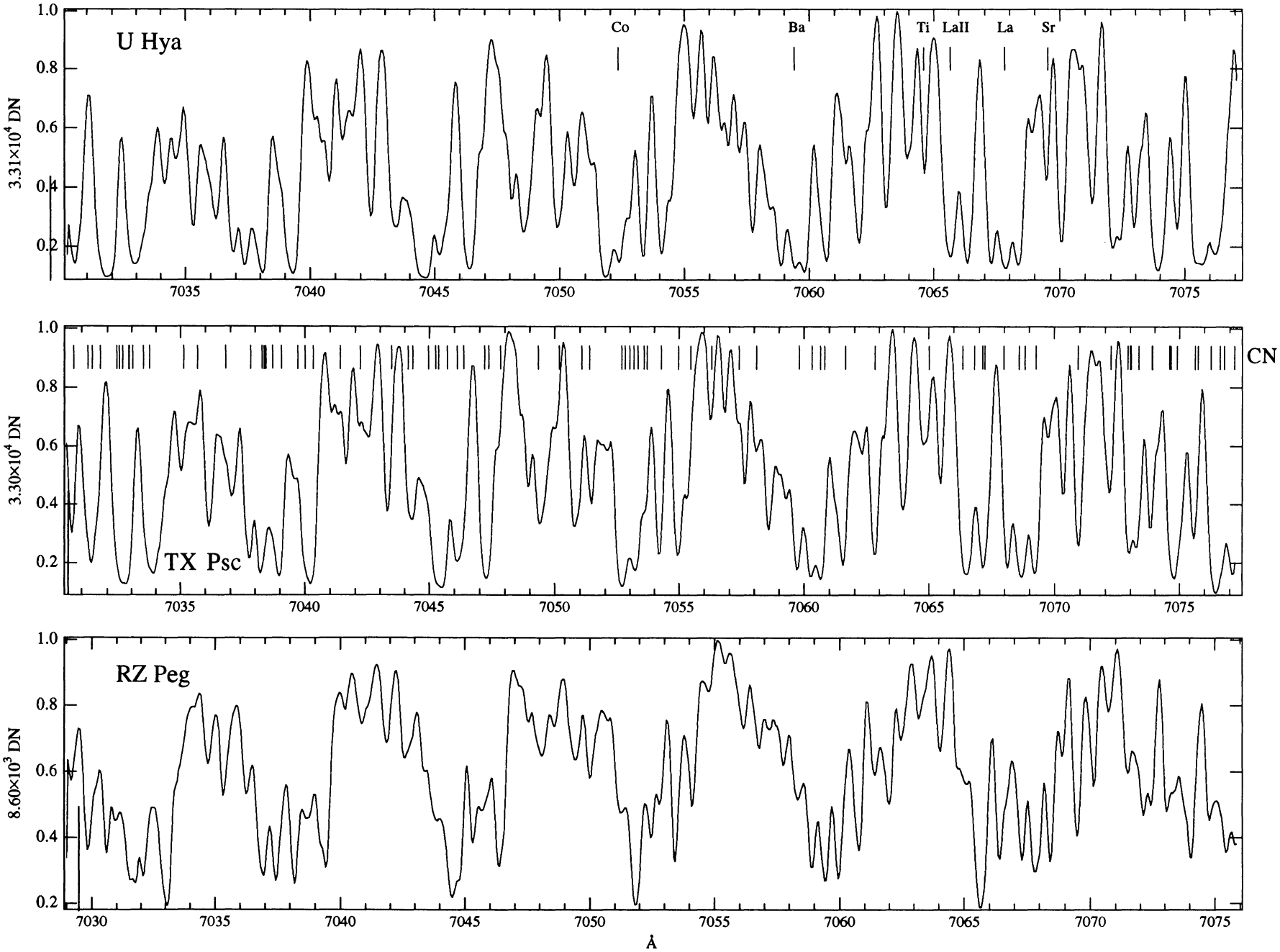

FIG. 36*a*

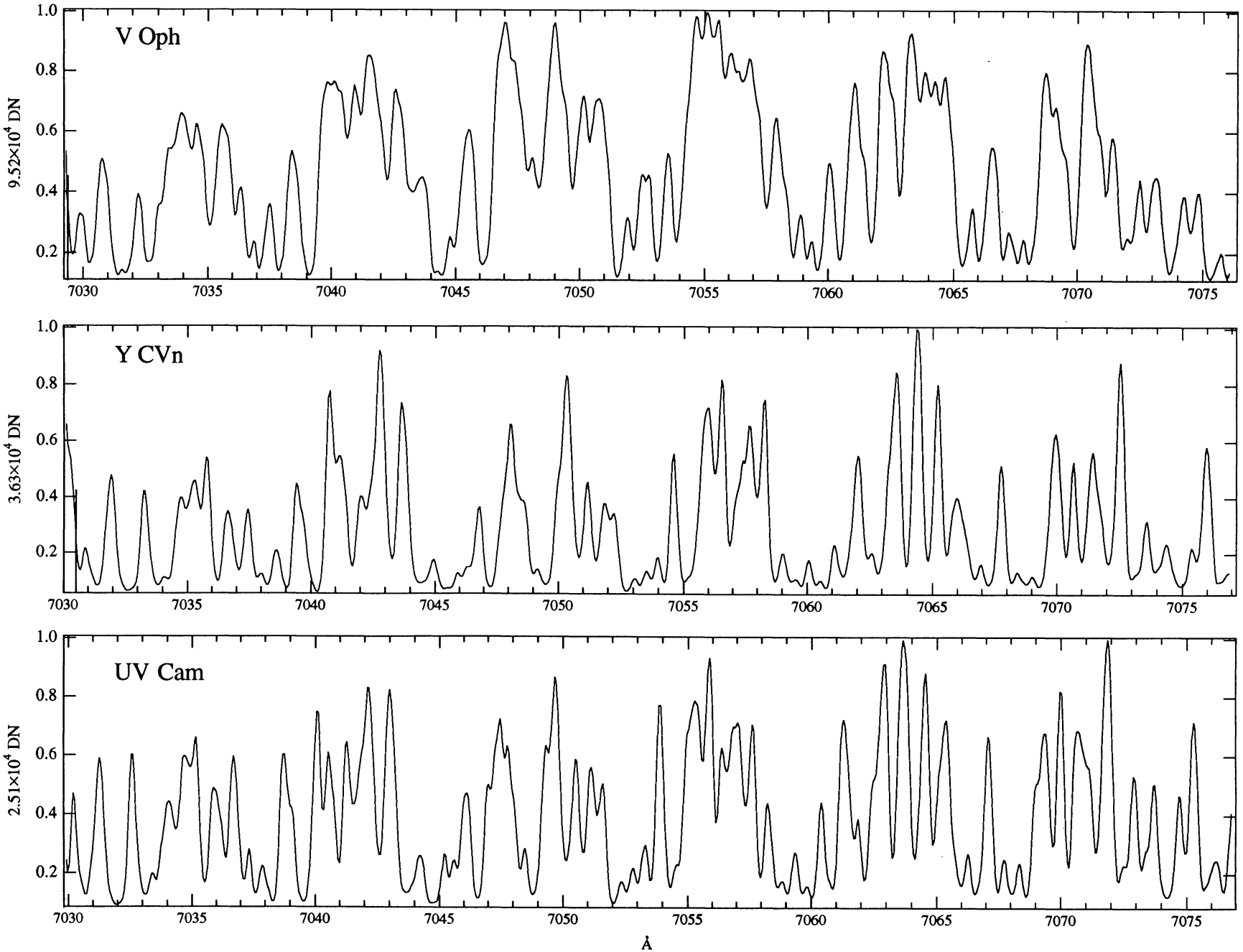

FIG. 36*b*

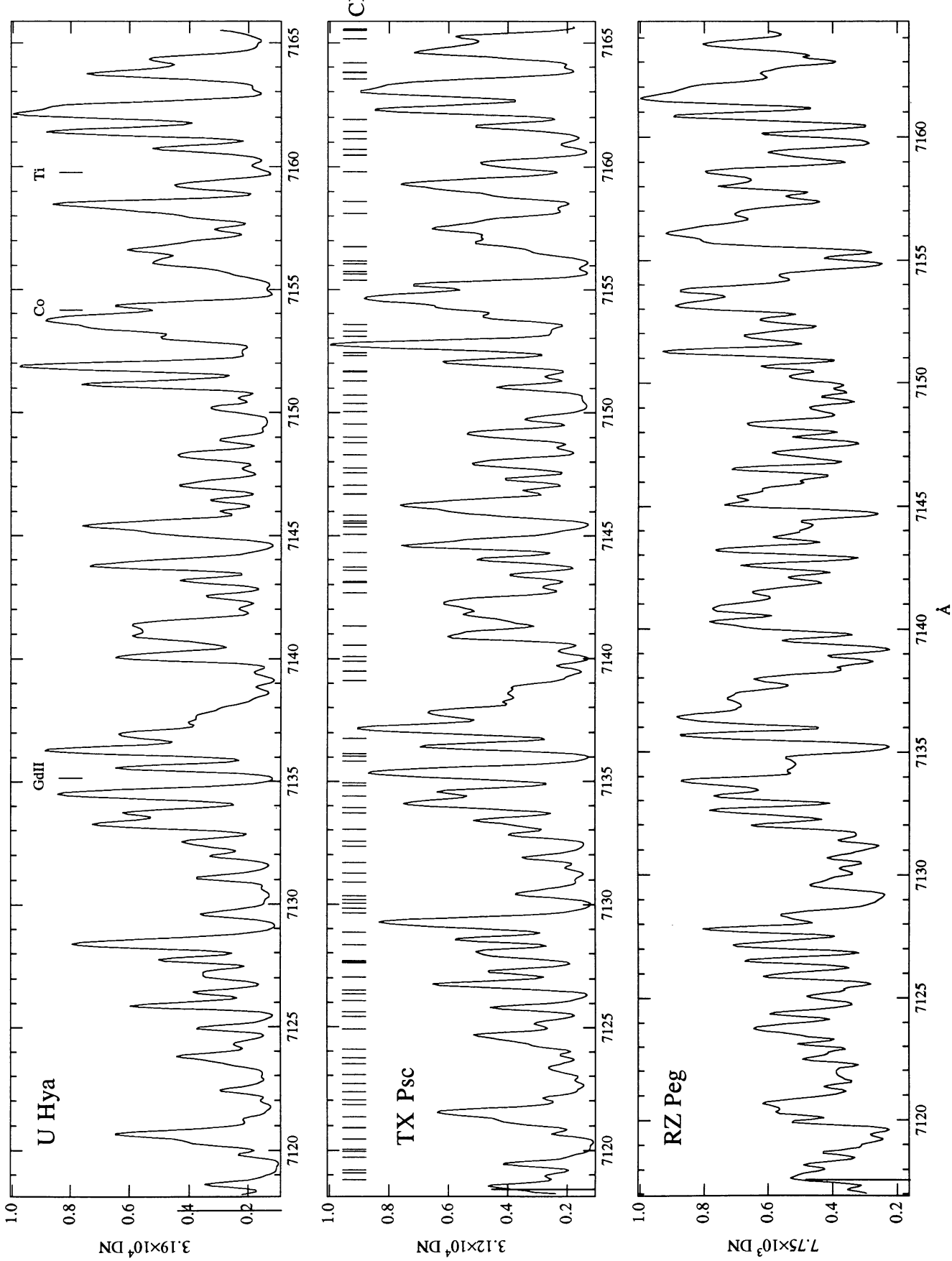

FIG. 37*a*

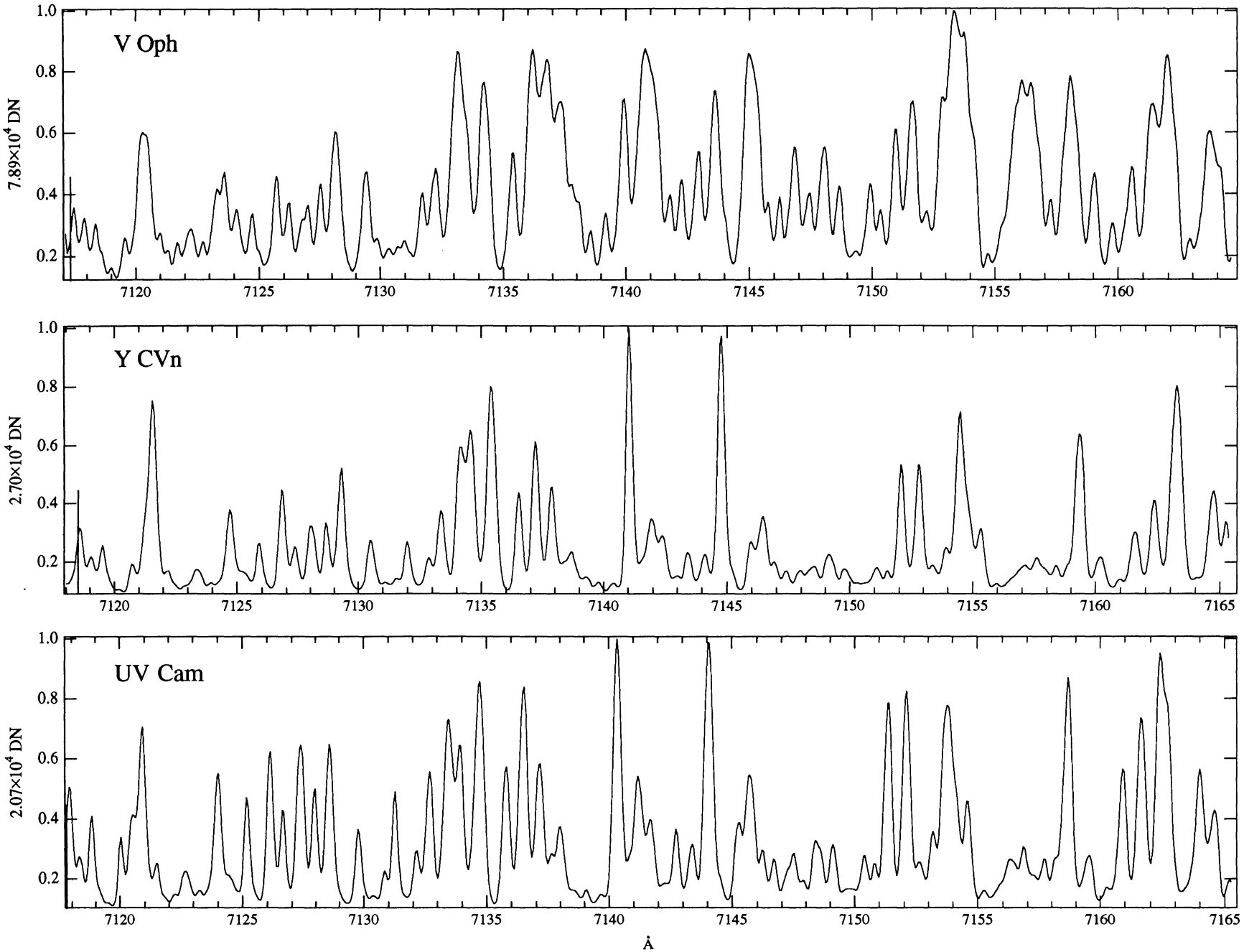

FIG. 37*b*

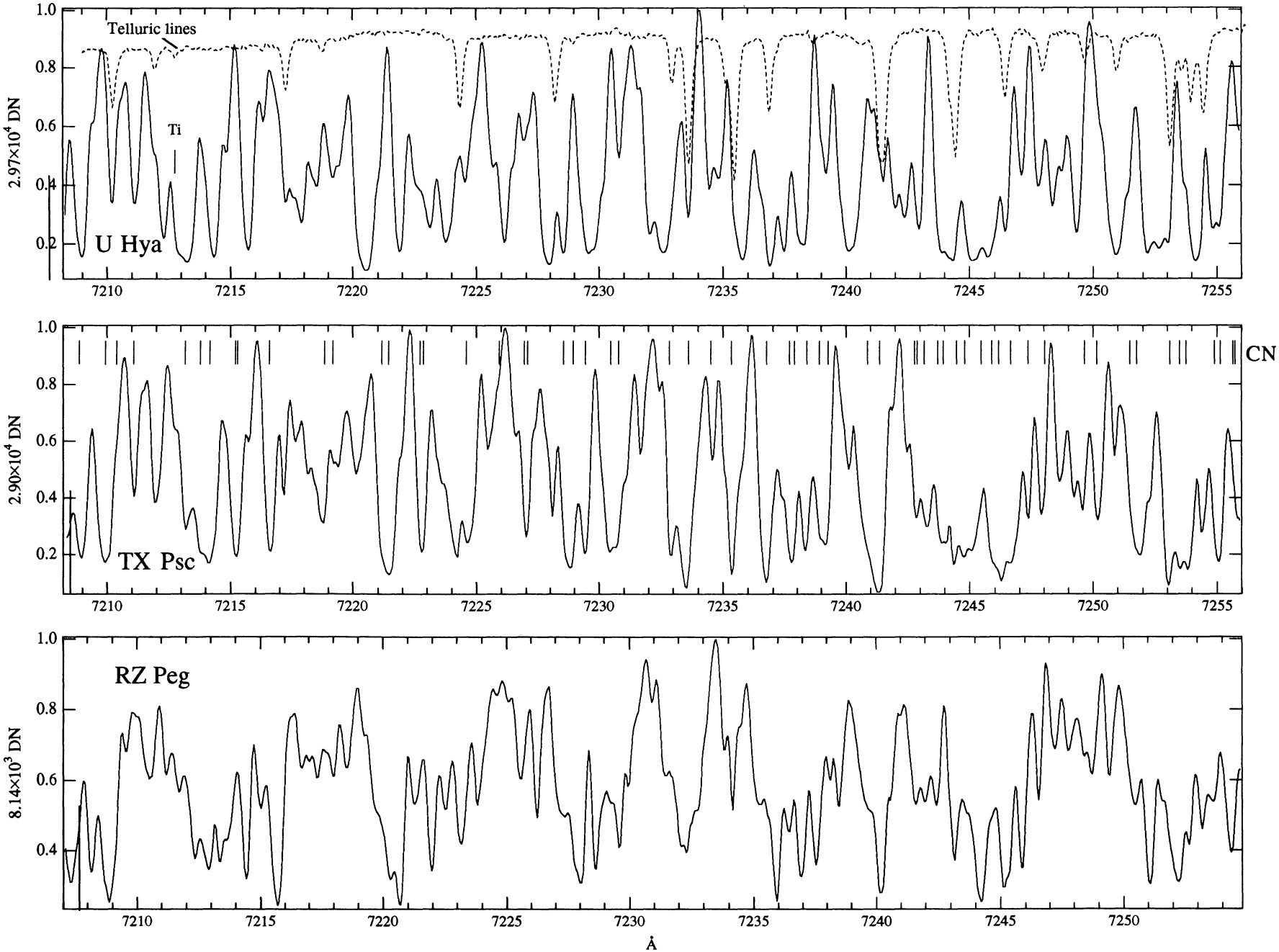

FIG. 38*a*

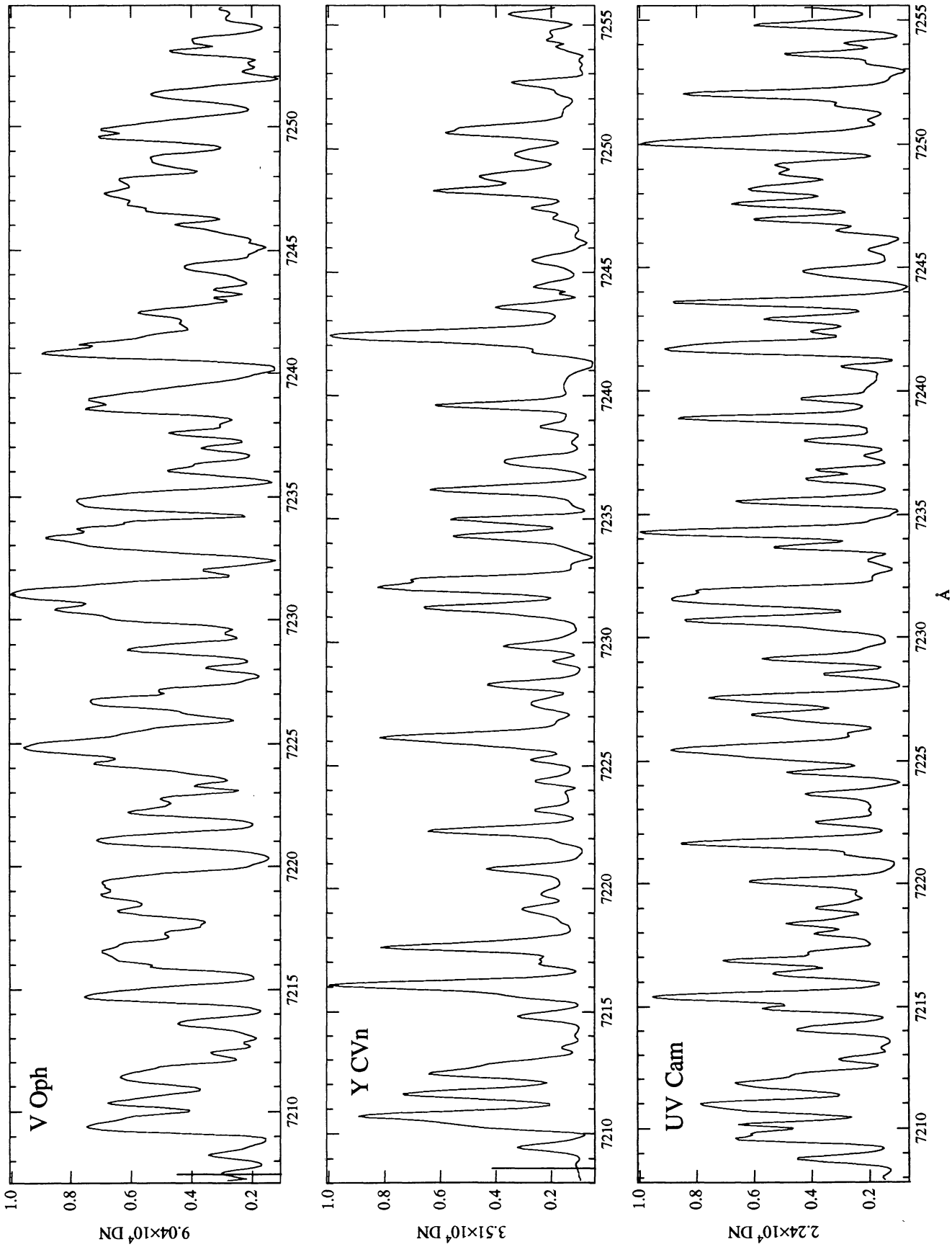

FIG. 38*b*

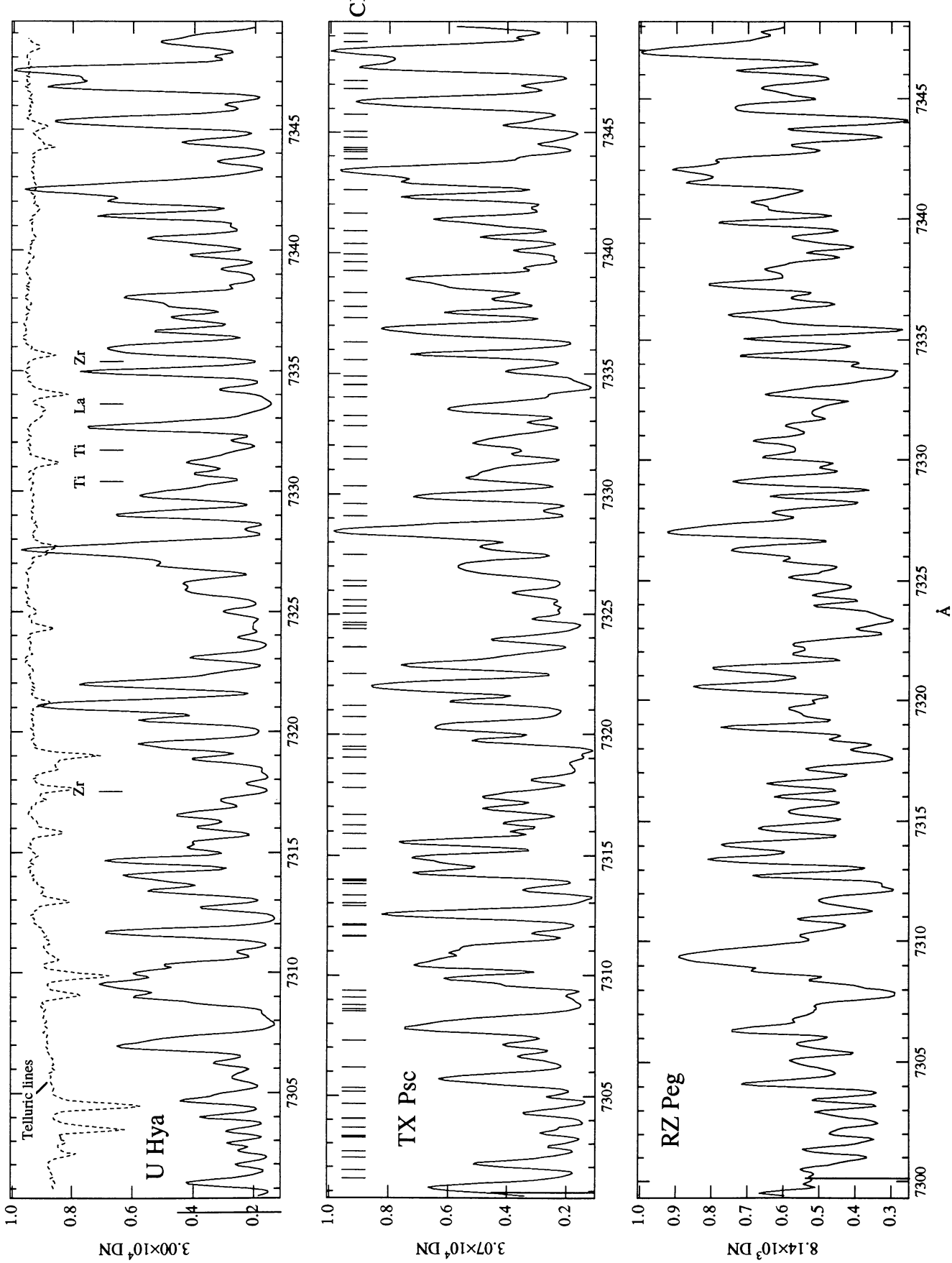

FIG. 39*a*

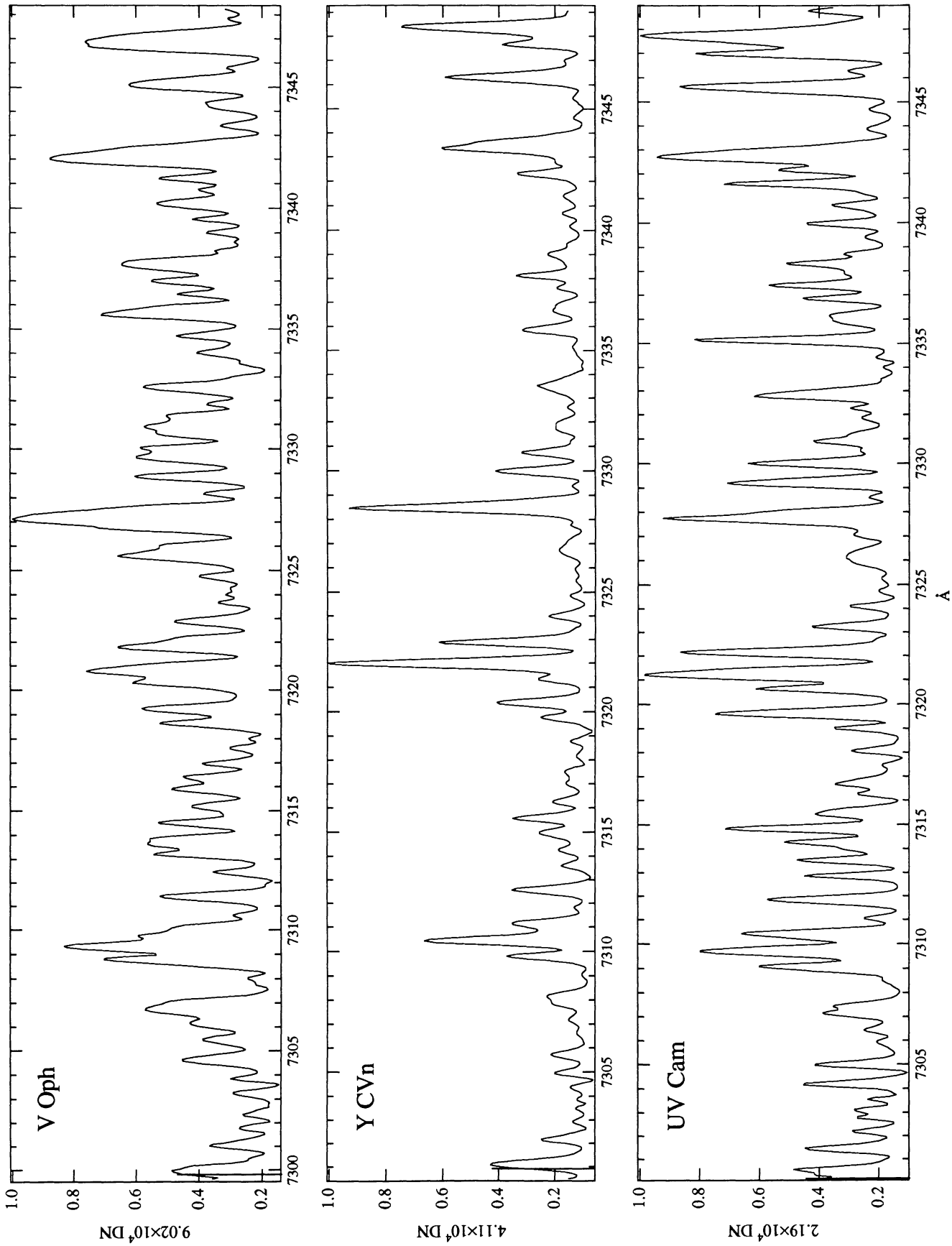

FIG. 39*b*

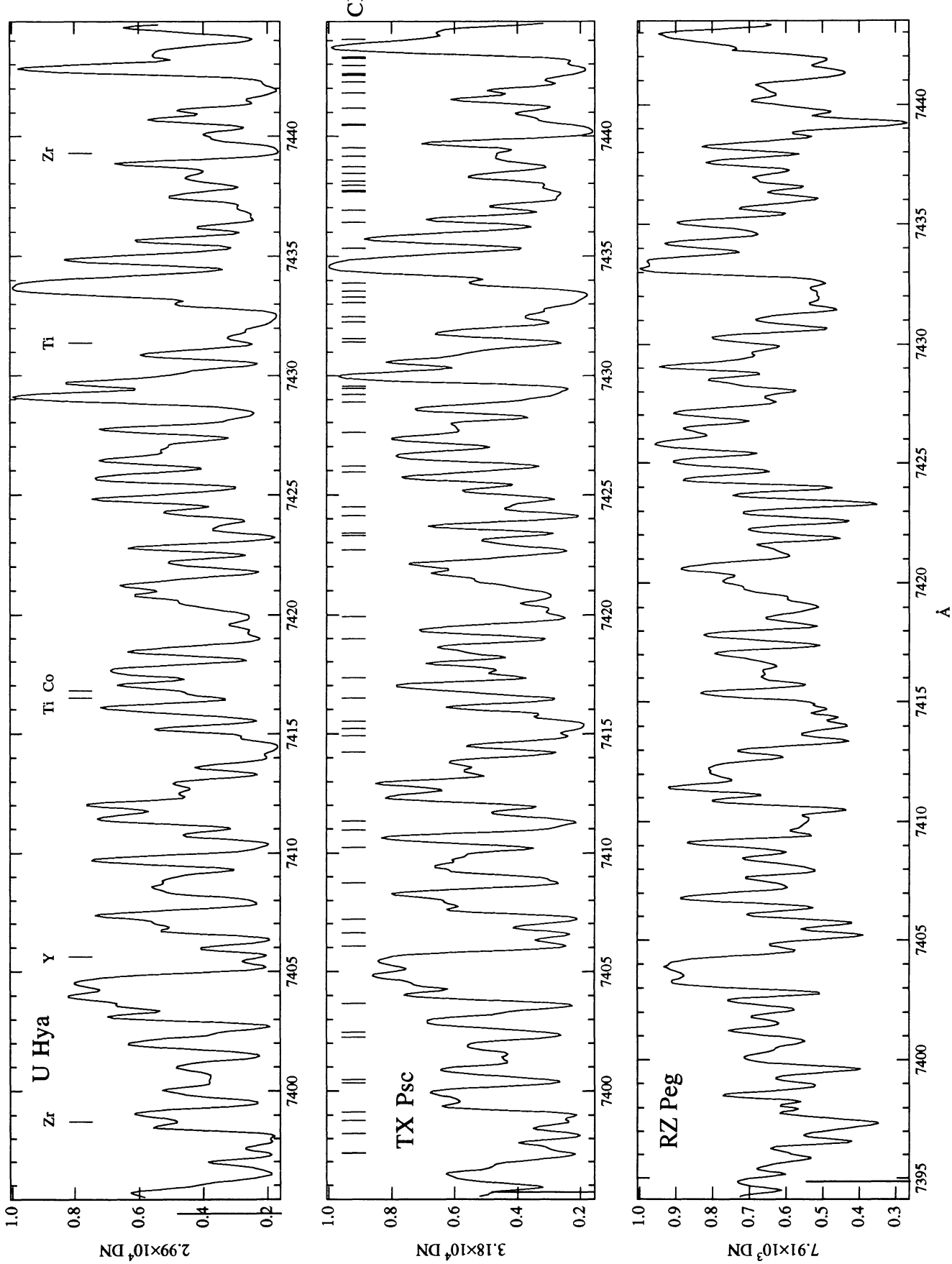

FIG. 40*a*

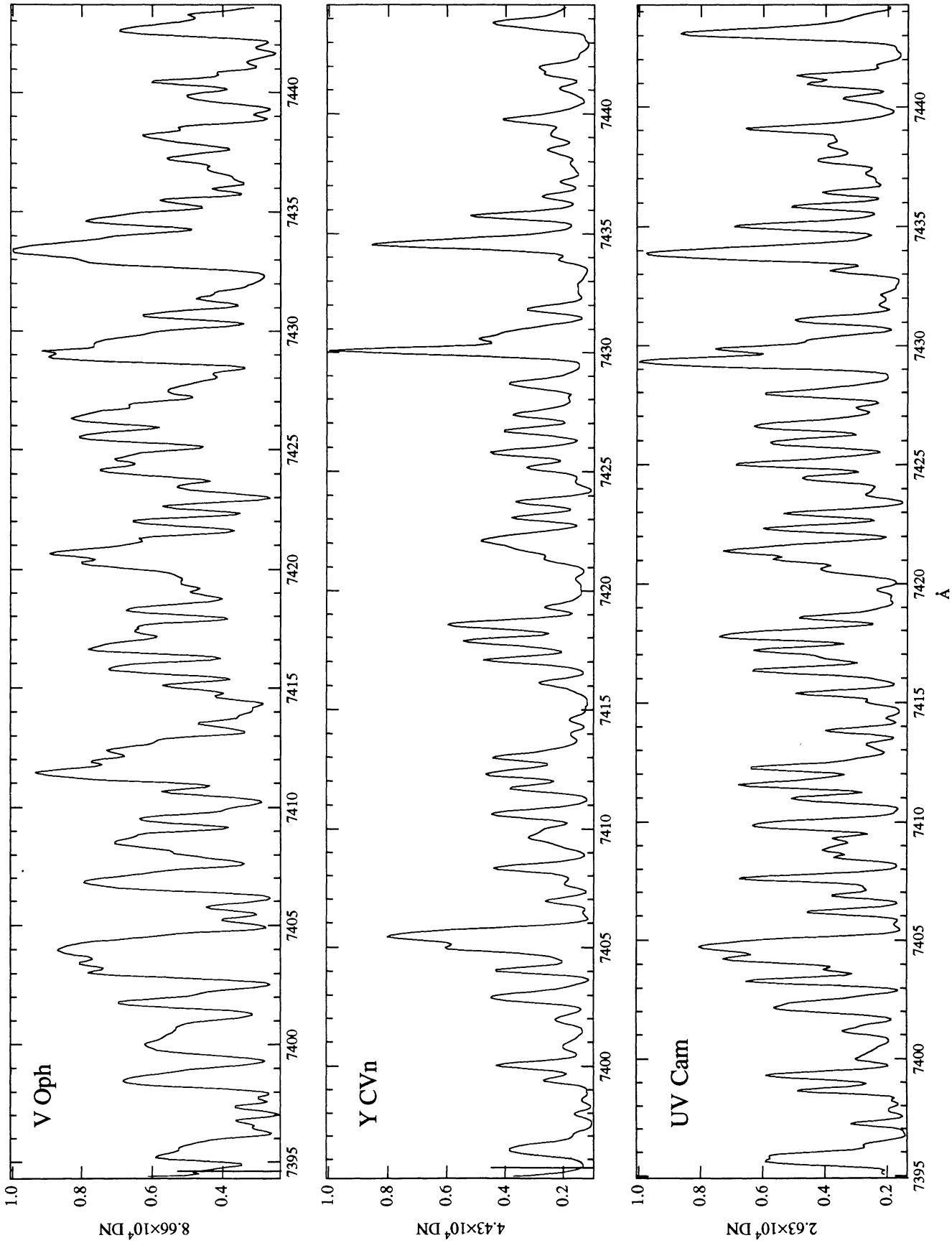

FIG. 40*b*

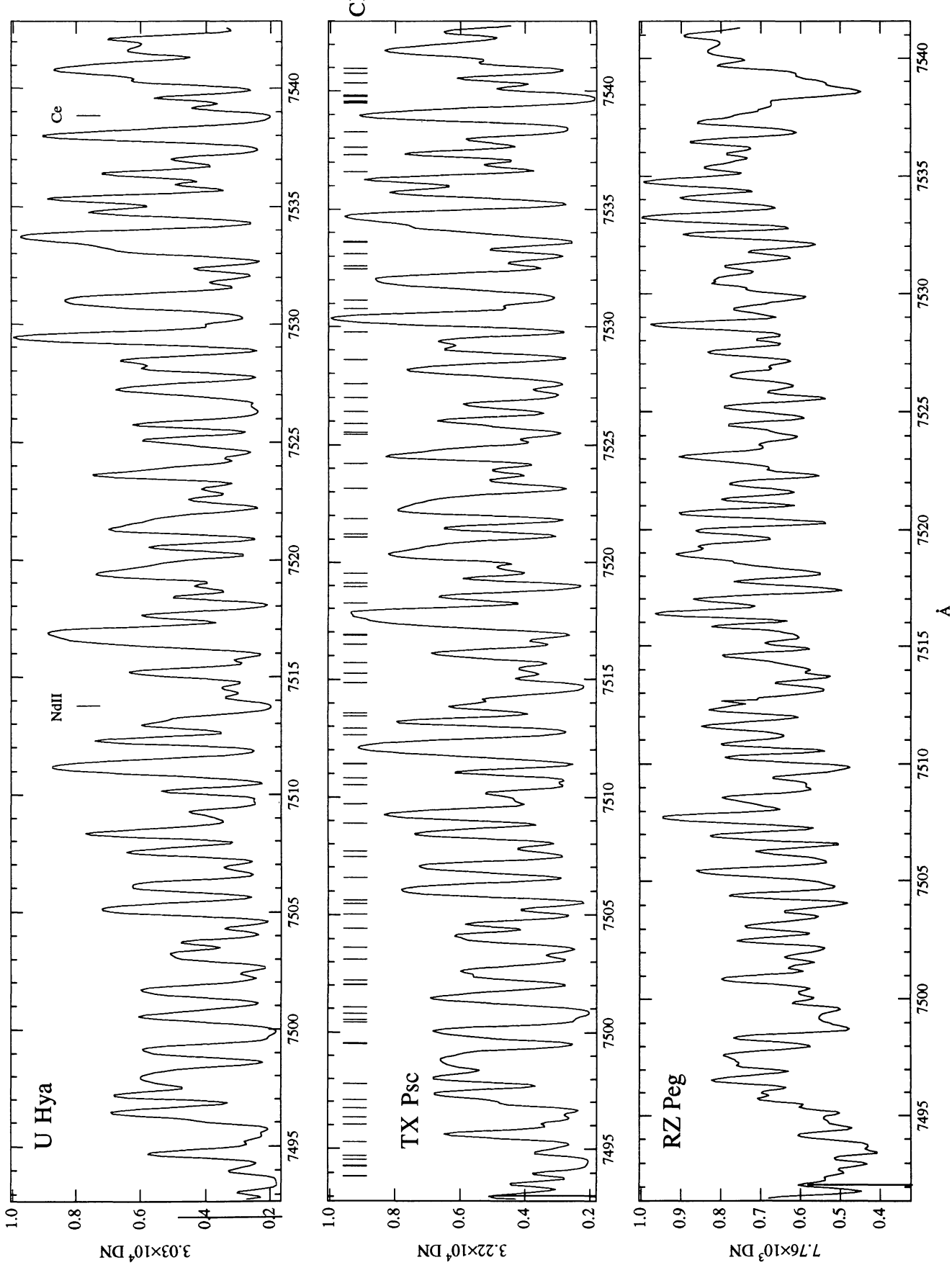

FIG. 41*a*

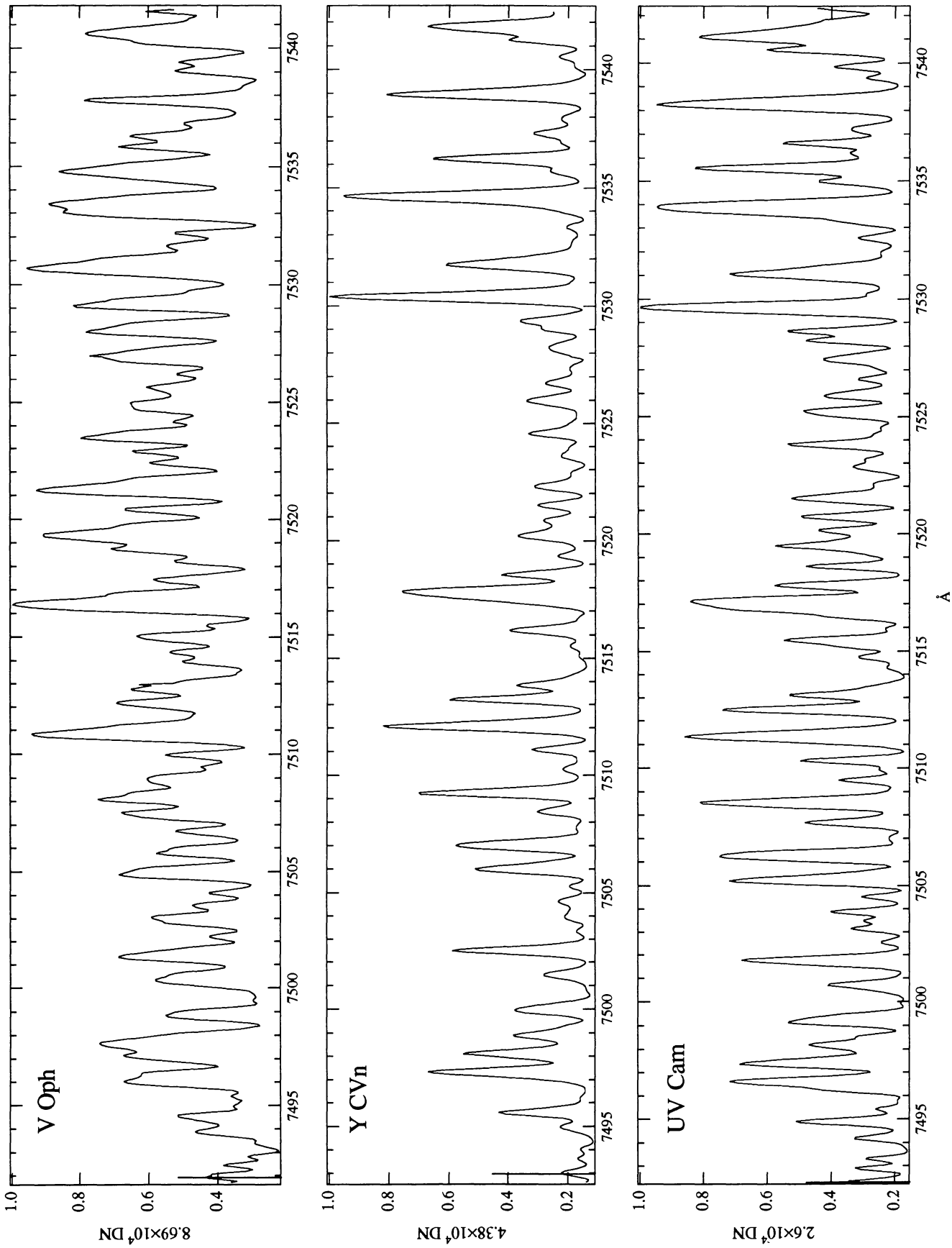

FIG. 41*b*

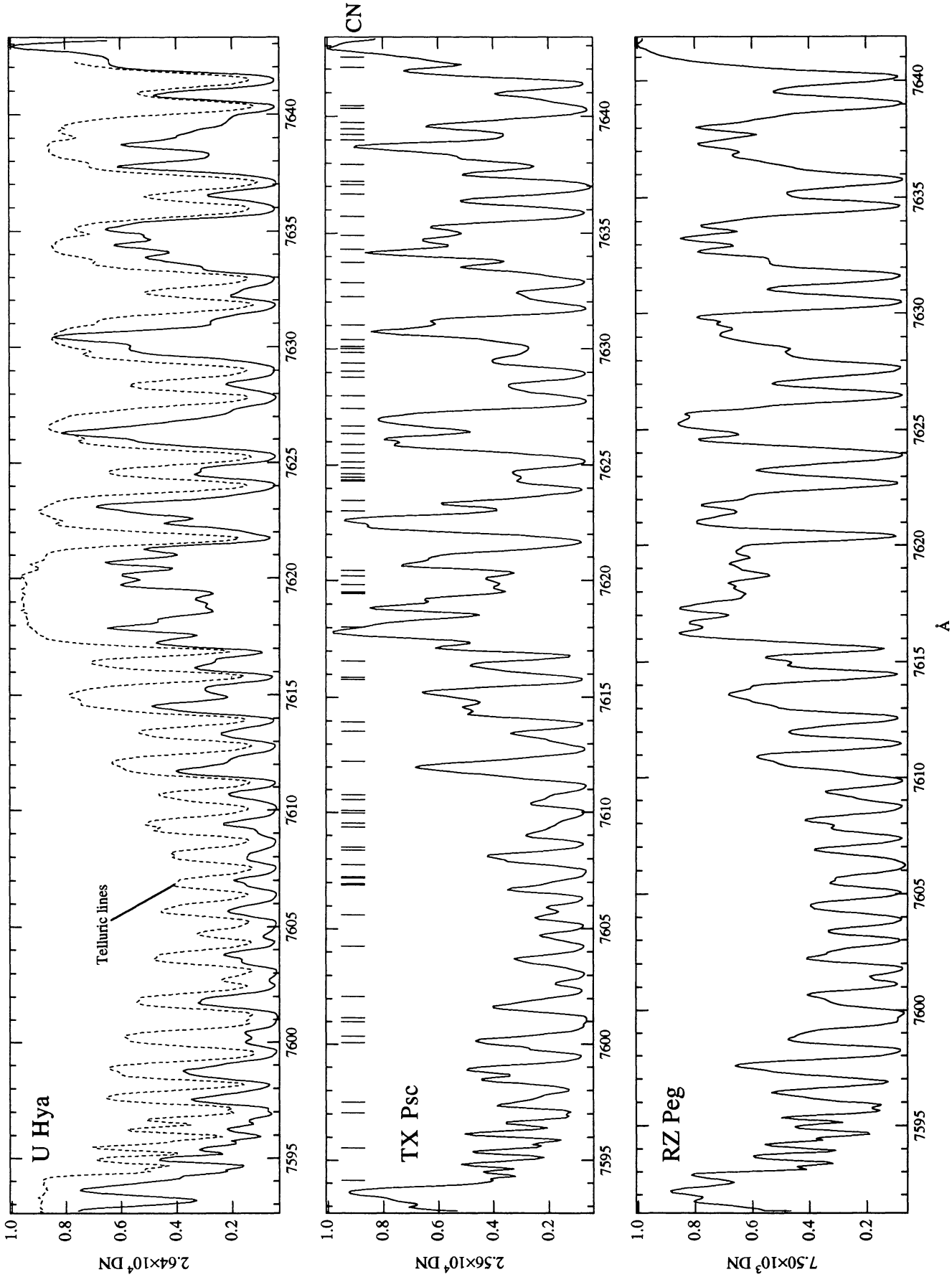

FIG. 42*a*

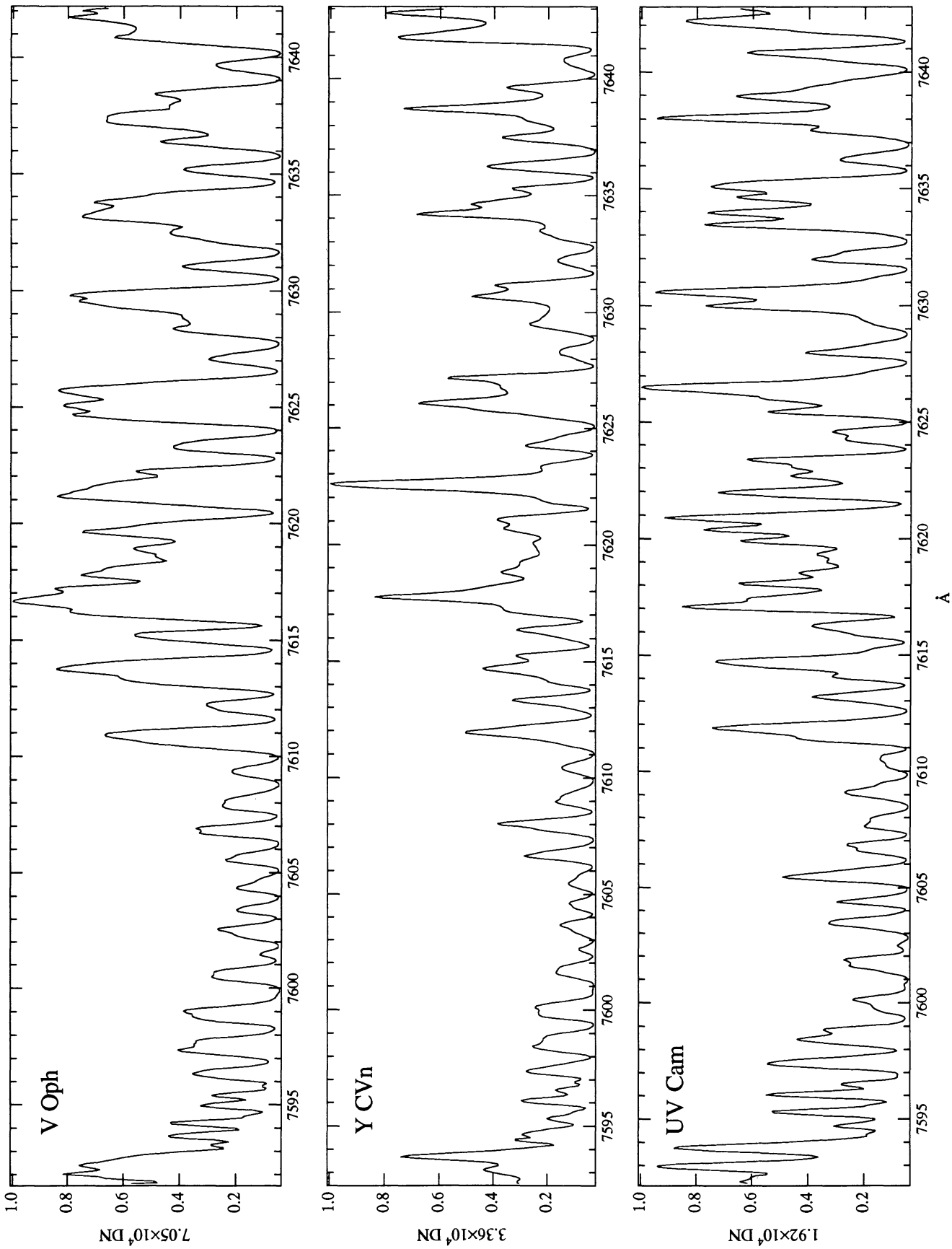

FIG. 42*b*

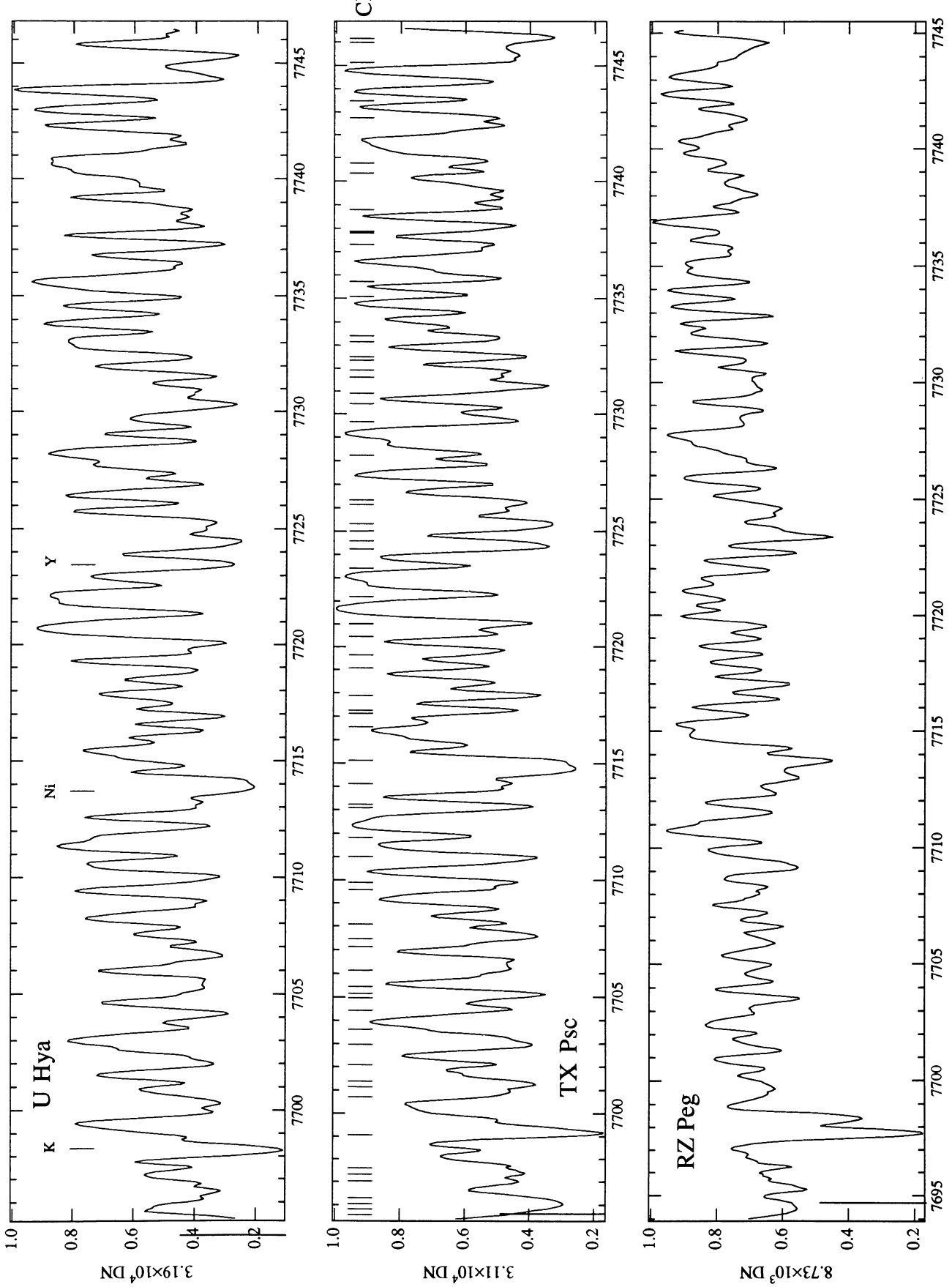

FIG. 43*a*

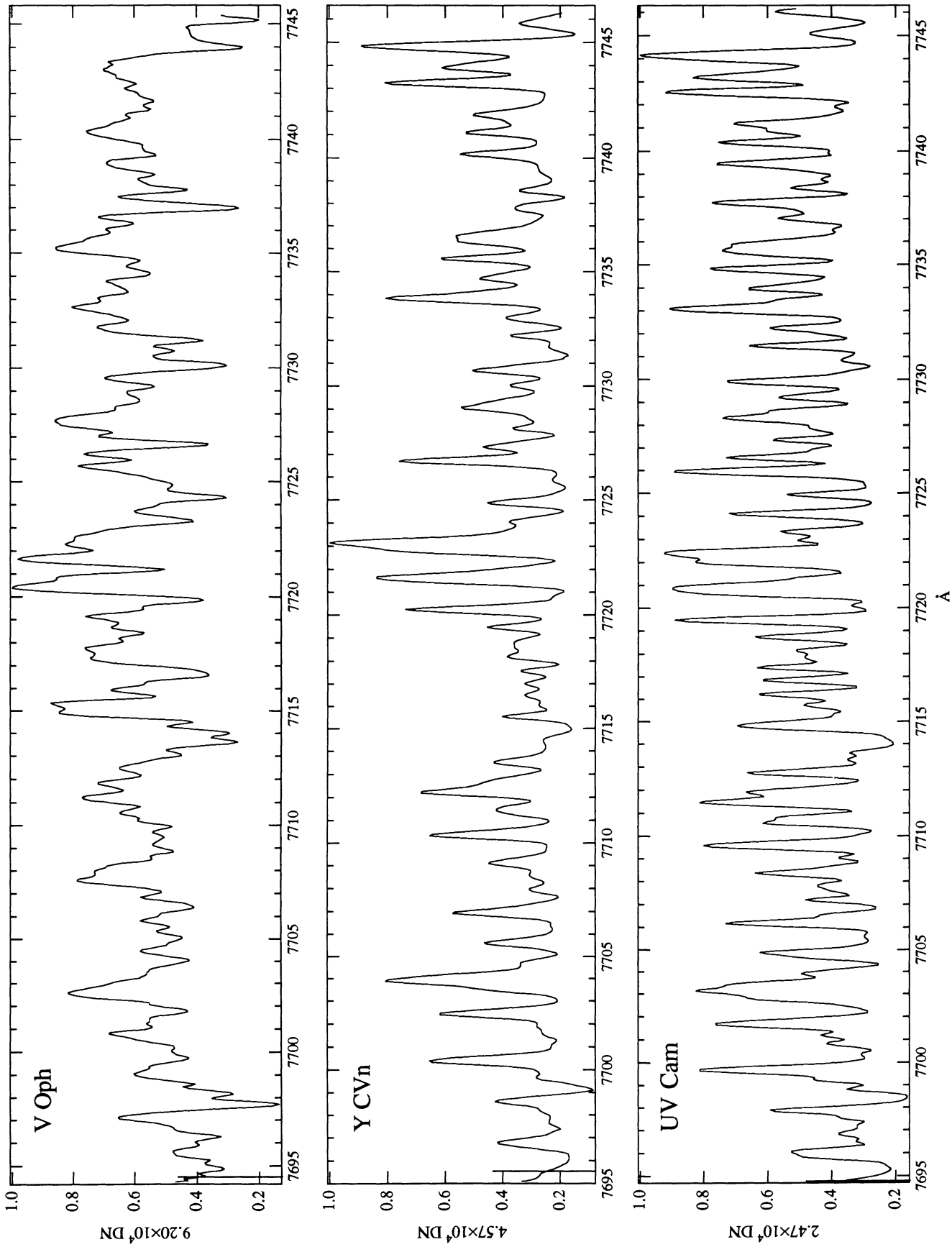

FIG. 43*b*

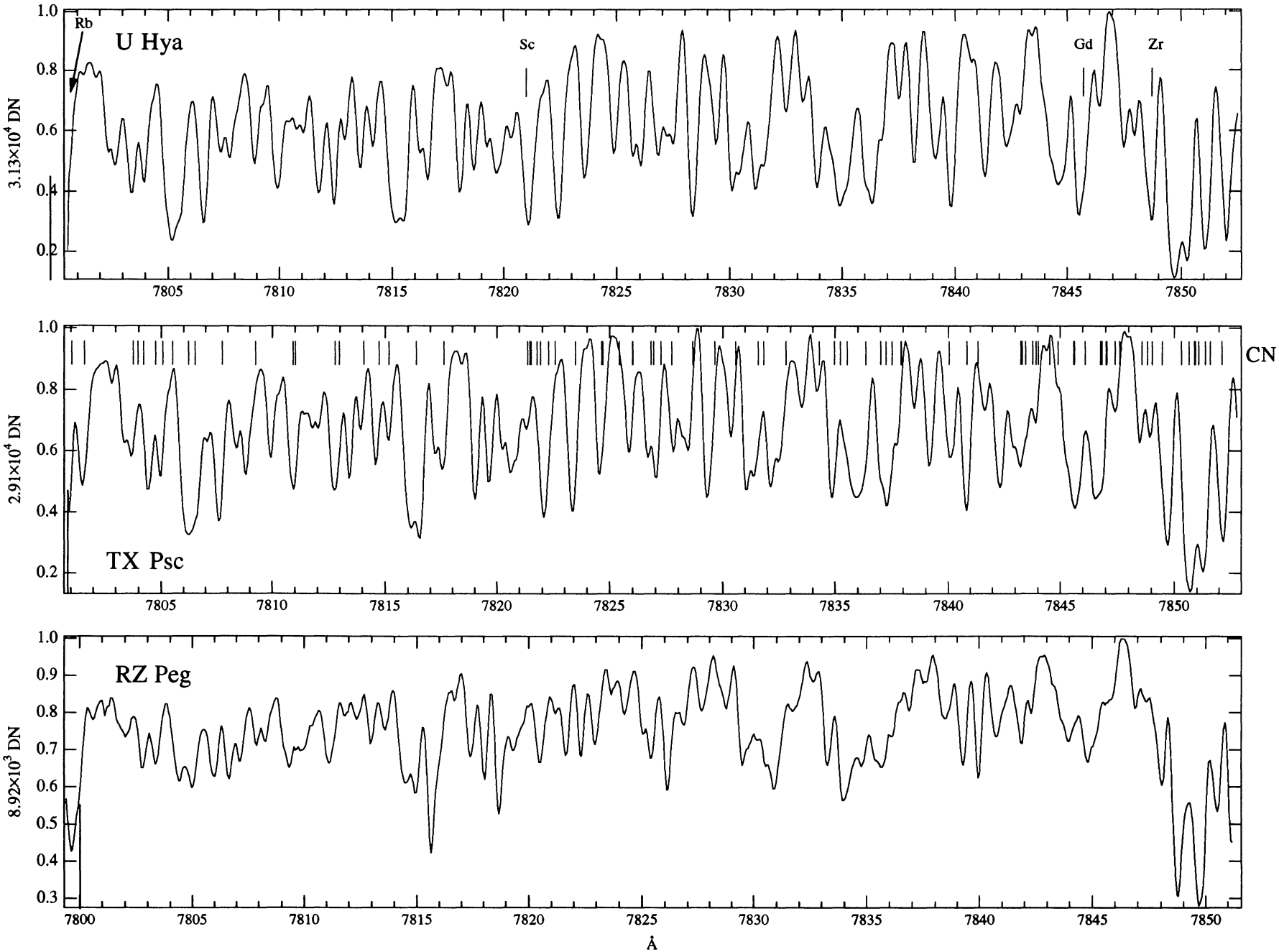

FIG. 44*a*

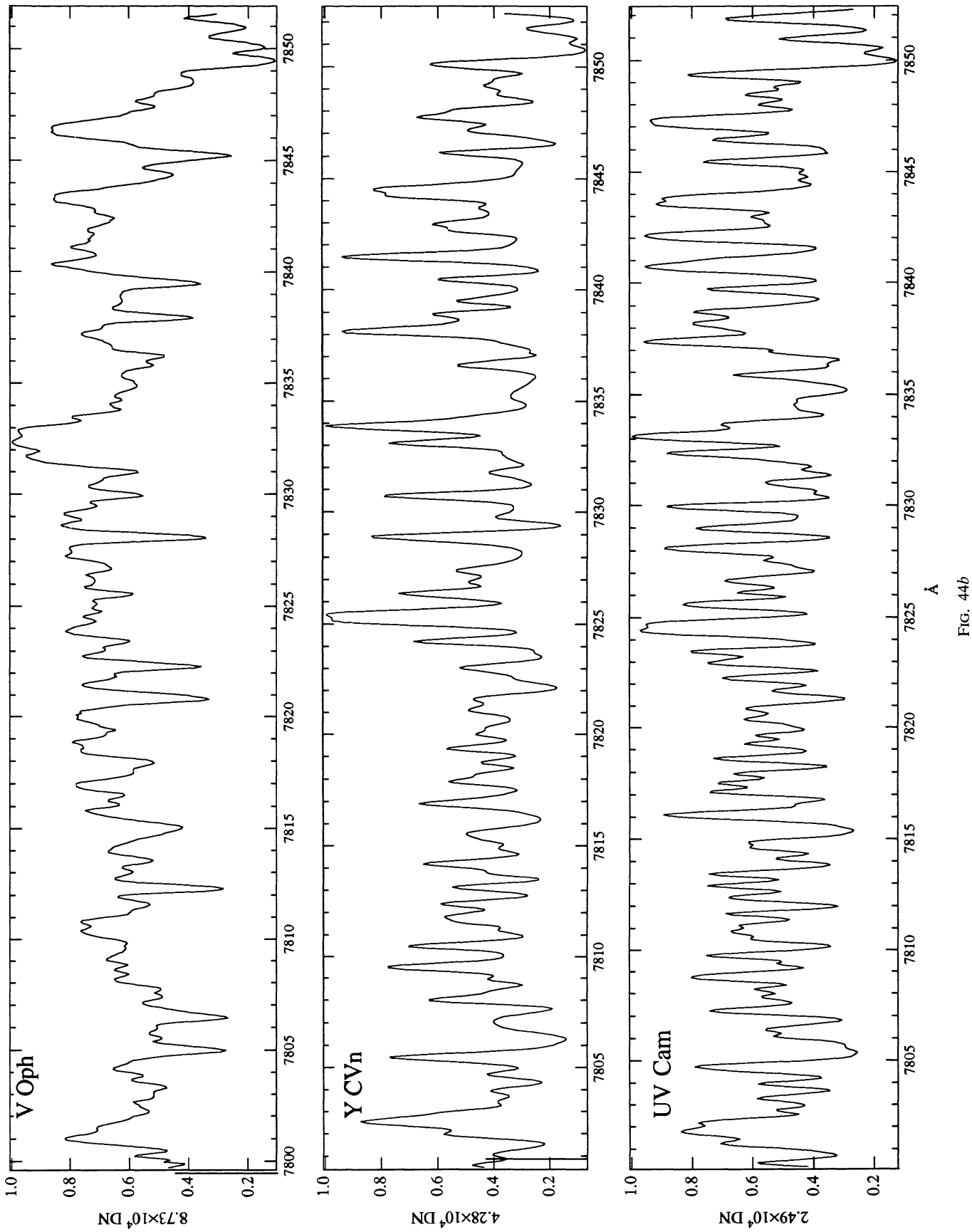

FIG. 44*b*

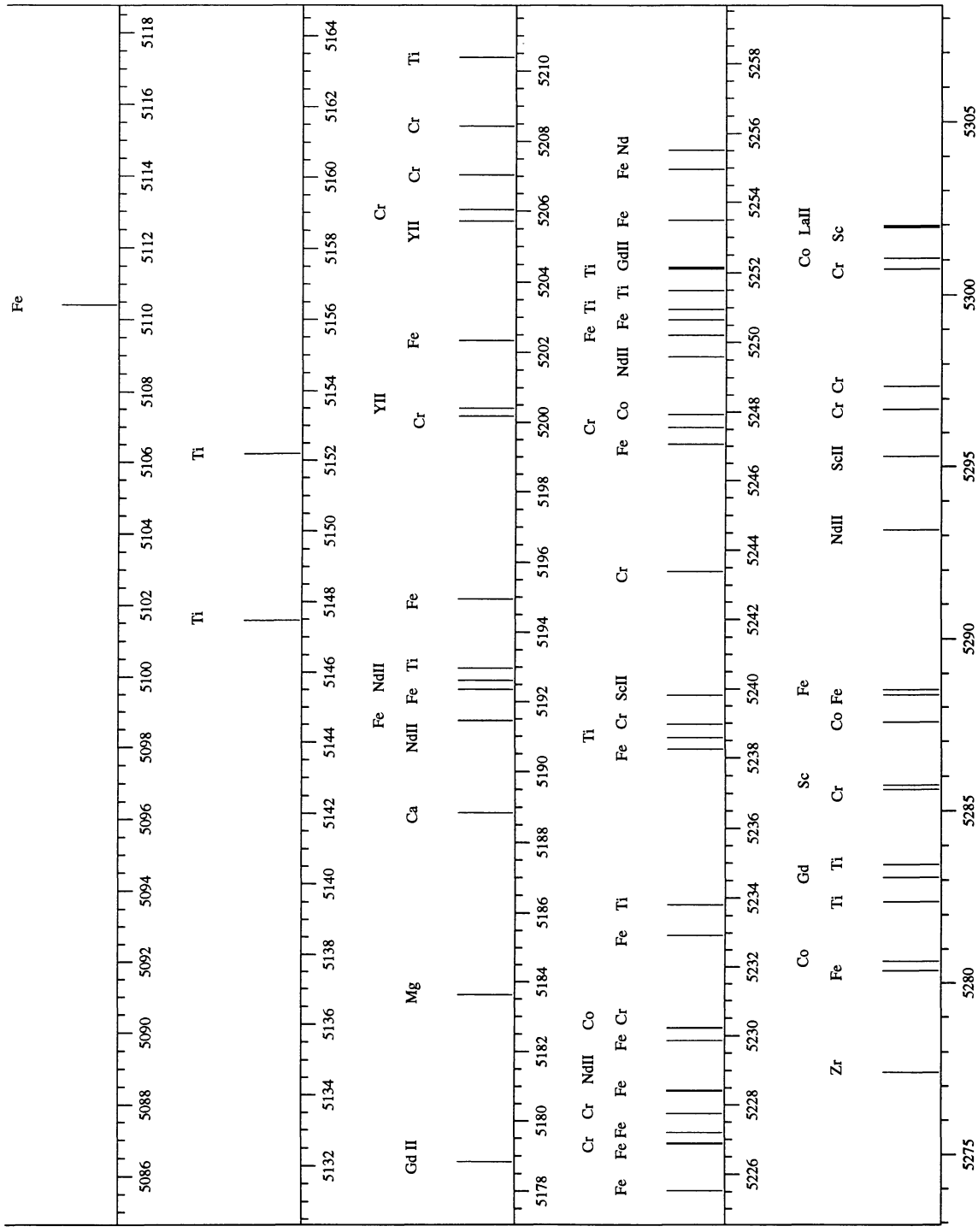

FIG. 45

FIGS. 45–52.—Template spectra of atomic absorption lines identified in the spectrum of U Hya. Aligning the "zero-velocity axis" of a stellar spectrum with the *y*-axis of the atomic plot brings the atomic features to rest velocity (see legend for Figs. 5–44). If the wavelength tick marks of a spectrum and template are positioned to coincide, any shift in wavelength of the atomic lines to the stellar features indicates the heliocentric stellar velocity.

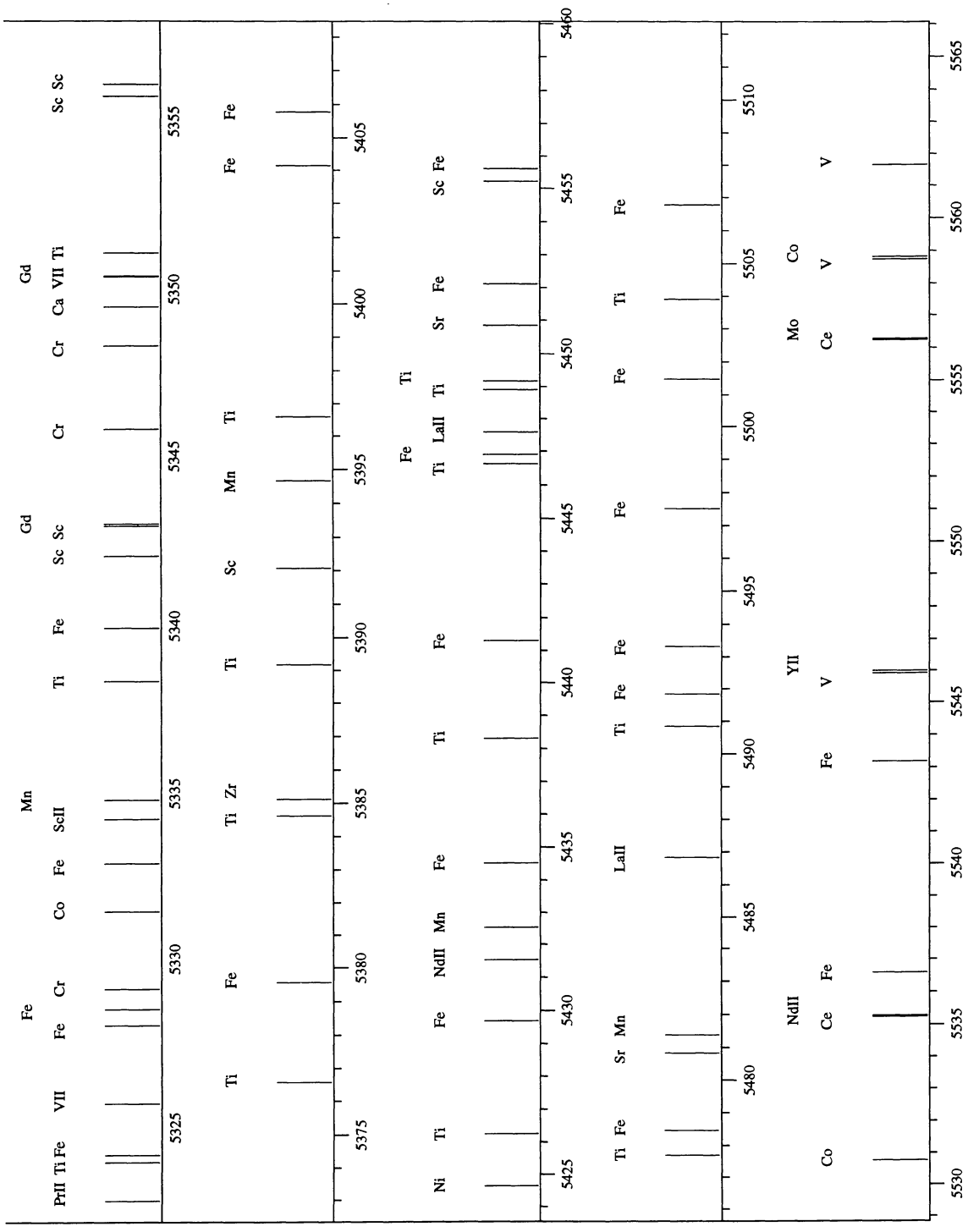

FIG. 46

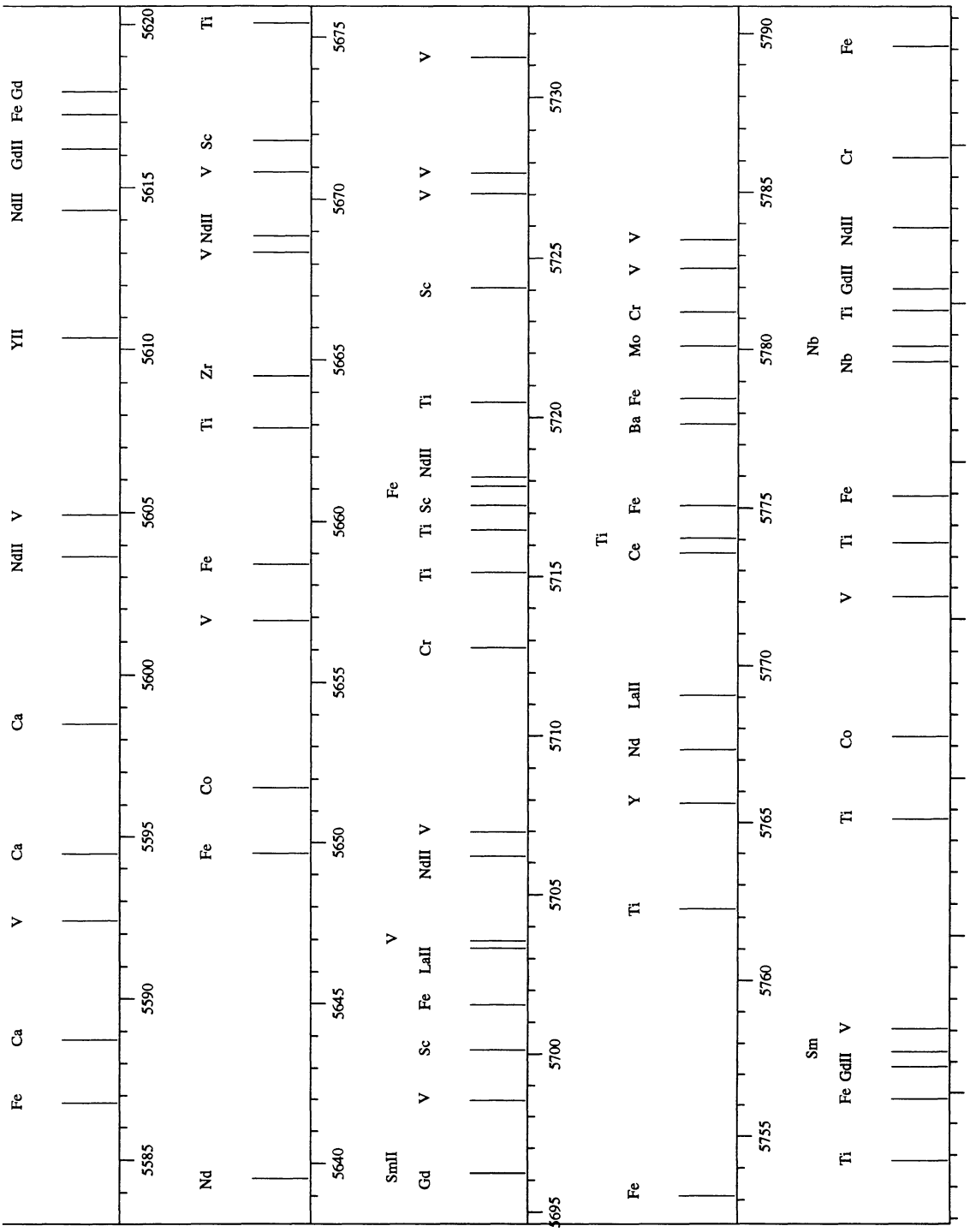

FIG. 47

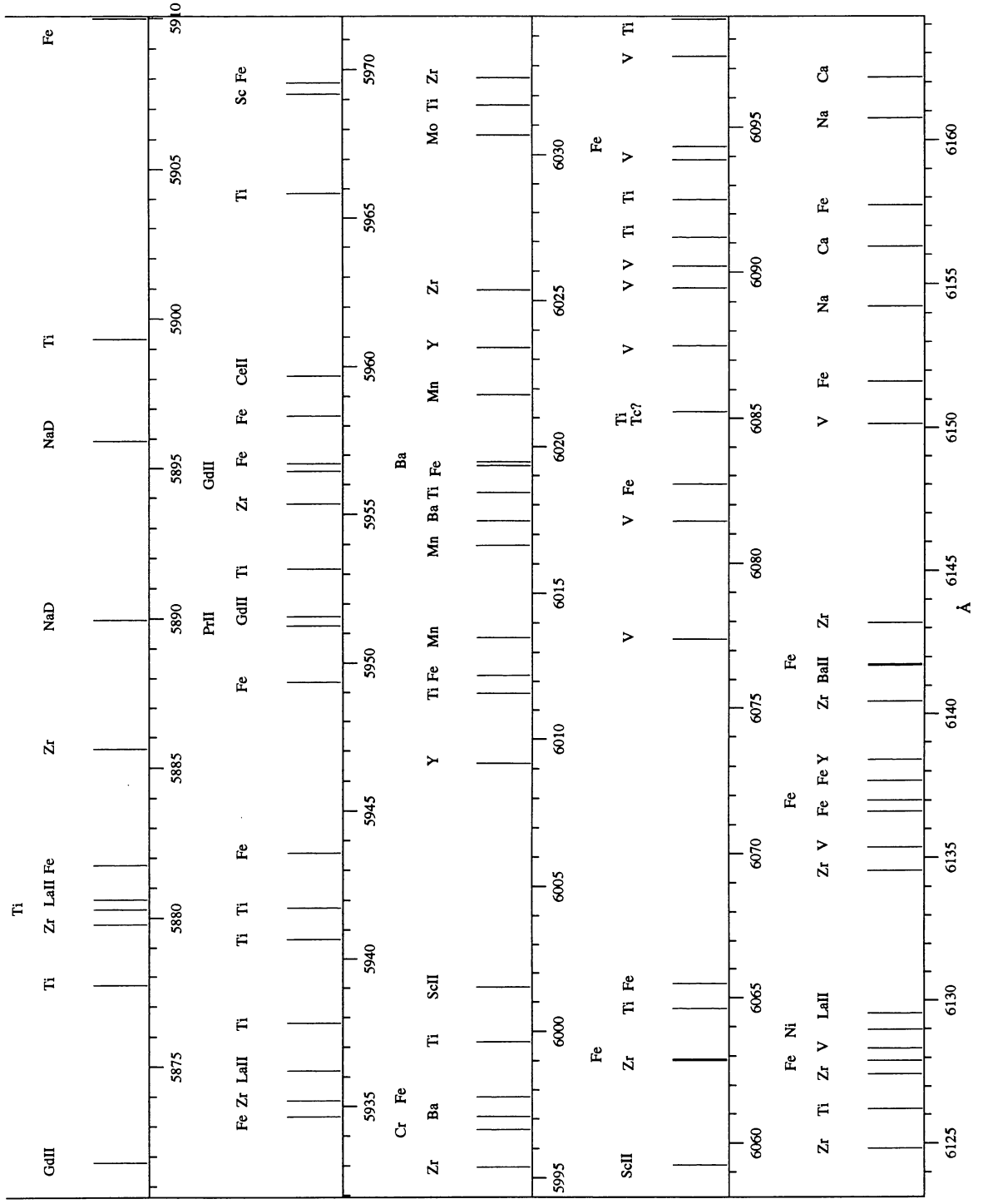

FIG. 48

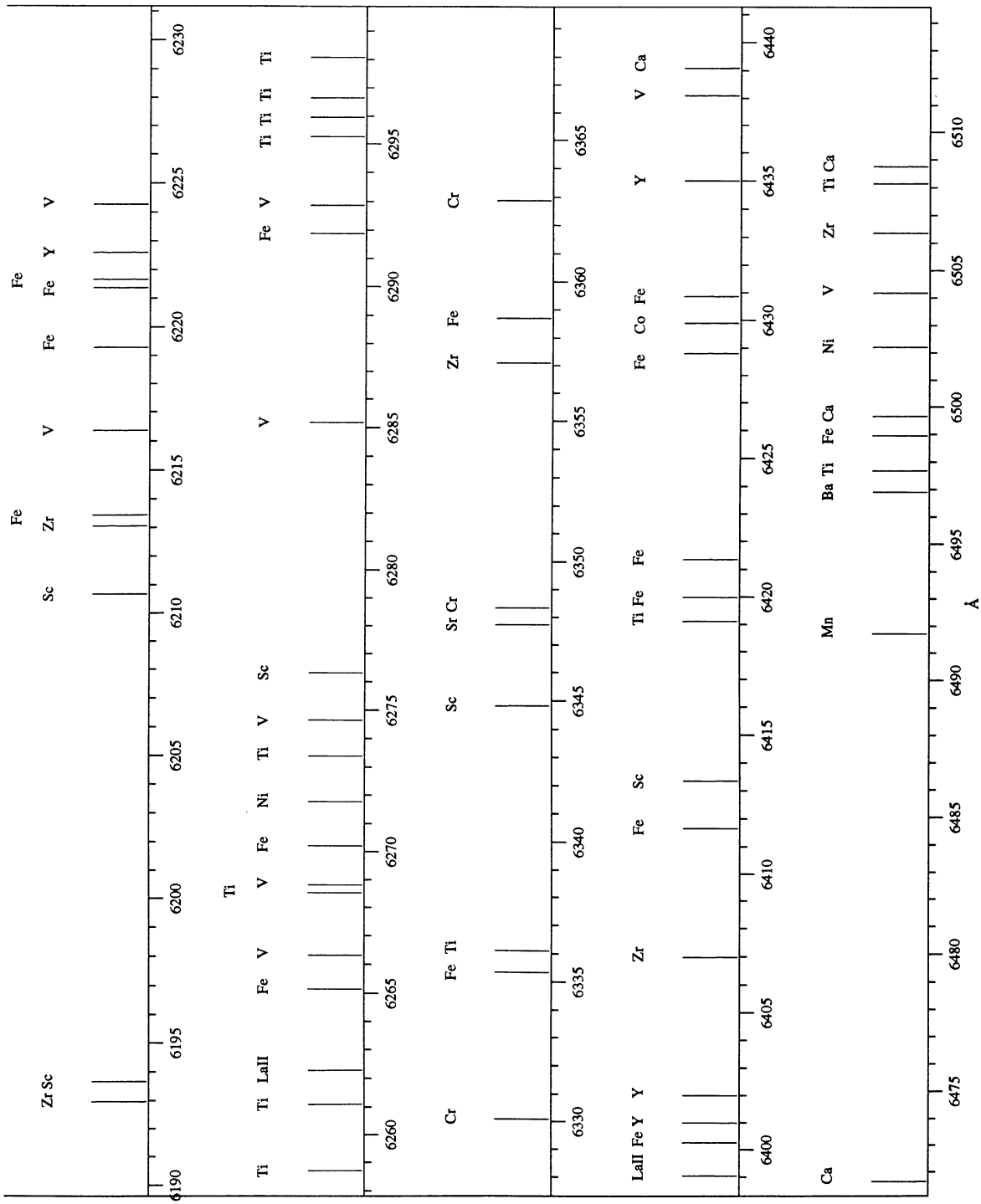

FIG. 49

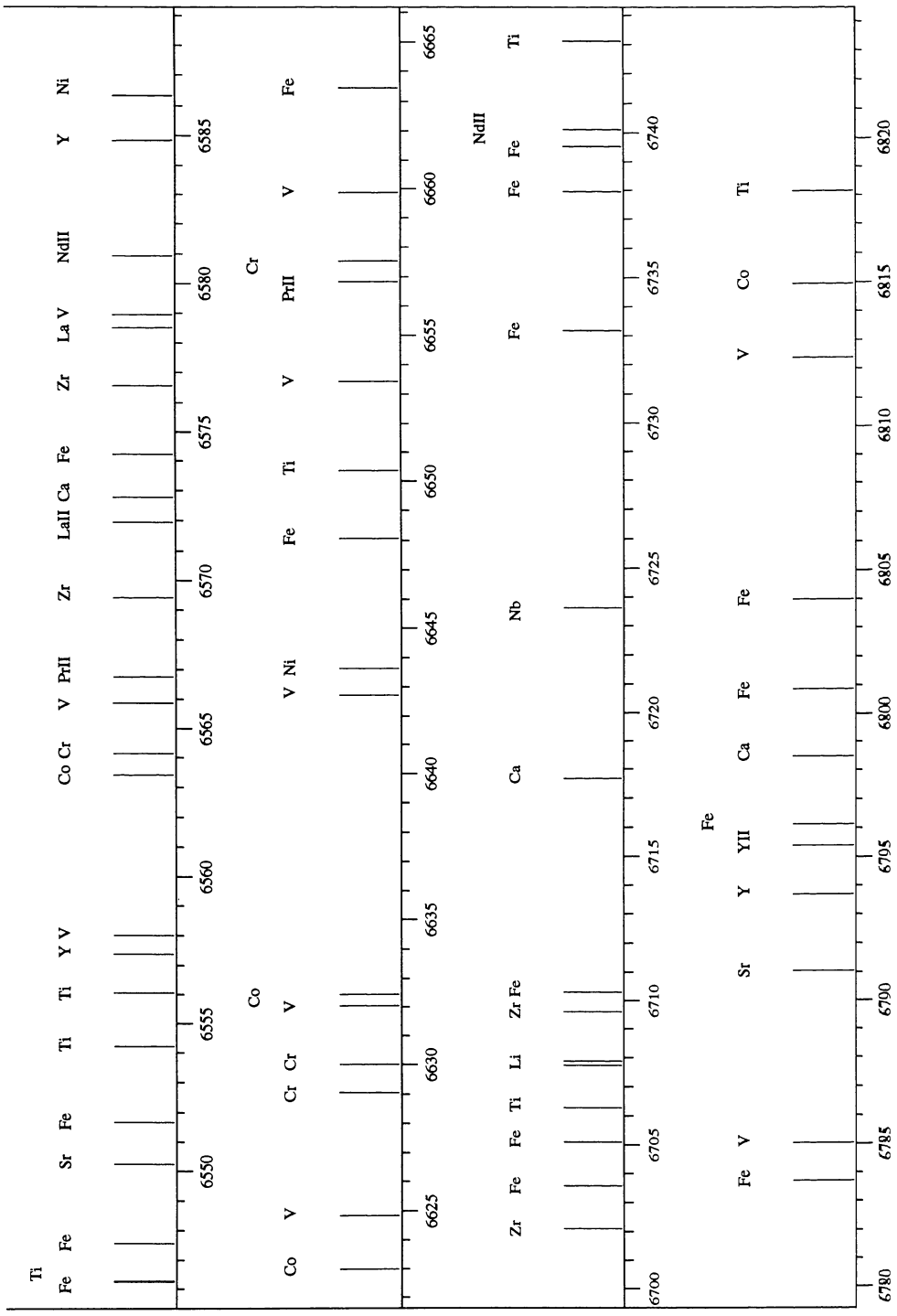

FIG. 50

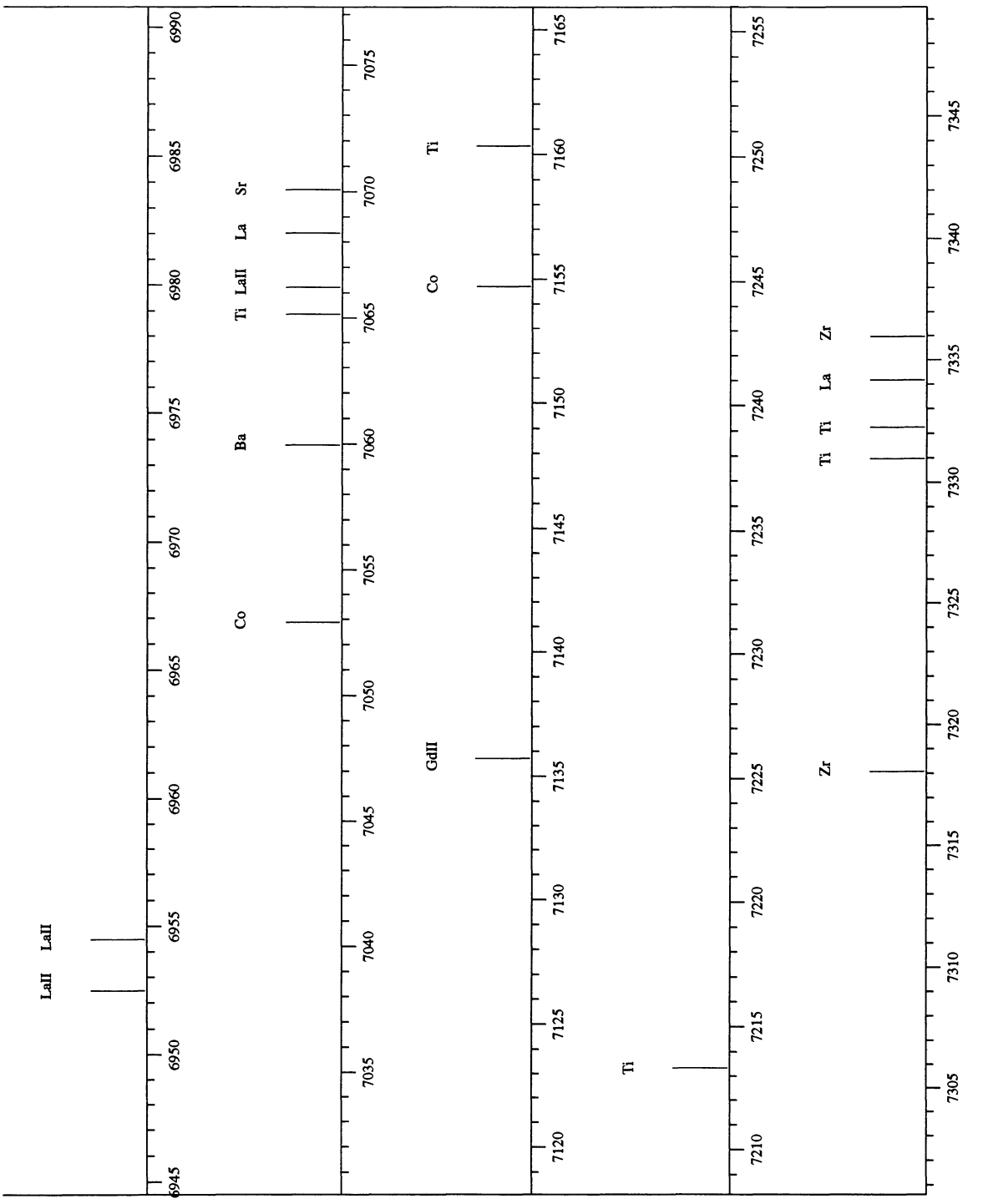

FIG. 51

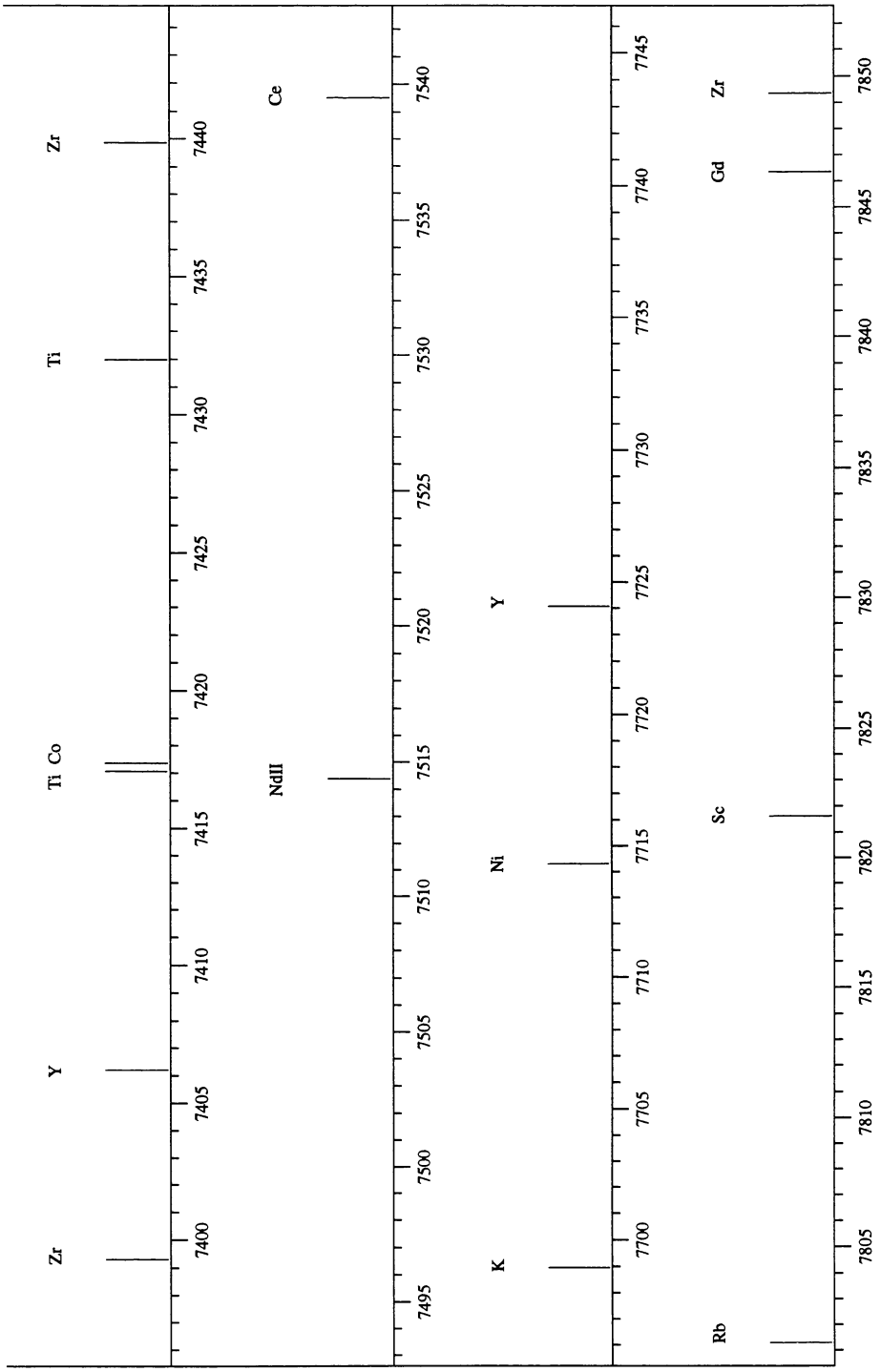

FIG. 52

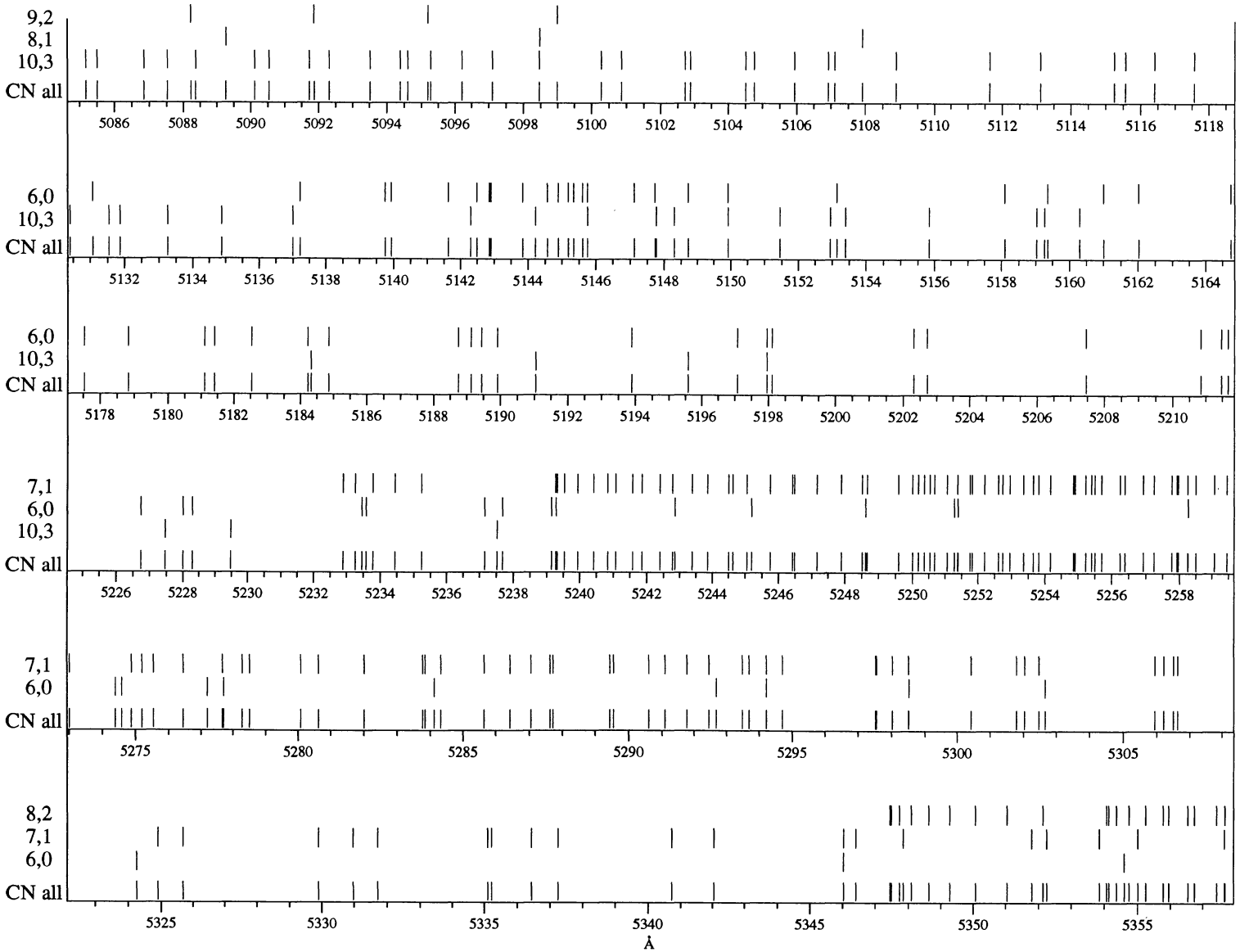

FIG. 53

FIGS. 53–60.—Template spectra of the Red System of CN from the tables of Davis & Phillips (1963). At the bottom of each spectrum all the overlapping vibrational-rotational transitions are plotted together, labeled "all." Above, the vibration lines are separated from each other, and each transition is labeled on the left. Aligning the zero-velocity axis of a stellar spectrum (see legend for Figs. 5–44) with the y-axis of the corresponding CN line template brings the stellar absorption features to rest velocity. If the wavelength tick marks of a spectrum and template are positioned to coincide, any shift in wavelength of the atomic lines to the stellar features indicates the heliocentric stellar velocity.

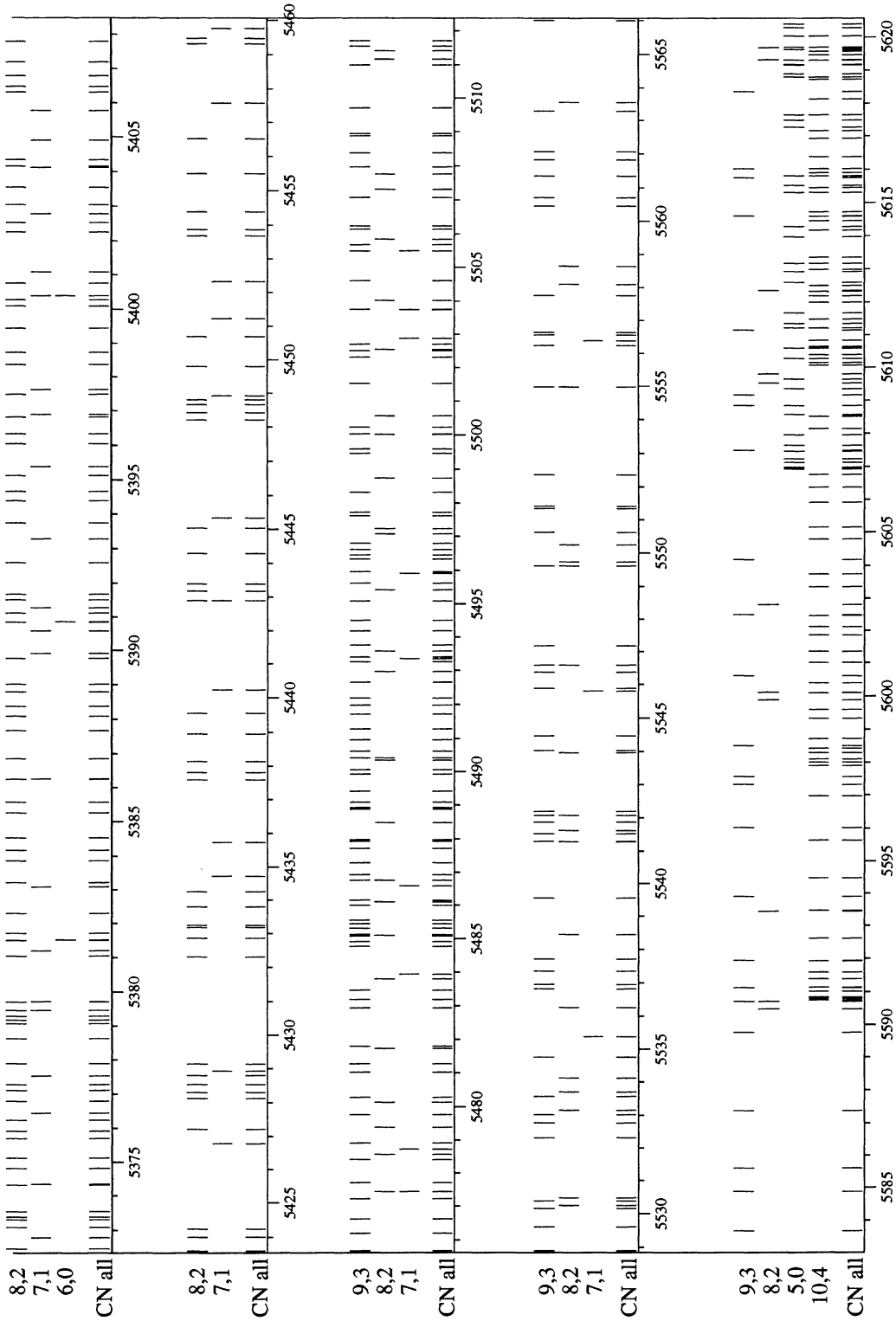

FIG. 54

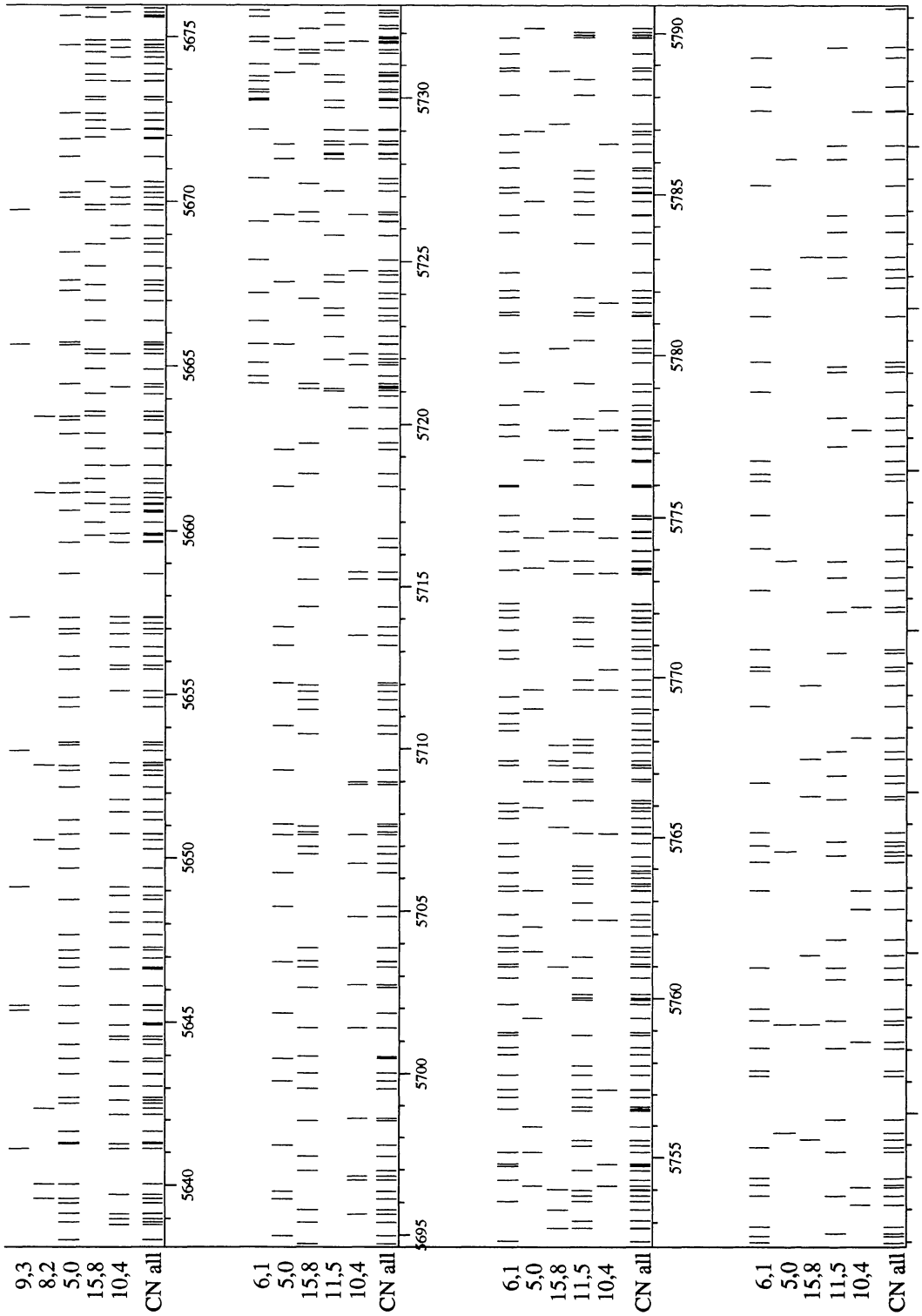

FIG. 55

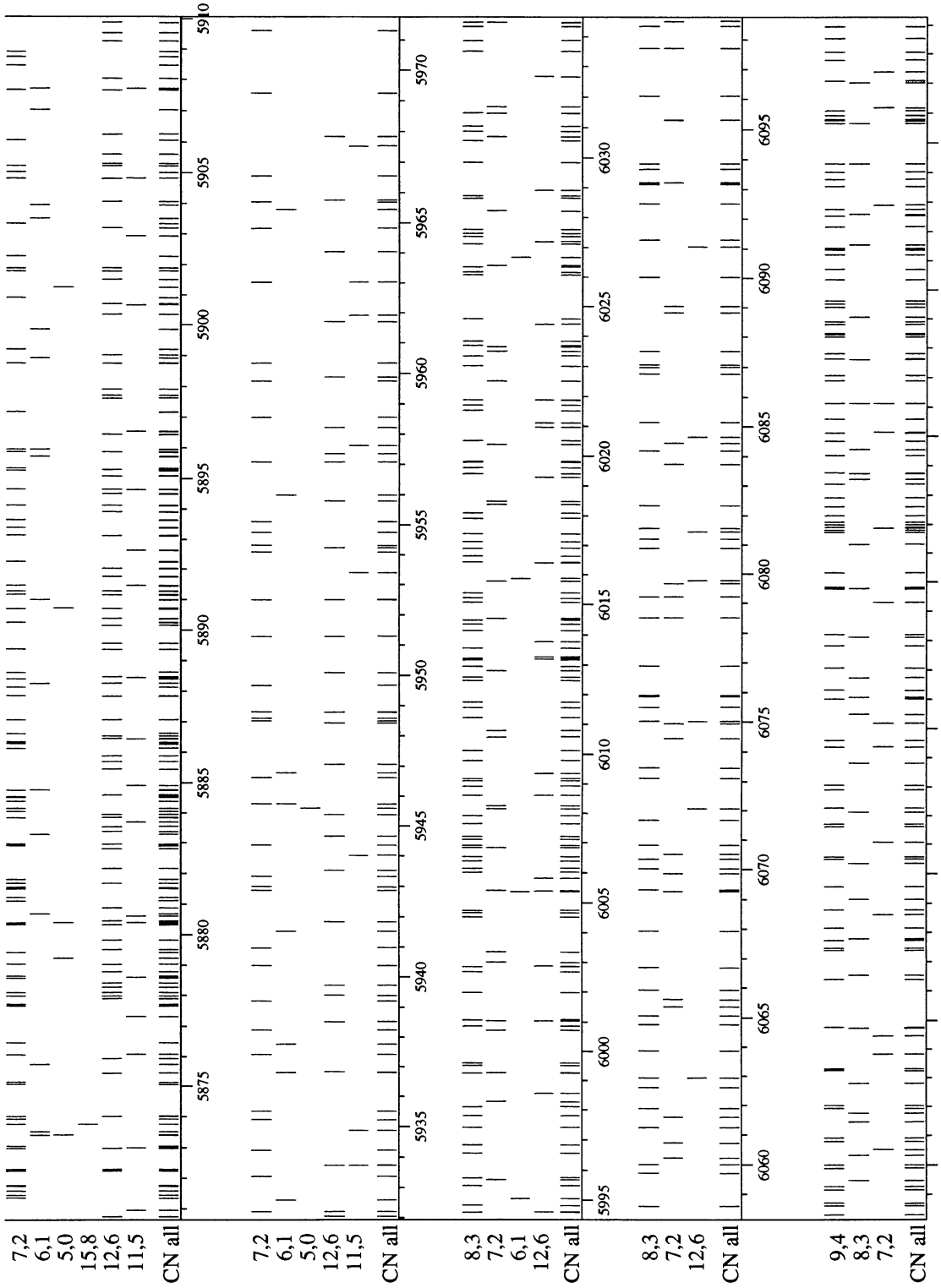

FIG. 56

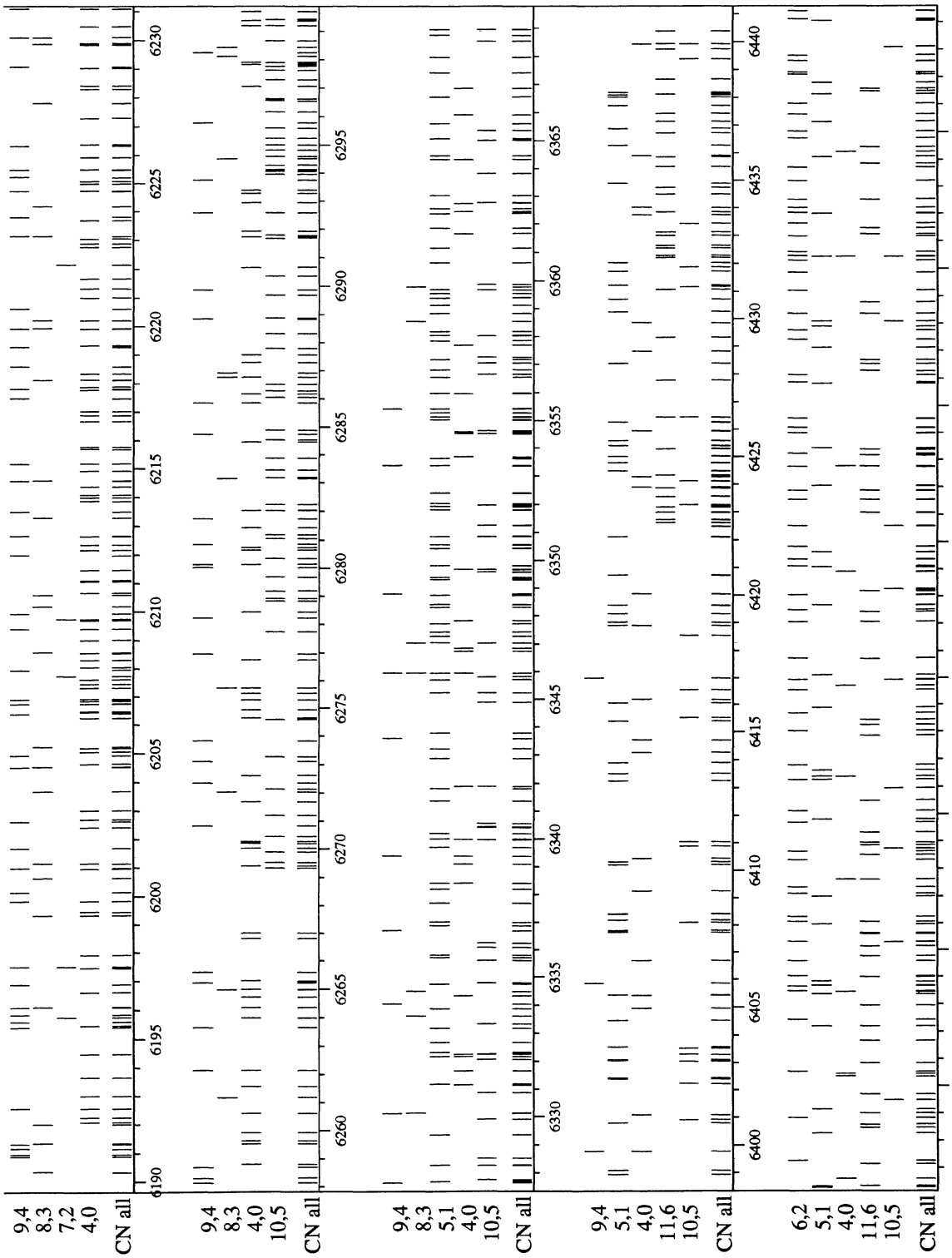

FIG. 57

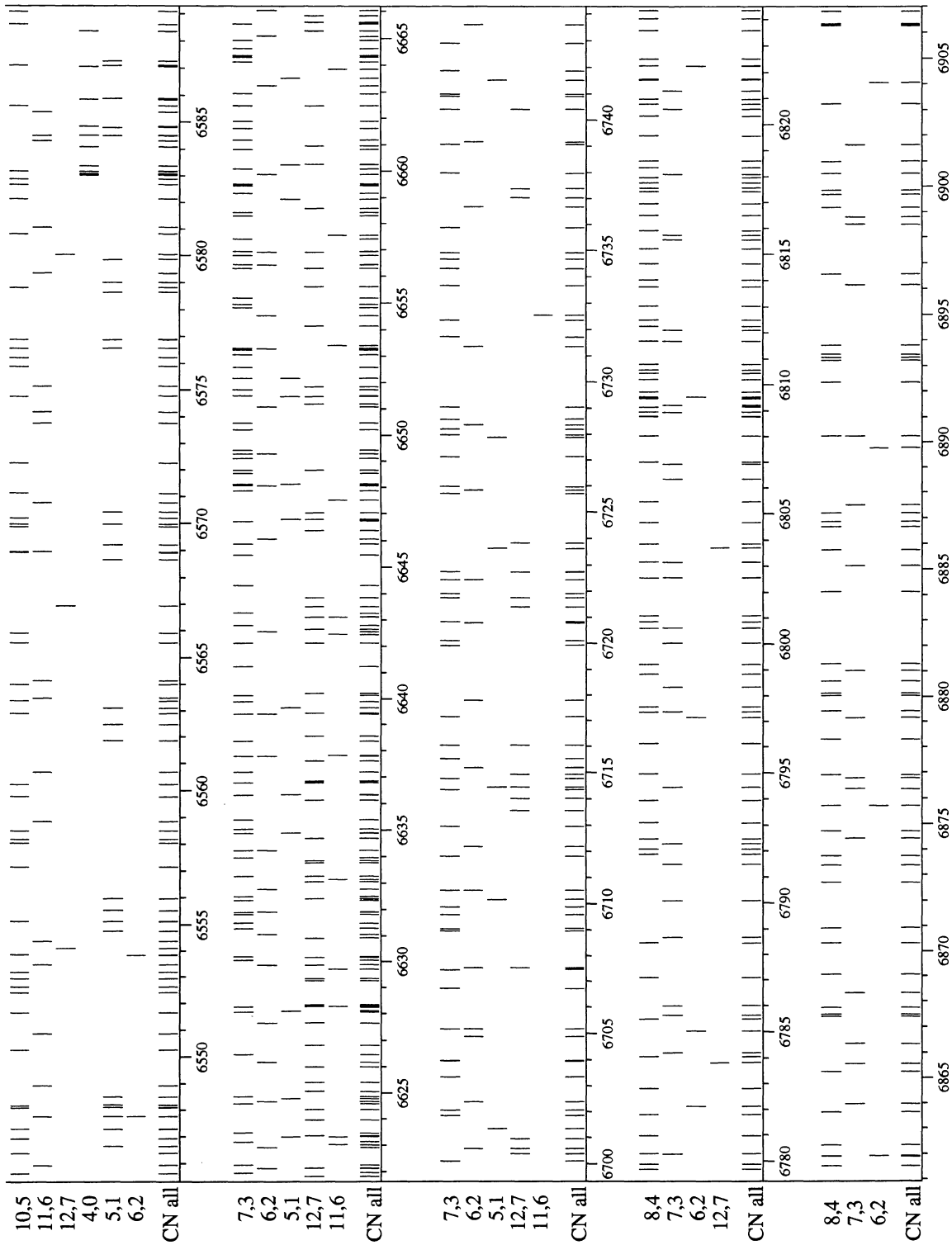

FIG. 58

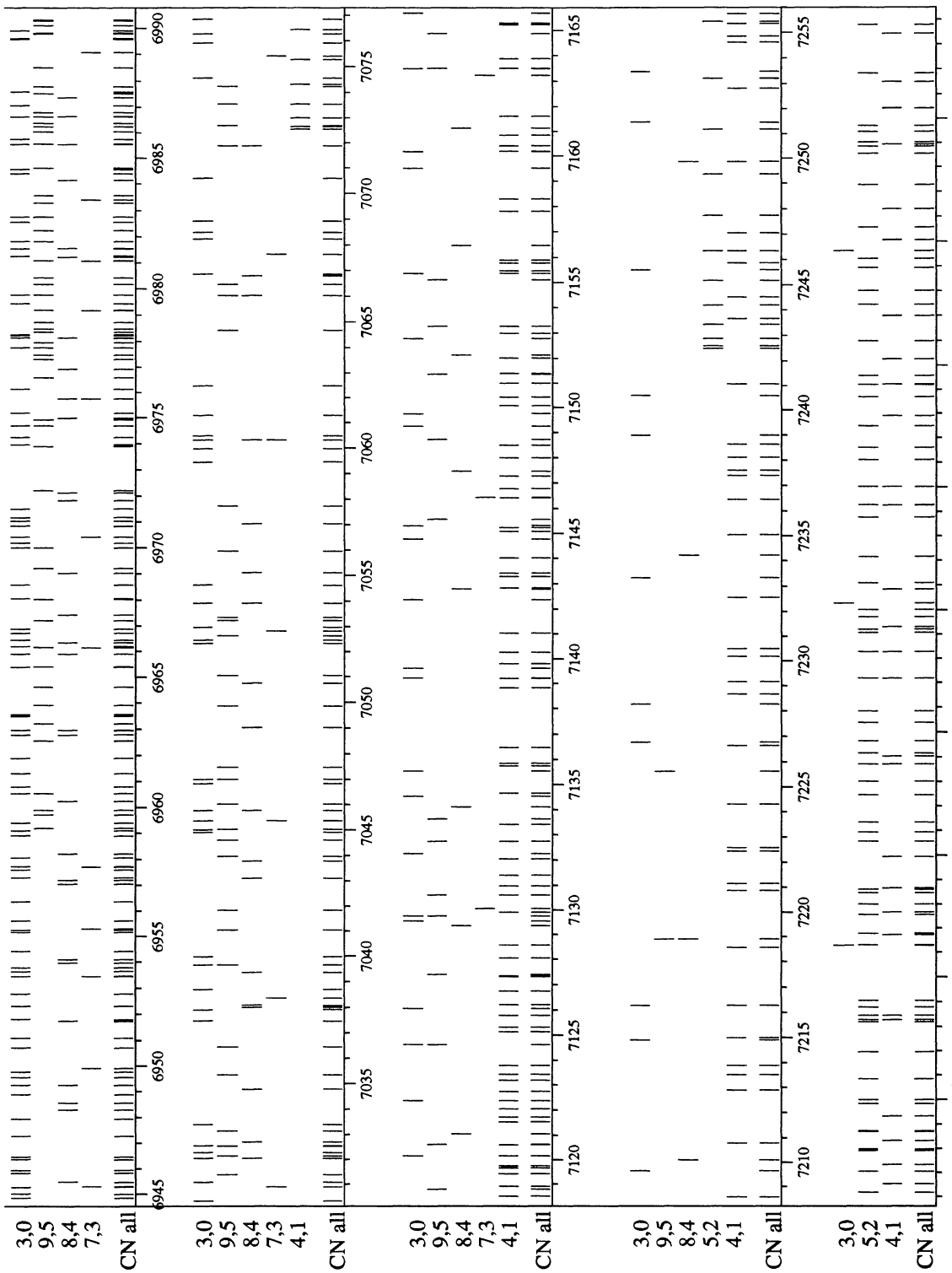

FIG. 59

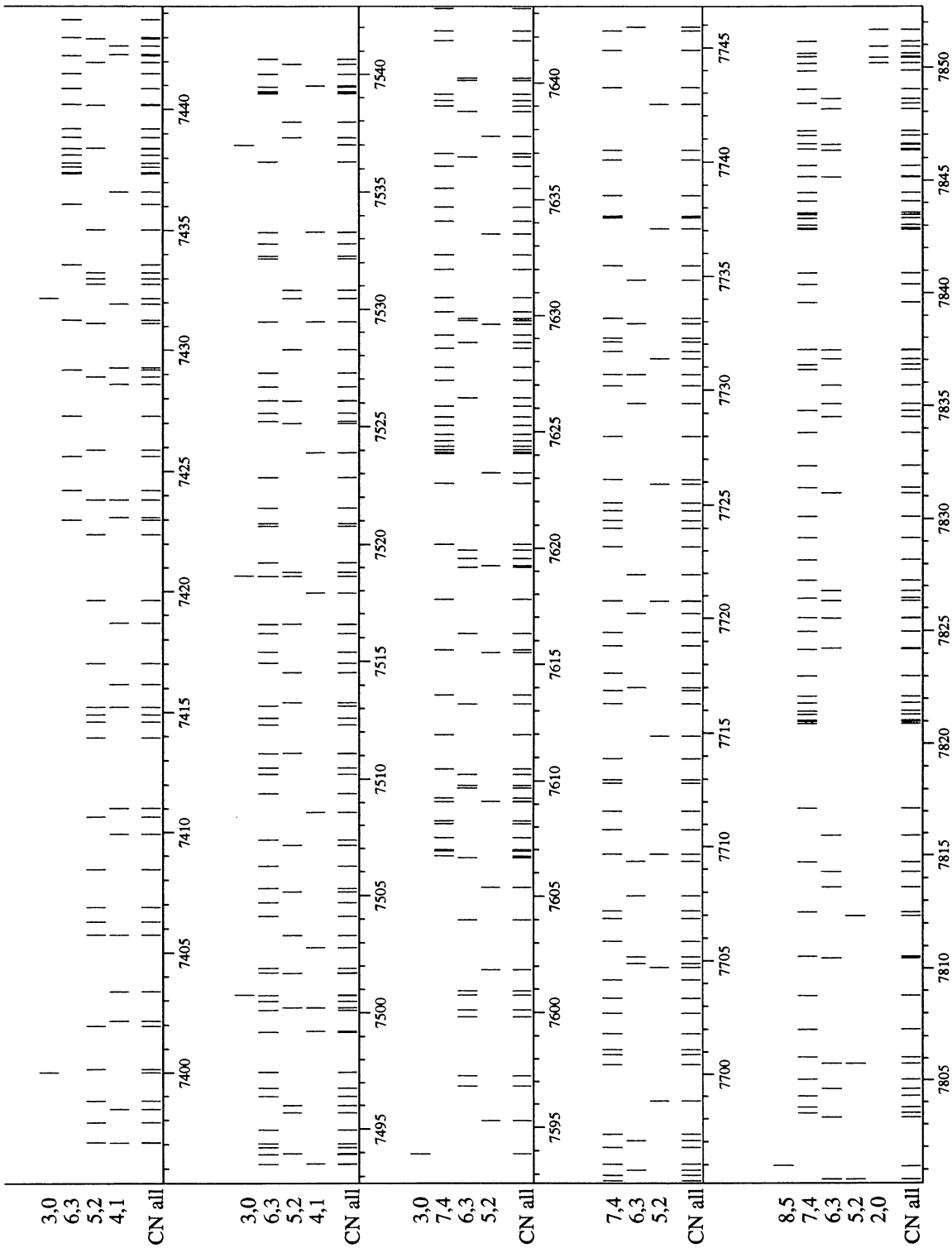

FIG. 60

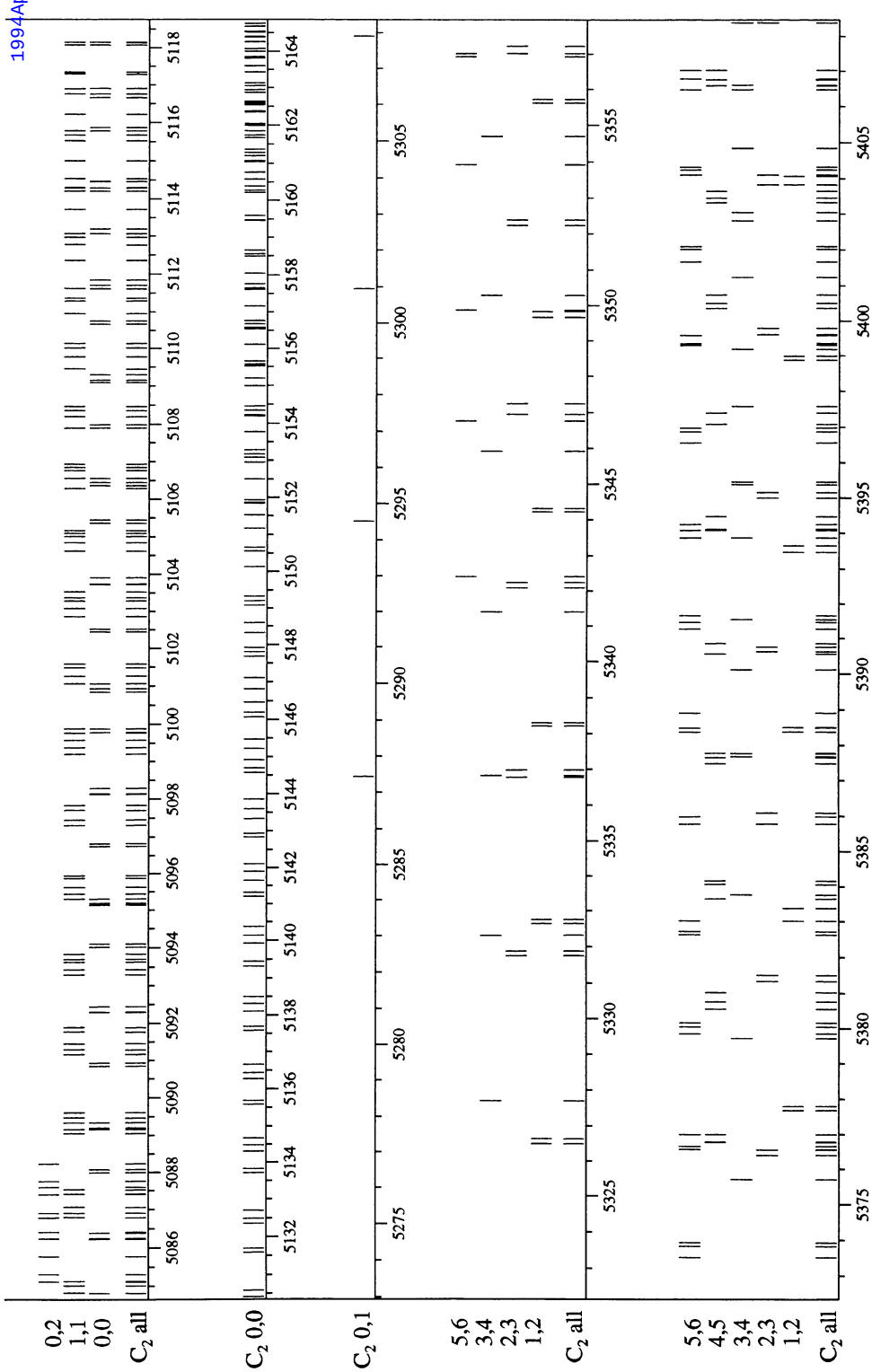

FIG. 61

FIGS. 61–65.—Template spectra of the Swan bands of C_2 from the tables of Phillips & Davis (1968). At the bottom of each spectrum all the overlapping vibrational-rotational transitions are plotted together, labeled "all." Above, the vibration lines are separated from each other, and each transition is labeled on the left. Aligning the zero-velocity axis of a stellar spectrum (see legend for Figs. 5–44) with the y-axis of the corresponding C_2 line template brings the stellar absorption features to rest velocity. If the wavelength tick marks of a spectrum and template are positioned to coincide, any shift in wavelength of the atomic lines to the stellar features indicates the heliocentric stellar velocity.

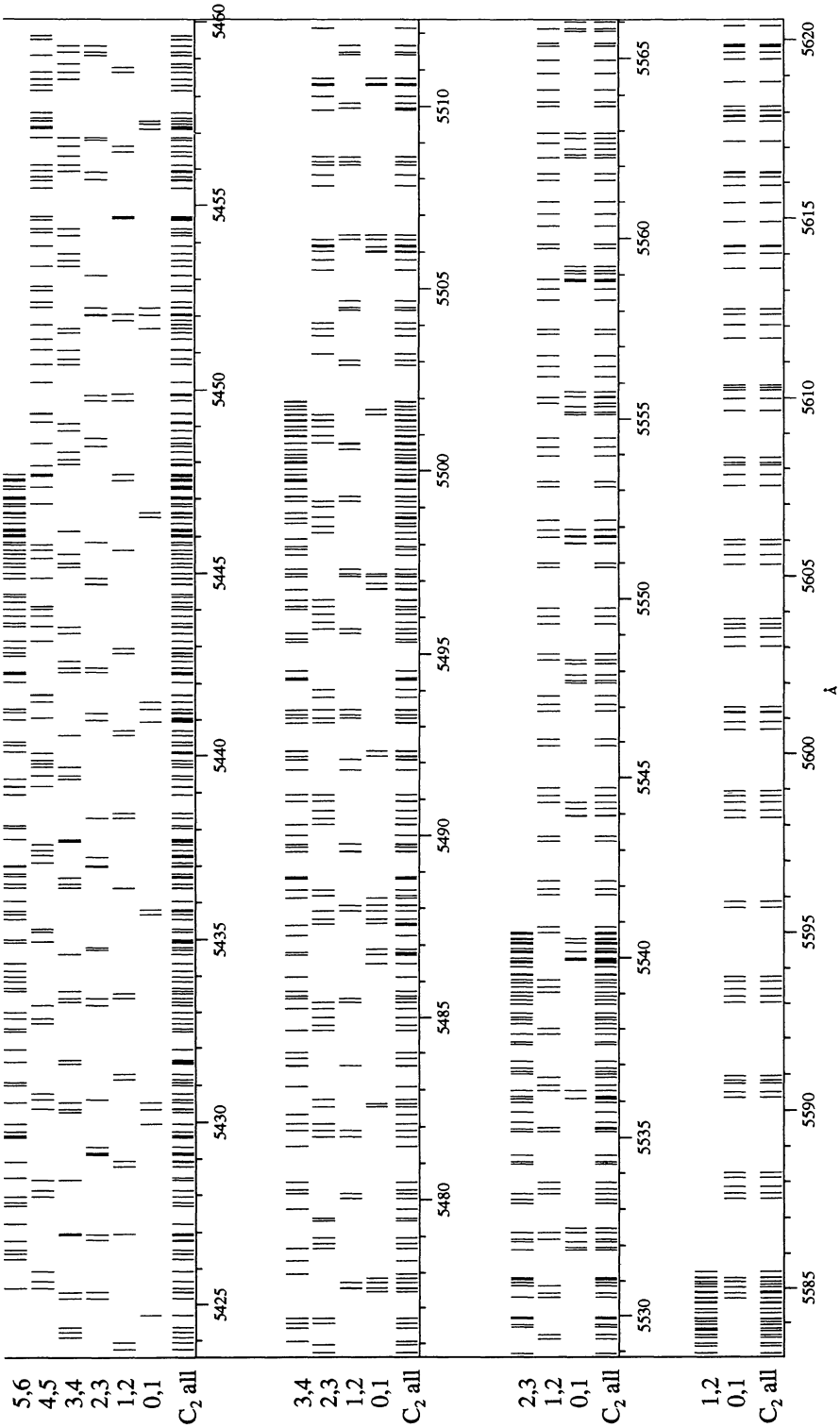

FIG. 62

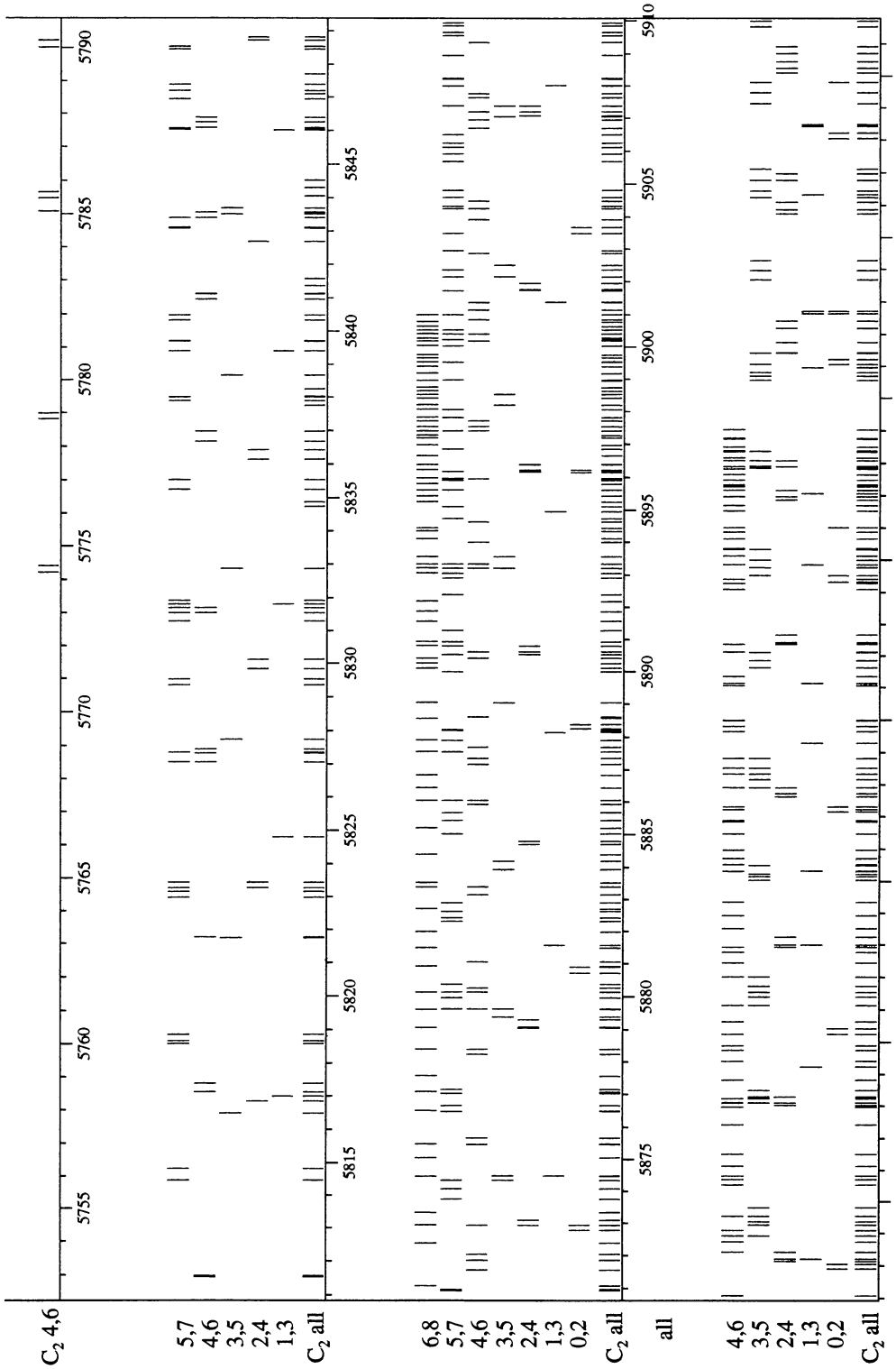

FIG. 63

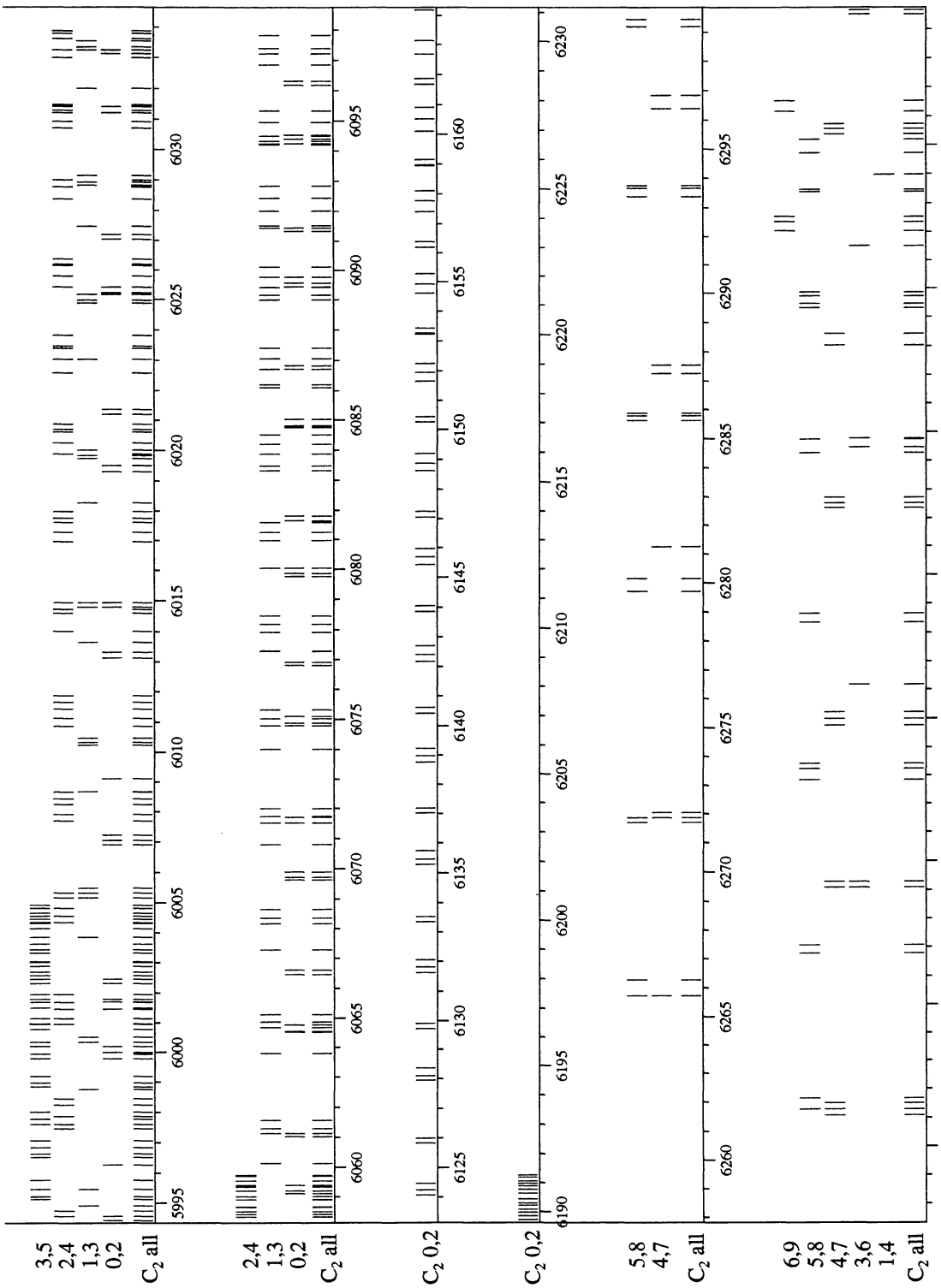

FIG. 64

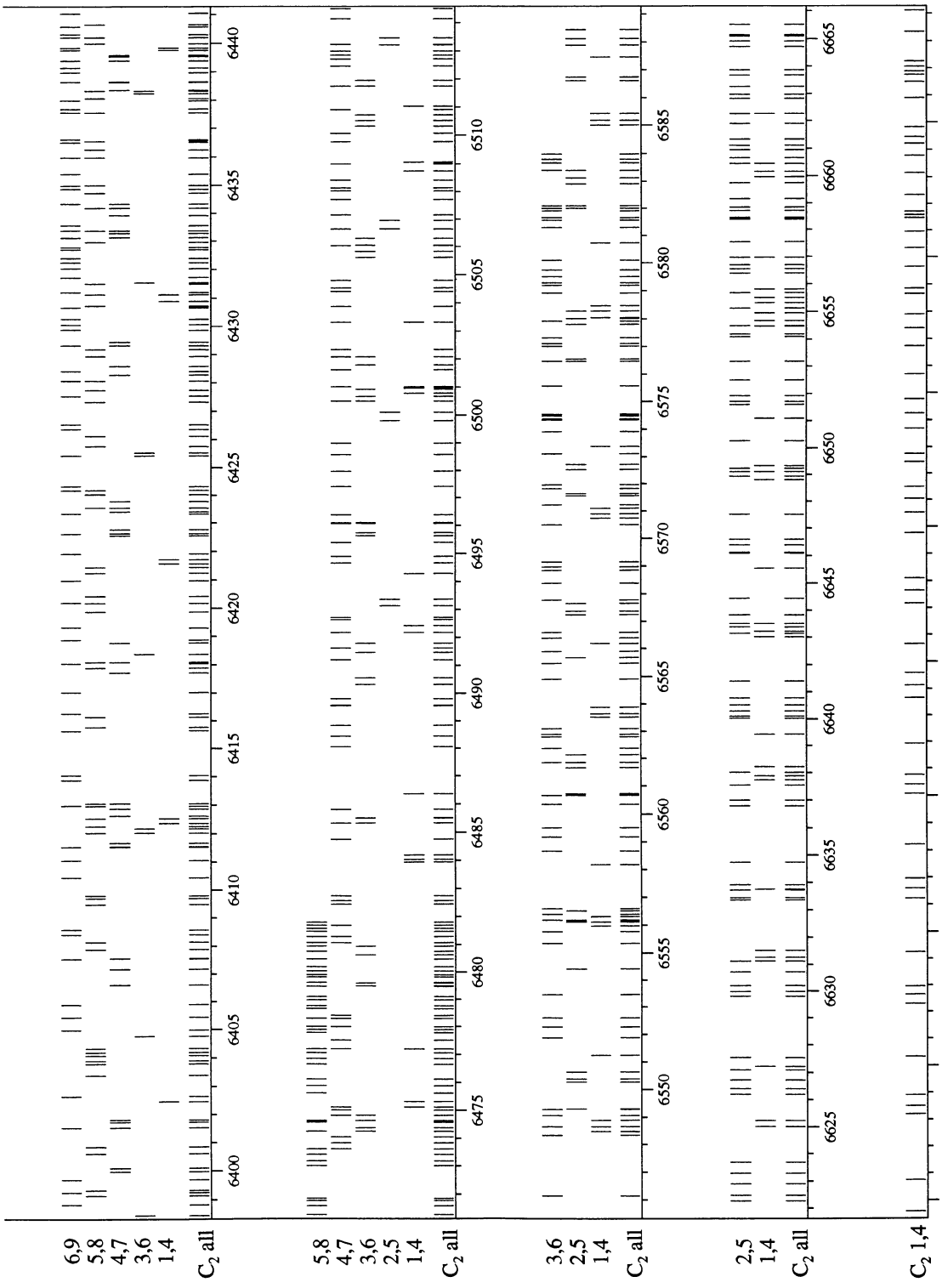

FIG. 65